

Electronic Thesis and Dissertation Repository

4-27-2020 10:00 AM

N-Heterocyclic Carbene Ligated Group 11 Trimethylsilylchalcogenolates: Building Blocks for Heterometallic Chalcogenide Molecules

Dickron Richard Nahhas
The University of Western Ontario

Graduate Program in Chemistry

A thesis submitted in partial fulfillment of the requirements for the degree in Master of Science

© Dickron Richard Nahhas 2020

Follow this and additional works at: <https://ir.lib.uwo.ca/etd>

 Part of the [Inorganic Chemistry Commons](#)

Recommended Citation

Nahhas, Dickron Richard, "N-Heterocyclic Carbene Ligated Group 11 Trimethylsilylchalcogenolates: Building Blocks for Heterometallic Chalcogenide Molecules" (2020). *Electronic Thesis and Dissertation Repository*. 6985.

<https://ir.lib.uwo.ca/etd/6985>

This Dissertation/Thesis is brought to you for free and open access by Scholarship@Western. It has been accepted for inclusion in Electronic Thesis and Dissertation Repository by an authorized administrator of Scholarship@Western. For more information, please contact wlsadmin@uwo.ca.

Abstract

The synthesis of heterometallic chalcogenide molecules requires the continued investigation into the appropriate reagents necessary to introduce metal – chalcogen bonds in a controlled fashion. Trimethylsilyl metallochalcogenolates (MESiMe₃) act as synthons introducing “ME⁻” in solution upon reacting with an appropriate ternary metal reagent, MX (X= halide, acetate, etc.). Recent work makes use of *N*-heterocyclic carbenes (NHCs) as a class of ancillary ligand that can stabilize these reagents and the heterometallic chalcogenide molecules obtained with them. Building on previous work, this thesis describes the synthesis of group 11 trimethylsilyl metallochalcogenolates stabilized by *bis*-1,3-tritylimidazole-2-ylidene (abbreviated ITr) to build this library of compounds and investigate their reactivity towards dinuclear chalcogenide molecules, [(ITr)₂M(μ₂-E)M'] (M=Cu, Ag, Au; E=S, Se). Surprisingly, the reaction of [ITrMESiMe₃] with [ITrMOAc] did not yield the desired products in a selective manner. Attempts are made to rationalize the failure to obtain both the homo and heterometallic compounds by this general method and by other previously established techniques.

Keywords: metal chalcogenides, heterometallic, trimethylsilyl metallochalcogenolates, *N*-heterocyclic carbenes (NHCs)

Summary for Lay Audience

Transition metal chalcogenides are compounds made of a combination of an element from the middle of the periodic table together with one of the chalcogens (oxygen, sulfur, selenium, or tellurium). These solids are found in nature as minerals and ores from which valuable metals can be extracted; however, recent work has shown their suitability for a wide variety of applications ranging from photovoltaic absorbers to catalysts. In engineering the material properties of these compounds further, chemists have learned that controlling the chemical bonding between these elements and forming discrete molecules allows for improved control of their material properties. The challenge of assembling these molecules in a controlled manner is often overcome using other organic molecules, known as ligands, which chemically bond to the metal or chalcogen atoms to effectively control the degree of bonding between these types of elements. The nature of the chemical bond between the ligand and the metal, as well as the ability for this ligand to encompass the metal atom, controls the ability to isolate molecular metal chalcogenides. The work in this field is ongoing, with homometallic (one metal) or heterometallic (two or more metal types) molecules having been made. To continue developing the synthesis of heterometallic chalcogenide molecules, the work in this thesis describes a contribution to the growing library of metal-chalcogen complexes incorporating *N*-heterocyclic carbenes (NHCs) as effective ligands, and investigating the chemical reactions thought to be able to produce a new class of dinuclear, heterometallic molecules.

Acknowledgments

The last two and a half years of my life at Western have been a whirlwind of learning and growth. London, Ontario, has been good to me and provided me with a chance to grow as a person and make new connections with many people, all of whom deserve thanks for their part in helping me come this far. First, I would like to thank the University for funding my two years here and extend my deepest and most humble feelings of gratitude and appreciation to Dr. John Corrigan for his patient tutelage and mentorship. Thank you for allowing me to be part of the lab and for helping me grow as a researcher, challenging my ideas and inspiring new ones. Your patience and guidance were always felt, and I look forward to reading about the work the group produces in the future.

In my time here, I have had the privilege of working with many members of the Corrigan group, past and present. Though there are many people to thank, I would like to make a special mention to Alex Polgar and Jay Kyungseeop Lee for being here at the start. Though I only had a year with Mr. Polgar, it was a memorable one filled with discussions about chemistry and life; I wish you all the success I know is already on its way to you. To Mr. Lee, who was here with me in the trenches for the entirety of my graduate studies, I owe a tremendous amount for being there to listen when reactions wouldn't work and for encouraging me when reactions did. You are a brilliant chemist and my hope is that you acknowledge yourself as such.

Thank you to Connor, Alicia, Rachel and Khayrat; every member of the Corrigan group that I encountered during my time here had to endure my long tangents about my research and theirs. While some happily reciprocated, others quietly and politely obliged me this pleasure. For this I am grateful. To the new members of the Corrigan group, I am sad our time was short but am confident you will do great things here. I look forward to hearing about the achievements of Zahra, Mansha, Johanna, Julia and Evie, as they move on from their undergraduate studies, and thank them for always being interested in learning about what we do. Having you all around in the lab and in group meetings made for a fun time and I am confident you will all succeed in your respective paths.

To the new graduate students Andy and Nils, I would like to offer my sincerest appreciation and gratitude for making the end of my time here very memorable. To Andy, thank you for always being willing to entertain my questions about your project. Dr. Cluster will go on to great things, of this I am sure. To Nils, the "crazy German guy" thank you for taking the time to befriend an old man and for always being willing to talk about chemistry with the same amount of (if not more) passion as I do. Your passion for your

research and your students is inspiring, and I hope you hold onto this passion as you work in the Corrigan lab and beyond.

To my parents, family, and friends thank you for always believing in me and supporting me. To my sister Vana thank you for always being excited to hear about the lab and for taking an interest in my work. To my mom and dad, thank you for patiently listening to my concerns and offering solutions where you could. A special mention to so many of my friends from the Toronto area, those I grew up with, those I met during my undergraduate studies and those I see in passing. Each of you helped in your way to keep me level – headed during my time as a student.

Last, but certainly not least, I would like to thank my partner Laura for all her love and support during my time as a Master's student. I came to London to earn a Master's degree and got lucky in finding a partner for life. Thank you for taking an (sometimes) earnest interest in my work in the lab. Thank you for putting up with the long nights, the early days and having me bring my work home with me. I am excited for what the future has in store for us and blessed to have you by my side. Though I can't promise I won't continue to bring chemistry home with me, I look forward to having our lives grow and be filled with so much more.

Table of Contents

Abstract	ii
Summary for Lay Audience	iii
Acknowledgments	iv
List of Schemes	viii
List of Tables	viii
List of Figures	ix
List of Appendices	xii
List of Abbreviations	xiii
Chapter 1	1
1 Introduction	1
1.1 Metal Chalcogenide, Chalcogenolate Nanoclusters and Complexes	2
1.2 Synthesis of Metal–Chalcogen Complexes: The Growing Use of Trimethylsilyl Reagents	7
1.3 Silyl Metallochalcogenolates: Synthons in Heterometallic Chalcogenide Cluster Chemistry	11
<i>1.3.1. Quantifying Ligand Effects: Tolman Electronic Parameter, Tolman Cone Angle and Percent Buried Volume</i>	<i>12</i>
<i>1.3.2. Phosphine stabilized trimethylsilyl group 11 metallochalcogenolates</i>	<i>14</i>
<i>1.3.3. NHC–stabilized trimethylsilyl group 11 metallochalcogenolates</i>	<i>16</i>
1.4 Scope of Thesis	19
1.5 References	19
Chapter 2	23
2 The Synthesis and Characterization of ITr–Protected Group 11 Trimethylsilylmetallochalcogenolates	23
2.1. Introduction	23
2.2 Results & Discussion	25
<i>2.2.1 Synthesis and Characterization of [ITrMOAc]</i>	<i>25</i>
<i>2.2.2. Syntheses and Characterization of [ITrMESiMe₃]</i>	<i>31</i>
2.3 Conclusions	43
2.4 Experimental	45
2.4.1 General Considerations	45
2.4.3 Measuring δ donor ability by $^1J_{C-H}$ coupling constants⁴⁵	50
2.5. References	50
Chapter 3	53

3 Toward the Synthesis of Heterometallic Chalcogenide Molecules: Attempted syntheses of [(ITr)₂M(μ₂-E)M'] from [ITrMX] (X = OAc, Cl, ESiMe₃)	53
3.1 Introduction	53
3.2 Results and Discussion	55
3.2.1. <i>Attempted syntheses of [(ITr)₂M₂(μ₂-E)] (M = Cu, Ag, Au; E = S, Se)</i>	55
3.2.2. <i>Attempted syntheses of [(ITr)₂M(μ₂-E)M']: Unexpected Reactivity Patterns of [ITrMESiMe₃]</i>	65
3.2.3. <i>The Inability to Synthesize Homometallic and Heterometallic [(ITr)₂M(μ₂-E)M']</i>	70
3.3 Conclusions	76
3.4 Experimental	78
3.4.1. <i>General Considerations</i>	78
3.4.2. <i>Syntheses</i>	78
3.4 References	80
Chapter 4	82
4 Conclusions and Outlook	82
4.1. Summary and Conclusions	82
4.2. Future Work	84
4.3. References	86
Appendix 1. Supporting Information for Chapter 2	88
Appendix 2. Supporting Information for Chapter 3	116
Curriculum Vitae	141

List of Schemes

Scheme 1.1: General reaction methods for the synthesis of metal chalcogenide nanoclusters, where $m = 1, 2, 3, \dots$; $n = 1, 2, 3, \dots$. Reactions are often carried out in the presence of a neutral, $2e^-$ ligand, L. :B = Bronsted base. R_3P = trialkylphosphine. X = anionic, $2e^-$ ligand.....	7
Scheme 1.2: General reaction methods toward the synthesis of molecular metal chalcogenolates, where $m = 1, 2, 3, \dots$; $n = 1, 2, 3, \dots$. Reactions are often conducted in the presence of a neutral, $2e^-$ ligand, L. X = anionic, $2e^-$ ligand. R = organic group (alkyl, aryl, etc.).....	8
Scheme 1.3: General reaction schema for use of trimethylsilylated chalcogen reagents, where $m = 1, 2, 3, \dots$; $n = 1, 2, 3, \dots$. Reactions are often conducted in the presence of a neutral, $2e^-$ ligand, L. X = anionic, $2e^-$ ligand. R = organic group (alkyl, aryl, etc.).....	9
Scheme 2.1: Syntheses of [ITrMOAc](2.1a–c).....	26
Scheme 2.2: Syntheses of [ITrMESiMe ₃](2.2a,b – 2.3a,b).....	31
Scheme 2.3: Proposed decomposition reaction of metallochalcogenolates($M = Cu^I, Ag^I, Au^I$; $E = S, Se$).	33
Scheme 2.4: Syntheses of [ITrAuESiMe ₃](2.2c – 2.3c).....	34
Scheme 3.1: Proposed synthesis of [(ITr) ₂ M ₂ (μ_2 -E)] from [ITrMOAc].....	56
Scheme 3.2: General reaction methodology for syntheses of [(ITr) ₂ M((μ_2 -E)M')]	65

List of Tables

Table 1.1: Electronic and steric parameters of selected ligands (phosphines and NHCs). %V _{bur} has been reported for LAuCl complexes and TEP for LNi(CO) ₃ , unless otherwise noted.* – crystal structure of ligand used in SambVca ⁸⁸ . **–Data from L ₂ AuX (X = Cl ⁻ , Ph ₂ EtAuSe(C ₆ H ₄) ₂ Se ⁻ , 4-phenyl-1H-1,2,3-triazol-5-yl) used in SambVca. ^{84,86,88–96}	14
Table 1.2: Melting points for group 11 trimethylsilyl metallochalcogenolates ^{51,71–73,97}	18
Table 2.1: ¹ H and ¹³ C NMR data comparing chemical shifts of the carbene (¹³ C), the carbonyl (¹³ C), and the methyl groups (¹³ C and ¹ H) in [ITrMOAc]. Data listed in ppm in CDCl ₃	28
Table 2.2: ¹ H & ¹³ C NMR data comparing the acetate resonance and carbenic carbon resonance of [ITrMOAc] and [IPrMOAc]. Data listed in ppm in the indicated solvent.....	29
Table 2.3: ¹ H NMR/ ¹³ C NMR resonance of ESiMe ₃ moiety for [(ITr)MSSiMe ₃](2.2a–c) and [(ITr)MSeSiMe ₃](2.3a–c), compared to [IPrMESiMe ₃]. Data obtained in CDCl ₃ from this work and others, reported in ppm. ^{17–19}	35
Table 2.4: ¹³ C NMR data for NCN resonances in NHC–M–X complexes (NHC = ITr, IPr; X = OOCCH ₃ , ESiMe ₃ ; E = S, Se). ^{17–19} Data reported in CDCl ₃ and/or at 25 °C unless otherwise indicated	36

List of Figures

- Figure 1.1:** Molecular structures of $[\text{Cu}_{70}\text{Se}_{35}(\text{PEt}_2\text{Ph})_{24}]$ (left) and $[\text{Cu}_{12}(\mu_6\text{-Te})_3(\mu_3\text{-TePh})_6(\text{PPh}_3)_6]$ (right). Phosphine ligands = wireframe, telluroate (TePh) ligands = capped stick. Cu^{I} = blue, Se = pink, Te = orange.^{6,7}.....2
- Figure 1.2:** Reaction scheme from Dehnen et al. showing the different types of copper selenide nanoclusters obtained as a function of reaction chemistry.⁸..... 3
- Figure 1.3:** Molecular structures of $[(^i\text{Pr}_3\text{P})_4(\text{CuSPh})_6]$ (left) and $[(^i\text{Pr}_3\text{P})_3(\text{CuSPh})_4]$ (right). Cu^{I} = blue, S = yellow, phosphine ligands = wireframe, R groups = wireframe. 4
- Figure 1.4:** Molecular structures of mixed copper selenide/thiolate cluster compounds $[\text{Cu}_{22}\text{Se}_6(\text{S-}p\text{-C}_6\text{H}_4\text{NO}_2)_{10}(\text{PPh}_3)_8]$ (top left), $[\text{Cu}_{28}\text{Se}_6(\text{S-}p\text{-C}_6\text{H}_4\text{Br})_{16}(\text{PPh}_3)_8]$ (top right) and $[\text{Cu}_{72}\text{Se}_{14}(\text{SPh})_{36}(\text{OAc})_8(\text{PPh}_3)_6]$ (bottom).^{5,14-16} R groups on chalcogenolates = capped stick, phosphines = wireframe. Cu = blue, Se = pink, S = yellow, P = purple, O = red, Br = brown, N = green.....5
- Figure 1.5:** Molecular structures of $[\text{Ag}_4(\text{Se}_2\text{fc})_3]^{2-}$ (left) and $[\text{Ag}_{74}\text{S}_{19}(\text{dppp})_6(\text{fc}(\text{C}\{\text{O}\}(\text{CH}_2)_2\text{S})_2)_{18}]$ (right).^{21,24} Ferrocenyl ligands = capped stick, phosphine = wireframe, inorganic core = ball and stick. Ag^{I} = blue, S = yellow, Se = pink, Fe = brown, P = purple, O = dark red. Counter ions, hydrogens and solvent omitted for clarity. 6
- Figure 1.6:** Molecular structures of $[\text{Cu}_{14}\text{In}_6\text{Se}_7(^i\text{PrSe})_{18}]$ (left) and $[\text{Au}_8\text{InSe}_4(\text{dppe})_4]^{3+}$ (right) as examples of heterometallic chalcogenide nanoclusters.⁵⁷⁻⁵⁸ Solvent molecules and disordered molecules deleted for clarity. Cu = blue, Se = pink, In = brown, Au = gold. Ancillary ligands = wireframe; selenolate R groups = capped stick. 10
- Figure 1.7:** Diagram of Tolman Cone Angle (left, highlighted in red) and hemisphere of coordination used for calculation of %Vbur (right). Listed are the average L – M bond lengths for phosphines (2.28 Å) and N–heterocyclic carbenes (2.00 Å)^{74,76} 13
- Figure 1.8:** Electronic structure of NHCs (diagram from Hopkinson et al.).⁸⁶ The lone pair at the carbenic carbon is stabilized by π -electron donation and σ -electron withdrawal. 16
- Figure 1.9:** NHCs used to stabilize group 11 trimethylsilyl metallochalcogenolates.^{64-66,105}..... 17
- Figure 2.1:** Reactions of $[\text{LCuESiMe}_3]$ illustrating the effect of the neutral, $2e^-$ ligand, L. The acetate (OAc) and trimethylsilyl (SiMe_3) moieties are coloured to illustrate the formation of the thermodynamically favored product. Below, the various ligands used are illustrated along with reported TEP and %Vbur values.^{22,23} Pr = n – propyl; Ph = phenyl; Et = ethyl; $i\text{Pr}_2$ – bimy = bis–1,3–(diisopropyl)benzimidazole–2–ylidene; $i\text{Pr}$ = bis–1,3–(2,6-diisopropylphenyl)imidazole–2–ylidene.24
- Figure 2.2:** Structure, electronic and steric data of bis–1,3–tritylimidazole–2–ylidene (ITr)²⁶..... 25
- Figure 2.3:** 400 MHz ^1H NMR spectra of $[\text{ITrMOAc}]$ (Cu^{I} = red, Ag^{I} = green, Au^{I} = green) in CDCl_3 at 25 °C. Acetate peaks indicated by arrows.27
- Figure 2.4:** Scatter plot of correlation between the HOMO–LUMO gap and chemical shift of carbenic carbon in various NHCs (data from Wong et al. and Roy et al.).^{26,37} Included are figures of each NHC compared in the graph, in order from left to right.31
- Figure 2.5:** ^1H NMR spectra of **2.1a** (blue) and after reaction with 1.07 eq. $\text{S}(\text{SiMe}_3)_2$ in CDCl_3 . Red stars = **2.2a**, blue stars = $[\text{ITrCuOAc}]$, orange stars = AcOSiMe_3 , black star = excess $\text{S}(\text{SiMe}_3)_2$ 32
- Figure 2.6:** ORTEP ellipsoid plot of $[(\text{ITr})\text{CuSSiMe}_3]$ (**2.2a**) at 50% probability level. Nitrogen (green), copper (blue), silicon (beige), sulfur (yellow) are colored for emphasis. Hydrogens and solvent

molecules omitted for clarity. Intramolecular contacts ($<\Sigma$ VVDW) shown in blue. Selected bond lengths and angles: Cu1–S1: 2.152(1) Å; S1–Si1: 2.111(2) Å; C17 – Cu1:3.030(3) Å; C41–Cu1: 3.005(4) Å; Cu1–S1–Si1: 105.87(6)°; C1–Cu1–S1: 172.6(1)°; Cu1–C1–N1: 130.4(2)°; Cu1–C1–N2: 125.1(2)°.....38

Figure 2.7: ORTEP ellipsoid plot of [(ITr)CuSeSiMe₃] (**2.3a**) at 50% probability level. Nitrogen (green), copper (blue), silicon (beige), sulfur (yellow) are colored for emphasis. Hydrogens and solvent molecules omitted for clarity. Intramolecular contacts ($<\Sigma$ VVDW) shown in blue. Selected bond lengths and angles: Cu1–S1: 2.152(1) Å; S1–Si1: 2.111(2) Å; C17 – Cu1:3.030(3) Å; C41–Cu1: 3.005(4) Å; Cu1–S1–Si1: 105.87(6)°; C1–Cu1–S1: 172.6(1)°; Cu1–C1–N1: 130.4(2)°; Cu1–C1–N2: 125.1(2)°.....39

Figure 2.8: Differences in orientation of –ESiMe₃ about the imidazole ring in [ITrCuSSiMe₃] (**2.2a**, top), [IPrCuSSiMe₃]· THF (**2.Ia**, middle) and [IPrCuSSiMe₃]·0.25 PhMe (**2.IIa**, bottom). Plane of the ring highlighted in blue and plane of Si-S-Cu drawn in red.¹⁷.....40

Figure 2.9: Diagram and table of structural differences that are statistically significant in select bond lengths and bond angles between [IPrCuESiMe₃] (E = S, **2.IIa**; Se, **2.IIIa**) and [ITrCuESiMe₃] (E = S, **2.2a**; Se, **2.3a**). Note that **2.IIa** is the toluene solvate, and **2.IIIa** is the THF solvate (see text).....41

Figure 2.10: UV– VIS Absorption spectra of [ITrMOAc] and [ITrMESiMe₃]. Graph is focused on 200–400 nm range and the absorbance has been normalized. All spectra acquired in 0.6 mM solution in tetrahydrofuran at 25 °C.....42

Figure 2.11: Proposed reactions for syntheses of heterometallic group 11 metal chalcogenide molecular frameworks44

Figure 3.1: Examples of copper sulfide molecules **3.I** – **3.III** from previous works. Figures also show molecular structure of IPr*, IPr and 7Dipp.....54

Figure 3.2: ¹H NMR spectra of the 2:1 reaction of [ITrCuOAc] (**3.1a**) and Se(SiMe₃)₂ in CDCl₃ (A – D). Spectrum E is [ITrCuCl] (**3.4**) in CDCl₃ Insets are expansions of the H_{4,5-imid} region and the –OAc region. **A)** –25 °C, 1 hr. **B)** –25 °C, 120 hr. **C)** 5 °C, 24 hr. **D)** 25 °C, 24 hr. *– **3.1a** *–**3.3a**. *–AcOSiMe₃. Note: *– δ 6.99 ppm correlates to **3.4**57

Figure 3.3: ¹H NMR spectra of [ITrCuCl] (**3.4**, purple) and reaction aliquots from 2:1 reactions of **3.4** and Na₂E (E = S, red; Se = blue) after stirring at room temperature for 24 hrs. All data shown in C₆D₆.....58

Figure 3.4: ¹H NMR spectra of the 2:1 reaction of [ITrAgOAc](**3.1b**) and E(SiMe₃)₂ in CDCl₃. E = S, maroon; E = Se, teal. Inset shows H_{4,5-imid} region and –ESiMe₃ region. No –SeSiMe₃ peak is evident.* – **3.1b/3.5**; *– **3.2b/3.3b**; *– AcOSiMe₃; *– Se(SiMe₃)₂.....60

Figure 3.5: ¹H NMR spectra of 2:1 reactions of [ITrAuOAc] **3.1c** and E(SiMe₃)₂ in CDCl₃. E = S, maroon; Se, teal. Inset shows ¹H–¹³C HMBC suggesting that new peaks at δ 6.95 ppm (E = S) and δ 6.96 ppm (E = Se) belong to carbene on ITr–Au–E. Inset, maroon, shows peak at δ 6.99 ppm corresponding to [ITrAuCl.]61

Figure 3.6: ¹H NMR spectrum, in CDCl₃, of aliquot from [ITrAuOAc] (**3.1c**) + ½ S(SiMe₃)₂ in THF. Inset shows only one major ITr bearing product thought to be [ITrAuSSiMe₃](**3.2c**) based on –SSiMe₃ peak, but integration is 1: 3 instead of 1:4.5. A PRESAT NMR pulse sequence was used to saturate PDMS grease peak at δ 0.07 ppm..... 62

Figure 3.7: ¹H NMR spectrum, in C₆D₆, of solids isolated from the 2:1 reaction of [ITrAuOAc] **3.1c** and S(SiMe₃)₂ in THF. Inset shows multiple ITr bearing compounds, with δ 6.44 ppm corresponding to [ITrAuSSiMe₃] (**3.2c**)..... 63

Figure 3.8: ¹H NMR spectrum in C₆D₆ of a 2:1 mixture of [ITrAuCl] (**3.5**) and Na₂S for 24 hours at 25

°C. Inset shows ^1H - ^{13}C HMBC showing correlations between peaks in $\text{C}_{4,5}$ -imid region and carbenic resonances characteristic to [ITr-Au-S]. Correlation (δ 6.49, δ 185.1) belonged to 3.5 , while peaks (δ 6.53, δ 194.2), (δ 6.56, δ 198.6) and (δ 6.44, δ 179.9) remain unidentified.....	64
Figure 3.9: ^1H NMR spectra of the reaction of [ITrCuESiMe ₃](E = S, 3.2a ; Se 3.3a) and [ITrAgOAc] (3.1b). (3.2a , maroon; 3.3a , teal). Inset shows expansions of regions of interest, labelling [ITrMESiMe ₃] with triangles, [ITrMOAc] with circles and using red and blue to distinguish between Ag and Cu compounds.....	66
Figure 3.11 Scatter plot tracking changes in peak area for select resonances in Figure 3.10 . T = -25 °C up to 60 min; T = -10 °C afterwards.....	67
Figure 3.10: Stacked ^1H NMR spectra of [ITrAuSSiMe ₃] and [ITrAgOAc] in CDCl ₃ . Data collected at -25 °C for first 60 minutes, then -10 °C for remaining 90 minutes	67
Figure 3.12: ^1H NMR spectrum of reaction of [ITrCuSeSiMe ₃] and [ITrAuOAc] in C ₆ D ₆ . Inset shows ^1H - ^{13}C HMBC for H _{4,5} -imid region and expansion of the peaks in the f1 axis. Peak at δ 2.00 ppm corresponds to -OAc for [ITrCuOAc].	68
Figure 3.13: ^1H NMR spectra of the reaction of [ITrAuSeSiMe ₃] and [ITrCuOAc]. Spectra in C ₆ D ₆ after 1 hour at -25 °C (red) and 24 hours at 25 °C (blue) superimposed to illustrate disappearance of -SeSiMe ₃	69
Figure 3.14: Space Filling Models of [(IPr*) ₂ Cu ₂ (μ_2 -S)],(3.I , top left), [(7Dipp) ₂ Cu ₂ (μ_2 -S)] (3.III , top right), [(7Dipp) ₂ Au ₂ (μ_2 -Cl)] ⁺ (3.V bottom right) and [(ITr) ₂ Au ₂ (μ_2 -Cl)] ⁺ (3.6 , bottom left). Solvent and counter ions omitted for clarity. Cl = lime green, S = yellow, Au = gold, N = green, C = grey	72
Figure 3.15: Steric maps of [(IPr*) ₂ Cu ₂ (μ_2 -S)] (3.I) generated from crystallographic data. Space filling model next to each image shows the molecule in the same orientation, with the appropriate atoms deleted. C = grey, Cu ^I = blue. See Appendix for details	74
Figure 3.16: Steric Maps of [(7Dipp) ₂ Cu ₂ (μ_2 -S)] (3.III) and [(NHC) ₂ Au ₂ (μ_2 -Cl)] ⁺ (NHC = 7Dipp, 3.V ; ITr, 3.6) in the same orientation seen in Figure 3.14 (Orientation C, see Appendix).....	76
Figure 4.1: N-Heterocyclic Carbenes (NHCs) used in the isolation of group 11 trimethylsilyl metallochalcogenolates.....	84
Figure 4.2: Example of silyl deprotection of [(NHC)Au(CH ₂ COCH ₃)] from Nolan et al. (NHC = IPr, top). Proposed use for future work toward synthesis of heterometallic dinuclear gold chalcogenides (bottom).....	86

List of Appendices

Appendix 1: Supporting Information for Chapter 2.	88
Appendix 2: Supporting Information for Chapter 3.	116

List of Abbreviations

°C	Degrees Celsius
ΔE	HOMO–LUMO energy gap
μ	Bridging coordination mode
η	Hapticity; uninterrupted number of atoms through which a ligand is coordinated
ε	Molar Absorptivity
δ	Chemical Shift
δ_p	Paramagnetic shielding term
δ_d	Diamagnetic shielding term
$\%V_{bur}$	Percent buried volume
ε	Molar Absorptivity
γ	Magnetogyric Ratio
ν	frequency (s^{-1})
θ_T	Tolman Cone Angle
λ_{max}	emission maximum
1D	One–Dimensional
2D	Two–Dimensional
3D	Three–Dimensional
7Dipp	<i>bis</i> -1,3-(2,6-diisopropylphenyl)-4,5,6,7-tetrahydro-1,3-diazepin-2-ylidene
Å	Angstrom
A	Alkali metal; Na, Li, K
AcOSiMe ₃	Acetoxytrimethylsilane
a. u.	absorbance units
Ar	Aromatic Group
:B	Brønsted Base
CAAC	Cyclic Alkyl Amino Carbene
CAAC ^{Cy}	2-(2,6-diisopropylphenyl)-3,3-dimethyl-2-azaspiro[4.5]dec-1-ylidene
cm	centimetre
cm ⁻¹	wavenumber
Cp	metallocene; cyclopentadienyl ring
Dipp	2,6-diisopropylphenyl
DFT	Density Functional Theory
dppe	1,2- <i>bis</i> (diphenylphosphino)ethane
dppm	1,1- <i>bis</i> (diphenylphosphino)methane
dppp	1,3- <i>bis</i> (diphenylphosphino)propane
E	Chalcogen; S, Se, or Te
E ²⁻	Chalcogenide; S ²⁻ , Se ²⁻ , or Te ²⁻
ER	Chalcogenolate; RE ⁻
ESI–MS	Electrospray Ionization Mass Spectrometry
Et	Ethyl – C ₂ H ₅
eV	Electron Volt – 1.6022 x 10 ⁻¹⁹ J
fc	ferrocenyl; [(C ₅ H ₄) ₂ Fe]
HMBC	Heteronuclear Multiple Bond Correlation
HOMO	Highest Occupied Molecular Orbital
Hz	Hertz (s^{-1})
ⁱ Pr	isopropyl; –CH(CH ₃) ₂

IPr	<i>bis</i> -1,3-(2,6-diisopropylphenyl) imidazole-2-ylidene
IPr·HCl	<i>bis</i> -1,3-(2,6-diisopropylphenyl) imidazolium chloride
IPr*	<i>bis</i> -1,3-(2,6-(diphenylmethyl)-4-methylphenyl)imidazole-2-ylidene
ⁱ Pr ₂ -bimy	<i>bis</i> -1,3-(diisopropyl)benzimidazole-2-ylidene
IR	Infrared
ITr	<i>bis</i> -1,3-tritylimidazole-2-ylidene
ITr·HOTf	<i>bis</i> -1,3-tritylimidazolium triflate
<i>J</i>	<i>J</i> – coupling constant
KHMDS	potassium hexamethyldisilazane
NHC	<i>N</i> -heterocyclic carbene
NMR	Nuclear Magnetic Resonance
L	Neutral, 2 electron donor ligands
LUMO	Lowest Unoccupied Molecular Orbital
Me	methyl; –CH ₃
MLCT	Metal-to-Ligand Charge Transfer
NCN	carbenic carbon
NCH	imidazole-2-ylidene proton; also referred to as H _{4,5-imid}
NMR	Nuclear Magnetic Resonance
OAc	acetate; CH ₃ C(O)O
O ₂ CR	carboxylate
OTf	triflate; ⁻ OSO ₂ CF ₃
Ph	phenyl; C ₆ H ₅
ppm	parts-per-million
R	organic group; alkyl group
RE – ER	diorganodichalcogenide
Samb/∇ca	Salerno at the MoLNaC Buried Volume Calculation
SCE	Saturated Calomel Electrode
SEM–EDX	Scanning Electron Microscopy – Electron Dispersive X-Ray
SIPr	<i>bis</i> -1,3-(2,6-diisopropyl phenyl)imidazolin-2-ylidene
SPAAC	Strain – Promoted Azide Alkyne Click reaction
SCXRD	Single Crystal X-Ray Diffraction
^t Bu	tertiary-butyl; –C(CH ₃) ₃
TEP	Tolman Electronic Parameter
THF	tetrahydrofuran; OC ₄ H ₈
THT	tetrahydrothiophene; SC ₄ H ₈
TMEDA	tetramethylene diamine
UV – VIS	ultraviolet – visible
X	Anionic, 2 electron donor ligands
XLCT	Anion – to – Ligand Charge Transfer

Chapter 1

1 Introduction

The tendency for oxygen and the heavier group 16 chalcogens sulfur, selenium and tellurium to form solids with various metals was well established in antiquity and reflected by the naming of this group, indicating that these elements were “born from ores” of various metals.¹ This propensity to bind to metals in extended three dimensional networks allows for a rich tapestry of diverse structures and properties, which translates to the use of these types of compounds in a wide variety of applications. Within these solid materials, the chalcogens can adopt coordination modes bridging multiple metal centres, binding to each other, or a combination of both. These unpredictable binding motifs may lead to solids with non – integer chemical formulae, making the discussion on the structure of even those solids containing only two elements a challenge. The smaller difference in electronegativity between the transition metals and the chalcogens, as opposed to the more ionic nature of alkali metal chalcogenides, allows for the possibility of metal–metal bonding in the former class of compounds. Transition metal chalcogenides can be “chalcogen–rich” or “metal–rich” phases of binary (two elements), ternary (three elements), or even quaternary composition (four elements); chalcogen–rich phases may or may not contain E–E bonds, while metal–rich phases may display M–M bonding.^{1,2} These non – stoichiometric phases may also arise due to the propensity for the transition metals to take on different oxidation states, which can lead to materials containing mixed valent systems that ultimately lead to non – stoichiometry.^{1,2}

The covalent nature of transition metal chalcogenides (*i.e.* sulfides, selenides, tellurides) leads to structural differences from those observed in the 3D lattices of the more ionic metal oxides.¹ These structural differences and the semiconducting nature of the late transition metal chalcogenides eventually made this class of compounds ideal in studying the quantum confinement effect, whereby the control of the three–dimensional growth of these extended solids into nanoparticles (crystallites with nanometer dimensions) resulted in tunable optoelectronic properties.³ In the process of developing nanoparticle research, and driven by the importance of similar metal–sulfide and metal–selenide compounds in bioinorganic chemistry, synthetic inorganic chemists began the work of making transition metal chalcogenides as molecular, atomically precise assemblies, often referred to as nanoclusters.⁴ The term has since come to encompass those molecules whose dimensions are, also, well below the nanometer range. Work in this field continues toward the discovery of new reagents or reaction methods to introduce metal–chalcogen bonds in a controlled, well–defined manner.

1.1 Metal Chalcogenide, Chalcogenolate Nanoclusters and Complexes

The structural diversity found in transition metal chalcogenide nanomaterials is a direct result of the flexible coordination chemistry of the chalcogens and, often, the metals. The anionic chalcogenide (E^{2-}) and chalcogenolate (RE^-) ligands can bridge two or more metal centres, doing so in a more stable manner than their neutral counterparts (H_2E , R_2E , REH).⁵ The structure and size of nanocluster compounds are affected by the role of these anionic ligands. Chalcogenides, with the ability to adopt dicoordinate (μ_2^-), tricoordinate (μ_3^-), tetracoordinate (μ_4^-) and even hexacoordinate (μ_6^-) geometries, can contribute to the higher nuclearity of nanoclusters, resulting in molecules ultimately bearing larger numbers of metal centres. This effect is more pronounced in going from $S \rightarrow Se \rightarrow Te$, as larger ionic radii and more diffuse, polarizable orbitals allow the heavier chalcogens to coordinate a greater number of metal centres.⁶ The chalcogenolates, with their pendant R groups, are more limited in the number of metal atoms they can coordinate and contribute to the lower nuclearity of nanoclusters. For example, $[Cu_{70}Se_{35}(PEt_2Ph)_{24}]$ and $[Cu_{12}(\mu_6^-Te)_3(\mu_3^-TePh)_6(PPh_3)_6]$ both contain chalcogenide ligands that are μ_6^- , with the copper selenide molecule displaying higher nuclearity as a result of the cumulative effect of having only hexacoordinated selenides (see **Figure 1.1**).^{7,8} The mixed telluride/tellurolate compound, on the other hand, showcases a more coordinatively limited phenyl tellurolate ligand, coordinating only three copper centres and organizing the pendant phenyl rings away from the cluster core, to avoid interrupting the Cu – Te interactions; this ultimately helps stabilize a molecule of lower nuclearity.⁸

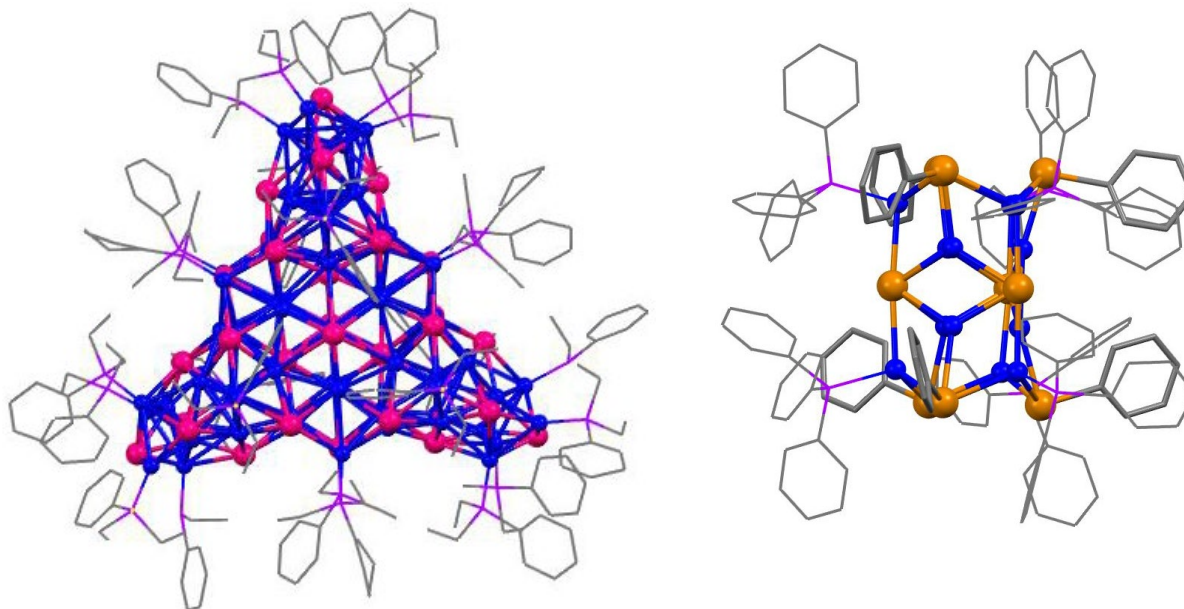


Figure 1.1: Molecular structures of $[Cu_{70}Se_{35}(PEt_2Ph)_{24}]$ (left) and $[Cu_{12}(\mu_6^-Te)_3(\mu_3^-TePh)_6(PPh_3)_6]$ (right). Phosphine ligands = wireframe, tellurolate (TePh) ligands = capped stick. Cu = blue, Se = pink, Te = orange.^{6,7}

Transition metal chalcogenide nanoclusters have been synthesized containing chalcogenide, chalcogenolate or mixed chalcogenide/chalcogenolate ligand systems. For those compounds containing only chalcogenides, the use of an ancillary ligand is often necessary to prevent further aggregation or condensation of the molecular species towards more thermodynamically favoured bulk phases. In some special circumstances, “naked” clusters with no ligands have also been demonstrated in the literature.⁹ In general, the identity of the metal, the ancillary ligand, the chalcogenide and the reaction conditions under which these components are introduced influence the product outcome. For example, a very comprehensive review by Dehnen *et al.* discusses the formation of copper chalcogenide clusters as a function of the chalcogen, phosphine and reaction conditions used, with an excerpt of the reaction schema relevant to copper selenides shown in **Figure 1.2**.⁹

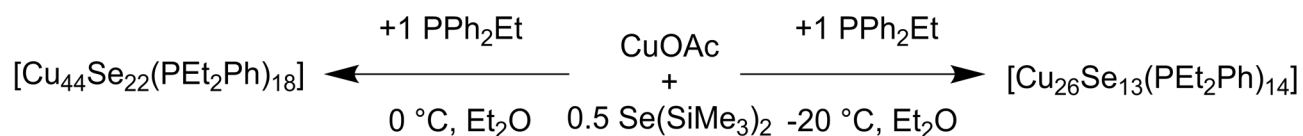


Figure 1.2: Reaction scheme from Dehnen *et al.* showing the different types of copper selenide nanoclusters obtained as a function of reaction chemistry.⁸

Molecular metal chalcogenolate compounds also owe their structure and size to the delicate balance between the interplay of the many factors used to kinetically stabilize them. In one extreme, sterically demanding R groups can make it possible to isolate mononuclear metal chalcogenolate complexes.¹⁰ On the other hand, very small organic groups in the absence of any additional ancillary ligands can only stabilize extended 1D or 2D coordination solids, which are often insoluble and difficult to characterize.¹¹ Organic moieties on the chalcogen centres that are intermediate in size can stabilize cyclic or oligomeric architectures, and these are often used in conjunction with other ancillary ligands to access metal chalcogenolate nanoclusters of intermediate nuclearity. The structures of trialkylphosphine stabilized copper (I) phenylchalcogenolates, for instance, were demonstrated to depend on phosphine to metal ratio, the synthetic routes used to obtain them, and the identity of the chalcogen and phosphine ligands.^{12,13} Though many compounds were ultimately studied, **Figure 1.3** shows the difference that phosphine ratio has in the final structure of the triisopropylphosphine stabilized copper (I) phenylthiolates.¹² Any

deficiency of phosphine relative to the number of copper centres ultimately resulted in molecular copper (I) phenylthiolates of higher nuclearity.¹²

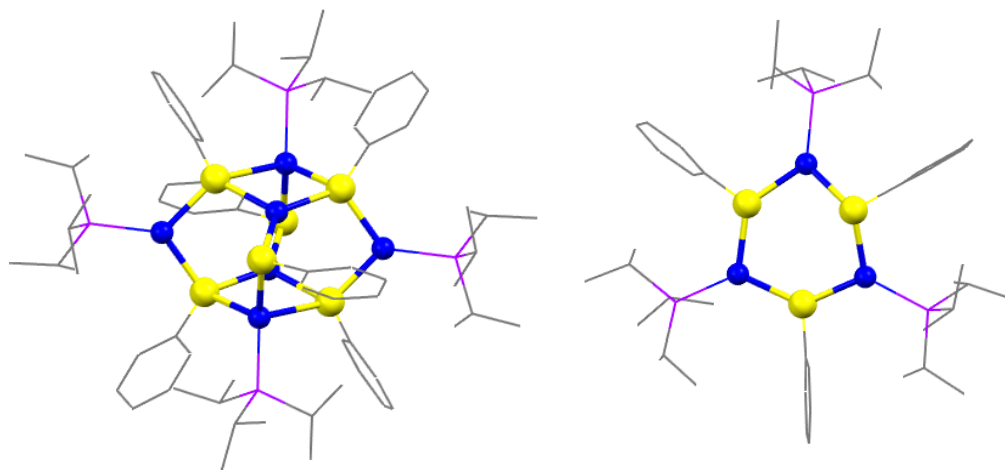


Figure 1.3: Molecular structures of binary thiolates $[(^1\text{Pr}_3\text{P})_4(\text{CuSPh})_6]$ (left) and $[(^1\text{Pr}_3\text{P})_3(\text{CuSPh})_4]$ (right). Cu^{I} = blue, S = yellow, phosphine ligands = wireframe, R groups = wireframe.¹⁰

In addition to these binary molecules, made of only two elements (i.e. **Figure 1.3**), nanoclusters have been made using the mixed chalcogenide/chalcogenolate system, containing E^{2-} and RE^- within the same inorganic molecule. As discussed above, the chalcogenolate ligands organize themselves to the surface of the cluster while the chalcogenide ligand bridges multiple metal centres together within the core. This layered composition has made it possible to isolate metal chalcogenide/chalcogenolate clusters with varying chalcogens, or ternary composition.^{6,14} **Figure 1.4** features just a few examples of these types of compounds in a series of copper selenide/thiolate clusters reviewed by MacDonald and Corrigan; it was determined that the swapping of interstitial or peripheral chalcogens resulted in observable differences in the UV–VIS absorption spectra of these compounds.^{6,15–17} Though mixed chalcogenide/chalcogenolate clusters can be made without ancillary ligands, it is more commonplace in the literature to find examples stabilized by both ancillary ligands and chalcogenolates.

In addition to the synthetic flexibility of mixing different chalcogens in the same molecule, the advantage of using chalcogenolate ligands in the synthesis of metal chalcogenide cores is the ability to use these pendant R groups to affect cluster stability, solubility and to impart additional functionality.^{6,18,19} In general, replacing the more traditionally used R groups (Ph, ^tBu, etc.) with those that have some advantageous chemical or physical property has allowed for the incorporation of more structural variety into this class of compounds. For example, the compounds in **Figure 1.4**, such as $[\text{Cu}_{28}\text{Se}_6(\text{S}-p\text{-C}_6\text{H}_4\text{-Br})_{16}(\text{PPh}_3)_8]$ and $[\text{Cu}_{22}\text{Se}_6(\text{S}-p\text{-C}_6\text{H}_4\text{-NO}_2)_{10}(\text{PPh}_3)_8]$ feature functional groups on the *para* position of

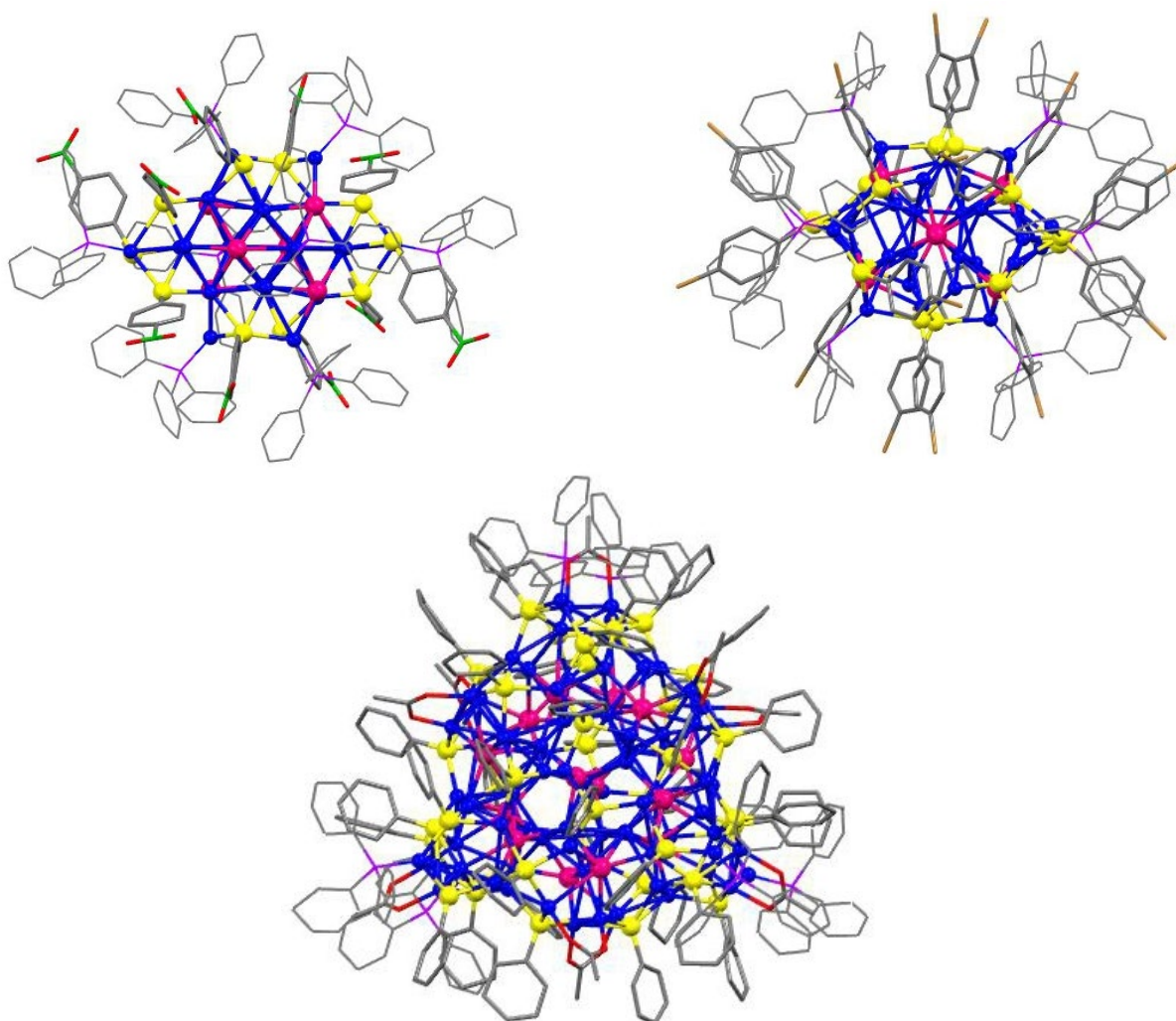


Figure 1.4: Molecular structures of mixed copper selenide/thiolate cluster compounds $[\text{Cu}_{22}\text{Se}_6(\text{S-p-C}_6\text{H}_4\text{NO}_2)_{10}(\text{PPh}_3)_8]$ (top left), $[\text{Cu}_{28}\text{Se}_6(\text{S-p-C}_6\text{H}_4\text{Br})_{16}(\text{PPh}_3)_8]$ (top right) and $[\text{Cu}_{72}\text{Se}_{14}(\text{SPh})_{36}(\text{OAc})_8(\text{PPh}_3)_6]$ (bottom).^{5, 14–16} R groups on chalcogenolates = capped stick, phosphines = wireframe. Cu = blue, Se = pink, S = yellow, P = purple, O = red, Br = brown, N = green

the phenylthiolate ligand, which can be reacted further to introduce new functional groups to the cluster surface, or to connect clusters together by vertex sharing.^{6,16,17,20} The idea of functionalization is not limited to the chalcogenolate ligand, as compounds such as $[\text{Cu}_{72}\text{Se}_{14}(\text{SPh})_{36}(\text{OAc})_8(\text{PPh}_3)_6]$ feature stimulus responsive acetate ligands that, hypothetically, can be removed under the appropriate reaction conditions to reveal bonding sites at the metal centre.¹⁵ The ability to use surface metal acetate functional groups (M – OAc) to afford chemical transformations to cluster compounds was recently exemplified in a work by Lee, which used a zinc phosphinidene cluster containing these moieties as a single source precursor for nanoparticulate zinc phosphide.²¹ In addition to the functionalization of cluster surfaces by chemical groups amenable to surface and/or cluster modification, functional groups which impart new material properties onto the cluster compounds have been used as chalcogenolate ligands. The use of

ferrocenyl chalcogenolate ligands, for instance, results in molecular species with potential applications in chemical sensing.^{18,22–24} As before, the nuclearity of the product can be affected by the presence of mixed chalcogen/chalcogenide systems, making the synthesis of ferrocene decorated chalcogenolates and chalcogenide/chalcogenolates well studied and reported. For instance, the structure of $[\text{Ag}_4(1,1'\text{-fcSe}_2)_3]^{2-}$ ($\text{fc} = [\text{Fe}(\eta_5\text{-C}_5\text{H}_4)_2]$) features bis-selenolate ligands on the ferrocenyl moieties, allowing for the isolation of a tetranuclear anionic structure (see **Figure 1.5**).²² In contrast, the mixed sulfide/thiolate compound $[\text{Ag}_{74}\text{S}_{19}(\text{dppp})_6(\text{fc}(\text{C}\{\text{O}\}\text{OCH}_2\text{CH}_2\text{S})_2)_{18}]$ ($\text{dppp} = 1,3\text{-bis}(\text{diphenylphosphino})\text{propane}$), is a multinuclear molecule with overall dimensions (including ligand sphere) in the nanometre range (see **Figure 1.5**).²⁵ Although not a chalcogenide/chalcogenolate system, Gunawardene *et al.* recently extended the idea of functionalized chalcogenolate ligands further by using azide functionalized thiolate ligands to make $[\text{Au}_{25}\text{SR}_{18}]^-$ clusters which were amenable to surface click chemistry via the Strain-Promoted Alkyne-Azide Cycloaddition (SPAAC) reaction.¹⁹ They demonstrated the ability to perform SPAAC reactions to introduce ferrocenyl alkynes to the surface of the gold chalcogenolate cluster compound.¹⁹

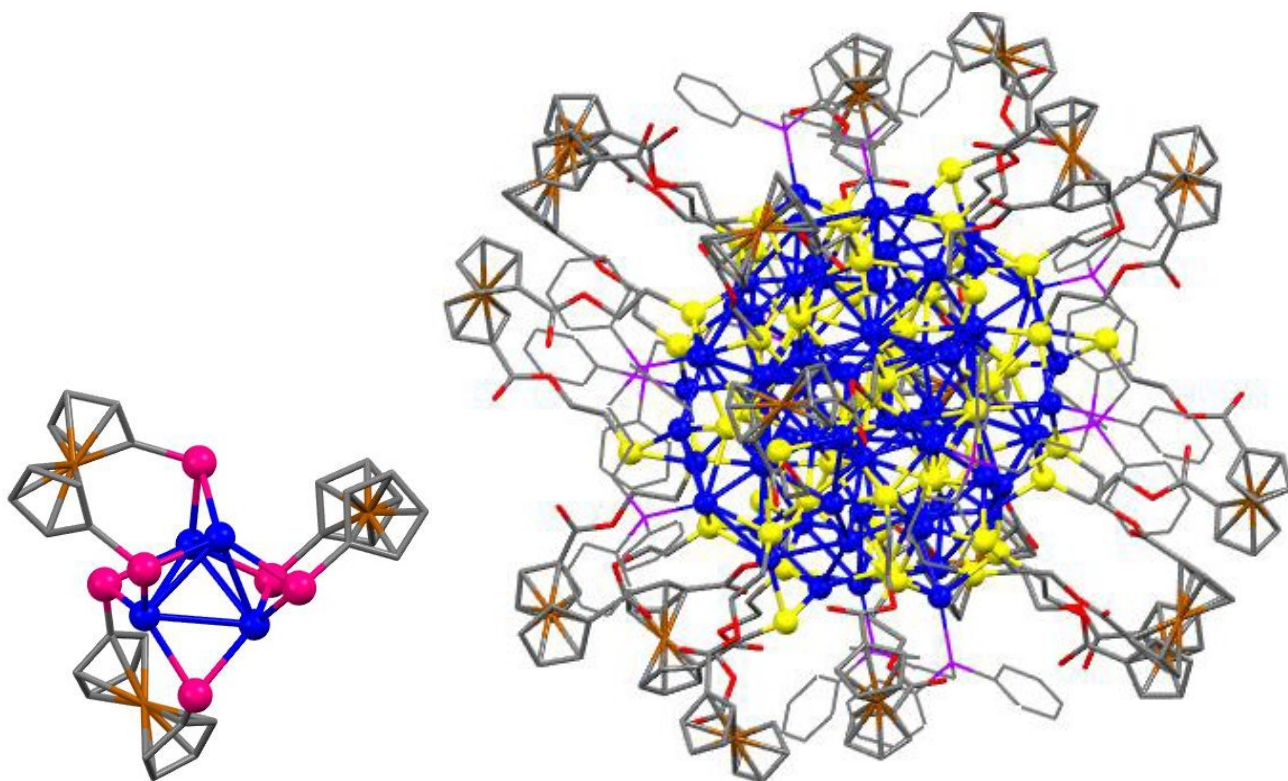
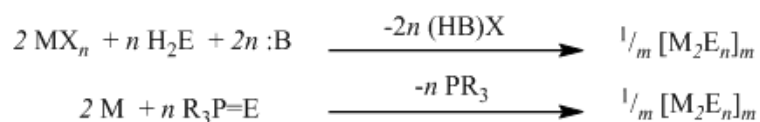


Figure 1.5: Molecular structures of $[\text{Ag}_4(\text{Se}_2\text{fc})_3]^{2-}$ (left) and $[\text{Ag}_{74}\text{S}_{19}(\text{dppp})_6(\text{fc}(\text{C}\{\text{O}\}(\text{CH}_2)_2\text{S})_2)_{18}]$ (right)^{21,24}. Ferrocenyl ligands = capped stick, phosphine = wireframe, inorganic core = ball and stick. Ag^{I} = blue, S = yellow, Se = pink, Fe = brown, P = purple, O = dark red. Counter ions, hydrogens and solvent omitted for clarity.

1.2 Synthesis of Metal–Chalcogen Complexes: The Growing Use of Trimethylsilyl Reagents

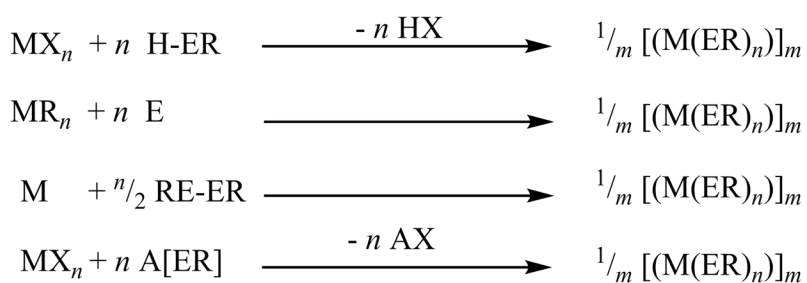
The syntheses of the compounds described has evolved as the chemistry of metal chalcogenide nanoclusters continues to develop. Historically, the syntheses of metal chalcogenide cluster compounds were conducted by the general schema shown below, where E^{2-} was introduced to the reaction mixture by *in situ* deprotonation of H_2E (see **Scheme 1.1**)²⁶ These toxic reagents were eventually replaced with relatively safer alkali metal chalcogenide salts, undergoing metathesis with the appropriate metal reagents in the presence of ancillary ligands to yield the final product. Though simple, these methods were effective in obtaining some of the first metal chalcogenide nanoclusters. Yam *et al.*, for instance, showed the reaction of $[Cu_2(\mu-dppm)_2(MeCN)_2](PF_6)_2$ and Na_2S led to the formation of the first tetranuclear $Cu_4^I(\mu_4-S)$ cluster.²⁷ Although effective, the reactions proceed by an inhomogeneous mixture, due to the limited solubility of the chalcogen starting material. A step toward a more soluble route was the use of phosphine chalcogenides as transfer reagents, able to deliver E^{2-} in solution.^{28–32} Though phosphine chalcogenides overcome the difficulties with the solubility of the aforementioned chalcogen reagents, they are limited by reaction conditions having to overcome the bond enthalpy of $P=E$ (i.e. higher reaction temperatures), which makes the lighter congeners better suited toward the synthesis of nanoparticles rather than nanoclusters.^{33–35} Phosphine chalcogenides featuring heavier chalcogens are more effective at chalcogenide cluster synthesis at the lower temperatures required for kinetic control; lighter phosphine chalcogenides have been shown to act as bridging ligands in complexes such as $[Cu_2(\mu-Cl)_2(dppeSe_2)_2]$ ($dppe = bis-1,2-(diphenylphosphino)ethane$) at room temperature.^{26,28,33,36}



Scheme 1.1: General reaction methods for the synthesis of metal chalcogenide nanoclusters, where $m = 1, 2, 3, \dots$; $n = 1, 2, 3, \dots$. Reactions are often carried out in the presence of a neutral, $2e^-$ ligand, L. $:B$ = Bronsted base. R_3P = trialkylphosphine. X = anionic, $2e^-$ ligand.

The presence of the R group on chalcogenolate reagents makes the syntheses of metal chalcogenolates less complicated by issues of solubility of the chalcogen. The solubility of the starting metal compound, however, is a synthetic challenge that often requires the use of higher reaction temperatures and, if left unchecked, can lead to the formation of compounds with more ambiguous composition (this is also true for the synthesis of metal chalcogenide nanoclusters). The simplest chalcogenolate reagents used are the

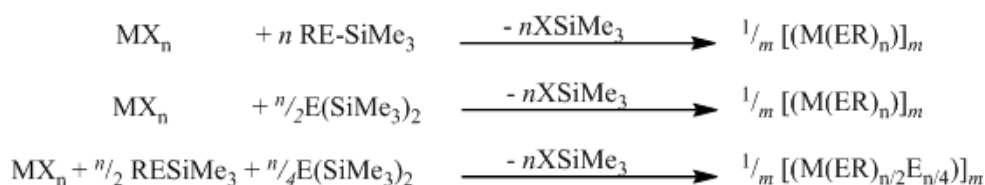
chalcogenols, which suffer from increased thermal and light sensitivity as the chalcogens are replaced S → Se → Te.³⁷ Deprotonation *in situ* generates “RE⁻” in solution which allows for coordination with the metal centre (**Scheme 1.2**); this methodology continues to be used, as exemplified in the synthesis of [Fe₂(μ-SR)₃(CO)₅X] from [Fe(CO)₄X₂] and HS-R in the presence of Et₃N (X⁻ = Br⁻, I⁻).³⁸⁻⁴¹ Conversely, the use of soluble alkyl metal complexes in conjunction with elemental chalcogens leads to insertion of the chalcogen into metal – carbon bonds, albeit at higher temperatures to circumvent the limited solubility of the chalcogen starting material.^{5,42-44} In this vein, Piers *et al.* have demonstrated the ability of tellurium to insert into scandium – carbon bonds and manganese–carbon bonds to make metal tellurolates at temperatures approaching 100 °C.⁴²⁻⁴⁴ The use of solid metal reagents in the presence of soluble diorganodichalcogenides is a protocol that has been investigated to generate metal chalcogenolates by oxidative addition onto the metal centre; this chemistry was originally used to probe the reactivity of metal – metal bonds.^{45,46} However, the reduction of diorganodichalcogenides by some transition metal reagents can be slow in cases where large R groups are used to stabilize the compounds. In lieu of oxidative addition of the diorganodichalcogenides directly onto a metal centre of interest, it is possible to first react with an alkali metal to form the alkali metal chalcogenolate A[ER], which subsequently reacts with the appropriate metal reagent to eliminate an alkali metal salt as a favoured by-product. In this way, Fujisawa *et al.* were able to probe the effect of temperature on metal chalcogenolate synthesis by reacting Na[S-*p*-C₆H₄Cl] with either [Cu(MeCN)₄]PF₆ or AgNO₃ in the presence of a halide source and under different reaction temperatures to obtain [M(S-*p*-C₆H₄X)₃]²⁻ or [M₄(μ-S-*p*-C₆H₄Cl)₆]²⁻ (M = Cu^I, Ag^I; X = Cl⁻, Br⁻), by elimination of NaPF₆ or NaX.⁴⁷ The general reaction schema for the examples mentioned is shown in **Scheme 1.2**.²⁶



Scheme 1.2: General reaction methods toward the synthesis of molecular metal chalcogenolates, where $m = 1, 2, 3, \dots$; $n = 1, 2, 3, \dots$. Reactions are often carried out in the presence of a neutral, 2e⁻ ligand, L. X = anionic, 2e⁻ ligand. R = organic group (alkyl, aryl, etc.)

Although the examples above were not an exhaustive list, synthetic inorganic chemists continued the development of new reagents and synthetic protocols to access metal chalcogenide cluster compounds.

An exciting development is the continued use of silyl chalcogenide and silyl chalcogenolate reagents, which are soluble in organic media, contain the chalcogen in the appropriate charge state, and are relatively easier to handle, bottleable, chalcogen – containing reagents. The organosilyl groups that act as protecting motifs (like the R groups on the chalcogenolate reagents shown above) are able to react because of the lower bond enthalpy of the E–Si bond (506 – 619 kJ/mol) compared to E–C bonds: the protecting silyl groups can be removed in the presence of nucleophiles that have a more thermodynamically favoured bond enthalpy with silicon (i.e. Si – O = 798 kJ/mol).^{48,49} The key to using these compounds is the addition of a metal salt (MX) with the appropriate counterions that form the favoured X–SiR₃ by-product, allowing for the formation of M–E bonds in a more controlled fashion. Therefore, the syntheses of metal chalcogenide, metal chalcogenolate, or mixed chalcogenide/chalcogenolate clusters could be realized more easily by soluble reagents in the respective stoichiometry shown below (see **Scheme 1.3**)^{48,50} While modifications have been made to the organosilyl moiety to obtain more stable reagents, it was found that deviating from the trimethylsilyl functionality caused issues with subsequent reactivity of the chalcogen–silicon bond.^{51,52}



Scheme 1.3: General reaction schema for use of trimethylsilylated chalcogen reagents, where $m = 1, 2, 3, \dots$; $n = 1, 2, 3, \dots$. Reactions are often carried out in the presence of a neutral, $2e^-$ ligand, L. X = anionic, $2e^-$ ligand. R = organic group (alkyl, aryl, etc.)

The use of trimethylsilylated chalcogenide and chalcogenolate reagents has allowed for fine tuning of the composition and structure of metal chalcogenide cluster compounds. In fact, the compounds illustrated in **Figure 1.3** – **Figure 1.5** were synthesized by one of the three general methods shown in **Scheme 1.3**. Although the exact mechanism is not understood, it is accepted that the thermodynamic stability of the XSiMe₃ by-product controls the formation of the cluster compounds in these reactions.⁹ Thus, cluster forming reactions can be done systematically in the presence of different ancillary ligands, metal salts and reaction conditions (temperature, solvent, etc.) to synthesize new and interesting structures which can be crystallized from these reaction mixtures unperturbed by the presence of the innocuous XSiMe₃ or E(SiMe₃)₂.^{6,9,52} For all the advantages offered by these reagents, the use of trimethylsilyl protected chalcogen sources continues to be developed especially with respect to the trimethylsilyl chalcogenolates, whose syntheses are analogous to those showcased in **Scheme 1.2**. The ability to introduce chalcogen functionality onto molecules in a protected state has led to the development of methods to transfer

$[E-SiMe_3]^-$ requiring reagents such as $A[ESiMe_3]$ ($A = Li, Na$): the lithium salts have been accessed by reaction of $E(SiMe_3)_2$ with 1 equivalent of nBuLi , while sodium analogues have been accessed by the reaction of $NaNH_2$ with $E(SiMe_3)_2$.⁵³⁻⁵⁵ Recent work has seen the development of “naked $^-ESiMe_3$ ” with the use of methylcarbonate ionic liquids to deprotect an equivalent of $-SiMe_3$ from $E(SiMe_3)_2$.⁴⁴ The organic salts generated ($R^+[ESiMe_3]^-$) have been used in the synthesis of homoleptic trimethylsilylchalcogenolato metallates $[M(ESiMe_3)_4]^-$ ($M = Ga, In; E=S, Se$), which can be reacted further to form reagents that act as single source precursors for $CuInS_2$.⁵⁶ This recent work is an example of, arguably, the biggest advantage behind the use of silylated chalcogen compounds; stepwise control of reactivity at the chalcogen allows access to heterometallic, ternary nanoclusters. Prior to the inception of these silylated chalcogen reagents, heterometallic structures had been accessed on the rare occasion that tetrachalcogenometallate anions could be reacted with heterometal ions to form ternary assemblies; the reaction of $[In(SET)_4]^-$ with $[Cu(MeCN)_4]^+$ to isolate the copper indium thiolate cluster $[Cu_6In_3(SET)_{16}]^-$ was a first example toward molecular heterometallic chalcogenides.⁵⁷ Subsequent examples, following the discovery of silylated reagents above, were isolated by the mixing metal salts in the presence of these reagents and ancillary ligands/coordinating solvent (see **Figure 1.6**).⁵⁷⁻⁶⁶

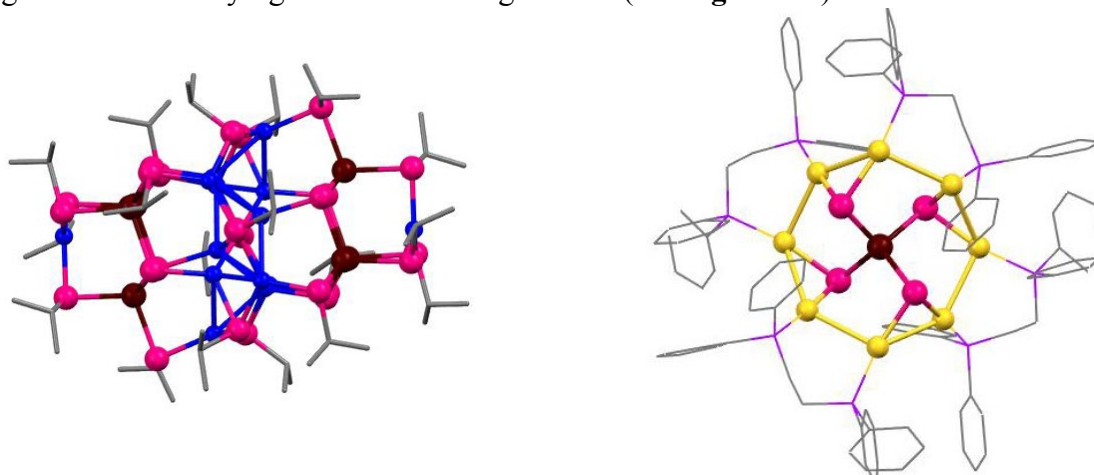


Figure 1.6: Molecular structures of $[Cu_{14}In_6Se_7(iPrSe)_{18}]$ (left) and $[Au_8InSe_4(dppe)_4]^{3+}$ (right) as examples of heterometallic chalcogenide nanoclusters.⁵⁶⁻⁵⁷ Solvent molecules and disordered molecules deleted for clarity. Cu = blue, Se = pink, In = brown, Au = gold. Ancillary ligands = wireframe; selenolate R groups = capped stick.

Although these reactions were successful, new and controlled methods were sought and inspired by other work using chalcogenolate reagents in nanoparticle synthesis, wherein metal chalcogenolate clusters could be used as single source precursors for these nanomaterials.⁶⁷⁻⁶⁹ These previous works investigated the thermal activation of $E-C$ bonds to remove the organic moiety and allow for subsequent particle growth. In analogy to this, and inspired by the lability of $E-Si$ bonds in the aforementioned silyl chalcogenide and silyl chalcogenolate reagents, a new class of compounds was made with a preformed

M–E bond between metals and silyl chalcogenolates (E–SiR₃).⁴⁸ These “silyl metallochalcogenolates” (MESiR₃) were the silyl analogues of metal chalcogenolates discussed above, amenable to the formation of heterometallic compounds by using the same patterns of reactivity established in **Scheme 1.3**.

1.3 Silyl Metallochalcogenolates: Synthons in Heterometallic Chalcogenide Cluster Chemistry

The “one-pot” reaction of silylated chalcogenide/chalcogenolate reagents with different metal salts was viable for the isolation of several ternary metal chalcogenide clusters. In the interest of expanding on the general techniques used for these syntheses, a strategy was developed involving the preformation of a M–E bond in a “silyl metallochalcogenolate” compound (MESiR₃). In analogy to chalcogenolates (RE⁻), silyl chalcogenolates allow for the controlled coordination about the chalcogen, just like their alkyl counterparts, but offer a more sensitive E–Si bond that can be cleaved in the presence of M'X (X = halide, acetate, etc.). This allows for the formation of XSiR₃ that drives bond formation between ME and M' to allow the synthesis of [MEM']_n to proceed under conditions of kinetic control (i.e. lower temperatures).

A review by DeGroot and Corrigan covers a wide variety of silyl metallochalcogenolate compounds known at the time of publication^{48,52} The stability and solubility of the silyl metallochalcogenolate was shown to depend on a balance between the R group on the silyl moiety and the identity and/or presence of ancillary ligands about the metal centre. Where large R groups are used, protection of the metallochalcogenolate from condensation reactions is realized by the limited coordination profile of E–SiR₃ and the steric bulk that renders the chalcogen less nucleophilic. Thus, the use of large R groups about the silyl functionality generally results in other ligands not being necessary for product stability or solubility. [Cu(SSiMe₂^tBu)₄], for instance, can be formed from [Li₂(TMEDA)₂(SSiMe₂^tBu)₂] and [Cu(CH₃CN)₄](PF₆) in acetonitrile at 0 °C, which contains only ancillary ligands left over from the synthesis requiring activation of a [SSiMe₂]₃ by ^tBuLi in TMEDA (TMEDA = tetramethyl ethylenediamine).⁷⁰ Smaller R groups on the silicon centre, then, require the presence of ancillary ligands about the metal to stabilize the silyl metallochalcogenolates against the formation of the more favoured bulk phases and to help solubilize the reagent. The less hindering the R group on the chalcogenolate, the more likely the chalcogen will coordinate to multiple metal centres and cascade to the decomposition of bulk solids; formation of E(SiMe₃)₂ from [M(ESiMe₃)_n] compounds in solution is well documented and driven by the formation of bulk metal chalcogenides.^{71–74} Ancillary ligands such as amines, Cp rings (as

in metallocene), phosphines and most recently, *N*-heterocyclic carbenes (NHCs) have been used to stabilize trimethylsilyl metallochalcogenolates of various metals.^{25,52,70,73–79}

As mentioned above, the reactivity of E–Si bonds is affected by the R groups on silyl chalcogenolates and is found to be limited when large R groups are used.⁴⁸ The Corrigan group, among others, developed a large variety of ligand stabilized trimethylsilyl metallochalcogenolates, which were used in subsequent heterometallic chalcogenide syntheses. DeGroot *et al.* reported the synthesis of the compound [(N,N'-TMEDA)Zn(ESiMe₃)₂] which has since been used in the syntheses of heterometallic cluster compounds of Cd, Mn and toward the synthesis of ZnE nanoparticles.^{75,80–83} In a relatively rare example of trimethylsilyl chalcogenolates without any ancillary ligands, Khadka *et al.* report the synthesis of Mn and Co mixed chalcogenide/trimethylsilylchalcogenolate anionic clusters, as well as the synthesis of [Mn(SSiMe₃)₄]²⁻.⁸³ Though these latter examples feature no ancillary ligands, the use of ancillary PR₃ and NHC ligands to stabilize trimethylsilyl metallochalcogenolates is often crucial in their isolation and use in subsequent reactions for heterometallic chalcogenide cluster syntheses.^{6,48,83,84}

1.3.1. Quantifying Ligand Effects: Tolman Electronic Parameter, Tolman Cone Angle and Percent Buried Volume

The nature of the stabilizing ligand is important for understanding the stability and future reactivity of the metal complexes to which they coordinate. The electronic properties of a given ligand have been characterised using the Tolman Electronic Parameter (TEP), probing the electron donating or withdrawing ability by evaluating the change in the IR frequency of the A₁ vibrational mode of the carbonyl moiety in a ligand stabilized metal carbonyl complex (traditionally nickel, though now replaced with less toxic indium or rhodium).^{85–88} Greater electron density about the metal centre results in a redshifted CO stretch due to the occupation of the π^*_{M-CO} orbital. In this way, the ability of a variety of ligands to donate electron density onto metal centres could be tabulated and reported, despite not being able to separate and understand the differences between σ and π effects.

Understanding the steric demand of ligands in a more quantitative way was established for phosphines by the introduction of the Tolman Cone Angle (θ_T), measured from crystallographic data as illustrated in **Figure 1.7**.⁸⁵ The larger the cone angle, the more sterically encumbering the phosphine ligand may be considered. The nature of this measure relies heavily on the geometry about the phosphorus centre and does not readily consider the differences that multidentate or even non-phosphine ligands would have when measuring steric contributions by this method. To overcome these limitations, the Nolan group

introduced the concept of percent buried volume ($\%V_{\text{bur}}$) to quantify the steric contribution of a wider variety of ligands (see **Figure 1.7**).⁸⁷ A coordination sphere is defined about the metal centre, the volume calculated, and the model mapped over the molecular structure obtained by SCXRD of a [LAuCl] complex, to calculate the percentage of this spherical space that is occupied by the ligand.^{87,89}

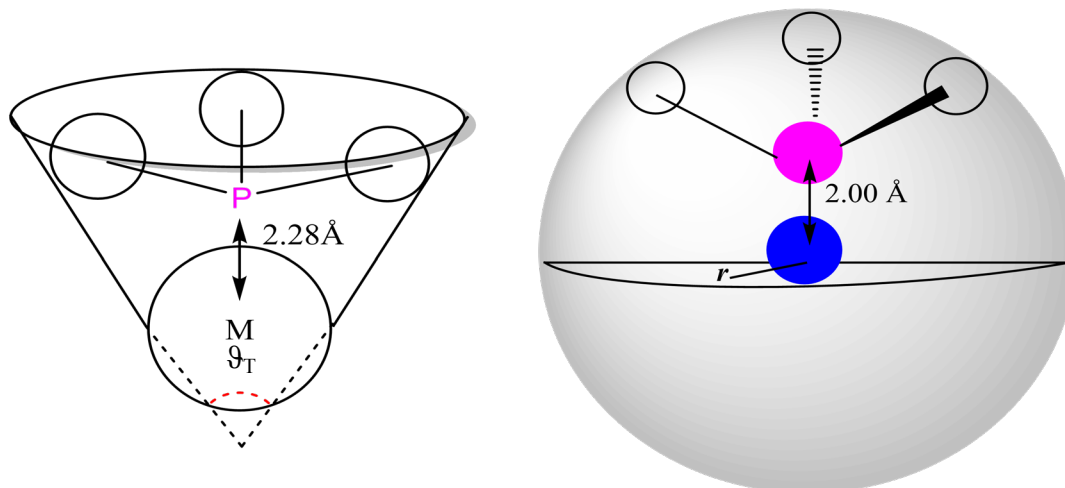



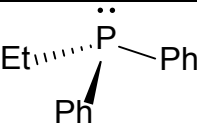
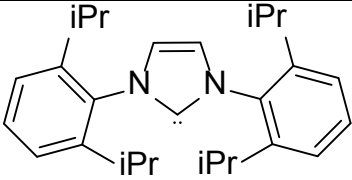
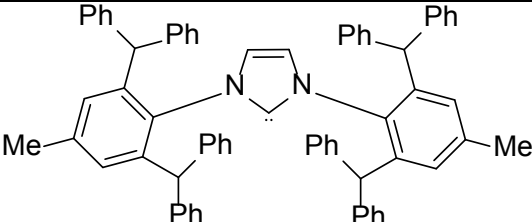
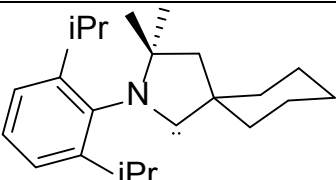
Figure 1.7: Diagram of Tolman Cone Angle (left, highlighted in red) and hemisphere of coordination used for calculation of $\%V_{\text{bur}}$ (right). Listed are the average L – M bond lengths for phosphines (2.28 Å) and N–heterocyclic carbenes (2.00Å)^{74, 76}

Though the online calculator they provide could be used with crystallographic data from any complex, the researchers set the precedent of reporting this quantity for data calculated from [(L)AuCl] to mitigate the effect of other coordinated counterions on the metal centre.⁸⁷ Additionally, the use of this parameter must take into consideration the radius of the sphere about the metal centre, as well as any difference in ligand – metal bond length for the comparison of different ligands.⁸⁷ Data for comparison of phosphines and NHCs, for instance, are calculated at the average bond length of both interactions and tabulated along with TEP (v) in **Table 1.1** (phosphine – M = 2.28 Å; NHC – M = 2.00Å). The same researchers have used DFT calculations to suggest that the radius of the coordination sphere around most metals should be set at 3.5 Å, however, this parameter can be changed as required.

In addition to this parameter, the online application has recently been modified to include contour plots that provide space – filling models of these coordination spheres, so as to visualize the steric effect of the ancillary ligand on the metal centre being studied.⁸⁷ In addition to a graphical representation, the $\%V_{\text{bur}}$ is quantified in the space around the atom at the centre of the coordination sphere and expressed as “free volume” ($\%V_{\text{free}}$) to illustrate and quantify the steric hindrance faced by nucleophiles trying to attack the metal in the centre of the sphere. While the role of the ancillary ligand is often to protect the metal centre

from further reactivity, many research fields seek to instead prevent unwanted reactivity, requiring the more intelligent design of ligands and making use of this information.

Table 1.1: Electronic and steric parameters of selected ligands (phosphines and NHCs). %V_{bur} has been reported for LAuCl complexes and TEP for LNi(CO)₃, unless otherwise noted.* – crystal structure of ligand used in SambVca⁸⁹. **–Data from L₂AuX (X = Cl⁻, Ph₂EtAuSe(C₆H₄)₂Se⁻, 4-phenyl-1H-1,2,3-triazol-5-yl) used in SambVca.^{85,87,97,89–96}

Ligand	Ref.	TEP (cm ⁻¹)	%V _{bur}	
			2.00 Å	2.28 Å
PEt₃ 	[^{85,87}]	2061.7	31.7	27.1
PPh₂Et 	[^{85,87,93}]	2066.7	35.2**	30.3**
IPr 	[^{87,94}]	2051.5	44.5	39.0
IPr* 	[^{90,95}]	2052.7	50.4	45.7
CAAC^{Cy} 	[^{96,97}]	2020.4	41.4**	36.5**

1.3.2. Phosphine stabilized trimethylsilyl group 11 metallochalcogenolates

Inspired by the work of Fenske *et al.*, Tran and Corrigan reported the first group 11 trimethylsilylmetallochalcogenolates, featuring a pendant ESiMe₃ group, by reacting (R₃P)₃CuOAc with E(SiMe₃)₂ in a 1:1 reaction stoichiometry at low temperature.^{8,9,13–15,77} This success set the Corrigan group

on the path toward accessing trimethylsilyl metallochalcogenolates of the rest of the group 11 metals, given the prevalence of these metals in the materials sciences and the rarity of obtaining such mononuclear trimethylsilylchalcogenolates for these elements.⁴⁸ Previous reactions of $E(\text{SiMe}_3)_2$ with mixtures of metal salts in the presence of phosphines were hypothesized to occur by these transient metallochalcogenolate species. The ability to isolate, characterize and bottle these compounds would allow a more rational design of subsequent ternary nanoclusters, given the ability for $[(\text{PR}_3)_3\text{MESiMe}_3]$ to act as a soluble source of $[\text{M}-\text{E}]^-$.^{52,77,98} As indicated above, the synthesis of the phosphine stabilized precursor was shown to depend on the ancillary ligand used, necessary to coordinatively saturate the group 11 metal. Additionally, the reaction stoichiometry and reaction conditions could also be modulated toward preventing formation of the bulk phases but allowing the activation of the E–Si bond.

In these group 11 trimethylsilyl metallochalcogenolates, SCXRD data of the cuprachalcogenolates demonstrated the copper centres were in a tetrahedral coordination geometry, characteristic to the closed shell group 11 cations; the argentochalcogenolates were also hypothesized to contain a minimum of 3 equivalents of phosphine to passivate the silver centre.^{52,77} Where these lighter congeners were accessed by the reaction of $[(\text{R}_3\text{P})_3\text{MOAc}]$ with $E(\text{SiMe}_3)_2$, the synthesis of the aurachalcogenolates was demonstrated by the reaction of $[\text{Ph}_3\text{PAuCl}]$ with $[\text{LiESiMe}_3]$ ($E = \text{S}, \text{Se}$).^{52,79} The reaction of the starting gold chlorido complex with $E(\text{SiMe}_3)_2$ was slow under the reaction conditions required for the stability of the final product, requiring the lithiation of $E(\text{SiMe}_3)_2$ ($E = \text{S}, \text{Se}$) to generate the more reactive lithium chalcogenolate species and push the reaction to completion. In these complexes, the propensity for gold to adopt linear coordination modes allowed the use of one equivalent of phosphine ligand to stabilize the molecules against decomposition. Following the synthesis of the phosphine stabilized group 11 trimethylsilyl metallochalcogenolates, the reactivity of the pendant E–Si bond in these compounds has been studied.^{52,77,79} The reactive nature of the silver compounds made isolation and handling of these compounds difficult, resulting in decomposition during isolation.⁵² For those reagents probed, the reactivity of the E–Si bond was demonstrated either in the ability to access heterometallic structures, or by post synthetic modification at the chalcogen centre. Tran *et al.* showed that reaction of $[(\text{PPr}_3)_3\text{CuESiMe}_3]$ with $\text{Hg}(\text{OAc})_2$ led to the formation of $[\text{Hg}_{15}\text{Cu}_{20}\text{E}_{25}(\text{PPr}_3)_{18}]$ ($E = \text{S}, \text{Se}$); the reaction of the cuprathiolate compound with InCl_3 was amenable to the formation of $[\text{Cu}_6\text{In}_8\text{Cl}_4\text{S}_{13}(\text{PEt}_3)_{12}]$.⁶² Borecki and Corrigan showed that treatment of $[(\text{PEt}_2\text{Ph})_3\text{CuSeSiMe}_3]$ with a small amount of protic solvent led to the formation of the respective selenol.⁵² Polgar *et al.* were able to use a trimethylsilyl aurathiolate to synthesize $[\text{Au}_4\text{Cu}_4\text{S}_4(\text{dppm})_2]$ (dppm = diphenylphosphinomethane) as a first example of a heterometallic group 11 chalcogenide containing the bridging chalcogenide motifs, $\text{AuCu}_2(\mu_3\text{-S})$.⁷⁹ Yet,

for all the advantages offered by these metallochalcogenolates, the thermal instability of these reagents in solution and as isolated solids remained a challenge in developing their use.^{52,62,77,79}

The work of Borecki and Corrigan was meant to address this thermal instability by investigating a library of metallochalcogenolates stabilized by different phosphines.⁵² While varying the electronic and steric parameters did show some effect, quantum chemical calculations suggest the phosphine – metal bond strength for the group 11 metals may have been the limiting factor in the stability of these trimethylsilyl metallochalcogenolates.⁹⁹ Indeed, the aurachalcogenolates were found to be the most stable from the collective, with the auraselenolate surviving in solution up to 5 °C likely due to the strength of the phosphine –gold interaction.⁷⁹ Thus, the only way to improve on these group 11 trimethylsilyl metallochalcogenolates was by the use of a different ligand system with a more thermodynamically favourable L – M interaction.

1.3.3. NHC–stabilized trimethylsilyl group 11 metallochalcogenolates

N–Heterocyclic carbenes (NHCs) are a class of ancillary ligands containing a divalent carbon atom, with a singlet lone pair localized in a sp^2 hybridized orbital (see **Figure 1.8**).^{87,88,100–102} The shape of the heterocyclic ring, the presence of the heteroatoms and the saturation of the backbone on the ring contribute to the stability of the lone pair in its singlet state.¹⁰⁰ Unlike traditional carbenes that are electrophilic because of their triplet character, the aforementioned structural features decrease the energy of the singlet ground state such that the HOMO of NHCs is the lone pair (singlet state), while the LUMO is the vacant p orbital. It is the interaction of this HOMO with an unoccupied orbital on a metal centre that contributes to the strong σ bonding interaction. Further research has shown the electronic character of NHCs makes

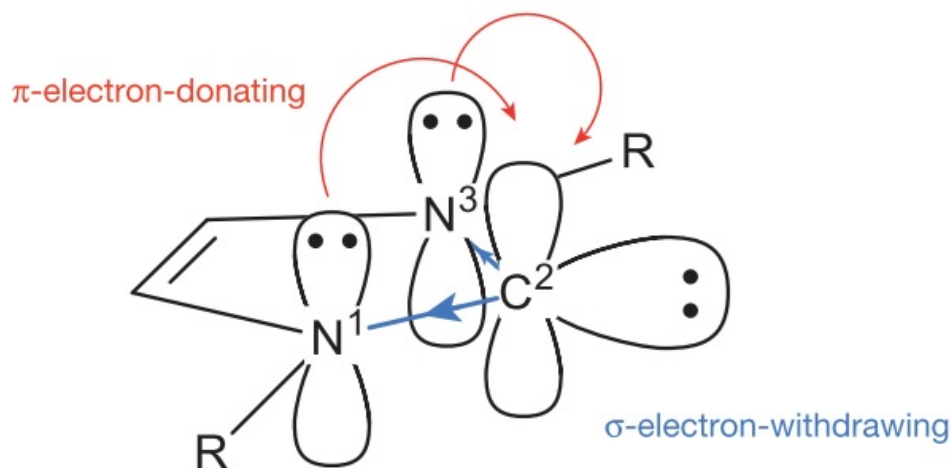


Figure 1.8: Electronic structure of NHCs (diagram from Hopkinson *et al.*).⁸⁵ The lone pair at the carbenic carbon is stabilized by π –electron donation and σ –electron withdrawal.

them well suited for the stabilization of a variety of reactive species, given their increased σ -donating ability and relatively weaker π -accepting properties, when compared to phosphines.

Although NHCs are weaker π acceptors than phosphines, NHC–M bonds have been shown to have a non-negligible π back-bonding component, depending on the energy of the LUMO and depending on the electron richness of the metal being coordinated.^{100–102} As such, they have found use in many different aspects of inorganic chemistry, stabilizing exotic and transient species of metals and main group elements.^{103–107} Like phosphines, their electronic and steric characteristics can be tuned, and like phosphines these parameters can be modulated independent of each other.

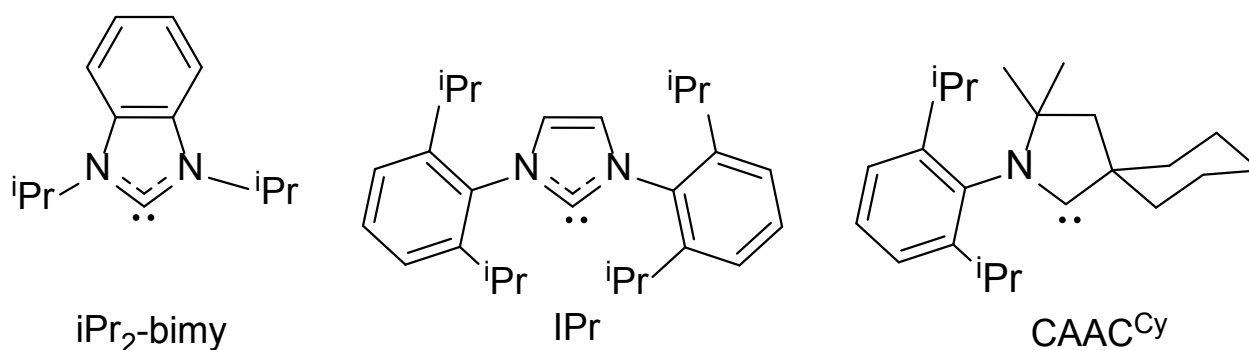


Figure 1.9: NHCs used to stabilize group 11 trimethylsilyl metallochalcogenolates.^{63–65,104}

In general, the electronic characteristics of NHC ligands are associated most closely with the saturation, size and type of heterocyclic ring (**Figure 1.9**). Stronger σ -donating ability is correlated with the stability of the free carbene which can be rationalized, in part, by the ability of the heteroatoms to donate electron density into the vacant p orbital on the carbenic carbon. Therefore, σ -donating ability generally follows the trend benzimidazole < imidazolylidene < imidazolidinyliene < pyrrolidinyliene and one can rationalize the trend as tracking with the decrease of delocalization of the lone pairs at nitrogen (i.e. π effects more localized about carbenic carbon). Pyrrolidinylienes, known in the literature as Cyclic Alkyl Amino Carbenes (CAACs), contain only one nitrogen in their saturated five-membered ring and can be considered an extreme to this trend, making this class of NHC a significantly stronger σ -donor while also having improved π -accepting capability.^{88,100,104}

While the electronics of NHCs are a continually studied topic, it is generally accepted that the nature of the substituents on the nitrogen centre of NHCs has been shown to generally have little effect on the electronic characteristics of the carbene, but greater implications for the steric profile of the NHC.^{87,88,100} In making this generalization, however, one ignores the true nature of the σ -donating and π -accepting

characteristics of NHCs, which are best described by frontier orbital calculations. Regardless, the use of NHCs has been generalized to the understanding that varying the R groups changes the steric parameters of the ligand, while modifications to the heterocyclic ring affect the electronic properties. As such, a wide variety of NHCs has been made with variable TEP and %V_{bur} values (see **Table 1.1** for examples).

Table 1.2: Melting points for group 11 trimethylsilyl metallochalcogenolates^{52,72–74,98}.

M = Cu	E = S	E = Se	E = Te
[(PEt₂Ph)₃CuESiMe₃]	–25 °C	–28 °C	–47 °C
[(PPh₂Et)₃CuESiMe₃]	5 °C (decomp.)	–15 °C	–25 °C
[(iPr₂–bimy)CuESiMe₃]₂	91–93 °C	–	–
IPrCuESiMe₃	171–172 °C	166–168 °C	178–180 °C
CAAC^{Cy}CuESiMe₃	168–171 °C	169–173 °C	–
M=Ag			
[(PEt₂Ph)₃AgESiMe₃]	–40 °C (decomp.)	–50 °C	–
[(PPh₂Et)₃AgESiMe₃]	–25 °C	–35 °C (decomp)	–
IPrCuESiMe₃	175–179	170–175 °C	–
M=Au			
IPrAuESiMe₃	185–186 °C	184–187 °C	177–182 °C

Following the syntheses of phosphine stabilized group 11 trimethylsilyl metallochalcogenolates, the Corrigan group was inspired by other work on group 11 NHC complexes to adopt the methodology to the trimethylsilyl metallochalcogenolates. The use of NHC ligands was successfully applied to the syntheses of group 11 chalcogenolates, phosphides and silyl phosphido complexes.^{108–110} Fard *et al.* eventually used *bis*–1,3–(diisopropyl)benzimidazole–2–ylidene (iPr₂–bimy) and *bis*–1,3–(2,6–diisopropylphenyl)imidazole–2–ylidene (IPr) to synthesize copper and silver trimethylsilyl chalcogenolates.^{73,74} The use of the iPr₂ – bimy and IPr resulted in the stabilization of either dimeric or monomeric copper and silver chalcogenolate compounds, which in turn could react with Hg(OAc)₂ to produce ternary chalcogenide clusters of varying nuclearity; lower TEP and %V_{bur} resulted in the formation of clusters of higher nuclearity.^{73,74} Polgar *et al.* went on to synthesize IPrAuESiMe₃ (E = S, Se, Te), which was subsequently reacted with group 11 metal acetates to obtain cluster compounds systematically altered at the heterometal and the chalcogen, tuning the optical properties of the resultant cluster compounds.^{72,98} In a different work,

Polgar *et al.* was also able to extend the library of compounds to [CAAC^{Cy}CuESiMe₃] (CAAC^{Cy}= 2-(2,6-diisopropyl-phenyl)-3,3-dimethyl-2-azaspiro[4.5]dec-1-ylidene) using these cuprachalcogenolates to access isomorphous analogues of the IPr stabilized clusters, showing the effect of the NHC on the optical properties of the cluster compounds.^{72,98} In all these reports, the use of NHCs to stabilize the trimethylsilyl metallochalcogenolates resulted in a pronounced increase of thermal stability for these compounds, both as solids and in solution. **Table 1.2** summarizes the NHCs used thus far in the isolation of group 11 trimethylsilyl metallochalcogenolates and contrasts their melting points to those of the phosphine stabilized group 11 trimethylsilyl metallochalcogenolates.

1.4 Scope of Thesis

This thesis continues work on expanding the library and reaction chemistry of NHC-stabilized group 11 trimethylsilylchalcogenolate reagents, by making metallochalcogenolates stabilized with a sterically demanding NHC, and subsequently probing the reactivity of these compounds. Chapter 2 focuses on the syntheses and characterization of group 11 trimethylsilyl metallochalcogenolates stabilized by the sterically demanding NHC bis-1,3-tritylimidazole-2-ylidene (ITr) and group 11 metal acetates stabilized by the same ligand.⁹⁴ Chapter 3 discusses the work on probing the reactivity of these compounds toward novel heterometallic chalcogenides. The suitability of the trimethylsilyl protection/deprotection strategy in this vein of metal chalcogenide chemistry is discussed and other limitations for reaction chemistry are reviewed. Chapter 4 summarizes the results of these two chapters and suggests future directions for the development of this chemistry toward the goals intended on in Chapter 3 and towards the syntheses of heterometallic chalcogenide compounds in general.

1.5 References

- (1) Bouroushian, M. In *Electrochemistry of Metal Chalcogenides*; Springer Berlin Heidelberg: Heidelberg, 2010; pp 1–56.
- (2) Franzen, H. F. *Prog. Solid State Chem.* **1978**, *12*, 1–39.
- (3) Brus, L. *J. Phys. Chem.* **1986**, *90*, 2555–2560.
- (4) Pinkard, A.; Champsaur, A. M.; Roy, X. *Acc. Chem. Res.* **2018**, *51*, 919–929.
- (5) Azizpoor Fard, M.; John Corrigan, S. F. The University of Western Ontario, 2015.
- (6) MacDonald, D. G.; Corrigan, J. F. *Philos. Trans. R. Soc. A Math. Phys. Eng. Sci.* **2010**, *368*, 1455–1472.
- (7) Cave, D.; Corrigan, J. F.; Eichhöfer, A.; Fenske, D.; Kowalchuk, C. M.; Rösner, H.; Scheer, P. *J. Clust. Sci.* **2007**, *18*, 157–172.
- (8) Corrigan, J. F.; Fenske, D. *Angew. Chemie Int. Ed. English* **1997**, *36*, 1981–1983.
- (9) Dehnen, S.; Eichhöfer, A.; Fenske, D. *Eur. J. Inorg. Chem.* **2002**, *2002*, 279–317.

- (10) Fujisawa, K.; Imai, S.; Moro-oka, Y. *Chem. Lett.* **1998**, *27*, 167–168.
- (11) Polgar, A. The University of Western Ontario, 2018.
- (12) Kluge, O.; Grummt, K.; Biedermann, R.; Krautscheid, H. *Inorg. Chem.* **2011**, *50*, 4742–4752.
- (13) Krautscheid, H.; Fenske, D.; Baum, G.; Semmelman, M. *Angew. Chem.* **1993**, *105*, 1364–1367.
- (14) Wang, X.-J.; Langetepe, T.; Persau, C.; Kang, B.-S.; Sheldrick, G. M.; Fenske, D. *Angew. Chem. Int. Ed.* **2002**, *41*, 3818–3822.
- (15) Fuhr, O.; Fernandez-Recio, L.; Fenske, D. *Eur. J. Inorg. Chem.* **2005**, *2005*, 2306–2314.
- (16) Fernandez-Recio, L.; Fenske, D.; Fuhr, O. *Zeitschrift für Anorg. und Allg. Chemie* **2008**, *634*, 2853–2857.
- (17) Langer, R.; Wünsche, L.; Fenske, D.; Fuhr, O. *Zeitschrift für Anorg. und Allg. Chemie* **2009**, *635*, 2488–2494.
- (18) MacDonald, D. G.; Kübel, C.; Corrigan, J. F. *Inorg. Chem.* **2011**, *50*, 3252–3261.
- (19) Gunawardene, P. N.; Corrigan, J. F.; Workentin, M. S. *J. Am. Chem. Soc.* **2019**, *141*, 11781–11785.
- (20) Corrigan, J. F.; Fuhr, O.; Fenske, D. *Adv. Mater.* **2009**, *21*, 1867–1871.
- (21) Lee, K.; Huang, Y.; Corrigan, J. F. *Chem. Commun.* **2019**, *55*, 11466–11469.
- (22) Wallbank, A. I.; Corrigan, J. F. *J. Clust. Sci.* **2004**, *15*, 225–232.
- (23) Wallbank, A. I.; Borecki, A.; Taylor, N. J.; Corrigan, J. F. *Organometallics* **2005**, *24*, 788–790.
- (24) Nitschke, C.; Wallbank, A. I.; Fenske, D.; Corrigan, J. F. *J. Clust. Sci.* **2007**, *18*, 131–140.
- (25) Liu, Y.; Khalili Najafabadi, B.; Azizpoor Fard, M.; Corrigan, J. F. *Angew. Chem. Int. Ed.* **2015**, *54*, 4832–4835.
- (26) DeGroot, M. W.; Corrigan, J. F. In *Comprehensive Coordination Chemistry II*; Fujita, M., Powell, A., Creutz, C. A., Eds.; Elsevier: San Diego, 2004; pp 58–64.
- (27) Yam, V. W.-W.; Lo, K. K.-W. *Comments Inorg. Chem.* **1997**, *19*, 209–229.
- (28) García-Rodríguez, R.; Hendricks, M. P.; Cossairt, B. M.; Liu, H.; Owen, J. S. *Chem. Mater.* **2013**, *25*, 1233–1249.
- (29) Stuczynski, S. M.; Kwon, Y.-U.; Steigerwald, M. L. *J. Organomet. Chem.* **1993**, *449*, 167–172.
- (30) Baistrocchi, P.; Cauzzi, D.; Lanfranchi, M.; Predieri, G.; Tiripicchio, A.; Tiripicchio Camellini, M. *Inorganica Chim. Acta* **1995**, *235*, 173–183.
- (31) Belletti, D.; Cauzzi, D.; Graiff, C.; Minarelli, A.; Pattacini, R.; Predieri, G.; Tiripicchio, A. *J. Chem. Soc., Dalton Trans.* **2002**, No. 16, 3160–3163.
- (32) Belletti, D. *Inorganica Chim. Acta* **2003**, *356*, 187–192.
- (33) Alvarado, S. R.; Shortt, I. A.; Fan, H.-J.; Vela, J. *Organometallics* **2015**, *34*, 4023–4031.
- (34) Zhang, Y.; Qiao, Z.-P.; Chen, X.-M. *J. Solid State Chem.* **2002**, *167*, 249–253.
- (35) Jiang, X.; Xie, Y.; Lu, J.; He, W.; Zhu, L.; Qian, Y. *J. Mater. Chem.* **2000**, *10*, 2193–2196.
- (36) Lobana, T. S.; Mahajan, R.; Castineiras, A. *Transit. Met. Chem.* **2001**, *26*, 440–444.
- (37) Sink, C. W.; Harvey, A. B. *J. Chem. Phys.* **1972**, *57*, 4434–4442.
- (38) Gysling, H. J. *Coord. Chem. Rev.* **1982**, *42*, 133–244.
- (39) Pearson, S.; Lu, H.; Stenzel, M. H. *Macromolecules* **2015**, *48*, 1065–1076.
- (40) Maiti, B. K.; Avilés, T.; Moura, I.; Pauleta, S. R.; Moura, J. J. G. *Inorg. Chem. Commun.* **2014**, *45*, 97–100.
- (41) Xiao, Z.; Jiang, R.; Jin, J.; Yang, X.; Xu, B.; Liu, X.; He, Y.; He, Y. *Dalton Trans.* **2019**, *48*, 468–477.
- (42) Piers, W. E.; MacGillivray, L. R.; Zaworotko, M. *Organometallics* **1993**, *12*, 4723–4725.
- (43) Piers, W. E. *J. Chem. Soc. Chem. Commun.* **1994**, *3*, 309–310.
- (44) McGregor, K.; Deacon, G. B.; Dickson, R. S.; Fallon, G. D.; Rowe, R. S.; West, B. O. *J. Chem. Soc. Chem. Commun.* **1990**, *19*, 1293–1294.
- (45) Canich, J. A. M.; Cotton, F. A.; Dunbar, K. R.; Falvello, L. R. *Inorg. Chem.* **1988**, *27*, 804–811.
- (46) Cotton, F. A.; Dunbar, K. R. *Inorg. Chem.* **1987**, *26*, 1305–1309.

- (47) Fujisawa, K.; Imai, S.; Suzuki, S.; Moro-oka, Y.; Miyashita, Y.; Yamada, Y.; Okamoto, K. *J. Inorg. Biochem.* **2000**, *82*, 229–238.
- (48) DeGroot, M. W.; Corrigan, J. F. *Zeitschrift für Anorg. und Allg. Chemie* **2006**, *632*, 19–29.
- (49) Spreight, J. G.; Lange, N. A. In *Lange's Handbook of Chemistry*; McGraw - Hill: New York, New York, 2005; pp 4.41-4.53.
- (50) Fuhr, O.; Dehnen, S.; Fenske, D. *Chem. Soc. Rev.* **2013**, *42*, 1871–1906.
- (51) Kückmann, T. I.; Hermsen, M.; Bolte, M.; Wagner, M.; Lerner, H.-W. *Inorg. Chem.* **2005**, *44*, 3449–3458.
- (52) Borecki, A.; Corrigan, J. F. *Inorg. Chem.* **2007**, *46*, 2478–2484.
- (53) Taher, D.; Wallbank, A. I.; Turner, E. A.; Cuthbert, H. L.; Corrigan, J. F. *Eur. J. Inorg. Chem.* **2006**, *2006*, 4616–4620.
- (54) Finger, L. H.; Scheibe, B.; Sundermeyer, J. *Inorg. Chem.* **2015**, *54*, 9568–9575.
- (55) Do, Y.; Simhon, E. D.; Holm, R. H. *Inorg. Chem.* **1983**, *22*, 3809–3812.
- (56) Guschlbauer, J.; Vollgraff, T.; Sundermeyer, J. *Inorg. Chem.* **2019**, *58*, 15385–15392.
- (57) Hirpo, W.; Dhingra, S.; Kanatzidis, M. G. *J. Chem. Soc., Chem. Commun.* **1992**, No. 7, 557–559.
- (58) Eichhöfer, A.; Fenske, D.; Olkowska-Oetzel, J. *Zeitschrift für Anorg. und Allg. Chemie* **2004**, *630*, 247–251.
- (59) Olkowska-Oetzel, J.; Sevillano, P.; Eichhöfer, A.; Fenske, D. *Eur. J. Inorg. Chem.* **2004**, *2004*, 1100–1106.
- (60) Hirpo, W.; Dhingra, S.; Sutorik, A. C.; Kanatzidis, M. G. *J. Am. Chem. Soc.* **1993**, *115*, 1597–1599.
- (61) Eichhöfer, A.; Fenske, D. *J. Chem. Soc. Dalton Trans.* **2000**, No. 6, 941–944.
- (62) Tran, D. T. T.; Beltran, L. M. C.; Kowalchuk, C. M.; Trefiak, N. R.; Taylor, N. J.; Corrigan, J. F. *Inorg. Chem.* **2002**, *41*, 5693–5698.
- (63) Senevirathna, D. C.; Werrett, M. V.; Pai, N.; Blair, V. L.; Spiccia, L.; Andrews, P. C. *Chem. - Eur. J.* **2017**, *23*, 8171–8175.
- (64) Ahlrichs, R.; Eichhöfer, A.; Fenske, D.; May, K.; Sommer, H. *Angew. Chem, Int. Ed.* **2007**, *46*, 8254–8257.
- (65) Sommer, H.; Eichhöfer, A.; Drebov, N.; Ahlrichs, R.; Fenske, D. *Eur. J. Inorg. Chem.* **2008**, *2008*, 5138–5145.
- (66) Lorenz, A.; Fenske, D. *Angew. Chem. Int. Ed.* **2001**, *40*, 4402–4406.
- (67) Levchenko, T. I.; Kübel, C.; Khalili Najafabadi, B.; Boyle, P. D.; Cadogan, C.; Goncharova, L. V.; Garreau, A.; Lagugné-Labarthe, F.; Huang, Y.; Corrigan, J. F. *J. Am. Chem. Soc.* **2017**, *139*, 1129–1144.
- (68) Levchenko, T. I.; Lucier, B. E. G.; Corrigan, J. F.; Huang, Y. *Inorg. Chem.* **2018**, *57*, 204–217.
- (69) Zhao, X.; Huang, Y.; Corrigan, J. F. *Inorg. Chem.* **2016**, *55*, 10810–10817.
- (70) Komuro, T.; Matsuo, T.; Kawaguchi, H.; Tatsumi, K. *Dalton Trans.* **2004**, *4*, 1618–1625.
- (71) Babcock, J. R.; Zehner, R. W.; Sita, L. R. *Chem. Mater.* **1998**, *10*, 2027–2029.
- (72) Polgar, A. M.; Weigend, F.; Zhang, A.; Stillman, M. J.; Corrigan, J. F. *J. Am. Chem. Soc.* **2017**, *139*, 14045–14048.
- (73) Fard, M. A.; Weigend, F.; Corrigan, J. F. *Chem. Commun. (Camb)*. **2015**, *51*, 8361–8364.
- (74) Azizpoor Fard, M.; Levchenko, T. I.; Cadogan, C.; Humenny, W. J.; Corrigan, J. F. *Chem. - Eur. J.* **2016**, *22*, 4543–4550.
- (75) DeGroot, M. W.; Corrigan, J. F. *Organometallics* **2005**, *24*, 3378–3385.
- (76) Partyka, D. V.; Deligonul, N. *Inorg. Chem.* **2009**, *48*, 9463–9475.
- (77) Tran, D. T. T.; Corrigan, J. F. *Organometallics* **2000**, *19*, 5202–5208.
- (78) Wallbank, A. I.; Borecki, A.; Taylor, N. J.; Corrigan, J. F. *Organometallics* **2005**, *24*, 788–790.
- (79) Polgar, A. M.; Khadka, C. B.; Azizpoor Fard, M.; Nikkel, B.; O'Donnell, T.; Neumann, T.; Lahring, K.; Thompson, K.; Cadogan, C.; Weigend, F.; et al. *Chem. - Eur. J.* **2016**, *22*, 18378–

18382.

- (80) DeGroot, M. W.; Taylor, N. J.; Corrigan, J. F. *J. Am. Chem. Soc.* **2003**, *125*, 864–865.
- (81) DeGroot, M. W.; Corrigan, J. F. *Angew. Chem. Int. Ed.* **2004**, *43*, 5355–5357.
- (82) DeGroot, M. W.; Khadka, C.; Rösner, H.; Corrigan, J. F. *J. Clust. Sci.* **2006**, *17*, 97–110.
- (83) Khadka, C. B.; Macdonald, D. G.; Lan, Y.; Powell, A. K.; Fenske, D.; Corrigan, J. F. *Inorg. Chem.* **2010**, *49*, 7289–7297.
- (84) Niebel, T.; MacDonald, D. G.; Khadka, C. B.; Corrigan, J. F. *Zeitschrift für Anorg. und Allg. Chemie* **2010**, *636*, 1095–1099.
- (85) Tolman, C. A. *Chem. Rev.* **1977**, *77*, 313–348.
- (86) Gusev, D. G. *Organometallics* **2009**, *28*, 6458–6461.
- (87) Clavier, H.; Nolan, S. P. *Chem. Commun.* **2010**, *46*, 841–861.
- (88) Nelson, D. J.; Nolan, S. P. *Chem. Soc. Rev.* **2013**, *42*, 6723–6753.
- (89) Poater, A.; Cosenza, B.; Correa, A.; Giudice, S.; Ragone, F.; Scarano, V.; Cavallo, L. *Eur. J. Inorg. Chem.* **2009**, *2009*, 1759–1766.
- (90) Gómez-Suárez, A.; Nelson, D. J.; Nolan, S. P. *Chem. Commun.* **2017**, *53*, 2650–2660.
- (91) El-Hellani, A.; Monot, J.; Tang, S.; Guillot, R.; Bour, C.; Gandon, V. *Inorg. Chem.* **2013**, *52*, 11493–11502.
- (92) Köster, S. D.; Alborzinia, H.; Can, S.; Kitanovic, I.; Wölfl, S.; Rubbiani, R.; Ott, I.; Riesterer, P.; Prokop, A.; Merz, K.; et al. *Chem. Sci.* **2012**, *3*, 2062–2072.
- (93) Taher, D.; Taylor, N. J.; Corrigan, J. F. *Can. J. Chem.* **2009**, *87*, 380–385.
- (94) Roy, M. M. D.; Lummis, P. A.; Ferguson, M. J.; McDonald, R.; Rivard, E. *Chem. - Eur. J.* **2017**, *23*, 11249–11252.
- (95) Beltrán, T. F.; Zaragoza, G.; Delaude, L. *Dalton Trans.* **2017**, *46*, 9036–9048.
- (96) Falivene, L.; Credendino, R.; Poater, A.; Petta, A.; Serra, L.; Oliva, R.; Scarano, V.; Cavallo, L. *Organometallics* **2016**, *35*, 2286–2293.
- (97) Zeng, X.; Frey, G. D.; Kinjo, R.; Donnadieu, B.; Bertrand, G. *J. Am. Chem. Soc.* **2009**, *131*, 8690–8696.
- (98) Polgar, A. M.; Zhang, A.; Mack, F.; Weigend, F.; Lebedkin, S.; Stillman, M. J.; Corrigan, J. F. *Inorg. Chem.* **2019**, *58*, 3338–3348.
- (99) Jacobsen, H.; Fink, M. J. *Eur. J. Inorg. Chem.* **2007**, *2007*, 5294–5299.
- (100) Hopkinson, M. N.; Richter, C.; Schedler, M.; Glorius, F. *Nature* **2014**, *510*, 485–496.
- (101) Jacobsen, H.; Correa, A.; Poater, A.; Costabile, C.; Cavallo, L. *Coord. Chem. Rev.* **2009**, *253*, 687–703.
- (102) Huynh, H. V. *Chem. Rev.* **2018**, *118*, 9457–9492.
- (103) Hussong, M. W.; Hoffmeister, W. T.; Rominger, F.; Straub, B. F. *Angew. Chem. Int. Ed.* **2015**, *54*, 10331–10335.
- (104) Welz, E.; Böhnke, J.; Dewhurst, R. D.; Braunschweig, H.; Engels, B. *J. Am. Chem. Soc.* **2018**, *140*, 12580–12591.
- (105) Smith, C. A.; Narouz, M. R.; Lummis, P. A.; Singh, I.; Nazemi, A.; Li, C.-H.; Crudden, C. M. *Chem. Rev.* **2019**, *119*, 4986–5056.
- (106) Wang, G.; Freeman, L. A.; Dickie, D. A.; Mokrai, R.; Benkő, Z.; Gilliard, R. J. *Inorg. Chem.* **2018**, *57*, 11687–11695.
- (107) Aprile, A.; Corbo, R.; Tan, K. V.; Wilson, D. J. D.; Dutton, J. L. *Dalton Trans.* **2014**, *43*, 764–768.
- (108) Humenny, W. J.; Mitzinger, S.; Khadka, C. B.; Najafabadi, B. K.; Vieira, I.; Corrigan, J. F. *Dalt. Trans.* **2012**, *41*, 4413–4422.
- (109) Khalili Najafabadi, B.; Corrigan, J. F. *Chem. Commun.* **2015**, *51*, 665–667.
- (110) Khalili Najafabadi, B.; Corrigan, J. F. *Dalt. Trans.* **2014**, *43*, 2104–2111.

Chapter 2¹

2 The Synthesis and Characterization of ITr-Protected Group 11 Trimethylsilylmetallochalcogenolates

2.1. Introduction

The synthesis of transition metal chalcogenide cluster compounds has important implications in the development of new materials with tuneable properties.^{1,2} The syntheses of these molecules requires the introduction of the appropriate reagents under conditions of kinetic control to prevent the formation of bulk solids. As the field has evolved, the reagents used continue to develop to allow for the isolation of molecular metal chalcogenides of varying nuclearity and composition.³⁻⁵ A powerful methodology is the use of trimethylsilyl metallochalcogenolate reagents “[MESiMe₃]” which can be isolated or generated *in situ* in order to access ternary metal chalcogenide clusters (MEM’).⁶ These trimethylsilyl metallochalcogenolates are considered soluble sources of “[ME]⁻”, whose pendant –SiMe₃ groups could be reacted with an appropriate heterometallic reagent, M’X (X = halide, acetate, etc.), to generate XSiMe₃ and drive bond formation between ME and M’ under conditions of kinetic control (i.e. lower temperature). The ability to apply these methods to many different metals has been established, however, the Corrigan group was the first to successfully apply these ideas to the group 11 metals.⁶⁻¹⁴ Inspired by “one-pot” reactions of MX, M’X and E(SiMe₃)₂ that were thought to proceed by “[MESiMe₃]” intermediates, it was shown that the use of ancillary phosphine ligands to coordinatively saturate the metal centre mitigated the propensity for chalcogenolates to bridge between multiple metals, allowing for the isolation of [(PR₃)_nMESiMe₃] (*n*=3, M=Cu, Ag; *n*=1, M=Au) from 1:1 reactions of [(PR₃)_nMX] and E(SiMe₃)₂ or Li[ESiMe₃] (X = Cl, OAc).^{7,13-16}

Following the use of phosphines as stabilizing ligands, the coinciding emergence of *N*-heterocyclic carbenes (NHCs) as improved versions of phosphine ligands subsequently led to the development of a collection of NHC-stabilized group 11 trimethylsilyl metallochalcogenolate compounds that were more thermally robust and easier to isolate for storage than their phosphine counterparts.¹⁷⁻²⁰ Like phosphines, it was shown that the electronic and steric modulation of the NHC ligands affected the structure, stability and reactivity of the subsequent metallochalcogenolates.^{13,17,18} **Figure 2.1** demonstrates the difference the ancillary ligand (L = phosphine, NHC) can have on the product ternary metal chalcogenide.

¹ A version of the chapter is to be submitted for publication, authors: D. R. Nahhas, J. F. Corrigan.

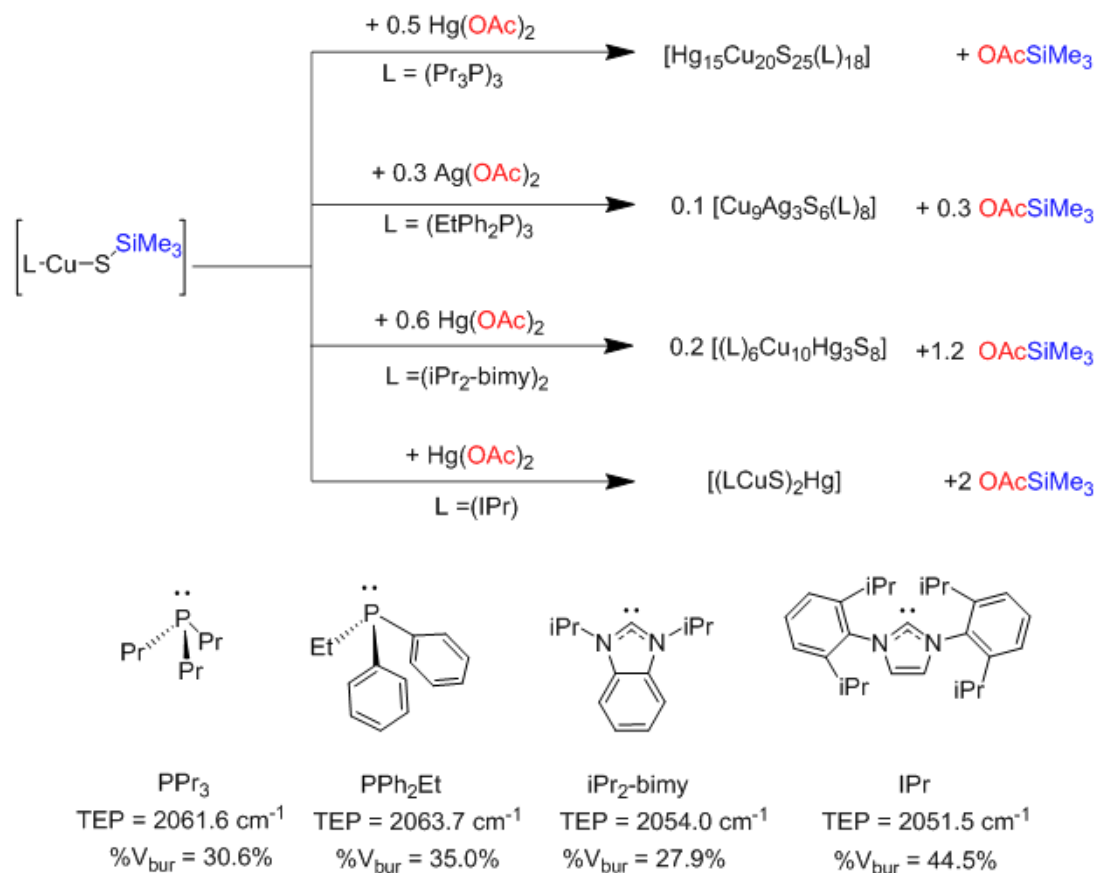
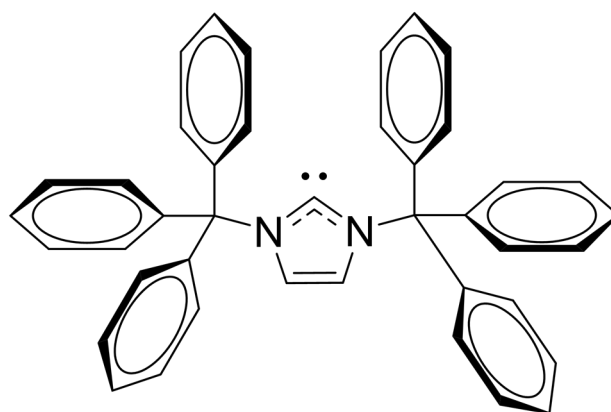


Figure 2.1: Reactions of $[\text{LCuESiMe}_3]$ illustrating the effect of the neutral, $2e^-$ ligand, L. The acetate (OAc) and trimethylsilyl (SiMe_3) moieties are coloured to illustrate the formation of the thermodynamically favored product. Below, the various ligands used are illustrated along with reported TEP and $\%V_{\text{bur}}$ values.^{22,23} Pr = n-propyl; Ph = phenyl; Et = ethyl; iPr_2 -bimy = bis-1,3-(diisopropyl)benzimidazole-2-ylidene; IPr = bis-1,3-(2,6-diisopropylphenyl)imidazole-2-ylidene.

The effect of phosphine ligands on the syntheses of binary copper chalcogenide clusters has been reviewed by Dehnen *et al.*, but the limited stability of the phosphine stabilized trimethylsilyl metallochalcogenolates makes a similar study on ternary group 11 chalcogenide compounds unfeasible.¹⁶ The greater stability of NHC-stabilized trimethylsilyl metallochalcogenolates has led to their use in the syntheses of heterometallic chalcogenide clusters, however, the library of NHC ligands used requires further development. Preliminary work by Fard *et al.* suggests NHCs with lower electron donating ability and smaller steric bulk (as measured by TEP and $\%V_{\text{bur}}$) result in ternary clusters of higher nuclearity.^{17,18,21-23} Recent work by Polgar *et al.* showed the ability to isolate very similar structures of the general type $[(\text{NHC})_4\text{M}_4(\mu_3\text{-E})_4\text{M}'_4]$ (NHC = bis-1,3-(2,6-diisopropylphenyl)imidazole-2-ylidene, IPr; 2-(2,6-diisopropylphenyl)-3,3-dimethyl-2-azaspiro[4.5]dec-1-ylidene, CAAC^{Cy}) when using either IPrAuESiMe_3 or $\text{CAAC}^{\text{Cy}}\text{CuESiMe}_3$ as starting materials, despite a drastic difference in their electronic properties.^{19,20,24,25} Therefore, the class of NHC-stabilized group 11 trimethylsilyl metallochalcogenolates

must continue to be developed, to allow for further comparative and exploratory studies. In the interest of expanding this class of compounds, this chapter describes the syntheses of group 11 trimethylsilyl metallochalcogenolates using a more sterically encumbering NHC, bis-1,3-tritylimidazole-2-ylidene, referred to hereafter as ITr (**Figure 2.2**).²⁶ This ligand has been used thus far for the attempted synthesis of monocoordinate silver ions and other work has demonstrated the utility of this ligand in stabilizing reactive main group compounds.^{26,27} Armed with a library of group 11 trimethylsilylmetallochalcogenolate compounds, future work will focus on the reactions that these compounds can undergo and the new heterometallic structures they can stabilize.



ITr

TEP = 2034.0 cm⁻¹

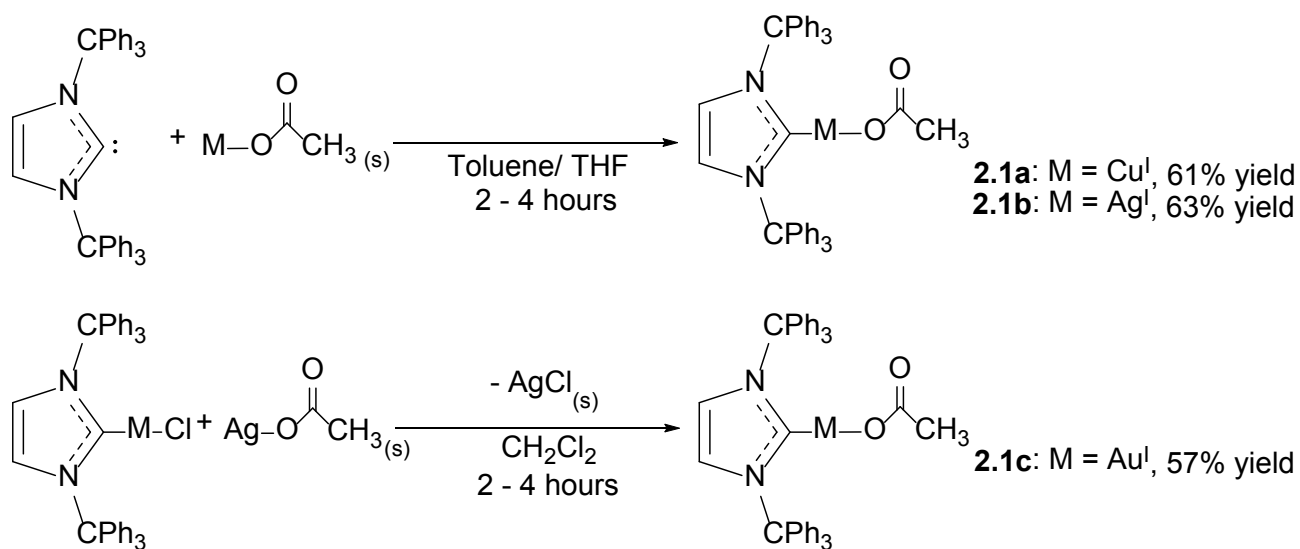
%V_{bur} = 57.3%

Figure 2.2: Structure, electronic and steric data of bis-1,3-tritylimidazole-2-ylidene (ITr)²⁶

2.2 Results & Discussion

2.2.1 Synthesis and Characterization of [ITrMOAc]

The synthesis of the metallochalcogenolates within this body of work began with the synthesis of the respective ITr-metal acetate complex. Where possible ([ITrCuOAc], **2.1a** and [ITrAgOAc], **2.1b**), the carbene was generated *in situ* from the deprotonation of the reported imidazolium triflate with 1 eq.



Scheme 2.1: Syntheses of [ITrMOAc](**2.1a–c**)

KHMDS, and mixed with the metal acetate in toluene; the resultant product showed limited solubility in toluene and thus a mixture of toluene and THF was used to allow for product filtration and purification. For [ITrAuOAc] (**2.1c**), the previously reported [ITrAuCl] was reacted by metathesis by mixing with AgOAc in CH₂Cl₂ and removing the insoluble by-product (AgCl) via filtration.²⁶ The metal acetate complexes were characterized by ¹H and ¹³C NMR spectroscopy and are expected to be linear molecules with a terminally coordinated acetate group, as this structural motif has been confirmed via crystallographic analysis of analogues with NHCs of comparable steric bulk.^{20,26,28} The ¹H NMR spectrum of the metal acetates, in CDCl₃, showed a singlet between δ 6.97 – δ 7.03 ppm for the imidazole-2-ylidene protons (NCH, 2H), with chemical shifts increasing in order from Cu (**2.1a**) < Au (**2.1c**) < Ag (**2.1b**) (**Figure 2.3**). Except for the copper acetate complex, the aromatic protons on the trityl groups appeared as two distinct multiplets between δ 7.15 – δ 7.35 ppm for the *ortho* (12 H) and *meta/para* protons (18 H). The *meta/para* protons were more deshielded than their *ortho* counterparts. Assignment of the individual multiplets observed in the spectra of [ITrAgOAc] (**2.1b**) and [ITrAuOAc] (**2.1c**) were confirmed by ¹H – ¹³C HMBC NMR experiments showing correlation between the *ortho* protons to the CPh₃ signal in the ¹³C NMR spectrum. Of note in the ¹H NMR data was the appearance of a singlet between δ 1.38 – δ 1.62 ppm that was assigned to the methyl protons of the acetate moiety (OAc, 3H). This assignment was based both on integration and ¹H – ¹³C HMBC NMR experiments that showed correlation to the ¹³C NMR resonance for the carbonyl carbon (δ 176.2 – δ 176.6 ppm) of the acetate. The ¹H NMR chemical shift of

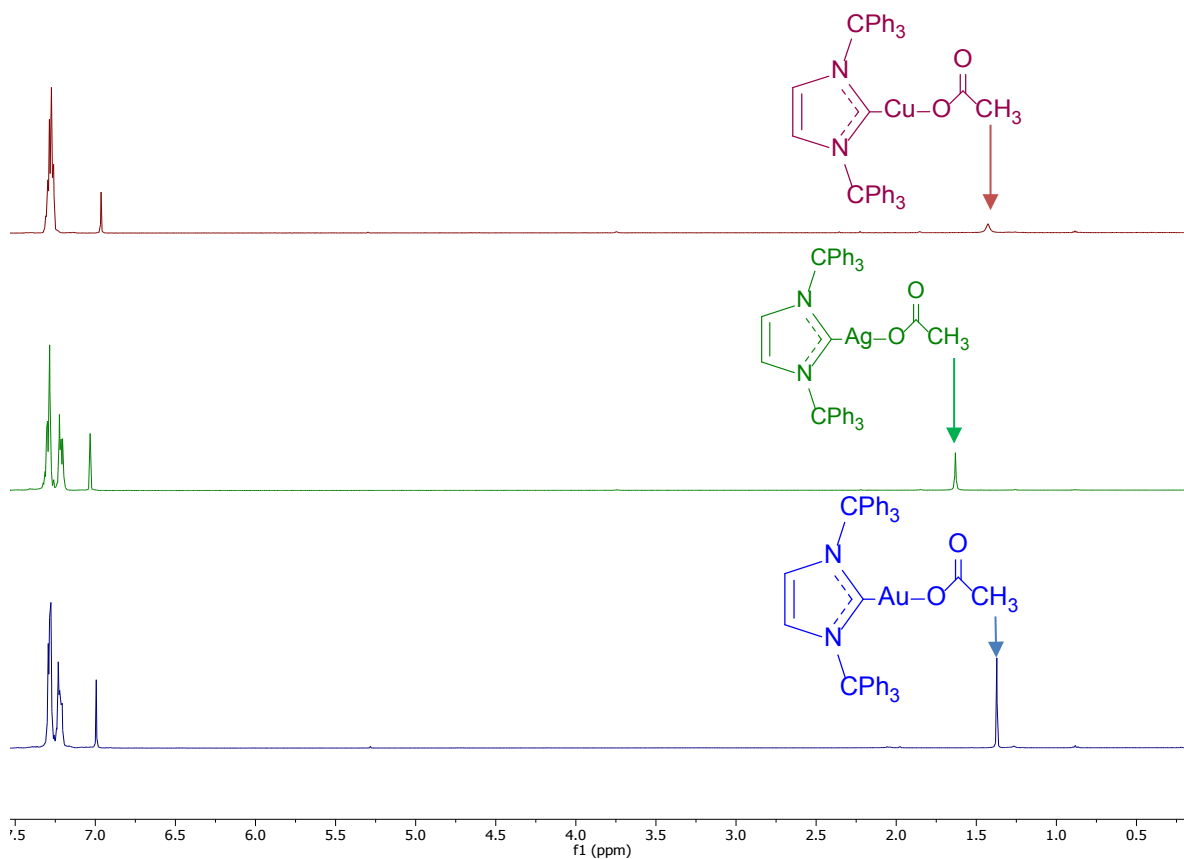


Figure 2.3: 400 MHz ^1H NMR spectra of [ITrMOAc] (Cu^{I} = red, Ag^{I} = green, Au^{I} = blue) in CDCl_3 at 25 $^\circ\text{C}$. Acetate peaks indicated by arrows.

this diagnostic resonance increased in order from Au (**2.1c**) < Cu (**2.1a**) < Ag (**2.1b**) (see **Figure 2.3**). The most characteristic ^{13}C NMR signal observed was the carbenic carbon (NCN) (δ 175.8 – δ 193.4 ppm). The chemical shift of this resonance was heavily influenced by the metal atom present also showing an increase in chemical shift from Au (**2.1c**) < Cu (**2.1a**) < Ag (**2.1b**) (see **Table 2.1** and **Figure 2.3**). For **2.1a** and **2.1c**, this signal was directly observed as a singlet at δ 186.2 ppm and δ 175.5 ppm, respectively, but the ^{13}C NMR spectra of **2.1b** showed no peak under standard $^{13}\text{C}\{^1\text{H}\}$ NMR conditions ($\tau = 5\text{s}$, 2048 scans). However, a pair of correlations in the $^1\text{H} - ^{13}\text{C}$ HMBC spectrum of **2.1b** was observed between the imidazole-2-ylidene protons (δ 7.03 ppm) and signals at δ 194.6 and δ 191.9 ppm. Given this pair of signals showed no correlation to any other protons in the ^1H NMR spectrum, it was thought that they belonged to the carbene resonance and were the result of coupling between the ^{13}C and $^{107/109}\text{Ag}$ nuclei. Coupling between the carbenic carbon and silver has been noted in the ^{13}C NMR spectra of other NHC – silver complexes, with these prior examples showing direct observation of the expected overlapping doublet pattern.^{29,30} It would thus be expected to see a pair of doublets for splitting by each isotope of

silver, however, this information was not resolved by $^1\text{H} - ^{13}\text{C}$ HMBC experiments. It was noted that the HMBC correlations were separated by $^1J_{\text{C-Ag}} \approx 270$ Hz, which was on the order of coupling values observed for similar complexes.^{29,30} Previous work by Roy *et al.* attempting to use the ITr ligand to stabilize a monocoordinate Ag^{I} complex did not report any data for this resonance in any of the silver complexes isolated; other researchers have justified this absence of signal due to the somewhat labile nature of NHC – Ag bonds in solution making them difficult to observe.^{27,31}

Table 2.1: ^1H and ^{13}C NMR data comparing chemical shifts of the carbene (^{13}C), the carbonyl (^{13}C), and the methyl groups (^{13}C and ^1H) in [ITrMOAc]. Data listed in ppm in CDCl_3 .

M =	$^{13}\text{C}(\text{NCN})$	$^{13}\text{C}(\text{OC}(\underline{\text{O}})\text{CH}_3)$	$^{13}\text{C}(\text{OC}(\text{O})\underline{\text{C}}\text{H}_3)$	$^1\text{H}(\text{OC}(\text{O})\underline{\text{C}}\text{H}_3)$
Cu (2.1a)	186.2	176.2	24.2	1.42
Ag (2.1b)	193.3	176.5	23.4	1.62
Au (2.1c)	175.7	177.8	24.6	1.38

The trends observed in the ^1H NMR chemical shift of the acetate moiety suggest the protons are more shielded in order from Ag (**2.1b**) < Cu (**2.1a**) < Au (**2.1c**). Comparison of the ^{13}C NMR chemical shifts of the carbonyl carbons and methyl carbons of the –OAc showed little difference between the carbonyl chemical shifts or the methyl chemical shifts (see **Table 2.1**). The most significant differences in the ^{13}C NMR data were observed for the carbenic carbon of which also showed a more shielded resonance in order from Ag (**2.1b**) < Cu (**2.1a**) < Au (**2.1c**) (see **Table 2.1**). A review by Jacobsen *et al.* stating that group 11 NHC–M–X complexes (X = Cl^- , Br^- , I^-) followed a similar trend for increasing NHC–M bond strength (Ag < Cu < Au), seemed to suggest that the increasingly shielded character of the carbenic carbon from Ag (**2.1b**) < Cu (**2.1a**) < Au (**2.1c**) was a function of the stronger NHC–M bond, resulting in a chemical shift less similar to the free carbene (δ 225.8 ppm in C_6D_6).^{26,30,32,33} This in turn could result in a stronger trans effect on the acetate ligand, resulting in a shielding effect on the acetate protons that increases the same way (Ag < Cu < Au). In the trends observed, it was interesting to note that the ^{13}C NMR spectra of [ITrAgOAc] (**2.1b**) bore a carbenic resonance that was especially deshielded compared to its copper and gold counterparts. Furthermore, this resonance was observed at a much higher frequency compared to resonances in similar silver acetate complexes.^{29,30} In fact, similar chemical shifts have been observed in complexes of $[(\text{SIPrAg})_2(\mu_2\text{-X})]^+$ (X = Cl^- , F^- , SIPr = *bis*-1,3-(2,6-diisopropyl phenyl)imidazolin-2-ylidene) and have been rationalized by the anomalous bonding between the SIPr and the silver centre.^{31,34} Given the supposed difference in the electronic nature of ITr (an imidazole-2-

ylidene) and SIPr (an imidazolin-2-ylidene), and in the attempts to rationalize the above hypothesis of the NHC's effect on the acetate resonances, it was felt that further investigation was warranted into the NMR data observed herein by comparison to NHC metal acetates previously reported in literature.^{26,35}

Table 2.2: ¹H & ¹³C NMR data comparing the acetate resonance and carbenic carbon resonance of [ITrMOAc] and [IPrMOAc]. Data listed in ppm in the indicated solvent.

M	2.1_ , ¹³ C (NCN)	[IPrMOAc] ¹³ C (NCN)	[IPrMOAc] ¹ H (OC(O)CH ₃)	2.1_ , ¹ H (OC(O)CH ₃)
Cu (a)	188.0 (C ₆ D ₆)	182.6 (C ₆ D ₆) ²⁸	1.93 (C ₆ D ₆) ²⁸	1.96 (C ₆ D ₆)
Ag (b)	193.4 (CDCl ₃)	184.3 (CDCl ₃) ²⁹	1.85 (CDCl ₃) ²⁹	1.62 (CDCl ₃)
Au (c)	175.5 (CDCl ₃)	175.9 (CD ₂ Cl ₂) ³⁶	1.65 (CD ₂ Cl ₂) ³⁶	1.38 (CDCl ₃)

The comparison of the ¹H NMR and ¹³C NMR data of [(ITr)MOAc] (M= Cu, **2.1a**; Ag, **2.1b**; Au, **2.1c**) to previous data on [IPrMOAc] (M= Cu, **2.1a**; Ag, **2.1b**; Au, **2.1c**) was made given their subsequent use in synthesis of [IPrMESiMe₃] and the similar imidazole-2-ylidene backbone on IPr and ITr.¹⁷⁻¹⁹ Comparing the ¹H NMR data showed no consistent trends; the OAc group of **2.1a** and **2.1c** showed chemical shifts that were slightly more deshielded than their IPr counterparts, but **2.1b** exhibited a more shielded resonance (see **Table 2.2**).^{28,29,36} The observation that the ¹H NMR chemical shifts of OAc for **2.1a** – **2.1c** were not consistently more shielded than their IPr counterparts may suggest the importance of anisotropic effects from the ligand influencing the chemical shift of these protons, which in turn is influenced by the solvent effects on the ligand. That **2.1b** contains an OAc resonance more shielded than [IPrAgOAc], yet **2.1a** is more deshielded than [IPrCuOAc] may point to the different effect the respective NMR solvent had on ITr vs. IPr. The relative insensitivity on the NMR spectroscopy of heteronuclei to solvent effects might allow a comparison of the ¹³C NMR data of the two NHC complexes to be less complicated by these differences and, perhaps, be more indicative of the electronic differences between the two ligands. In fact, comparison of the ¹³C NMR data of **2.1a** – **2.1c** suggested a more deshielded carbenic resonance than [IPrMOAc] for all complexes compared.^{28,29,36} While this was the opposite of the effect more electron donation and stronger NHC – M bonding was expected to have on the chemical shift of the carbenic resonances, Roy *et al.* reported that flanking arene – M interactions for the [(ITr)Rh(CO)₂Cl] probe complex used to measure electron donation likely contribute to the lower TEP reported for ITr in comparison to most imidazole-2-ylidene type NHCs.²⁶ Thus, one possible explanation for the deshielded nature of the carbenic resonance of ITr could be the flanking aryl – metal interactions

in this ligand; these would increase electron richness about the metal centre, mitigating σ donation from the NHC and deshielding the carbenic carbon more than other ligands where this aryl donation is not possible.^{26,30}

The chemical shift of nuclei in NMR experiments are governed by the equation:

$$\delta = \delta_p + \delta_d$$

where the paramagnetic shielding term, δ_p , is related to the changes in paramagnetic electron circulation and often dominates nuclei such as ^{13}C ; the diamagnetic term, δ_d , correlates directly to the amount of electron density about a nucleus and often dominates nuclei such as ^1H . The ^{13}C NMR trends above suggested more at play than a shift in electron density between the different NHC metal acetates. In a work by Wong *et al.*, Density Functional Theory (DFT) calculations on a series of [NHC–Ag–O₂CR] complexes (R = Me, Ph, 4–MeC₆H₄, 4–ClC₆H₄) showed that the chemical shifts of the carbenic resonance were dominated by a large δ_p term; variation in bonding of the NHCs to the Ag centre had a limited effect on the chemical shift of the carbenic carbon.³⁷ Using the common knowledge that δ_p results from the transition of electrons between symmetry related occupied and unoccupied orbitals, the researchers made a compelling argument to show that the differences in chemical shift between the [NHC–Ag–O₂CR] complexes they investigated were a function of the HOMO–LUMO gap (ΔE) of the NHCs used.^{37,38} They confirmed in their work that the NHC silver carboxylate complexes with a smaller ΔE displayed carbenic resonances that were shifted to higher frequency. The HOMO–LUMO gap reported by Wong *et al.* was calculated from an optimized geometry for [IPrAgOAc], not used in the work of Roy *et al.*, making it difficult to compare to the data available for the ligand used in this work ($\Delta E_{\text{ITr}} = 4.806$ eV; $\Delta E_{\text{IPrAgOAc}} = 4.58$ eV).^{26,37} Fortunately, Wong *et al.* make mention that the ΔE values calculated for the silver complexes showed a linear correlation to the ^{13}C NMR chemical shift of the free NHC ligands.³⁷ Plotted in **Figure 2.5** below, it was evident that ITr bore a carbenic resonance more deshielded than IPr, suggesting a smaller ΔE value for [ITrAgOAc] (**2.1b**) by this correlation. Thus, a full explanation on the difference in the NMR data of the metal acetates within this work would require quantum chemical calculations of the δ_p terms for the signals of interest. As a preliminary result, it may suffice to say that the NHC–M bond strength increases for **2.1a** – **2.1c** from M = Ag^I < Cu^I < Au^I, causing the differences in the series of NMR spectra

for [ITrMOAc], while comparison to other NHC metal acetates must take into account the difference in the HOMO–LUMO gap for the respective ligands.^{32,37}

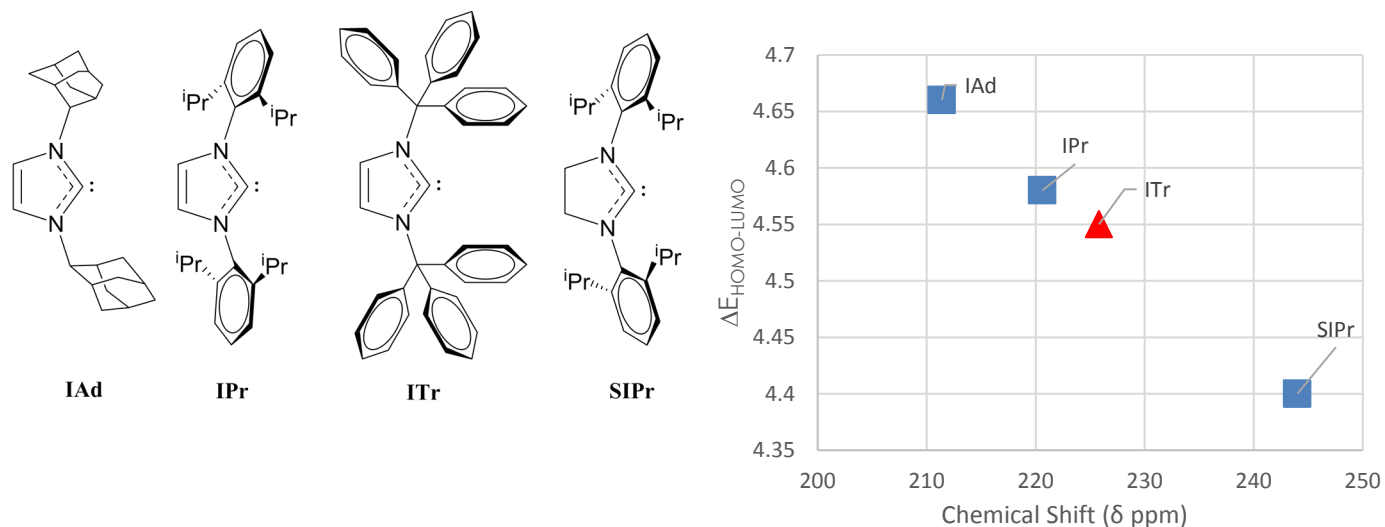
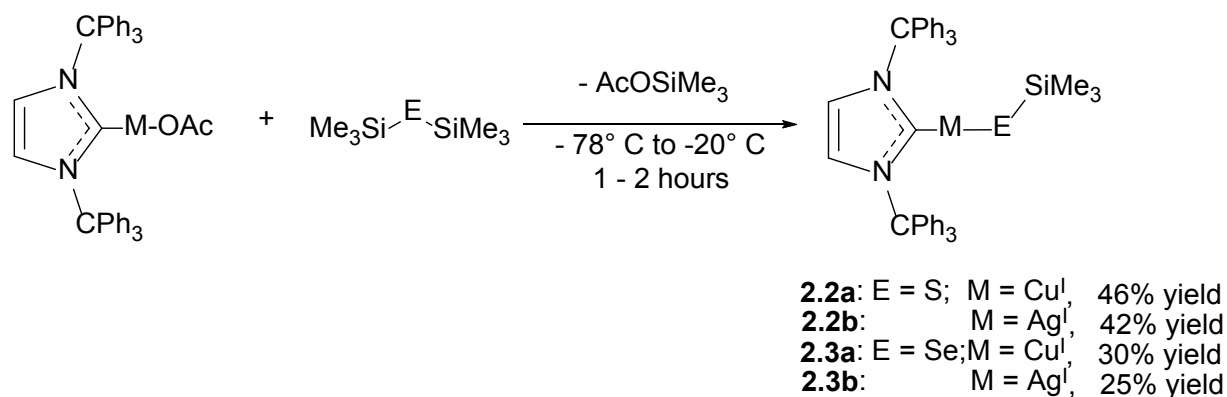


Figure 2.4: Scatter plot of correlation between the HOMO–LUMO gap and chemical shift of carbenic carbon in various NHCs (data from Wong et al. and Roy et al.).^{26,37} Included are figures of each NHC compared in the graph, in order from left to right.

2.2.2. Syntheses and Characterization of [ITrMESiMe₃]

Following the syntheses of the starting acetate complexes, the respective copper and silver chalcogenolates were made by the general method outlined in **Scheme 2.2**. This chemistry has been well established and has been used to access NHC metallochalcogenolates of copper and silver.¹¹ As hypothesized, the use of [(ITr)MOAc] (M= Cu, **2.1a**; Ag, **2.1b**) in an equimolar reaction with E(SiMe₃)₂ (E = S, Se) allowed for



Scheme 2.2: Syntheses of [ITrMESiMe₃] (**2.2a,b** – **2.3a,b**)

activation of a single E – Si bond to selectively produce [(ITr)CuESiMe₃] (E = S, **2.2a**; Se, **2.3a**) or [ITrAgESiMe₃] (E = S, **2.2b**; Se, **2.3b**). This was determined by using ¹H NMR spectroscopy to observe the concomitant formation of AcOSiMe₃ as a by-product in a 1:1 ratio to the chalcogenolate when conducting the reaction in CDCl₃. For instance, the addition of S(SiMe₃)₂ to a solution of **2.1a** at –20 °C in CDCl₃ (¹H NMR, δ_{OAc} = 1.42 ppm) followed by stirring for 1 hour at this temperature resulted in complete consumption of the acetate complex as determined via the disappearance of the signal at δ 1.42 ppm (**Figure 2.5**). Concomitant formation of AcOSiMe₃ (δ 2.05 ppm, 3H; δ 0.28 ppm, 9H) and **2.2a** was observed to confirm reaction completion (**Figure 2.5**).

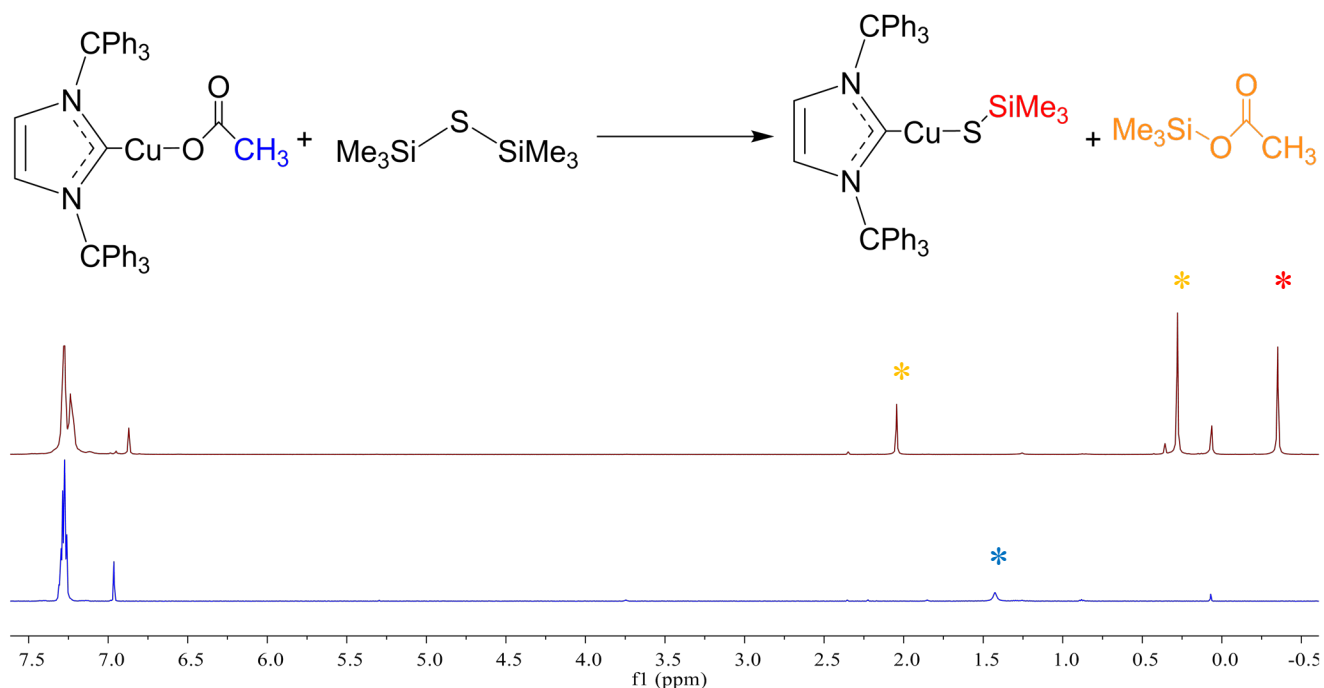
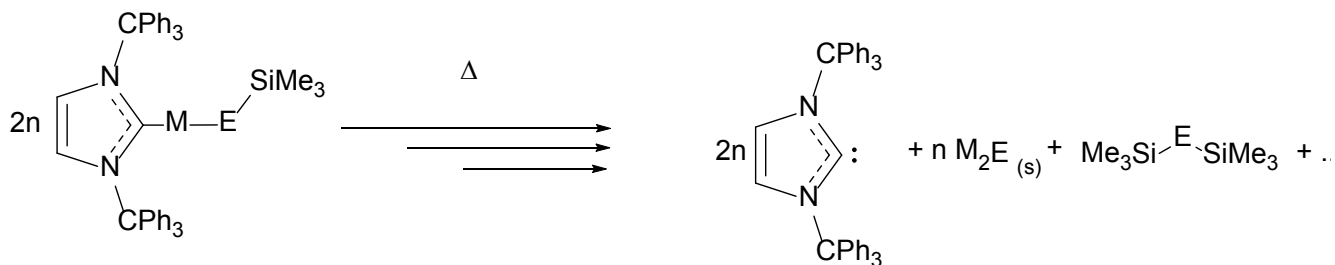


Figure 2.5: ¹H NMR spectra of **2.1a** (blue, bottom) and reaction mixture of **2.1a** with 1.07 eq. S(SiMe₃)₂ (red, top) in CDCl₃. Peaks of interest in both spectra have been colour coded.

Reactions for the synthesis of **2.2a** began with addition of S(SiMe₃)₂ at –20 °C, where previous reports for the syntheses of [IPrCuSSiMe₃] required initiation at –45 °C to avoid unwanted condensation reactions.^{17,18,39} Additionally, the ¹H NMR spectrum of [ITrCuSeSiMe₃] (**2.3a**) in CDCl₃ showed evidence of only ~20% decomposition over 16 hours at room temperature, as monitored by the production of Se(SiMe₃)₂ via the proposed decomposition mechanism in **Scheme 2.3**. This solution stability was in stark contrast to that shown by the argentochalcogenolates, which required NMR analysis at low temperatures. When dissolved in CDCl₃ at room temperature, samples of isolated crystalline [ITrAgESiMe₃] (E = S, **2.2b**; Se **2.3b**) immediately darkened, producing a black precipitate thought to be bulk Ag₂E. The ¹H and

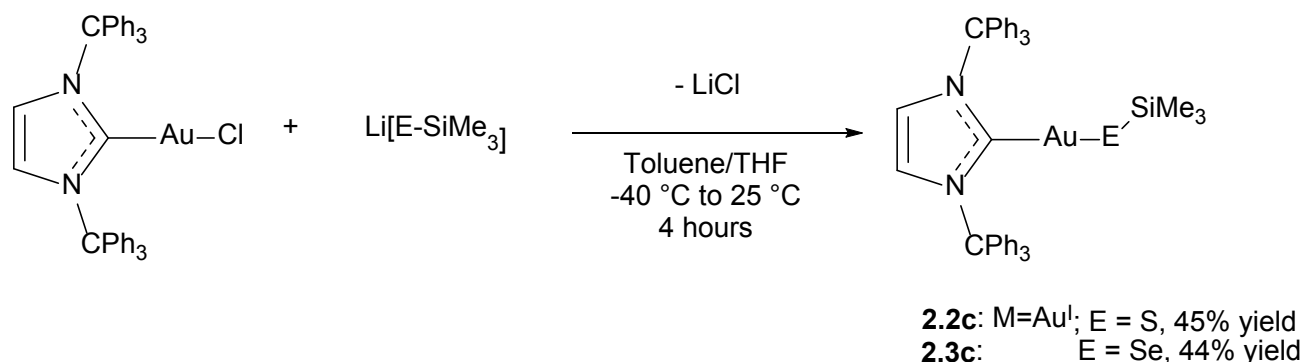
^{13}C NMR spectra suggested a mixture of NHC bearing products and the formation of $\text{E}(\text{SiMe}_3)_2$. From the spectra of **2.2b** and **2.3b** at room temperature, resonances belonging to the argento-chalcogenolates could be extrapolated from the mixture of signals observed and the assignment of ESiMe_3 was confirmed using integration and ^1H - ^{13}C HMBC. The instability of this system agreed with the behaviour of previously synthesized analogues and the increased propensity of Ag-E units to agglomerate to bulk silver chalcogenide species.¹⁸ Though decomposing, the silver compounds in this work were long lived enough to be observable by both spectroscopic methods. The identity of the ITr bearing by-product of decomposition was not confirmed, although it was hypothesized to be some polynuclear silver chalcogenide species. A review of the literature also suggested that ITr=E compounds were a possibility, though imidazole-2-chalcogenones with the ITr framework have not yet been reported.⁴⁰ In addition to differences in solution stability, some observations were made on the reactivity of $[\text{ITrMOAc}]$ toward the $\text{E}(\text{SiMe}_3)_2$ reagents. ^1H NMR analysis on aliquots from the reaction of $[\text{ITrCuOAc}]$ (**2.1a**) with $\text{S}(\text{SiMe}_3)_2$ stirred in CDCl_3 at temperatures below $-20\text{ }^\circ\text{C}$ showed no appreciable sign of reaction completion, as evidenced by the presence of peaks for both **2.1a** and $\text{S}(\text{SiMe}_3)_2$. Assessing the reactivity of $[\text{ITrAgOAc}]$ (**2.1b**) toward the production of $[\text{ITrAgESiMe}_3]$ proved more difficult, given the propensity for aliquots removed from reactions at cryogenic temperatures to decompose within seconds of warming to room temperature on removal.



Scheme 2.3: Proposed decomposition reaction of metallochalcogenolates ($\text{M} = \text{Cu}^{\text{I}}, \text{Ag}^{\text{I}}, \text{Au}^{\text{I}}$; $\text{E} = \text{S}, \text{Se}$).

In the syntheses of $[(\text{ITr})\text{MSSiMe}_3]$ ($\text{M} = \text{Cu}$, **2.2a**; Ag , **2.2b**) and $[(\text{ITr})\text{MSeSiMe}_3]$ ($\text{M} = \text{Cu}$, **2.3a**; Ag , **2.3b**), the driving force of these reactions was the tendency for the silicon centre to form thermodynamically favoured chemical bonds in AcOSiMe_3 , which in turn allowed for the introduction of a M-E bond to form the desired product.⁶ Though Si-Cl bonds are thermodynamically favoured, it was found that the reaction of $[\text{ITrAuCl}]$ directly with $\text{E}(\text{SiMe}_3)_2$ did not provide the desired metallochalcogenolate in a well-controlled fashion. The syntheses of $[\text{Ph}_3\text{PAuESiMe}_3]$ by Polgar *et al.* was shown to suffer the same limitations, which inspired the synthesis of $[\text{ITrAuESiMe}_3]$ ($\text{E} = \text{S}$ **2.2c**;

Se **2.3c**) in a method similar to this previous work.¹⁴ A lithiation reaction of $E(\text{SiMe}_3)_2$ made the chalcogenolate reagent more reactive, by converting it to $\text{Li}[E\text{SiMe}_3]$.^{4,14} Further reaction with $[\text{ITrAuCl}]$ led to the syntheses of **2.2c** – **2.3c** via the precipitation of LiCl , which was removed by filtration in toluene (see **Scheme 2.4**).^{19,4} Like previous NHC metallochalcogenolates, the gold compounds were found to be the most stable in solution, showing no signs of decomposition even after 24 hours at room temperature under inert atmosphere.¹⁹



Scheme 2.4: Syntheses of $[\text{ITrAuESiMe}_3]$ (**2.2c** – **2.3c**)

Compounds **2.2a–c** and **2.3a–c** were characterized by ^1H and ^{13}C NMR spectroscopic studies and Single Crystal X-Ray Diffraction (SCXRD) studies (see **Table S2.1** and **Table S2.2**) were conducted on **2.2a** and **2.3a**. The spectroscopic and crystallographic data suggest all the NHC metallochalcogenolates synthesized are linear about the metal centre with terminal ESiMe_3 coordination. This is further supported by previous studies on analogous compounds and the similar coordination characteristics of the group 11 metallochalcogenolates.^{3,10,18} The ^1H NMR spectra for the metallochalcogenolates show a slight change in the chemical shift of the imidazole-2-ylidene protons, causing them to become more shielded upon terminal coordination of $-\text{ESiMe}_3$. Replacing $-\text{OAc}$ for $-\text{ESiMe}_3$ also led to resolution of the aromatic protons on the cuprachalcogenolates (**2.2a** – **2.3a**) such that two multiplets corresponding to the *meta/para* and *ortho* protons appeared in the aromatic region (see **Figure 2.5**, δ 7.16 – δ 7.30 ppm). The most characteristic resonance that appeared in the ^1H NMR spectra was a high field singlet assigned to the $-\text{ESiMe}_3$ group. Comparison of the chemical shift for $-\text{ESiMe}_3$ (at room temperature) for all compounds synthesized in this work showed the most deshielded resonance belonged to $[\text{ITrAgESiMe}_3]$ (**2.2b** – **2.3b**), however the metalloselenolates (**2.3a** – **2.3c**) generally exhibited a more deshielded singlet than their metallothiolate counter parts (**2.2a** – **2.3c**). The apparent deshielding of the trimethylsilyl protons by less electronegative chalcogenolates (**2.2** = S; **2.3** = Se) has been a well documented trend in these types of

compounds and has been explained previously by the importance of anisotropic effects influencing chemical shift as larger, less electronegative chalcogens are used.^{42,43} A discussion on the effect of the metal on the NMR data for the complexes of this work was limited by the inability to compare and contrast any trends in this work to those for the family of [IPrMESiMe₃], because the NMR data for the latter class of compounds have been reported at various temperatures.^{17–19} Still, the trend in chemical shift of –ESiMe₃ when compared at room temperature (Ag < Au ≤ Cu) is similar to the trend observed in the ¹H NMR chemical shift of OAc in that the silver compounds are most deshielded.

Table 2.3: ¹H NMR/¹³C NMR resonance of ESiMe₃ moiety for [(ITr)MSSiMe₃] (**2.2a–c**) and [(ITr)MSeSiMe₃] (**2.3a–c**), compared to [IPrMESiMe₃]. Data obtained in CDCl₃ from this work and others, reported in ppm.^{17–19}

M	–SSiMe ₃ (2.2)		–SeSiMe ₃ (2.3)	
	ITr	IPr	ITr	IPr
Cu (a)	–0.36 ^a / 6.8 ^a	–0.17 ^a / 6.7 ^a	–0.32 ^a / 7.3 ^a	–0.04 ^a / 7.3 ^a
Ag (b)	–0.32 ^b / 6.8 ^b	–0.13 ^b / 7.0 ^b	–0.17 ^b / 7.5 ^b	–0.02 ^b / 7.6 ^b
Au (c)	–0.35 / 5.9	–0.11 / 6.4	–0.20 / 6.7	0.01 / 7.0

^a *T* = –10 °C ; ^b *T* = –30 °C

Unlike their acetate counterparts, comparison of the ¹H and ¹³C NMR data of [(ITr)MSSiMe₃] (M = Cu, **2.2a**; Ag, **2.2b**; Au, **2.2c**) and [(ITr)MSeSiMe₃] (M = Cu, **2.3a**; Ag, **2.3b**; Au, **2.3c**) to those for the previously synthesized [IPrMESiMe₃] suggested greater electron donation in compounds of this work (see **Table 2.3**).^{17–19} The ¹H NMR resonances of the –SiMe₃ moiety listed in **Table 2.3** are more shielded for [ITrMESiMe₃] than [IPrMESiMe₃], however, the ¹³C NMR signals were less sensitive to the proposed increase in electron density about the metal centre; [ITrCuSSiMe₃] (**2.2a**) has a more deshielded –SSiMe₃ ¹³C NMR resonance than [IPrCuSSiMe₃].¹⁷ Though these data do agree with increased electron density about the –ESiMe₃ group, anisotropic effects from the different ligand environments (ITr vs. IPr) should not be ignored. The data in **Table 2.4** (see below) revealed the carbenic resonances of the metallothiolate (**2.2a–c**) and metalloselenolate (**2.3a–c**) compounds in this work behaved like the metal acetates (**2.1a–2.1c**) in that they were more deshielded than their IPr counterparts, likely due to a smaller HOMO–LUMO gap for ITr than IPr.³⁷ For those data obtained at the same temperature, replacing –OAc with the

–ESiMe₃ group resulted in a deshielding of the carbenic carbon regardless of the identity of the NHC. Based on earlier discussion on the chemical shift of carbenic carbons in metal acetates, the deshielding of the carbenic resonances on coordination to –ESiMe₃ could be a result of the change in the paramagnetic shielding term for this resonance, changing as a function of the changing electronic structure of the metallochalcogenolate.³⁷ Further evidence for this change in electronic structure is given by the similarity in the changes in chemical shift conserved between NHCMeSiMe₃; both instances have the gold selenolates containing the most deshielded carbenic carbon.^{17,19}

Table 2.4: ¹³C NMR data for NCN resonances in NHC–M–X complexes (NHC = ITr, IPr; X = OOCCH₃, ESiMe₃; E = S, Se).^{17–19} Data reported in CDCl₃ and/or at 25 °C unless otherwise indicated.

	OC(O)CH ₃		ESiMe ₃			
	ITr 2.1	IPr	ITr, E = S 2.2	IPr, E = S	ITr, E = Se 2.3	IPr, E = Se
Cu (a)	188.0 ^c	182.6 ^c	189.9	182.8 ^c	190.2	181.6 ^a
Ag (b)	193.3	184.3	–	–	–	–
Au (c)	176.6	175.9 ^d	194.1	187.1	195.7	188.9

^a *T* = –10 °C; ^b *T* = –30 °C; ^c C₆D₆²⁸; ^d CD₂Cl₂³²

Single Crystal X–Ray Diffraction (SCXRD) studies (see **Table S2.1** and **Table S2.2**) of [(ITr)CuSSiMe₃] (**2.2a**) and [(ITr)CuSeSiMe₃] (**2.3a**) confirmed the proposition that the metallochalcogenolates in this work were linear molecules with terminal coordination of the –ESiMe₃ moiety. Both compounds crystallized in the space group *P* $\bar{1}$ as THF solvates. Both compounds showed near linear coordination about the copper centre (**2.2a** = 172.6(1)°; **2.3a** = 171.3(1)°) and, as expected, **2.3a** displayed a longer E–Si bond (2.265(1) Å vs. 2.111(2) Å) and a longer Cu–E bond (2.2656(7) Å vs. 2.152(1) Å). Along with the contraction of the Cu–E–Si bond angle in **2.3a** (102.72(4)° vs. 105.87(6)°), these trends have been noted in similar compounds when changing from S→Se→Te.¹⁷

Given the analysis by Roy *et al.* on the coordination characteristics of the ITr ligand, it was thought that the SCXRD data might be able to provide some insight as to whether the trityl rings in the ligand were coordinating to the *d*¹⁰ metal centre in these metallochalcogenolates.²⁶ The data available for [(ITr)CuI], the most comparable complex whose molecular structure was reported, suggested intramolecular contacts

between the aryl rings and the copper centre consistent with η_2 coordination on either aryl ring (see **Figure S2.1**).²⁶ For both [(ITr)CuSSiMe₃] (**2.2a**) and [(ITr)CuSeSiMe₃] (**2.3a**), contacts with a distance less than the sum of the Van der Waals radii ($\Sigma_{C-Cu} = 3.1\text{\AA}$) were found between carbons of opposing trityl rings and the copper centre (see **Figure 2.6** and **Figure 2.7**). On both **2.2a** and **2.3a**, the trityl group *cis* to the –SiMe₃ group showed a contact via the *ipso* carbon, (Cu1–C17 = 3.030(3) Å for **2.2a**; 3.004(4) Å for **2.3a**) while the ring *trans* to the –SiMe₃ group showed contact to the *ortho* carbon (Cu1–C41 = 3.005(4) Å for **2.2a**; 2.969(5) Å for **2.3a**). Comparing structural details between [(ITr)CuI], **2.2a** and **2.3a**, it was found that the compounds in this work displayed more acute R – N – C_{NHC} bond angles, despite having shorter Cu – X (X = I, –ESiMe₃) contacts and effectively pulling the –SiMe₃ moiety closer to the trityl groups. In response, it was noted that the copper centre in **2.2a** and **2.3a** was biased away from the –SiMe₃ group, and these conformational changes likely culminated to disrupt η_2 interactions otherwise possible in these compounds. The effect was exacerbated on changing the chalcogen in [(ITr)CuESiMe₃] from S → Se, likely due to a more acute Cu – E – Si bond angle. Although DFT calculations would be required to confirm these observations, the presence of longer contacts between the copper centre and other carbon atoms ($0.3\text{\AA} \geq \Sigma_{C-Cu}$) suggested that the η_2 interactions present in [(ITr)CuI] may have been interrupted in **2.2a** and **2.3a** due to steric hindrance on coordination of [(ITr)Cu]⁺ to –ESiMe₃ (see **Figure S2.1**).

The structural data of **2.2a** · 1.25 THF and **2.3a** · 1.25 THF were compared to those for [IPrCuESiMe₃], as the compounds of this work were only a second example of imidazole–2–ylidene stabilized cuprachalcogenolates whose structural data is reported.^{17–19} As can be seen in **Figure 2.8**, the molecular structure of [(IPr)CuSSiMe₃]·THF (**2.Ia**), which crystallized in the C2/c space group, featured the molecule with the –ESiMe₃ group in the same plane as the imidazole backbone; this was not the case for the compounds of this work.¹⁸ Conversely, crystals of [(IPr)CuSSiMe₃]·PhMe (**2.IIa**) exhibited molecules in a similar conformation and space group ($P\bar{1}$) as [(ITr)CuESiMe₃] · 1.25 THF (see **Figure 2.8**).³⁹ Thus, the structural details of **2.2a** and **2.IIa** were compared, despite having different solvent and solvent effects. Summarized in **Figure 2.9**, the SCXRD data of **2.IIa** and **2.2a** suggested longer S – Si, Cu – S, C_{NHC} – Cu and C_{NHC} – N bonds for the latter, with only one of the two C_{NHC} – N bonds showing a statistically significant increase.^{17,39} Additionally, the copper atom was more skewed in its coordination to ITr than it was to IPr, likely due to the excessive steric bulk from the trityl groups. Despite all this, **2.2a** displayed more acute R – N – C_{NHC} bond angles, which could be rationalized by the propensity for the trityl groups to coordinate to the copper centre. These structural changes observed were not shown to occur when comparing the molecular structures of [IPrCuX] (X = I, OAc, ESiMe₃), suggesting that the structural differences in this comparison were the result of the different NHCs and their effect^{17,28,39,44} As such, they

are thought to be consistent with the propensity of the trityl groups to sit closer to the metal centre, given the proposed arene – M interactions in the compounds of this work. Similar structural differences were also observed between [(ITr)CuSeSiMe₃] · 1.25 THF (**2.3a**) and [(IPr)CuSeSiMe₃] · THF (**2.IIIa**), however, these comparisons are made more carefully given the conformational difference between these compounds and their differing space groups (**2.3a** = $P\bar{1}$, **2.IIIa** = $C2/c$).

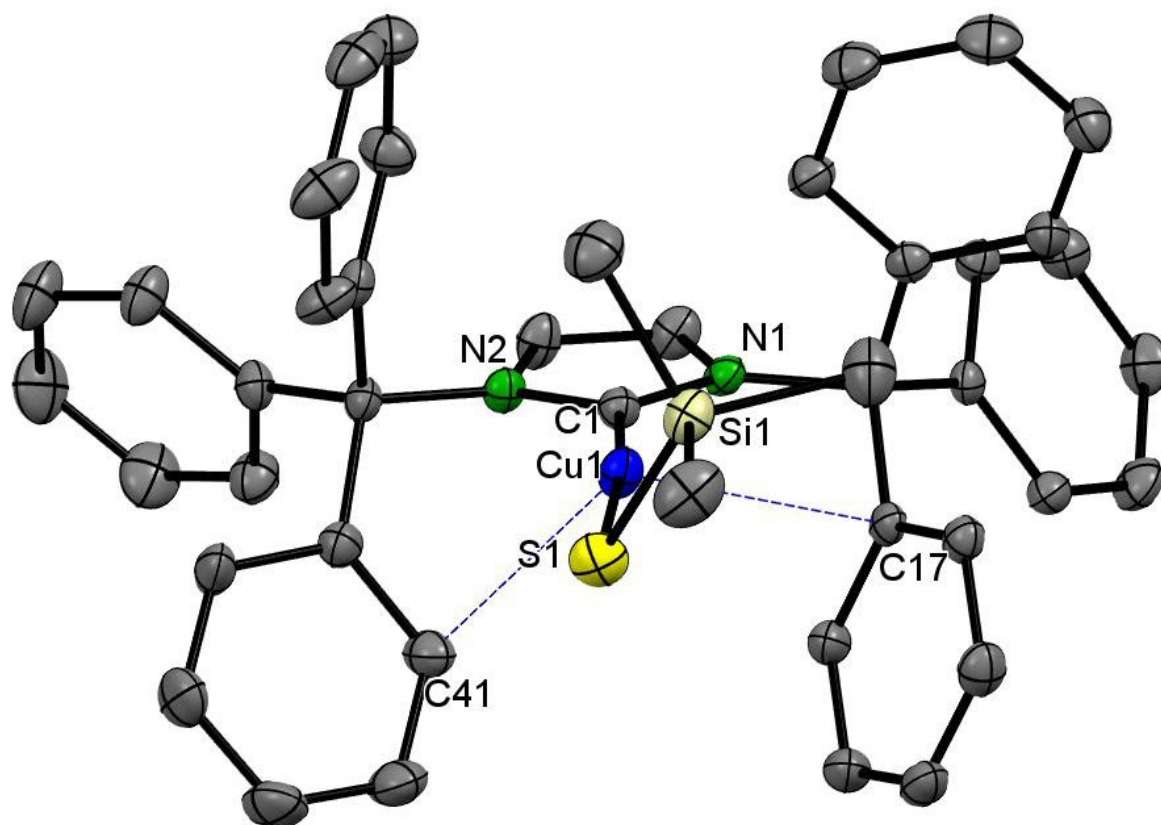


Figure 2.6: ORTEP ellipsoid plot of [ITrCuSSiMe₃] (**2.2a**) at 50% probability level. Nitrogen (green), copper (blue), silicon (beige), sulfur (yellow) are colored for emphasis. Hydrogens and solvent molecules omitted for clarity. Intramolecular contacts ($<\Sigma_{VDW}$) shown in blue. Selected bond lengths and angles: Cu1–S1: 2.152(1) Å; S1–Si1: 2.111(2) Å; C17 – Cu1: 3.030(3) Å; C41–Cu1: 3.005(4) Å; Cu1–S1–Si1: 105.87(6)°; C1–Cu1–S1: 172.6(1)°; Cu1–C1–N1: 130.4(2)°; Cu1–C1–N2: 125.1(2)°.

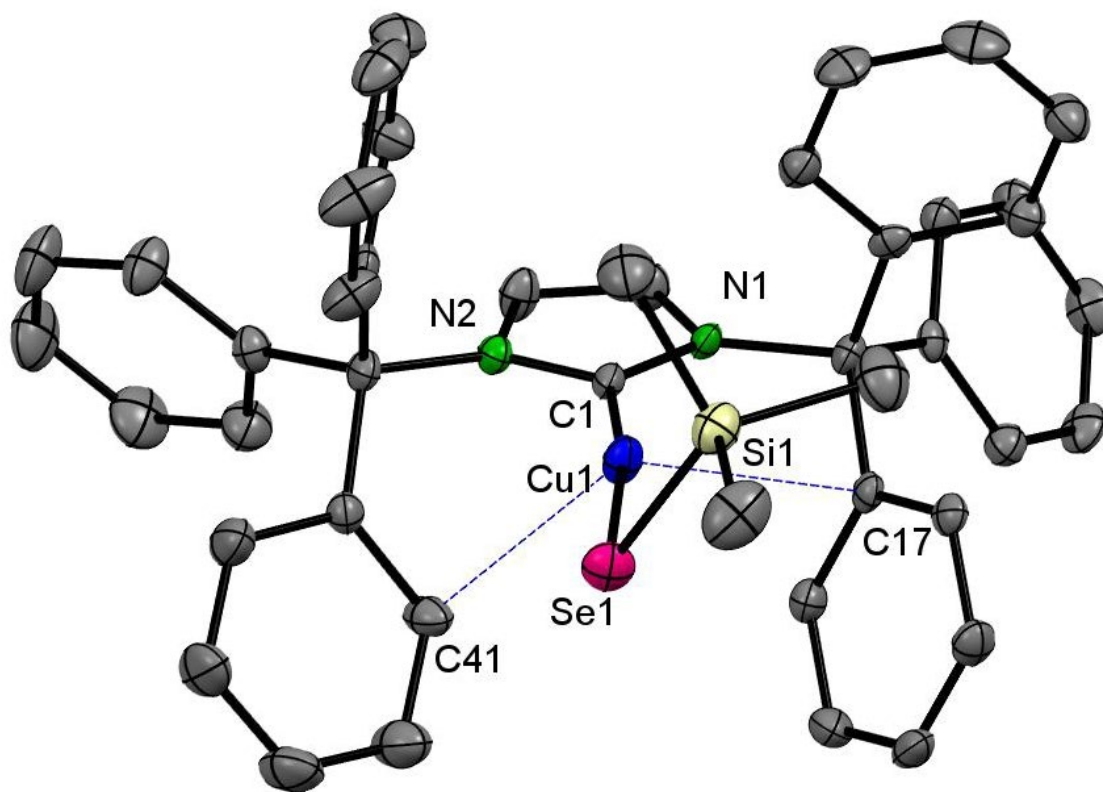


Figure 2.7: ORTEP ellipsoid plot of [ITrCuSeSiMe₃] (**2.3a**) at 50% probability level. Nitrogen (green), copper (blue), silicon (beige), and selenium (red) are colored for emphasis. Hydrogens and solvent molecules omitted for clarity. Intramolecular contacts ($<\Sigma_{VDW}$) shown in blue. Selected bond lengths and angles: Cu1–Se1: 2.2656(7) Å; Se1–Si1: 2.265(1) Å; C17 – Cu1: 3.004(4) Å; C41–Cu1: 2.969(5) Å Cu1–Se1–Si1: 102.72(4)°; C1–Cu1–Se1: 171.3(1)°; Cu1–C1–N1: 130.0(3)°; Cu1–C1–N2: 125.8(8)°.

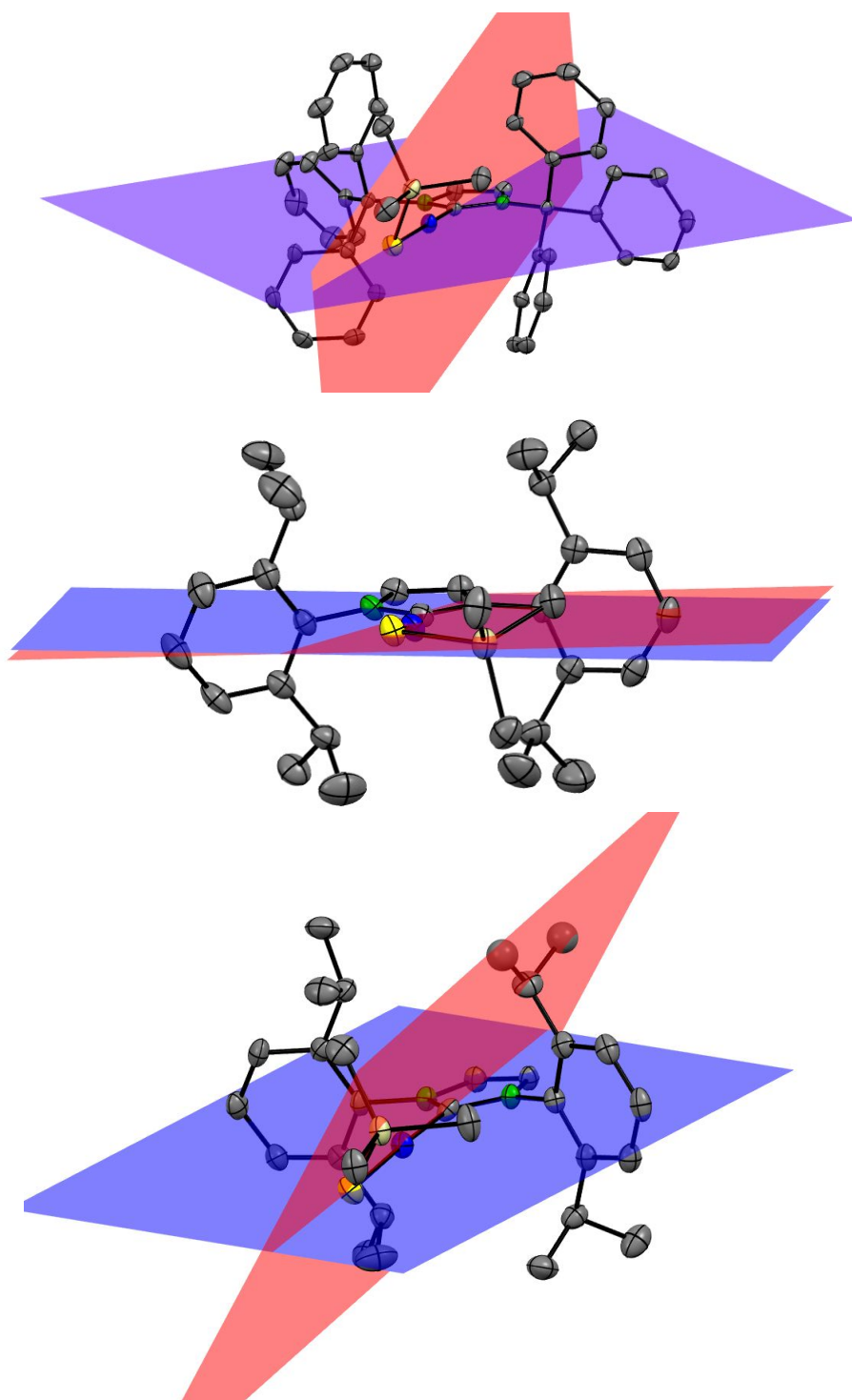
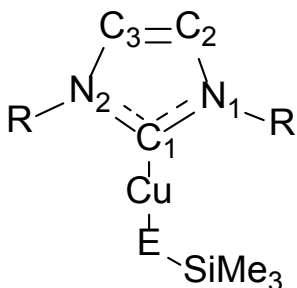


Figure 2.8: Differences in orientation of $-\text{SSiMe}_3$ about the imidazole ring in $[\text{ITrCuSSiMe}_3]$ (**2.2a**, top), $[\text{IPrCuSSiMe}_3] \cdot \text{THF}$ (**2.Ia**, middle) and $[\text{IPrCuSSiMe}_3] \cdot 0.25 \text{ PhMe}$ (**2.IIa**, bottom). Plane of the ring highlighted in blue and plane of Cu–S–Si drawn in red.¹⁷



	2.2a	2.IIa	$\Delta_{2.2a-2.IIa}$	2.3a	2.IIIa	$\Delta_{2.3a-2.IIIa}$
	E = S	E = S		E = Se	E = Se	
N₁ – R (Å)	1.501(4)	1.442(5)	+0.059	1.492(6)	1.442(2)	+0.050
N₂ – R (Å)	1.499(4)	1.440(5)	+0.059	1.503(5)	1.442(2)	+0.061
C₁ – N₁ (Å)	1.359(4)	1.335(6)	+0.024	–	–	–
C₁ – Cu (Å)	1.917 (4)	1.872(6)	+0.045	1.913(4)	1.884(1)	+0.029
Cu – E (Å)	2.152(1)	2.120(2)	+0.032	2.2656(7)	2.2431(7)	+0.0225
E – Si (Å)	2.111(2)	2.082(2)	+0.029	2.265(1)	2.2502(7)	+0.0148
C₁ – Cu – E (°)	172.6(1)	176.5(2)	–3.9	171.3(1)	170.68(5)	+0.6
Cu – E – Si (°)	105.87(6)	98.27(7)	+7.6	102.72(4)	100.42(2)	+2.3
C₃ – N₂ – R (°)	127.0(3)	123.8(4)	+3.2	127.2(3)	124.8(1)	+2.4
C₂ – N₁ – R (°)	127.5(3)	123.9(4)	+3.6	127.7(3)	125.2(1)	+2.5
R – N₁ – C₁ (°)	121.8(3)	123.8(4)	–2.0	–	–	–
R – N₂ – C₁ (°)	121.5(3)	125.3(4)	–3.8	121.0(3)	123.6(1)	+2.6
N₁ – C₁ – Cu (°)	130.4(2)	128.6(4)	+1.8	130.3(3)	131.4(6)	–1.1
N₂ – C₁ – Cu (°)	125.2(2)	127.4(4)	–2.2	125.8(3)	124.6(1)	+1.2

Figure 2.9: Diagram and table of structural differences that are statistically significant in select bond lengths and bond angles between [IPrCuESiMe₃] (E = S, **2.IIa**; Se, **2.IIIa**) and [ITrCuESiMe₃] (E = S, **2.2a**; Se, **2.3a**). Note that **2.IIa** is the toluene solvate, and **2.IIIa** is the THF solvate (see text)

The shorter $C_{\text{NHC}} - \text{Cu}$ bonds in the IPr-stabilized metallocalcoenolates suggested a stronger σ – bond in these compounds, despite all other indication that ITr was the better electron donor.^{17,39} Therefore, a second method was used to compare the σ -donor effect of ITr and IPr by comparing the $^1J_{\text{C-H}}$ coupling constants for the imidazolium salts of the two NHCs, as this information was recently shown to correlate to the σ -donating ability of the respective NHC ligand (see Experimental).⁴⁵ By this method, the ITr ligand was found to be a marginally better σ -donor than IPr, given a smaller $^1J_{\text{C-H}}$ constant (218.8 Hz vs. 223.7 Hz) correlated to less s character in the $\text{C-H}_{\text{imidazolium}}$ bond of ITr·HOTf than IPr·HCl.⁴⁵ With a more sp^2 like lone pair, this suggested that ITr should be a stronger σ -donor than IPr and the statistical differences in the structures compared were opposite to what would be expected (see **Figure 2.9**). The longer $C_{\text{NHC}} - \text{Cu}$ bonds in [(ITr)CuESiMe₃] may have been due to the presence of arene – M interactions mitigating σ – donation, but a quantum chemical investigation would be required to better understand the electronic differences between the two classes of compounds.

2.2.3 UV–VIS Absorption Spectra of [ITrMOAc] and [ITrMESiMe₃]

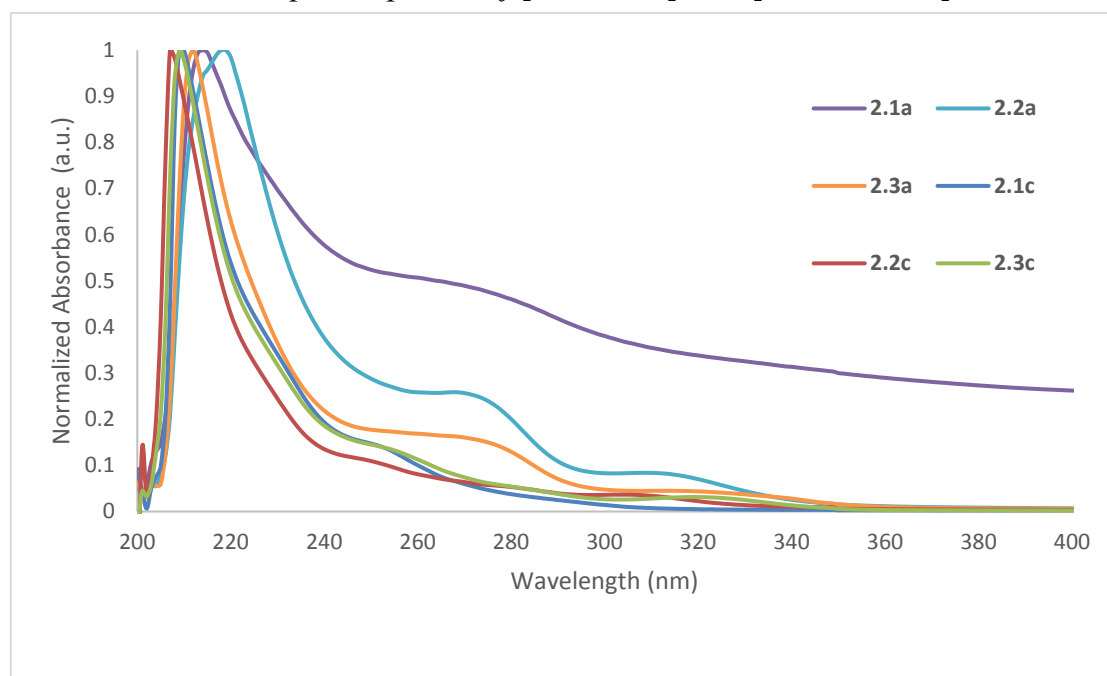


Figure 2.10: UV– VIS Absorption spectra of [ITrMOAc] and [ITrMESiMe₃]. Graph is focused on 200 – 400 nm range and the absorbance has been normalized. All spectra acquired in 0.6 mM solution in tetrahydrofuran at 25 °C.

The UV–VIS absorption spectra were obtained for the copper (**2.1a – 2.3a**) and gold (**2.1c – 2.3c**) compounds in dilute THF solution at room temperature; **2.1b – 2.3b** were too unstable for comparison at room temperature. In all the compounds analyzed, an absorption maximum ca. 210 – 220 nm was observed and assigned to intraligand $\pi \rightarrow \pi^*$ transitions on the ITr backbone, given their presence and limited

difference in wavelength as a function of the identity of the metal and the chalcogen/acetate ligand. [(ITr)CuX] (X = OAc, **2.1a**; SSiMe₃, **2.2a**; SeSiMe₃, **2.3a**) showed an absorption maximum at ~272 nm, with a hypsochromic shift to ~253 nm for [(ITr)AuX] (X = OAc, **2.1c**; SSiMe₃, **2.2c**; SeSiMe₃, **2.3c**). Thus, these peaks were assigned to the ¹MLCT state with the understanding that a similar transition in the UV–VIS spectrum of [IPrCuCl] was assigned at 310 nm in acetonitrile; it was determined that the ligand (–Cl, –OAc or –ESiMe₃) could have a pronounced effect on the energy of this transition in Cu(I) complexes.⁴⁶ Though comparable spectroscopic data on the IPr family of compounds is not known in literature, Polgar showed that a similar transition existed for the CAAC^{Cy} copper acetate and chalcogenolates (ca. 290 nm) that were red shifted relative to the maxima in this work; the assignment of these transitions are made in comparison to those made by Polgar, bearing in mind the improved π accepting properties of cyclic alkyl amino carbenes.^{41,43} The absorption bands at ~310 – 320 nm were assigned to ¹XLCT(AcO[–]/Me₃SiE[–]→ITr) given their similarity to the maxima observed by Polgar for the CAAC^{Cy} cuprachalcogenolates (ca. 330 – 350 nm). This assignment was consistent with the minimal change in the absorption maxima as a function of the metal and the blueshifting observed as a function of the heavier chalcogen.^{41,43} Additionally, the hypsochromic shift of these bands relative to those observed in the CAAC^{Cy} family of compounds was consistent with the assignment of the transition, given the weaker π accepting character of ITr in comparison to CAAC^{Cy}.^{41,43}

2.3 Conclusions

In conclusion, the syntheses of ITr stabilized metal acetates has been described and their use for the syntheses of ITr stabilized group 11 metallochalcogenolates has been developed. A more rigorous study of the NMR data suggested that ITr may be an example of an NHC with a smaller HOMO–LUMO gap than imidazole–2–ylidenes previously used, though there have been no subsequent implications on the preparation of metallochalcogenolates with this type of ligand. Indeed, the propensity for this NHC to donate electron density has been determined by previous experiments measuring the TEP of the ligand and by work here measuring the ¹J_{C–H} coupling constant from ¹H NMR spectroscopic data.^{26,45} By an analysis of the NMR spectra and SCXRD data for the cuprachalcogenolates, the electron richness of the metal centre relative to previously synthesized NHC–metallochalcogenolates has been established; further quantum chemical calculations would be required to provide a definitive answer on whether there existed π donation between the phenyl rings and the copper centre, though preliminary data suggests a propensity for the R–groups of this ligand to swing toward the metal centre.^{17–19,26,45} The changes in the coordination environment of the ITr metallochalcogenolates differs from their predecessors by the inclination to direct

the R groups toward the metal centre and the swinging of the trimethylsilyl group out of the plane of the imidazole backbone.¹⁷ While the structural implications on the electronic differences between ITr and IPr metallochalcogenolates require a more rigorous quantum chemical investigation, there existed no analogous UV – VIS absorption data against which to compare the spectra obtained in this work. In general, assignment of the electronic transitions involved was possible by comparison to CAAC^{Cy} stabilized copper complexes like the work herein.²⁰ Given the more π accepting nature of CAAC ligands, the $M \rightarrow \text{NHC}$ transitions were hypsochromically shifted in this work and it remains to be seen how the proposed smaller HOMO – LUMO gap ultimately would affect the transitions in IPr stabilized metallochalcogenolates.

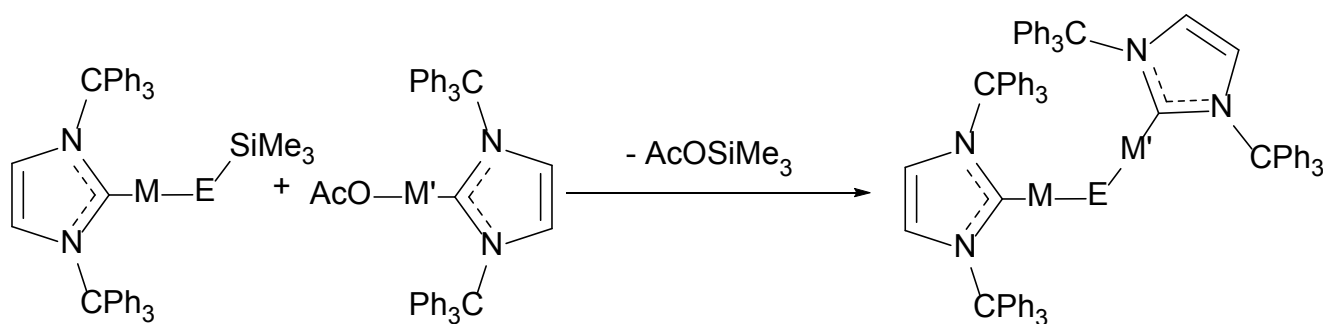


Figure 2.11: Proposed reactions for syntheses of heterometallic group 11 metal chalcogenide molecular frameworks.

Future work regarding the synthesis and characterization of these compounds could be taken in many directions. In the attempt to understand this growing library of trimethylsilyl metallochalcogenolates, quantum chemical investigations on the compounds of this work, the IPr trimethylsilyl metallochalcogenolates, the CAAC^{Cy} cuprachalcogenolates and the iPr–bimy metallochalcogenolates would cement the understanding of the electronic nature of these ligands and perhaps shed light on the effects, if any, the NHC has on the trimethylsilylchalcogenolate groups.^{17–20} Ultimately, this growing knowledge base would help to direct future uses of these compounds. Given the sterically and (arguably) electronically stabilized group 11 metal centre in this ITr family of compounds, future work should be conducted toward the use of these compounds as reagents for heterometallic metal chalcogenide molecular frameworks. The compounds can be reacted with metal acetates to probe the effect of the NHC on the structure of the cluster obtained, per the work of Polgar et al. .^{19,20} Additionally, they hold the potential to access hitherto unmade heterometallic chalcogenide frameworks, extending beyond the group 11 metals. Work in the group has attempted to use this class of compounds in reactions with various BiX₃ salts, ultimately finding ligand transfer to be a puzzling concern with all but the aurachalcogenolates. While

further work was done on the development of these compounds, some unexpected results prompted a different research direction, investigating the synthesis of heterometallic binuclear group 11 chalcogenide complexes using the compounds synthesized above as synthons toward these structures. The reagents herein were ideal for this synthetic target, given the pendant E–SiMe₃ bonds which could be reactive towards the acetate moiety, using the same thermodynamic driving force that made these compounds to drive the reaction between them to completion. While it was not known whether the ITr ligand was sterically encumbering enough to protect the final products, the next chapter of this thesis describes attempts toward the synthesis of these heterometallic molecular chalcogenides using the ITr stabilized trimethylsilylmetallochalcogenolates.

2.4 Experimental

2.4.1 General Considerations

All syntheses described were carried out using standard double-manifold Schlenk-line techniques, under an atmosphere of high-purity dry nitrogen. Non-chlorinated solvents (tetrahydrofuran, toluene, hexanes, pentane) were dried and collected using an MBraun MB-SP Series solvent purification system and stored over 3 Å molecular sieves. Tetrahydrofuran was often degassed further by three to five freeze-pump-thaw cycles just prior to use. Deuterated chloroform and deuterated benzene were purchased from Caledon and dried over P₂O₅ and NaK alloy respectively, refluxing under N₂ prior to collecting by distillation. Celite® was dried under dynamic vacuum at 220°C for 24 hours and stored under nitrogen in a sealed flask. Many chemicals required for the syntheses of starting materials were used as received from commercial sources (Alfa Aesoar, Sigma Aldrich, Caledon). S(SiMe₃)₂, Se(SiMe₃)₂, Li[SSiMe₃], Li[SeSiMe₃], CuOAc, trityl imidazole, trityl triflate, [THTAuCl] (THT = tetrahydrothiophene), ITrHOTf and [ITrAuCl] were made according to previous literature preparations, with slight modifications for ITrHOTf and [ITrAuCl].^{4,19,26,47} For ITrHOTf, isolation of the imidazolium salt was done under inert conditions, pipetting away the benzene mother liquor and washing the insoluble yellow precipitate three times with fresh benzene, followed by three washes with hydrocarbons before drying *in vacuo* and storing in a glovebox under nitrogen atmosphere. The synthesis of ITrAuCl was adapted from a previous work, mixing ITr and THTAuCl in a toluene solution overnight, evacuating to dryness and triturating in hydrocarbon to obtain a white solid that was stored in a glovebox refrigerator at –40 °C.

All NMR spectra were recorded on Inova 400 and Inova 600 spectrometers. ^1H and $^{13}\text{C}\{^1\text{H}\}$ NMR chemical shifts are reported relative to SiMe_4 at 25 °C using either the residual solvent signals or silicone grease as internal references. Heteronuclear Multiple Bond Correlation Experiments were performed for $^{13}\text{C}\text{--}^1\text{H}$ to confirm peak assignments or to improve signal to noise for the detection of carbenic carbons. Elemental Analysis was conducted by Saint Mary's University (Halifax, NS, Canada) with samples being dried *in vacuo* for at least 8 hours prior to shipment.

Solution state UV–VIS absorption spectroscopy was conducted on a Cary 5000 instrument with solutions being prepared in a glovebox and transferred to quartz cuvette with a Teflon cap. All samples were scanned between 200 to 1000 nm at a 2 nm/s scan rate. The spectra displayed in this work were normalized to the highest absorption peak.

Samples of $[(\text{ITr})\text{CuSSiMe}_3]\cdot 1.25 \text{ THF}$ (**2.2a**) and $[(\text{ITr})\text{CuSeSiMe}_3]\cdot 1.25 \text{ THF}$ (**2.3a**) for SCXRD experimental analysis were submitted to the X–Ray Facility at Western University. The respective sample was mounted on a Mitegen polyimide micromount with a small amount of Paratone N oil. All X–ray measurements were made on a Bruker Kappa Axis Apex2 diffractometer at a temperature of 110 K. The unit cell dimensions of **2.2a** were determined from a symmetry constrained fit of 9927 reflections with $5.0^\circ < 2\theta < 54.88^\circ$ and the dimensions for **2.3a** were determined from a symmetry constrained fit of 9964 reflections with $4.58^\circ < 2\theta < 55.24^\circ$. The data collection strategy was a number of w and j scans which collected data up to 56.734° (2θ) for **2.2a** and 50.0° (2θ) for **2.3a**. The frame integration was performed using SAINT.⁴⁷ The resulting raw data were scaled, and absorption corrected using a multi–scan averaging of symmetry equivalent data using TWINABS for **2.2a** and SADABS for **2.3a**.^{48–49} For **2.2a**, only the major component of a non–merohedrally twinned data was used for structure refinement.

The structures were solved by using a dual space methodology using the SHELXT program.⁵⁰ All non–hydrogen atoms were obtained from the initial solution. The hydrogen atoms were introduced at idealized positions and were allowed to ride on the parent atom. The structural model was fit to the data using full matrix least–squares based on F^2 . The calculated structure factors included corrections for anomalous dispersion from the usual tabulation. The structure was refined using the SHELXL program from the SHELXTL suite of crystallographic software.⁵¹ Graphic plots were produced using the NRCVAX program suite.⁵²

2.4.2 Synthesis

Synthesis of ITrCuOAc(2.1a) – In a Schlenk tube, ITrHOTf (0.98 g, 1.39 mmol) and KHMDS (0.29 g, 1.45 mmol) were stirred in 45 mL of toluene for 24 hours, producing a pale–yellow slurry with white precipitate. The reaction mixture was filtered through a ~3 cm plug of Celite and dropped into a collection flask charged with CuOAc (0.18 g, 1.42 mmol) and stir bar. The clear yellow solution began to produce white precipitate within 5 – 10 minutes of stirring. 100 mL of THF was added to remove turbidity in the solution, and the mixture was stirred for one hour. The solution was filtered through Celite once more, to remove unreacted starting material, then evacuated to dryness to produce an off white – yellow powder. Pure white product was obtained by stirring the product in hydrocarbons overnight, pipetting off the mother liquor and washing thrice in hydrocarbon (61% **yield**); **M.p** 176 – 178 °C (decomp). ¹H NMR (CDCl₃, 399.76 MHz, 25 °C): δ 7.19 – 7.32 (m, 30 H, ArH), δ 6.97 (s, 2H, NCH), δ 1.42 ppm (s, 3H, OAc); ¹³C{¹H} NMR (CDCl₃, 100.53 MHz, 25 °C): δ 186.2 (NCN), δ 176.2 (C = O, OOCCH₃), δ 142.3 (ArC), δ 129.9 (ArC), δ 128.2 (ArC), δ 128.0 (ArC), δ 120.9 (NCH), δ 78.1 (CPh₃), δ 24.2 ppm (CH₃, OOCCH₃). **Anal. Calc'd for C₄₃H₃₅CuN₂O₂**: C, 76.48; H, 5.22; N, 4.15.; **Found** C, 75.10; H, 5.09; N, 4.07. λ_{max} : 215 nm ($\epsilon = 2365 \text{ cm}^{-1} \text{ M}^{-1}$); 275 nm ($\epsilon = 1133 \text{ cm}^{-1} \text{ M}^{-1}$).

Synthesis of ITrCuSSiMe₃(2.2a) – In a Schlenk tube charged with **2.1a** (0.032g, 0.0474 mmol), 2.2 mL of CHCl₃ was added and the clear, pale yellow – green solution was cooled to –20 °C. After cooling for 5 – 10 minutes S(SiMe₃)₂ (0.01 mL, 0.0474 mmol) was added and the reaction stirred at this temperature for one hour. The product was often generated *in situ* using these reaction conditions; when isolated, the solvent was removed at –10 °C *in vacuo* and the remaining beige – white product was washed in hydrocarbons with three aliquots at room temperature (0.016g, 46% **yield**). It was also found the product was stable at –25 °C while in solution, and as such could be generated by addition of S(SiMe₃)₂ at any temperature ≤ -20 °C, followed by storage in a freezer at –25 °C overnight. Crystals suitable for SCXRD experiments were grown by layering a THF solution with pentane ~3 times the volume of the reaction mixture. **M.p**: 183 – 187 °C ; ¹H NMR (CDCl₃, 600 MHz, 25 °C): δ 7.26 – 7.30 (m, 18H, m,p –ArH), δ 7.21 – 7.25 (o, 12H, m – ArH), δ 6.87 (s, 2H, NCH), δ –0.35ppm (s, 9H, SiMe₃); ¹³C{¹H} NMR (CDCl₃, 150.90 MHz, 25 °C): δ 189.9 (NCN), δ 142.5 (ArC), δ 130.0 (ArC), δ 128.0 (ArC), δ 128.0 (ArC), δ 127.9 (ArC), δ 120.2 (NCH), δ 77.8 (CPh₃), δ 6.5 ppm (SiMe₃). λ_{max} : 219 nm ($\epsilon = 3354 \text{ cm}^{-1} \text{ M}^{-1}$); 268 nm ($\epsilon = 868 \text{ cm}^{-1} \text{ M}^{-1}$); 315 nm ($\epsilon = 268 \text{ cm}^{-1} \text{ M}^{-1}$).

Synthesis of ITrCuSeSiMe₃(2.3a) – To a Schlenk tube charged with stir bar **2.1a** (0.101g, 0.150 mmol), 7 mL of CHCl₃ was added, and the clear yellow solution was cooled to –45 °C. Se(SiMe₃)₂ (0.04 mL,

0.160 mmol) was added to the stirring solution and the reaction mixture was warmed to $-20\text{ }^{\circ}\text{C}$. After stirring for 1 hour between $-20\text{ }^{\circ}\text{C}$ to $-10\text{ }^{\circ}\text{C}$, the reaction mixture was evacuated at $-10\text{ }^{\circ}\text{C}$, to isolate a white – beige powder. The product was washed thrice in 10 mL aliquots of hexane. Analysis of the residue left behind in the mother liquor and the final product confirm the presence of only the final product (0.047g, 42% **yield**). Crystals suitable for SCXRD were grown by layering a THF solution with pentane at ~ 3 times the volume and storing in freezer overnight at $-25\text{ }^{\circ}\text{C}$. **M.p.** 164 – 166 $^{\circ}\text{C}$. **^1H NMR (CDCl_3 , 399.76 MHz, 25 $^{\circ}\text{C}$):** δ 7.26 – 7.33 (m, m,p – ArH, 18H), δ 7.21 – 7.25 (m, o – ArH, 12H), δ 6.88 (s, NCH, 2H), δ -0.19 ppm (s, SiMe_3 , 9H). **$^{13}\text{C}\{^1\text{H}\}$ NMR (CDCl_3 , 100.53 MHz, 25 $^{\circ}\text{C}$):** δ 190.2 (NCN), δ 142.7 (ArC), δ 130.2 (ArC), δ 128.2 (ArC), δ 128.0 (ArC), δ 119.5 (NCH), δ 77.9 (CPh_3), δ 7.13 ppm (SiMe_3). λ_{max} : 212 nm ($\epsilon = 2470\text{ cm}^{-1}\text{ M}^{-1}$); 271 nm ($\epsilon = 392\text{ cm}^{-1}\text{ M}^{-1}$); 318 nm ($\epsilon = 110\text{ cm}^{-1}\text{ M}^{-1}$).

Synthesis of ITrAgOAc (2.1b) – An 11 mL solution of freshly prepared ITr in toluene (0.234g, 0.423 mmol) was added by L – joint to a Schlenk tube charged with a stir bar and AgOAc (0.0735g, 0.440 mmol) with an additional 2 mL toluene to wash ITr into reaction flask. The 13 mL clear yellow solution was left stirring at room temperature. Within 30 – 40 minutes of stirring, the solution became turbid. 20 mL of THF was added to get a clear, yellow solution which was filtered through Celite to get a pale–yellow solution. The total reaction time from the moment of ITr addition to the moment of filtration through Celite was 2.5 hours. The filtrate was evacuated to dryness to get a white powder, caked with a yellow, oily impurity. The product was recrystallized by layering a 10 mL THF solution with 25 mL hexanes and storing at room temperature for two days. The white crystalline solid was isolated and washed with 10 mL pentane. The mother liquor was collected and evacuated to dryness to obtain an additional crop of off – white to yellow product (as confirmed by ^1H NMR) which was also washed in 10 mL pentane. The crystalline powder (0.080g) was used for subsequent analysis, however reactions were successfully conducted with solids isolated from mother liquor (0.110g, total yield: 0.190g, 63% **yield**). **M.p.** 182 $^{\circ}\text{C}$ (decomp.) **^1H NMR (CDCl_3 , 399.76 MHz, 25 $^{\circ}\text{C}$):** δ 7.26 – 7.32 (m,p – ArH, 18H), δ 7.18 – 7.25 (o – ArH, 12H), δ 7.03 (s, NCH, 2H), δ 1.63 (s, OAc, 3H). **$^{13}\text{C}\{^1\text{H}\}$ NMR (CDCl_3 , 100.53 MHz, 25 $^{\circ}\text{C}$):** δ 193.3 (d, $^1J_{\text{C-Ag}} = 271\text{ Hz}$, NCN), δ 176.5 (C = O, OAc), δ 142.4 (ArC), δ 130.1 (ArC), δ 128.2 (ArC), δ 128.1 (ArC), δ 120.7 (NCH), δ 78.4 (CPh_3), δ 23.4 ppm (CH_3 , OAc). **Anal. Calc'd for $\text{C}_{43}\text{H}_{35}\text{AgN}_2\text{O}_2$:** C, 71.77; H, 4.90; N, 3.89; **Found:** C, 71.24; H, 4.68; N, 3.81.

Synthesis of ITrAgSSiMe₃ (2.2b) – To a Schlenk tube charged with a stir bar and **2.1b** (0.105g, 0.146mmol), 6 mL of THF was added to obtain a clear, yellowish – brown solution which was cooled to $-70\text{ }^{\circ}\text{C}$. Upon cooling, $\text{S}(\text{SiMe}_3)_2$ (0.032 mL, 0.153 mmol) was added and the mixture was warmed to

–30 °C and stirred for one hour. 18 mL of heptane was cooled to –30 °C and the white slurry evacuated at low temperature to concentrate. The mother liquor was decanted and the white solid evacuated to dryness *in vacuo*. (0.034g, 30% **yield**). Crystals could be grown as colourless needles by layering a THF solution of the product with ~ 3 times the volume in hexanes and storing at –25 °C. **M.p.** 165 – 167 °C. **¹H NMR (CDCl₃, 399.76 MHz, –30 °C):** δ 7.27 – 7.34 (m, p-ArH, 18H), δ 7.15 – 7.22 (o – ArH, 12H), δ 6.96 (s, NCH, 2H), δ –0.32 ppm (s, SiMe₃), 9H). **¹³C{¹H} NMR (CDCl₃, 100.53 MHz, –30 °C)** δ 142.4 (ArC), δ 130.1 (ArC), δ 128.1 (ArC), δ 128.0 (ArC), δ 119.9 (NCH), δ 77.8 (CPh₃), δ 6.8 (SeSiMe₃) ppm.

Synthesis of ITrAgSeSiMe₃ (2.3b) – To a Schlenk tube charged with a stir bar and **2.1b** (0.112g, 0.156mmol), 6 mL of THF was added and the yellow solution cooled to –78° C. Se(SiMe₃)₂ (0.04 mL, 0.160mmol) was added and the solution was allowed to warm to –30 °C and stirred for 1 hour at this temperature. 18 mL of heptane was cooled to –30 °C and the white slurry evacuated at low temperature to concentrate. The mother liquor was separated from the yellow precipitate and evacuated at low temperature to yield the off – white solid. (0.032g 25% **yield**). **M.p.** 162 – 167 °C. **¹H NMR (CDCl₃, 399.76 MHz, –30 °C):** δ 7.25 – 7.36 (m,p-ArH, 18H), δ 7.16 – 7.24 (o – ArH, 12H), δ 6.96 (s, NCH, 2H), δ –0.16 ppm (s, SiMe₃), 9H). **¹³C{¹H} NMR (CDCl₃, 100.53 MHz, –30 °C)** δ 142.3 (ArC), δ 130.1 (ArC), δ 128.2 (ArC), δ 128.1 (ArC), δ 120.0 (NCH), δ 77.8 (CPh₃), δ 7.5ppm (SeSiMe₃) .

Synthesis of ITrAuOAc (2.1c) – To a Schlenk tube charged with ITrAuCl²⁶ (0.202g, 0.257 mmol) and a stir bar, 7 mL of CH₂Cl₂ and the solution was transferred to a Schlenk tube charged with a stir bar and AgOAc (0.0452g, 0.271 mmol). The reaction mixture was stirred in the dark for ~ 2 hours at room temperature and then filtered through Celite. The reaction flask was washed with 2 x 5mL of CH₂Cl₂ and the Celite pad washed once with 5 mL of CH₂Cl₂. The filtrate was concentrated *in vacuo* and 20 mL of heptane was added to induce precipitation. To complete precipitation of the product and avoid oiling of the solids, the CH₂Cl₂/heptane mixture was evacuated, allowing the more volatile chlorinated solvent to be evaporated more quickly and ultimately precipitating the desired product. The mother liquor was decanted, product washed in pentanes and evacuated to dryness yielding a grey – white powder (0.139g, 67 % **yield**). **M.p.** 120 °C (decomp). **¹H NMR (CDCl₃, 399.76 MHz, 25 °C)** δ 7.26 – 7.33 (m, m,p – ArH, 18H), δ 7.18 – 7.25 (o – ArH, 12H), δ 6.99 (s, NCH, 2H), δ 1.37 ppm (OOCCH₃, 3H). **¹³C{¹H} NMR (CDCl₃, 100.53 MHz, 25 °C):** δ 176.6 (OOCCH₃), δ 175.7 (NCN), δ 142.1 (ArC), δ 130.5 (ArC), δ 128.1 (ArC), δ 128.0 (ArC), δ 120.2 (NCH), δ 78.9 (CPh₃), δ 24.6 ppm (OOCCH₃). **λ_{max}:** 210 nm (ε = 1566 cm⁻¹ M⁻¹); 252 nm (ε = 221 cm⁻¹ M⁻¹).

Synthesis of ITrAuSSiMe₃ (2.2c) & ITrAuSeSiMe₃ (2.3c) – The syntheses of these compounds was inspired by the work of Polgar *et al.*.¹⁹ A solution of Li[ESiMe₃] was prepared in THF by addition of *n*-butyllithium to a solution of E(SiMe₃)₂ at 0 °C, stirred for 30 minutes and then warmed to room temperature and stirred for an additional 30 minutes.⁴ After cooling back down to –30 °C, a THF solution of ITrAuCl was added dropwise to and the mixture allowed to stir at room temperature for 4 hours. The mixture was evacuated to dryness, taken up in toluene and filtered through Celite. The solution was concentrated to a minimal volume and the product precipitated by addition of hexanes. The mother liquor was removed/decanted, and the product evacuated to dryness. Data for **2.2c** (E = S): **yield**, 83%. **M. p.** 194 – 196 °C. **¹H NMR (CDCl₃, 399.76 MHz, 25 °C)** δ 7.25 – 7.30 (m, m,p – ArH, 18H), δ 7.18 – 7.25 (m, o – ArH, 12H), δ 6.89 (s, NCH, 2H), δ –0.35 ppm (SSiMe₃, 9H). **¹³C{¹H} NMR (CDCl₃, 100.53 MHz, 25 °C):** δ 194.1 (NCN), δ 142.4 (ArC), δ 130.6 (ArC), δ 128.0 (ArC), δ 127.9 (ArC), δ 119.7 (NCH), δ 78.5 (CPh₃), δ 5.9 ppm (SSiMe₃). **λ_{max}:** 207 nm (ε = 1426 cm⁻¹ M⁻¹); 253 nm (ε = 145 cm⁻¹ M⁻¹); 307 nm (ε = 51 cm⁻¹ M⁻¹). Data for **2.3c** (E = Se): **yield** 45%. **M. p.** °C. **¹H NMR (CDCl₃, 399.76 MHz, 25 °C)** δ 7.25 – 7.30 (m, m,p – ArH, 18H), δ 7.18 – 7.25 (m, o – ArH, 12H), δ 6.90 (s, NCH, 2H), δ –0.20 ppm (SSiMe₃, 9H). **¹³C{¹H} NMR (CDCl₃, 100.53 MHz, 25 °C):** δ 195.7 (NCN), δ 142.4 (ArC), δ 129.9 (ArC), δ 128.2 (ArC), δ 128.0 (ArC), δ 119.7 (NCH), δ 78.5 (CPh₃), δ 6.7 ppm (SeSiMe₃). **λ_{max}:** 209 nm (ε = 3024 cm⁻¹ M⁻¹); 256 nm (ε = 391 cm⁻¹ M⁻¹); 324 nm (ε = 91 cm⁻¹ M⁻¹).

2.4.3 Measuring δ donor ability by ¹J_{C-H} coupling constants⁴⁵

According to the work by Meng *et al.* the ¹H NMR spectra of ITrHOTf synthesized in this work by previous methods was analyzed, in detail, to resolve ¹J_{C-H} coupling information for the imidazolium triflate.²⁶ Unfortunately, due to overlap of the ¹³C satellites with other resonances, the information required had to be extrapolated per the following method. The imidazolium proton in ITrHOTf appeared in the ¹H NMR spectrum as a triplet centred at δ 7.92 ppm, *J* = 1.8 Hz (Δδ = 0.0045 ppm). The triplet satellite with the corresponding *J* value was selected as one half of the ¹J_{C-H} satellite, and the distance from the satellite triplet to the central peak at δ 7.92 ppm (0.2735 ppm) was doubled before being used to calculate the ¹J_{C-H} constant of 218.8 Hz. Attempting to find the other half of the satellite was not possible due to overlap with other signals. Per the work by Meng *et al.* this suggested a C–H bonding orbital with less *s* character than that found in IPr (¹J_{C-H} = 223.7 Hz), which in turn suggested better δ donating ability for ITr than IPr.⁴⁵

2.5. References

- (1) Jin, R. *Acta Phys. – Chim. Sin.* **2018**, *34*, 737–739.
- (2) Jin, R.; Zeng, C.; Zhou, M.; Chen, Y. *Chem. Rev.* **2016**, *116*, 10346–10413.
- (3) MacDonald, D. G.; Corrigan, J. F. *Philos. Trans. R. Soc. A* **2010**, *368*, 1455–1472.
- (4) Taher, D.; Wallbank, A. I.; Turner, E. A.; Cuthbert, H. L.; Corrigan, J. F. *Eur. J. Inorg. Chem.* **2006**, *2006*, 4616–4620.
- (5) Corrigan, J. F.; Fuhr, O.; Fenske, D. *Adv. Mater.* **2009**, *21*, 1867–1871.
- (6) DeGroot, M. W.; Corrigan, J. F. *Z. Anorg. Allg. Chem.* **2006**, *632*, 19–29.
- (7) Tran, D. T. T.; Corrigan, J. F. *Organometallics* **2000**, *19*, 5202–5208.
- (8) Kückmann, T. I.; Hermsen, M.; Bolte, M.; Wagner, M.; Lerner, H.–W. *Inorg. Chem.* **2005**, *44*, 3449–3458.
- (9) DeGroot, M. W.; Corrigan, J. F. *Angew. Chem., Int. Ed.* **2004**, *43*, 5355–5357.
- (10) DeGroot, M. W.; Corrigan, J. F. *Organometallics* **2005**, *24*, 3378–3385.
- (11) Khadka, C. B.; Macdonald, D. G.; Lan, Y.; Powell, A. K.; Fenske, D.; Corrigan, J. F. *Inorg. Chem.* **2010**, *49*, 7289–7297.
- (12) Khadka, C. B.; Eichhöfer, A.; Weigend, F.; Corrigan, J. F. *Inorg. Chem.* **2012**, *51*, 2747–2756.
- (13) Borecki, A.; Corrigan, J. F. *Inorg. Chem.* **2007**, *46*, 2478–2484.
- (14) Polgar, A. M.; Khadka, C. B.; Azizpoor Fard, M.; Nikkel, B.; O'Donnell, T.; Neumann, T.; Lahring, K.; Thompson, K.; Cadogan, C.; Weigend, F.; Corrigan, J. F. *Chem. – Eur. J.* **2016**, *22*, 18378–18382.
- (15) Fuhr, O.; Dehnen, S.; Fenske, D. *Chem. Soc. Rev.* **2013**, *42*, 1871–1906.
- (16) Dehnen, S.; Eichhöfer, A.; Fenske, D. *Eur. J. Inorg. Chem.* **2002**, *2002*, 279–317.
- (17) Fard, M. A.; Weigend, F.; Corrigan, J. F. *Chem. Commun. (Camb)*. **2015**, *51*, 8361–8364.
- (18) Azizpoor Fard, M.; Levchenko, T. I.; Cadogan, C.; Humenny, W. J.; Corrigan, J. F. *Chem. – Eur. J.* **2016**, *22*, 4543–4550.
- (19) Polgar, A. M.; Weigend, F.; Zhang, A.; Stillman, M. J.; Corrigan, J. F. *J. Am. Chem. Soc.* **2017**, *139*, 14045–14048.
- (20) Polgar, A. M.; Zhang, A.; Mack, F.; Weigend, F.; Lebedkin, S.; Stillman, M. J.; Corrigan, J. F. *Inorg. Chem* **2019**, *58*, 53.
- (21) Tolman, C. A. *Chem. Rev.* **1977**, *77*, 313–348.
- (22) Gómez-Suárez, A.; Nelson, D. J.; Nolan, S. P. *Chem. Commun.* **2017**, *53*, 2650–2660.
- (23) Clavier, H.; Nolan, S. P. *Chem. Commun.* **2010**, *46*, 841–861.
- (24) Zeng, X.; Frey, G. D.; Kinjo, R.; Donnadiou, B.; Bertrand, G. *J. Am. Chem. Soc.* **2009**, *131*, 8690–8696.
- (25) Beltrán, T. F.; Zaragoza, G.; Delaude, L. *Dalton Trans.* **2017**, *46*, 9036–9048.
- (26) Roy, M. M. D.; Lummis, P. A.; Ferguson, M. J.; McDonald, R.; Rivard, E. *Chem. – Eur. J.* **2017**, *23*, 11249–11252.
- (27) Roy, M. M. D.; Ferguson, M. J.; McDonald, R.; Rivard, E. *Chem. Commun.* **2018**, *54*, 483–486.
- (28) Mankad, N. P.; Gray, T. G.; Laitar, D. S.; Sadighi, J. P. *Organometallics* **2004**, *23*, 1191–1193.
- (29) Partyka, D. V.; Deligonul, N. *Inorg. Chem.* **2009**, *48*, 9463–9475.
- (30) Hussong, M. W.; Hoffmeister, W. T.; Rominger, F.; Straub, B. F. *Angew. Chem., Int. Ed.* **2015**, *54*, 10331–10335.
- (31) Wong, V. H. L.; White, A. J. P.; Hor, T. S. A.; Hii, K. K. (Mimi). *Chem. Commun.* **2015**, *51*, 17752–17755.
- (32) Jacobsen, H.; Correa, A.; Poater, A.; Costabile, C.; Cavallo, L. *Coord. Chem. Rev.* **2009**, *253*, 687–703.
- (33) Hussong, M. W.; Rominger, F.; Kramer, P.; Straub, B. F. *Angew. Chem., Int. Ed.* **2014**, *53*, 9372–9375.

- (34) Tate, B. K.; Wyss, C. M.; Bacsá, J.; Kluge, K.; Gelbaum, L.; Sadighi, J. P. *Chem. Sci.* **2013**, *4*, 3068.
- (35) Nelson, D. J.; Nolan, S. P. *Chem. Soc. Rev.* **2013**, *42*, 6723–6753.
- (36) Gaillard, S.; Slawin, A. M. Z.; Nolan, S. P. *Chem. Commun.* **2010**, *46*, 2742.
- (37) Wong, V. H. L.; Vummaleti, S. V. C.; Cavallo, L.; White, A. J. P.; Nolan, S. P.; Hii, K. K. M. *Chem.–Eur. J.* **2016**, *22*, 13320–13327.
- (38) Tapu, D.; Dixon, D. A.; Roe, C. *Chem. Rev.* **2009**, *109*, 3385–3407.
- (39) Zhai, J.; Hopkins, M. D.; Hillhouse, G. L. *Organometallics* **2015**, *34*, 4637–4640.
- (40) Kimani, M. M.; Watts, D.; Graham, L. A.; Rabinovich, D.; Yap, G. P. A.; Brumaghim, J. L. *Dalton Trans.* **2015**, *44*, 16313–16324.
- (41) Polgar, A. M.; Zhang, A.; Mack, F.; Weigend, F.; Lebedkin, S.; Stillman, M. J.; Corrigan, J. F. *Inorg. Chem.* **2019**, *58*, 3338–3348.
- (42) Drake, J. E.; Glavincevski, B. M.; Humphries N D Abdul Majid, R. A.; Glavin, B. M. *Can. J. Chem.* **1979**, *57*, 3253–3256.
- (43) Polgar, A. Coinage Metal Chalcogenide Clusters with N– Heterocyclic Carbene Ancillary Ligands The University of Western Ontario, 2018.
- (44) Díez–González, S.; Escudero–Adán, E. C.; Benet–Buchholz, J.; Stevens, E. D.; Slawin, A. M. Z.; Nolan, S. P. *Dalton Trans.* **2010**, *39*, 7595.
- (45) Meng, G.; Kakalis, L.; Nolan, S. P.; Szostak, M. *Tetrahedron Lett.* **2019**, *60*, 378–381.
- (46) Vogler, A. *Inorg. Chem. Commun.* **2017**, *84*, 81–83.
- (47) Davis, D. P.; Kirk, K. L.; Cohen, L. A. *J. Heterocycl. Chem.* **1982**, *19*, 253–256.
- (48) Bruker–AXS, SAINT version 2013.8, **2013**, Bruker–AXS, Madison, WI 53711, USA
- (49) Bruker–AXS, TWINABS version 2012.1, **2012**, Bruker–AXS, Madison, WI 53711, USA
- (50) Bruker–AXS, SADABS version 2012.1, **2012**, Bruker–AXS, Madison, WI 53711, USA
- (51) Sheldrick, G. M., *Acta Cryst.* **2015**, *A71*, 3–8
- (52) Sheldrick, G. M., *Acta Cryst.* **2015**, *C71*, 3–8
- (53) Gabe, E. J.; Le Page, Y.; Charland, J. P.; Lee, F. L. and White, P. S. *J. Appl. Cryst.* **1989**, *22*, 384–387

Chapter 3

3 Toward the Synthesis of Heterometallic Chalcogenide Molecules: Attempted syntheses of [(ITr)₂M(μ₂-E)M'] from [ITrMX] (X = OAc, Cl, ESiMe₃)

3.1 Introduction

N-Heterocyclic Carbenes (NHCs) have recently been investigated for their ability to stabilize metal chalcogenide molecules (see **Figure 3.1** below).¹⁻⁴ Compared to other ligands generally used in this research field, NHCs have been shown to be inherently stronger σ-donors, which has resulted in their use for the synthesis of complexes that are often more thermally stable than their phosphine-stabilized analogues.⁵⁻⁸ The electronic character of NHCs has been modulated by changing the saturation or conjugation on the heterocyclic backbone, while the steric profile of these ligands has been shown to depend most on the different R groups on these backbones.^{5-7,9,10} The electronic and steric stabilization offered to the metal centres protects the NHC-stabilized metal chalcogenides from condensation with themselves, preventing the formation of thermodynamically favoured bulk phases, M_xE_y.^{1,2,9-12} Zhai *et al.* used both *bis*-1,3-(2,6-(diphenylmethyl)-4-methylphenyl)imidazole-2-ylidene (IPr*) and *bis*-1,3-(2,6-diisopropylphenyl)imidazole-2-ylidene (IPr) to synthesize molecular copper sulfide [(IPr*)₂Cu₂(μ₂-S)] (**3.I**) and copper thiolate [(IPr)₂Cu₂(μ₃-SSiMe₃)]⁺ (**3.II**) in works meant to target fragments of the inorganic active site of nitrous oxide reductase.^{1,2} Jordan *et al.* recently reported the synthesis of molecular copper sulfide [(7Dipp)₂Cu₂(μ₂-S)] (**3.III**), analogous to the work of Zhai *et al.*, making use of 1,3-bis-(2,6-diisopropylphenyl)-4,5,6,7-tetrahydro-1,3-diazepin-2-ylidene (7Dipp) to stabilize this inorganic framework and study its reactivity with nitrosonium ions.³ Polgar *et al.* reported the use of 2-(2,6-diisopropylphenyl)-3,3-dimethyl-2-azaspiro[4.5]dec-1-ylidene (CAAC^{Cy}) and IPr to stabilize [(NHC)₄M₈(μ₃-S)₄] (NHC = CAAC^{Cy}, M = Cu; NHC = IPr, M = Au) that were studied for their tuneable luminescent properties.^{11,12}

The synthesis of these molecular compounds has been investigated by various methods. Zhai *et al.* described three general methods for the synthesis of their copper sulfide molecule: salt metathesis of NHC metal chlorides with Na₂S, acid-base deprotection strategies using NHC metal thiols and NHC metal

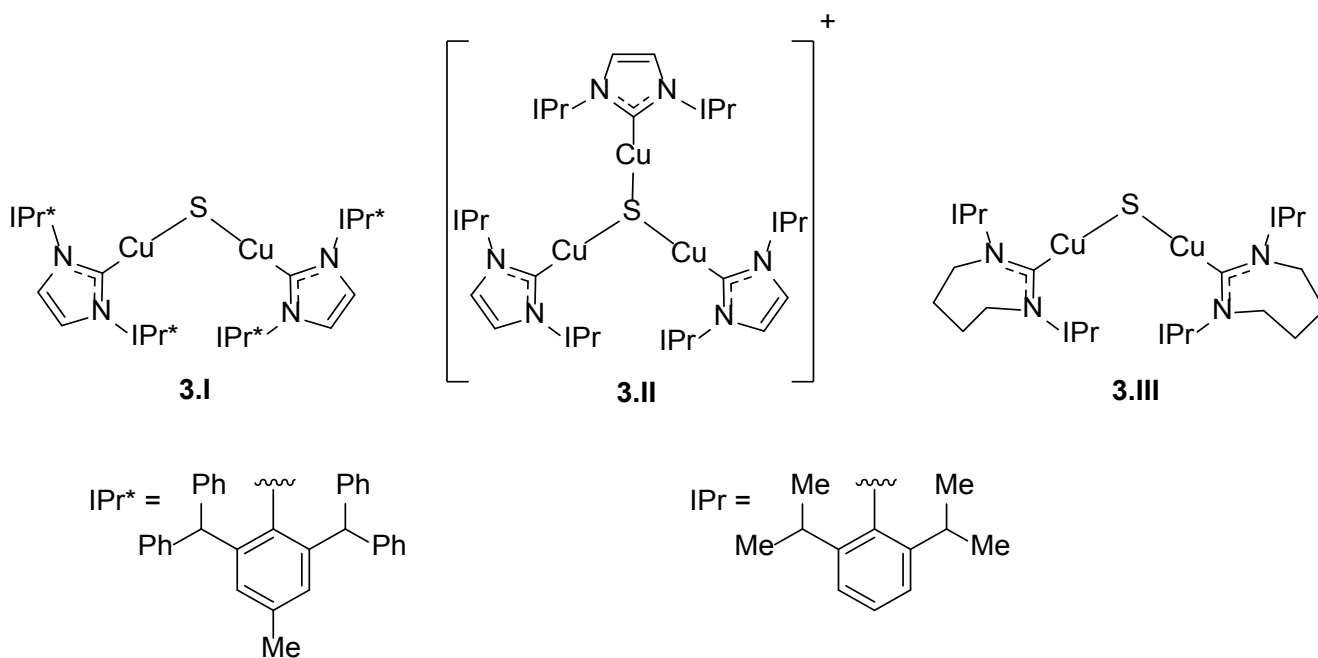


Figure 3.1: Examples of copper sulfide molecules **3.I** – **3.III** from previous works. Figures also show molecular structure of IPr*, IPr and 7Dipp.

alkoxides, and the use of NHC–stabilized trimethylsilyl metallothiolates with NHC metal fluorides.^{1,2} Of these three methods, Jordan *et al.* applied salt metathesis and acid–base deprotection strategies toward the synthesis of $[(7\text{Dipp})_2\text{Cu}_2(\mu_2\text{-S})]$ (**3.III**).^{1–3} Polgar *et al.* made use of the silyl deprotection strategy to synthesize their cluster compounds from NHC–stabilized trimethylsilyl metallochalcogenolates $[(\text{NHC})\text{MESiMe}_3]$ (NHC = CAAC^{Cy}, IPr; M = Cu, Au; E = S), in reactions with $[(\text{L})\text{MOAc}]$ (L = Ph_3P , $\{2,4\text{-}^t\text{Bu}(\text{C}_6\text{H}_3\text{O})_3\text{P}\}$); the structural effect of the NHC in this case was minimal as both NHCs produced octanuclear cluster compounds.^{11,12} Of these three methods, the use of the trimethylsilyl metallochalcogenolates ($[\text{MESiMe}_3]$) can offer significant advantages in accessing molecular metal chalcogenides given their ease of handling and storage, their relative stability in solution over their metal chalcogenol counterparts, and their ability to selectively undergo further chemical transformations.^{9,10,13–18} The use of these reagents operates on the principle that the pendant -SiMe_3 moiety acts as a removable protecting group, reacting in the presence of nucleophiles that can form thermodynamically favoured bonds to silicon (X = OAc, Cl, Br, etc.).¹³ This controlled reactivity about the chalcogen centre in $[\text{MESiMe}_3]$ has been used in the development of heterometallic or ternary metal chalcogenide molecules, with ternary compounds of Zn, Cu, Ag, and Au stabilized by a variety of ancillary ligands having been accessed by this reaction chemistry.^{1,2,11,12,15–17,19–23} As has been observed for phosphines, preliminary

work with NHCs has shown that the choice of ancillary ligand may affect the structure and nuclearity of the heterometallic cluster compounds obtained.^{9,11,15,20,24}

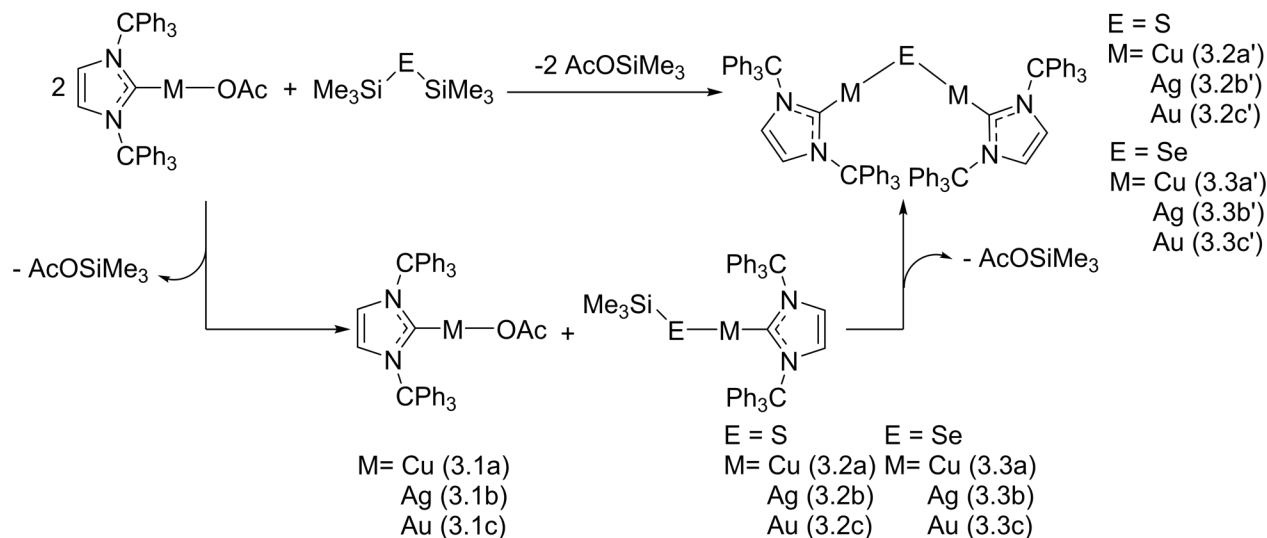
Given the recent interest in the homometallic molecules [(NHC)₂Cu(μ₂-S)] (**3.I** – **3.III**), it is interesting to probe the limits of the types of ligands and synthetic methods required to access heterometallic analogues for these compounds.¹⁻³ Because of the demonstrated utility and reactivity of [(NHC)₂Cu(μ₂-S)] compounds, heterometallic versions of this general structure (i.e. **3.I** and **3.III**) could be investigated for their ability to modulate the native reactivity of the dicopper sulfide compounds towards electrophiles or oxidizing agents.^{2,3} Additionally, the ability to vary the chalcogenido bridging ligand could affect the stability and reactivity of these dinuclear compounds [(NHC)₂M(μ₂-E)M']₂. Inspired by the successes of IPr* (%V_{bur} = 50.4%) and 7Dipp (%V_{bur} = 52.6%) on stabilizing this general type of compound, the work below describes the attempts toward [(NHC)₂M(μ₂-E)M']₂ (M = Cu^I, Ag^I, Au^I; E = S, Se) using trimethylsilyl metallochalcogenolates stabilized by *bis*-1,3-tritylimidazole-2-ylidene (ITr), which is an easy to synthesize, more electron donating and sterically more demanding ligand than even 7Dipp (%V_{bur} = 57.3%; TEP = 2034.0 cm⁻¹).²⁵ The steric bulk and electron donation offered by the NHC, coupled with the removable -SiMe₃ moiety on the metallochalcogenolates, was hypothesized to be appropriate for the syntheses of the dinuclear metal chalcogenide molecules. In addition to attempts made with [ITrMESiMe₃] and [ITrM'OAc], the work below also describes reactions toward the synthesis of the homometallic compounds via salt metathesis of [ITrMCl] (M = Cu, Au).

3.2 Results and Discussion

3.2.1. Attempted syntheses of [(ITr)₂M₂(μ₂-E)] (M = Cu, Ag, Au; E = S, Se)

The attempted synthesis of the homometallic dinuclear compounds was initially attempted by the reaction of [ITrMOAc] with E(SiMe₃)₂ in the stoichiometry shown in **Scheme 3.1**, which contrasted the methods used in the syntheses of [(NHC)₂Cu₂(μ₂-S)] (NHC = IPr*, **3.I**; 7Dipp, **3.III**) that required the isolation of intermediate reagents.^{2,3} As discussed in Chapter 2, the reaction of [ITrMOAc] (M = Cu^I, **3.1a**; Ag^I, **3.1b**; Au^I, **3.1c**) with one equivalent of E(SiMe₃)₂ resulted in the quantitative formation of [ITrMESiMe₃] (E = S, **3.2a** – **3.2c**; Se, **3.3a** – **3.3c**). It was thought that a 2:1 reaction of the starting materials would proceed by the selective formation of the ITr-metallochalcogenolate *in situ*, which could then react with the second equivalent of the ITr-metal acetate. The analysis of these reaction mixtures was carried out by NMR spectroscopy, using the ¹H NMR chemical shifts of the alkenyl protons on the imidazole backbone

(H_{4,5-imid}) to elucidate the presence of new compounds; the appearance/disappearance of other characteristic peaks (–OAc, –ESiMe₃) was also used in assessing reaction progression and completion. In addition, ¹H–¹³C HMBC experiments were performed as a relatively quick way to confirm the chemical shifts of carbenic resonances in the NMR sample and, using the information from the previous chapter, provided hints on the connections about that carbon atom.



Scheme 3.1: Proposed synthesis of [(ITr)₂M₂(μ₂-E)] from [ITrMOAc].

For instance, reactions of [ITrCuOAc] (**3.1a**) with Se(SiMe₃)₂ would be evaluated for reaction completion by the disappearance of the –OAc and –SeSiMe₃ resonances in the ¹H NMR spectrum. The appearance of any new peaks in the H_{4,5-imid} region would be checked against ¹³C NMR data obtained by ¹H–¹³C HMBC NMR experiments. The desired product was expected to show a correlation to a carbenic carbon with a chemical shift that was consistent with ITr–Cu–Se structural fragments (δ ~190 ppm). The ideal reaction conditions were sought to allow for selective formation of the desired product, as attempting to crystallize from a mixture of NHC metal complexes could often be tedious due to the co-crystallization of said complexes.² Where crystallization has not yet been successful, Electrospray Ionization – Mass Spectrometry (ESI–MS) was conducted in the hopes that the molecular ion could be observed and some confirmation on the structure obtained, in lieu of the structural data that would normally be elucidated by Single Crystal X–Ray Diffraction (SCXRD) studies. The *in-situ* generation of [ITrMSSiMe₃] (**3.2a** – **3.2c**) and [ITrMSeSiMe₃] (**3.3a** – **3.3c**) was confirmed by NMR spectroscopy in all of the following attempts with the general methodology in **Scheme 3.1**.

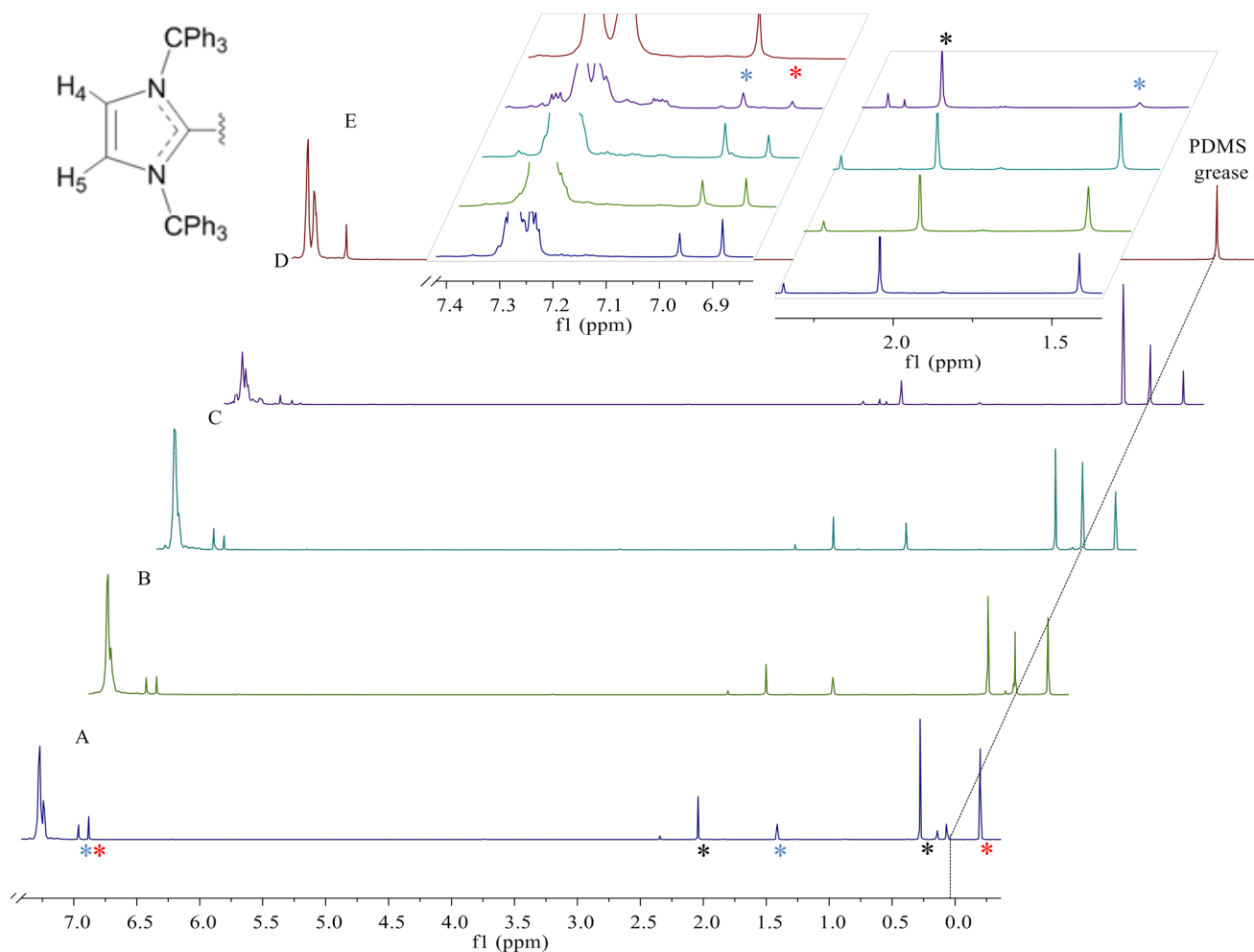


Figure 3.2: ^1H NMR spectra of the 2:1 reaction of $[\text{ITrCuOAc}]$ (**3.1a**) and $\text{Se}(\text{SiMe}_3)_2$ in CDCl_3 (A – D). Spectrum E is $[\text{ITrCuCl}]$ (**3.4**) in CDCl_3 . Insets are expansions of the $\text{H}_{4,5}$ -imid region and the -OAc region (see diagram). **A)** $-25\text{ }^\circ\text{C}$, 1 hr. **B)** $-25\text{ }^\circ\text{C}$, 120 hr. **C)** $5\text{ }^\circ\text{C}$, 24 hr. **D)** $25\text{ }^\circ\text{C}$, 24 hr. * - **3.1a** * - **3.3a** * - AcOSiMe_3 . Note: * - δ 6.99 ppm correlates to **3.4**.

In a 2:1 reaction of $[\text{ITrCuOAc}]$ (**3.1a**) with $\text{Se}(\text{SiMe}_3)_2$ in CDCl_3 , there was no sign of reactivity between **3.1a** and $[\text{ITrCuSeSiMe}_3]$ (**3.3a**), generated *in situ*, when the reaction was stirred cold ($\leq 5\text{ }^\circ\text{C}$) for prolonged periods of time (≥ 24 hours). This was determined by the observation of the Cu–acetate (δ 1.42 ppm) and Cu–selenolate (δ -0.19 ppm) resonances in the ^1H NMR spectra (**Figure 3.2 A–C**). Instead, the biggest difference observed under these conditions was the change in the relative intensities of the $\text{H}_{4,5}$ -imid peaks for **3.1a** (δ 6.99 ppm) and **3.3a** (δ 6.89 ppm), changing from 1:1 to 2:1, respectively. Coupled with the observation of increasing turbidity in the reaction solution, the decreasing amount of **3.3a** was thought to reflect the decomposition of this compound. The persistence of the $\text{H}_{4,5}$ -imid for **3.1a** after stirring for 24 hours at room temperature initially suggested the presence of $[\text{ITrCuOAc}]$ (**3.1a**), but closer inspection showed the signals expected for **3.1a** were no longer internally consistent as the relative

intensity of the acetate peak was lowered (**Figure 3.2 D**). This, instead, was indicative of another ITr-bearing species in solution with an overlapping chemical shift. Attempts toward the isolation of single crystals from these reaction mixtures for SCXRD studies yielded either **3.1a** or [ITrCuCl] (**3.4**). The targeted synthesis of the latter and characterization by NMR spectroscopy yielded spectra in CDCl₃ with a H_{4,5-imid} peak at δ 6.99 ppm (**Figure 3.2 E**), suggesting the presence of chlorinated solvent was somehow leading to the formation of [ITrCuCl] (see Experimental). Similar attempts with **3.1a** and S(SiMe₃)₂ in CDCl₃ also resulted in the isolation of **3.1a** or **3.4**, with spectra appearing like what is shown in **Figure 3.2**.

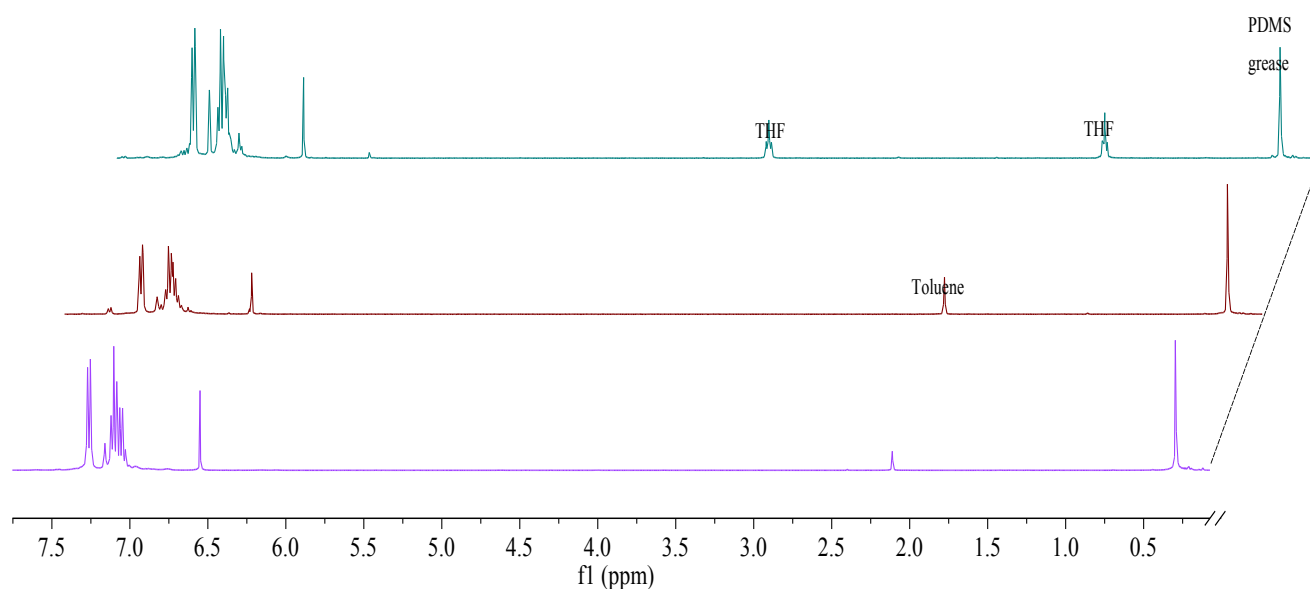


Figure 3.3: ¹H NMR spectra of [ITrCuCl] (**3.4**, purple) and reaction aliquots from a 2:1 reaction of **3.4** and Na₂E (E = S, red; Se = blue) after stirring at room temperature for 24 hrs. All data shown in C₆D₆.

The production of **3.4** when working in CDCl₃, could support the hypothesis that the cuprachalcogenolates were decomposing at room temperature faster than they could react with **3.1a**, somehow generating [ITrCu]⁺ in the process. Though never isolated, Roy *et al.* reported the use of ITr towards the synthesis of monocoordinate [ITrAg]⁺, with the closest result being the isolation of dimeric [(ITr)₂Ag₂]²⁺ from CH₂Cl₂ solutions.²⁶ Further investigation into the work of Zhai *et al.* suggested, instead, that compounds of the general formula [(NHC)₂Cu₂(μ₂-E)] may be prone to decomposition in the presence of haloalkanes, given the previously reported reactivity of [(IPr*)₂Cu₂(μ₂-S)] (**3.1**).² Given these observations, reactions toward [(ITr)₂Cu₂(μ₂-E)] (E = S, **3.2a'**; Se, **3.3a'**) were also attempted by the salt metathesis method, mixing one equivalent of Na₂E with two equivalents of [ITrCuCl] (**3.4**) and avoiding subsequent analysis

in CDCl_3 . The attempts toward **3.2a'** were expected to mimic the results reported by previous researchers, wherein stirring a solution of $[(\text{NHC})\text{CuCl}]$ and Na_2S resulted in clean conversion to the dinuclear compounds; the synthesis of **3.I** was reported as a slower reaction at room temperature than the synthesis of $[(7\text{Dipp})_2\text{Cu}_2(\mu_2\text{-S})]$ (**3.III**) under similar conditions, with reactions toward **3.I** showing a conversion rate of 50% over 24 hours in contrast to the complete conversion to **3.III**.^{2,3} A ^1H NMR spectrum of an attempt toward **3.2a'** suggested very minimal changes after 2 hours at 40 °C, when compared to the ^1H NMR spectrum of **3.4** in C_6D_6 (**Figure 3.3**). Stirring the reaction at room temperature for 24 – 48 hours resulted in a colour change from yellow to dark orange/brown, however, the NMR data remained mostly unchanged (**Figure 3.3**). In C_6D_6 , the chemical shift of the $\text{H}_{4,5\text{-imid}}$ were shifted to slightly higher frequency from δ 6.54 ppm to δ 6.55 ppm, with the carbenic resonance displaying a similar deshielding from δ 188.7 ppm to δ 189.2 ppm. A similar attempt toward $[(\text{ITr})_2\text{Cu}_2(\mu_2\text{-Se})]$ (**3.3a'**) produced identical NMR data combined with a colour change to brownish–red; heating was avoided as the copper selenide molecule was expected to be more thermally unstable in solution. SEM–EDX analysis of crystalline solids isolated from this reaction toward **3.3a'** suggested a 1:1 atomic ratio of Cu to Cl, indicating minimal or no reaction progress (see **Figure S3.1** in Appendix). Because of the similar chemical shifts in the spectra for the attempts toward **3.2a'** and **3.3a'**, subsequent analysis of the former was not conducted. The black–brown precipitate formed by both reactions was thought to be Cu_xE_y , but ultimately not characterized any further.

In addition to the attempted synthesis of ITr–stabilized dicopper chalcogenides **3.2a'** and **3.3a'**, analogous reactions were conducted toward the respective silver and gold compounds. Given the propensity of molecular silver chalcogenides to form clusters of higher nuclearity, only a few attempts were made toward $[(\text{ITr})_2\text{Ag}_2(\mu_2\text{-E})]$ (E = S, **3.2b'**; Se, **3.3b'**) by reacting $[\text{ITrAgOAc}]$ (**3.1b**) with $\text{E}(\text{SiMe}_3)_2$ in CDCl_3 . ^1H NMR spectra for these reactions revealed the consumption of **3.1b** by the disappearance of the –OAc resonance (δ 1.62 ppm), however, it was often the case that the trimethylsilyl resonance of $[\text{ITrAgESiMe}_3]$ (E = S, **3.2b**, δ –0.29 ppm; Se, **3.3b**, δ –0.14 ppm) would be observed in the respective spectrum, along with other NHC bearing compounds (δ 7.05 ppm) (**Figure 3.4**). Attempting to analyze reaction aliquots at room temperature immediately led to discoloration of the reaction solution and the formation of black precipitates, with evidence of this thermal decomposition presenting itself in the

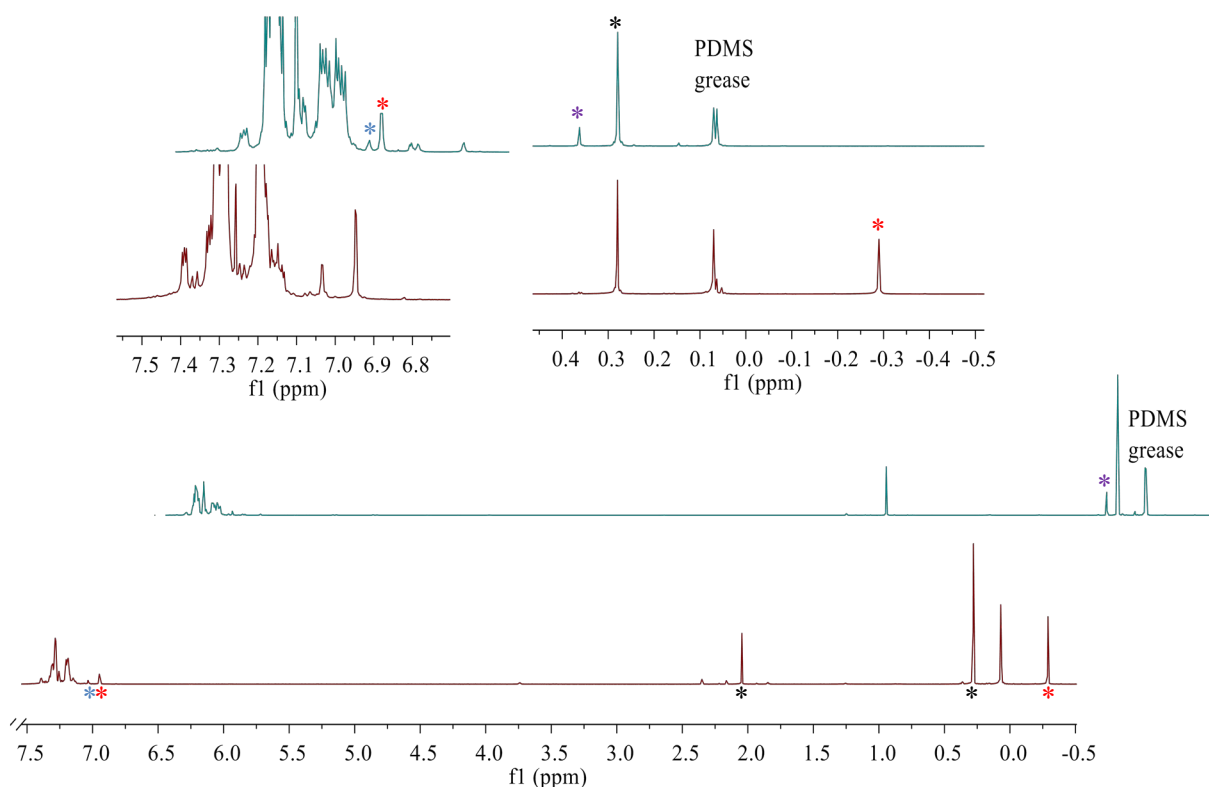


Figure 3.4: ^1H NMR spectra of a 2:1 reaction of $[\text{ITrAgOAc}](\mathbf{3.1b})$ and $\text{E}(\text{SiMe}_3)_2$ in CDCl_3 . E = S, maroon; E = Se, teal. Inset shows $\text{H}_{4,5\text{-imid}}$ region and $-\text{ESiMe}_3$ region. No $-\text{SeSiMe}_3$ peak is evident. * - $\mathbf{3.1b/3.5}$; * - $\mathbf{3.2b/3.3b}$; * - AcOSiMe_3 ; * - $\text{Se}(\text{SiMe}_3)_2$

^1H NMR spectra by the appearance of $\text{E}(\text{SiMe}_3)_2$ (**Figure 3.4**). Preliminary SCXRD experimental data collected on single crystals grown from these mixtures at colder temperatures ($-25\text{ }^\circ\text{C}$) have thus far suggested the formation of $[\text{ITrAgCl}](\mathbf{3.5})$ likely formed due to the decomposition of $[(\text{ITr})_2\text{Ag}_2(\mu_2\text{-E})]$ (E = S, $\mathbf{3.2b'}$; Se, $\mathbf{3.3b'}$) in the presence of chlorinated solvent, in much the same way as reported for $[(\text{IPr}^*)_2\text{Cu}_2(\mu_2\text{-S})](\mathbf{3.I})$ (see **Table S3.1**, **Figure S3.2 – Figure S3.4**).² In lieu of synthesizing $\mathbf{3.5}$ directly, it was proposed that the unidentified peak at $\delta\ 7.05\text{ ppm}$ belonged to this compound, given the observed similarity between $[\text{ITrCuOAc}]$ and $[\text{ITrCuCl}]$ by ^1H NMR spectroscopy, and the similarity between this resonance and the $\text{H}_{4,5\text{-imid}}$ peak for $[\text{ITrAgOAc}](\mathbf{3.1b})$. Additionally, the presence of a characteristic pair of doublets at $\delta\ 193.9\text{ ppm}$ ($^1J_{109\text{Ag}-13\text{C}} = 277\text{ Hz}$) and $\delta\ 193.9\text{ ppm}$ ($^1J_{107\text{Ag}-13\text{C}} = 239\text{ Hz}$) in the $^{13}\text{C}\{^1\text{H}\}$ NMR spectrum from an aliquot of the attempt toward $\mathbf{3.2b'}$ suggested that this major product bore an I Tr – Ag fragment (see **Figure S3.3** in Appendix). Just like the similarity in the NMR spectra of $[\text{ITrCuCl}]$ and $[\text{ITrCuOAc}]$, this carbenic resonance was similar to that which was observed for $[\text{ITrAgOAc}](\mathbf{3.1b})$

and the $^1J_{\text{Ag-C}}$ value was a good match to previous estimates of this data for **3.1b**. Due to the favorable interaction between Ag and Cl, salt metathesis reactions were not attempted for these compounds.

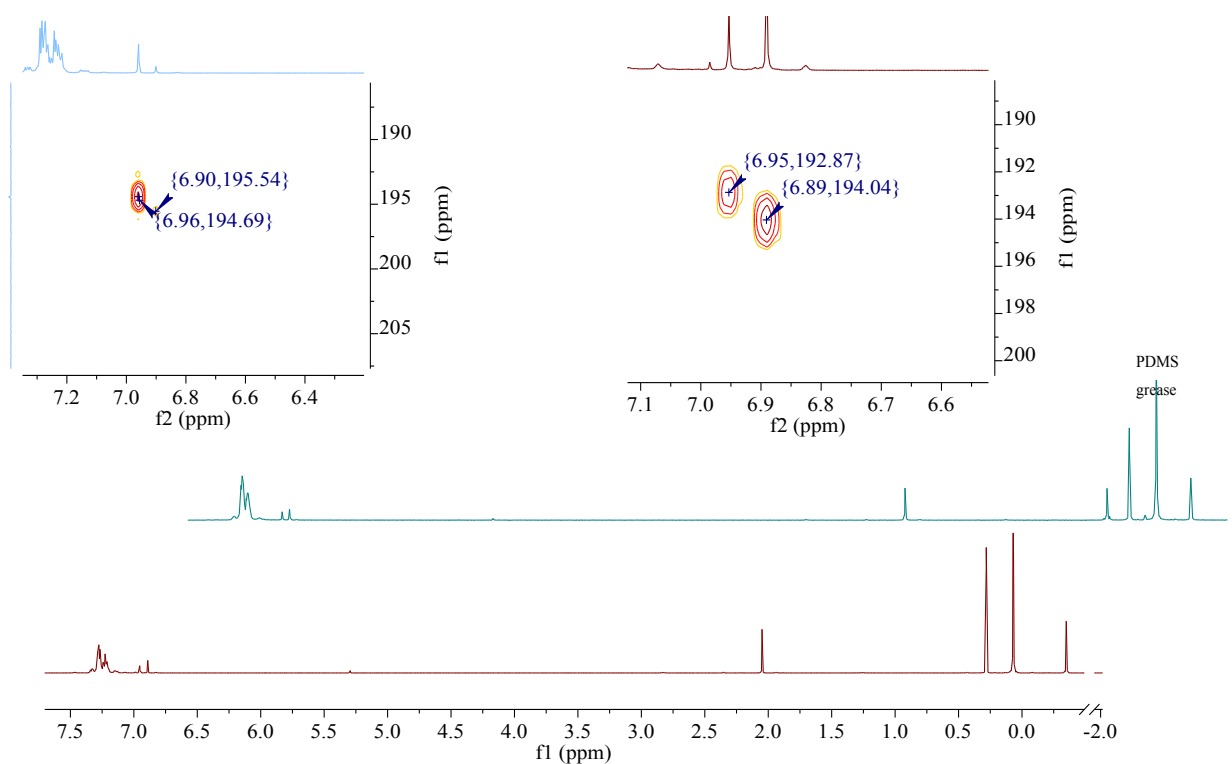


Figure 3.5: ^1H NMR spectra of 2:1 reactions of $[\text{ITrAuOAc}]$ **3.1c** and $\text{E}(\text{SiMe}_3)_2$ in CDCl_3 . E = S, maroon; Se, teal. Inset shows ^1H - ^{13}C HMBC suggesting that new peaks at $\delta 6.95$ ppm (E = S) and $\delta 6.96$ ppm (E = Se) belong to carbene on ITr-Au-E. Inset, maroon, shows peak at $\delta 6.99$ ppm corresponding to $[\text{ITrAuCl}]$.

The attempted synthesis of $[(\text{ITr})_2\text{Au}_2(\mu_2\text{-E})]$ (E = S, **3.2c'**; Se, **3.3c'**) was pursued in the same way as the copper analogues. Reactions between $[\text{ITrAuOAc}]$ (**3.1c**) and $\text{E}(\text{SiMe}_3)_2$ in CDCl_3 often resulted in the formation of two products, as determined by NMR spectroscopy. Analysis of ^1H NMR spectra in CDCl_3 confirmed the presence of $[(\text{ITr})\text{AuESiMe}_3]$ (E = S, **3.2c**; Se, **3.3c**) and a second ITr bearing compound; **3.2c** and **3.3c** were confirmed by the appearance of a $-\text{ESiMe}_3$ resonance (see **Figure 3.5**). ^{13}C NMR data obtained by ^1H - ^{13}C HMBC experiments indicated the new unidentified $\text{H}_{4,5\text{-imid}}$ peak (E = S, $\delta 6.95$ ppm; Se, $\delta 6.96$ ppm) in these reaction data correlated to a carbenic carbon similar to, yet distinct from $[\text{ITrAuESiMe}_3]$, suggesting perhaps the presence of another ITr-Au-E moiety ($\delta_{\text{E=S}} 192.9$ ppm; $\delta_{\text{E=Se}} 194.4$ ppm **Figure 3.5** inset). Though single crystals have not yet been obtained for these unknown compounds, ESI-MS spectra of fractions of these reactions containing mostly the unknown compound gave evidence for the molecular ion ($[\text{M-H}^+]$) of **3.2c'** and **3.3c'**. Despite multiple attempts,

the reactions conducted by the silyl deprotection method always resulted in a mixture of products when conducted in CDCl_3 , making further characterization of these compounds difficult because of these mixed product systems. Prolonged reaction times or attempts to crystallize the products identified above from CDCl_3 mixtures resulted instead in the isolation of $[\text{ITrAuCl}]$ (**3.6**) in a different habit than that previously reported by Roy *et al.* (see **Figure S3.6**, Appendix)..²⁵ Indeed, the ^1H NMR spectra of mixtures left in the chlorinated solvent showed the eventual formation of the chlorido complex, as evident by the peak at δ 6.99 ppm, which increased in intensity with longer reaction times (**Figure 3.5** inset, maroon).²⁵

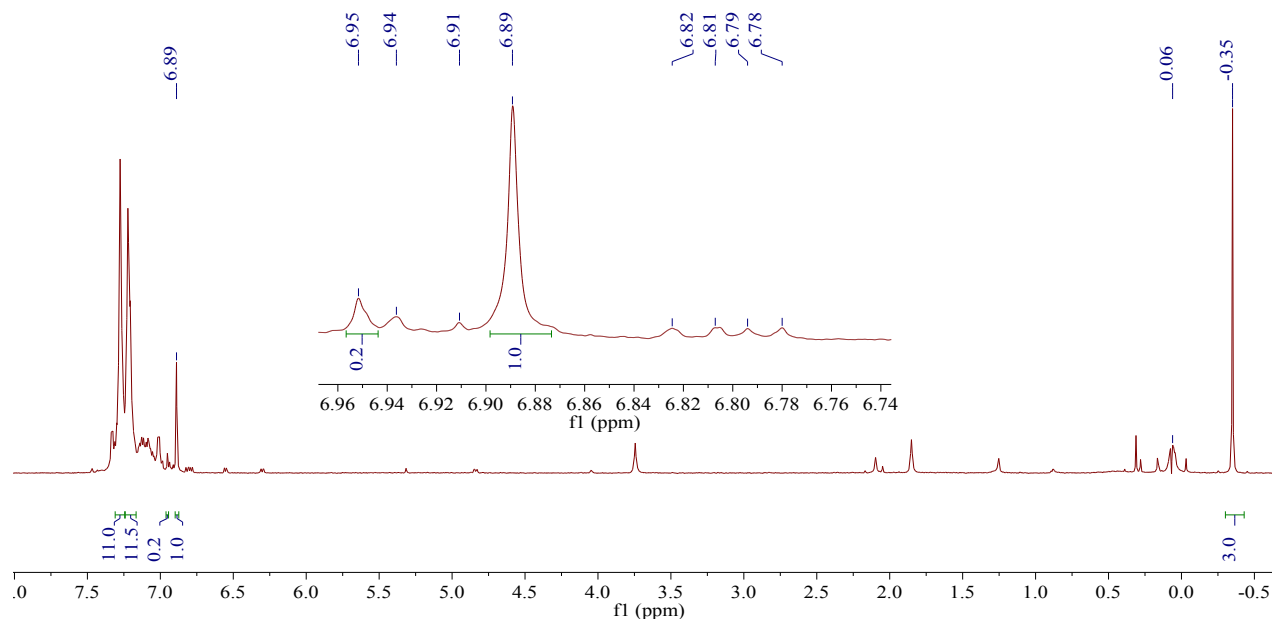


Figure 3.6: ^1H NMR spectrum, in CDCl_3 , of aliquot from $[\text{ITrAuOAc}]$ (**3.1c**) + $\frac{1}{2}$ $\text{S}(\text{SiMe}_3)_2$ in THF. Inset shows only one major ITr bearing product thought to be $[\text{ITrAuSSiMe}_3]$ (**3.2c**) based on $-\text{SSiMe}_3$ peak, but integration is 1: 3 instead of 1:4.5. A PRESAT NMR pulse sequence was used to saturate PDMS grease peak at δ 0.07 ppm.

Prior to the knowledge that chlorinated solvents were problematic for this system, a reaction of $[\text{ITrAuOAc}]$ (**3.1c**) with $\text{S}(\text{SiMe}_3)_2$ was conducted in THF, with a reaction aliquot analyzed in CDCl_3 and the solids isolated from the reaction serendipitously analyzed in C_6D_6 (**Figure 3.6** & **Figure 3.7**). The ^1H NMR spectrum in CDCl_3 suggested the presence of $[\text{ITrAuSSiMe}_3]$ (**3.2c**) as the major reaction product, however, the integration ratio between the $\text{H}_{4,5-\text{imid}}$ and $-\text{SSiMe}_3$ peak was not 1: 4.5 as expected, but rather 1: 3 (**Figure 3.6**). The presence of a peak at δ 6.95 ppm may indicate product formation, however, the distribution of products in **Figure 3.6** was dissimilar to what was observed in **Figure 3.5**.

Subsequent analysis of the solids in C_6D_6 suggested a mixture of products, including [ITrAuSSiMe₃] (**3.2b**), with its peaks integrating correctly after resolution of the other products' NMR signals by C_6D_6 (**Figure 3.7**). It was interesting to note that these data were different than data obtained from reactions conducted in $CDCl_3$, suggesting the presence of halogenated solvent somehow helps product formation, but inevitably prevents selective isolation of the desired product. The reactions behaved similarly when conducted with $Se(SiMe_3)_2$.

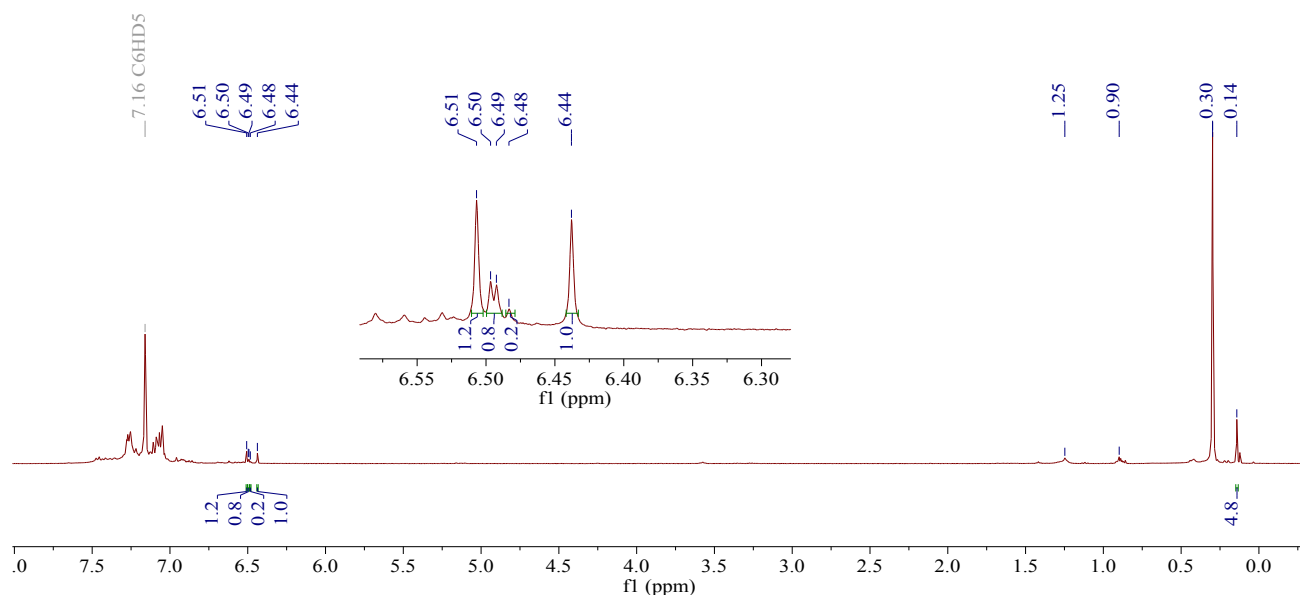


Figure 3.7: ¹H NMR spectrum, in C_6D_6 , of solids isolated from a 2:1 reaction of [ITrAuOAc] **3.1c** and $S(SiMe_3)_2$ in THF. Inset shows multiple ITr bearing compounds, with δ 6.44 ppm corresponding to [ITrAuSSiMe₃] (**3.2c**).

While the data in **Figure 3.5** suggested an ability to make the intended dinuclear gold chalcogenides, the tentative results and the data in **Figure 3.6** – **Figure 3.7** suggested that the trimethylsilyl deprotection strategy was, for reasons unknown, not selective in obtaining the desired product. Therefore, syntheses of the gold chalcogenide molecules were also attempted by the salt metathesis reaction to obtain the compounds in a supposedly more selective way. It was often observed that addition of a solution of [ITrAuCl] (**3.5**) in THF to a suspension of Na_2E , also in THF, caused immediate and drastic colour change to black. Attempting to initiate the reactions at lower temperatures showed a colour change first to purple, eventually darkening to black at room temperature. This colour change to purple suggested the presence of colloidal gold nanoparticles, implying the reduction of [ITrAuCl] (**3.5**) to some Au^0 species.²⁷ A review of the literature has found previous works confirming the tendency for gold chalcogenides to form mixed valence species during the synthesis of nanoparticles using H_2E ; evidence of Au^0 and E^0 is reported.²⁸

Thus, cyclic voltammetry of **3.5** in MeCN was performed, but, revealed no reduction peak when scanning to potentials as low as -2.4V vs. SCE (see **Figure S3.7** in Appendix). This suggested stability against reduction as was already demonstrated for phosphine-stabilized gold chlorido complexes and negated reduction as a possible competing side reaction.²⁹ SEM-EDX analysis of the black solids isolated shortly after warming a reaction mixture of **3.5** and Na_2Se to room temperature showed the presence of Na, Se, Au and Cl, with the atomic ratios between these elements ($\sim 2.48 : 1 : 0.35 : 0.37$) indicating Na_2Se was likely present. A reaction of **3.5** and Na_2S stirred as a black turbid slurry for 24 hours at room temperature led to the formation of a mixture of compounds, with the ^1H NMR and ^{13}C NMR data suggesting the presence of **3.5** (δ_{H} 6.49 ppm, δ_{C} 185.1 ppm) and two unidentified minor products likely containing ITr-Au-S fragments (δ_{H} 6.53 ppm, δ_{C} 194.7 ppm; δ_{H} 6.56 ppm, δ_{C} 198.6 ppm) (see **Figure 3.8**).

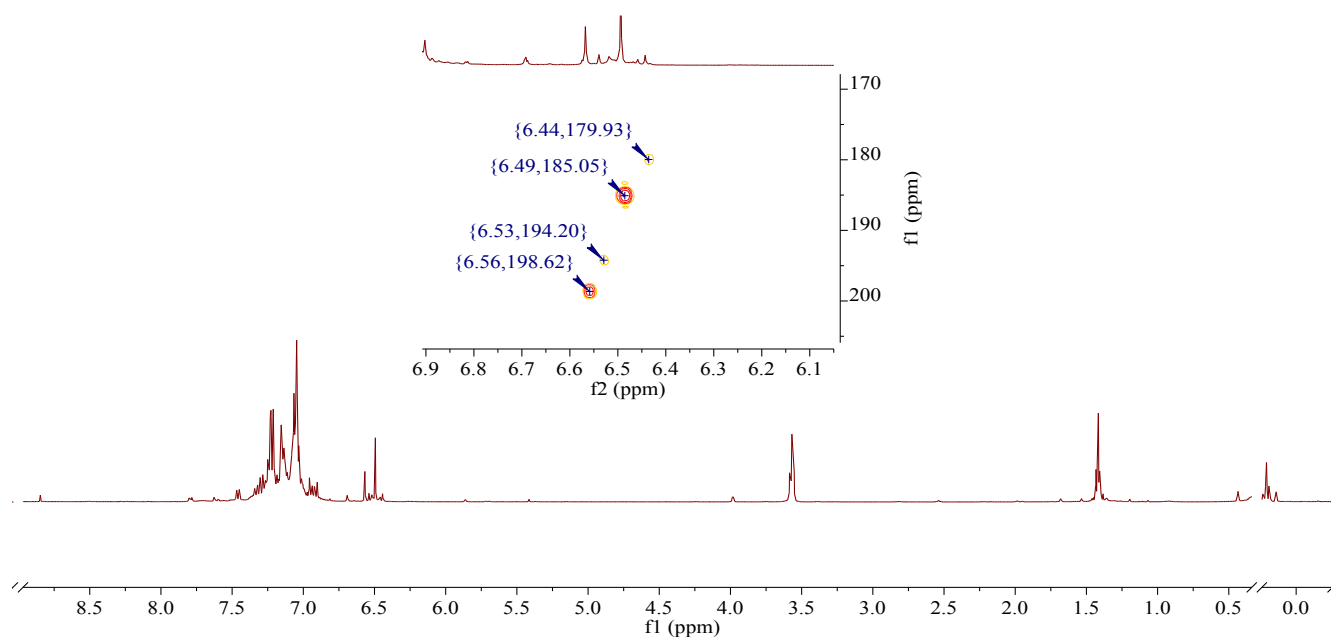


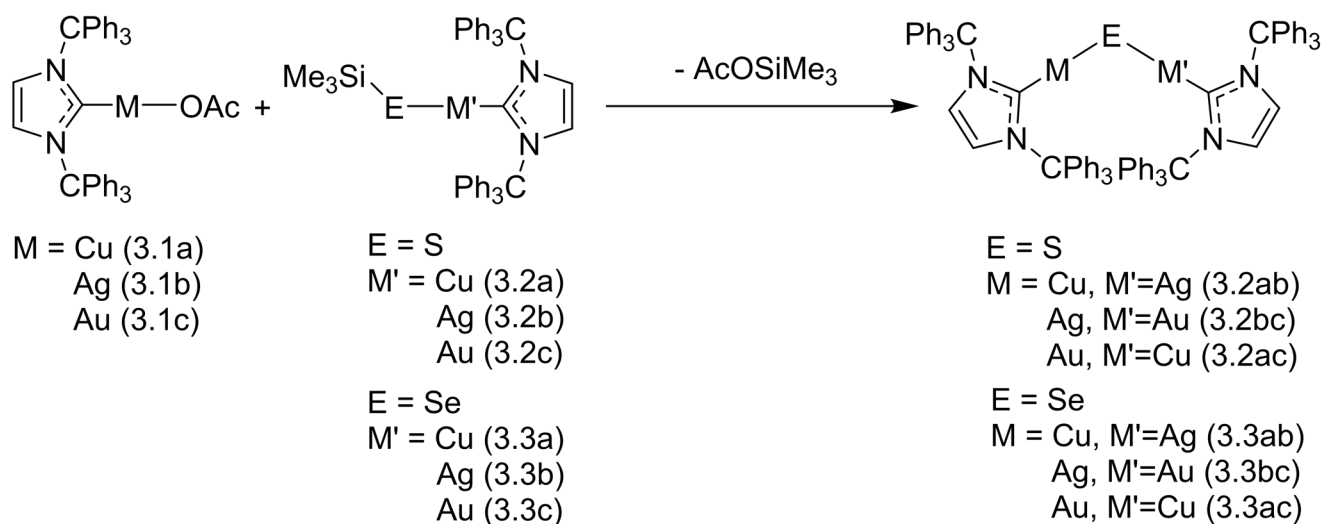
Figure 3.8: ^1H NMR spectrum in C_6D_6 of a 2:1 reaction mixture of $[\text{ITrAuCl}]$ (**3.5**) and Na_2S for 24 hours at $25\text{ }^\circ\text{C}$. Inset shows ^1H - ^{13}C HMBC showing correlations between peaks in $\text{H}_{4,5\text{-imid}}$ region and carbenic resonances characteristic to $[\text{ITr-Au-S}]$. Correlation ($\delta 6.49$, $\delta 185.1$) belonged to **3.5**, while peaks ($\delta 6.53$, $\delta 194.2$), ($\delta 6.56$, $\delta 198.6$) and ($\delta 6.44$, $\delta 179.9$) remain unidentified.

Ultimately, the mixture of products could not be effectively separated and no subsequent analyses by SCXRD or ESI-MS was able to confirm the intended structure. It was not known why salt metathesis did not selectively generate the desired compounds, however, closer inspection of **Figure 3.8** suggested the peak at $\delta 6.53$ ppm in the ^1H NMR spectrum belonged to $[(\text{ITr})_2\text{Au}_2(\mu_2\text{-Se})]$ (**3.3c'**), as discussed in **Figure 3.5**, given the similarity of its correlated carbenic resonance to this previous attempt ($\delta 194.7$ ppm). Given the presence of an additional, deshielded, unidentified peak at $\delta 6.56$ ppm, it was thought that **3.3c'** may

have been converted to another sulfur-bearing complex as this ^1H NMR resonance showed correlation to a carbenic resonances at δ 198.6 ppm. Given the deshielded nature of this second carbenic resonance, it was thought the second compound (δ 198.6 ppm) could be $[(\text{ITr})_3\text{Au}_3(\mu_3\text{-S})]\text{Cl}$, formed because of unselective reactivity of **3.5**. These compounds are known in the literature with phosphine ligands, however, the NHC supported complexes remain unreported.³⁰

3.2.2. Attempted syntheses of $[(\text{ITr})_2\text{M}(\mu_2\text{-E})\text{M}']$: Unexpected Reactivity Patterns of $[\text{ITrM}(\text{E}(\text{SiMe}_3)_3)]$

In addition to the attempted syntheses of homometallic chalcogenide molecules, reactions were conducted in the attempts of accessing heterometallic compounds (**Scheme 3.2**). While the results above did not bode well for the ability to isolate homometallic metal chalcogenides with ITr, the reactions discussed below were attempted with the hope that the combination of heterometallic reagents might affect the reactivity or stability of the products in an advantageous way.



Scheme 3.2: General reaction methodology for syntheses of $[(\text{ITr})_2\text{M}(\mu_2\text{-E})\text{M}']$.

To access $[(\text{ITr})_2\text{Ag}(\mu_2\text{-E})\text{M}']$ ($\text{E}=\text{S}$: $\text{M}' = \text{Cu}^{\text{I}}$ **3.2ab**, Au^{I} **3.2bc**; $\text{E}=\text{Se}$: $\text{M}' = \text{Cu}^{\text{I}}$ **3.3ab**, Au^{I} **3.3bc**) preliminary attempts were made using $[\text{ITrM}'\text{ESiMe}_3]$ ($\text{E}=\text{S}$: $\text{M}' = \text{Cu}^{\text{I}}$ **3.2a**, Au^{I} **3.2c**; $\text{E}=\text{Se}$: $\text{M}' = \text{Cu}^{\text{I}}$ **3.3a**, Au^{I} **3.3c**) and $[\text{ITrAgOAc}]$ (**3.1b**), given the relatively greater solution stability of the other metallochalcogenolates than $[\text{ITrAgESiMe}_3]$ ($\text{E}=\text{S}$ **3.2b**, **Se 3.3b**). Aliquots of the reactions between **3.2a – 3.3a** with **3.1b**, stirred at low temperatures (≤ -25 °C) in CDCl_3 , suggested transfer of the $-\text{ESiMe}_3$ instead of activation of the $\text{E} - \text{Si}$ bond. This observation was supported by the appearance of ^1H NMR data for the argentochalcogenolates and $[\text{ITrCuOAc}]$ despite having started with cuprachalcogenolates and $[\text{ITrAgOAc}]$ (**Figure 3.9**). Warming these mixtures to room temperature resulted in an unextractable

mixture of products. The transfer of chalcogenolate ligands between Cu and Ag is unprecedented in the literature for the heavier chalcogens (E = S, Se, Te). More surprising still is the inability for the OAc to activate the reactive E–Si bonds, given the syntheses of **3.2b** and **3.3b** by a similar process. Attempting to use other techniques to analyze the products of the reaction were not fruitful; ESI–MS only showed peaks whose isotopic patterns and *m/z* match fragments of [ITrCu]⁺ and [ITrCu(Im–CPh₃)]⁺.

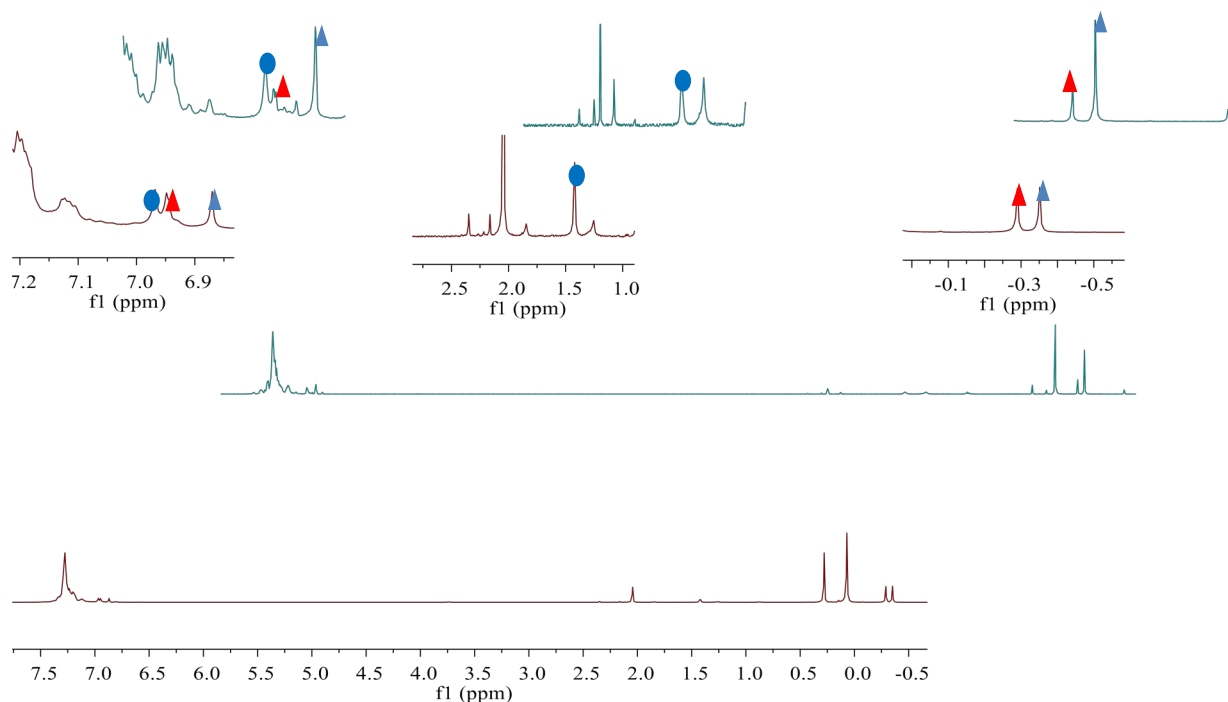


Figure 3.9: ¹H NMR spectra of the reaction of [ITrCuESiMe₃](E = S, **3.2a**; Se **3.3a**) and [ITrAgOAc] (**3.1b**). (**3.2a**, maroon; **3.3a**, teal). Inset shows expansions of regions of interest, labelling [ITrMESiMe₃] with triangles, [ITrMOAc] with circles and using red and blue to distinguish between Ag and Cu compounds.

In contrast to this, reactions attempted with [ITrAuESiMe₃] (E = S, **3.2c**; Se, **3.3c**) and [ITrAgOAc] (**3.1b**) in CDCl₃ showed evidence of reaction progression, however, the data were not always consistent with a selective reaction. Mixing **3.2c** and **3.1b** in CDCl₃ and monitoring the reaction at –25 °C showed little progress over the course of one hour at this temperature, as indicated by the presence of the –OAc (δ 1.62 ppm) and –SSiMe₃ (δ –0.35 ppm) peaks in the ¹H NMR spectra (see **Figure 3.10**). Warming the reaction to –10 °C and stirring for an additional 90 minutes resulted in the apparent consumption of **3.1b** while the signals for **3.2c** persisted. This suggested consumption of **3.1b** by some other, unidentified means. Monitoring reaction progress by integration of signals of interest indicated the rate of consumption of **3.1b** and **3.2c** was approximately equal for the two reagents up to warming to –10 °C, wherein the rate of consumption of **3.2c** (dark blue, **Figure 3.11**) slowed down relative to **3.1b** (green, **Figure 3.11**). In the

spectra, new peaks began to appear at δ 1.85 ppm and δ 2.19 ppm (**Figure 3.10**). Integration of these areas also increased, suggesting they were the products of some other side reaction (**Figure 3.11**). Similar results were observed in the reaction of **3.3c** with **3.1b** which showed the persistence of the selenolate and the appearance of the spurious, unidentified peak at δ 2.17 ppm. This chemical shift was consistent with an OAc fragment, but inconsistent with AcOSiMe_3 (δ 2.05 ppm, OAc, 3H; δ 0.28 ppm, SiMe_3 , 9H).

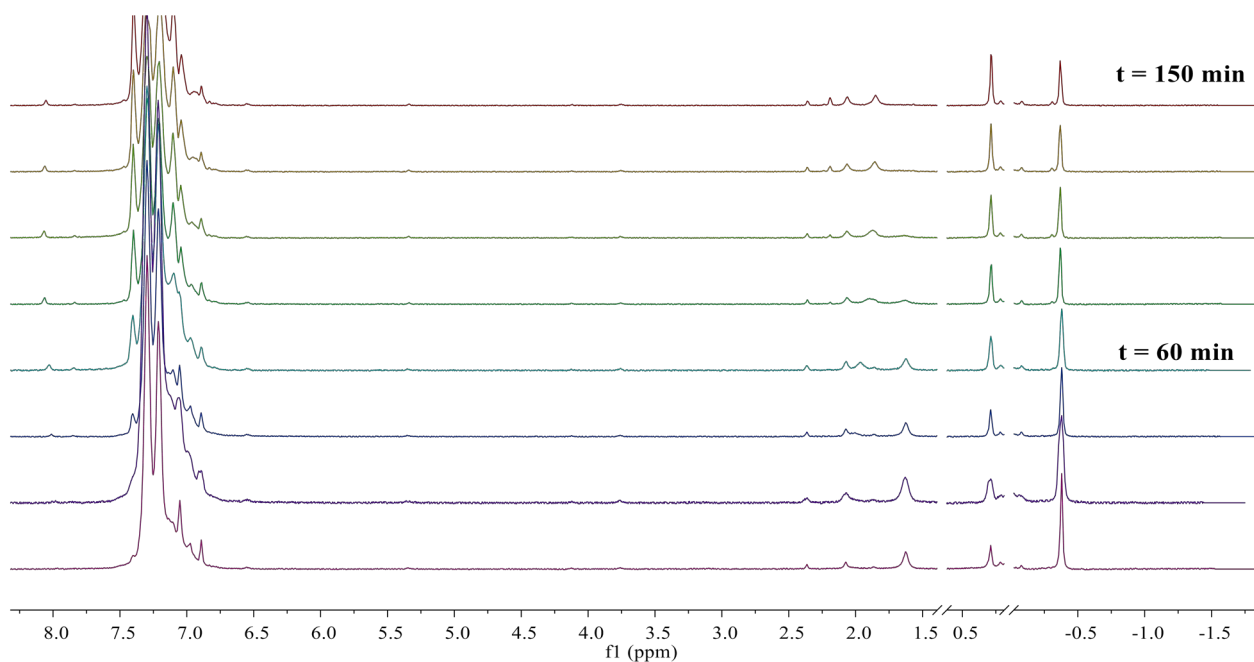


Figure 3.10: Stacked ^1H NMR spectra of the 1:1 reaction of $[\text{ITrAuSSiMe}_3]$ and $[\text{ITrAgOAc}]$ in CDCl_3 . Data collected at $-25\text{ }^\circ\text{C}$ for first 60 minutes, then $-10\text{ }^\circ\text{C}$ for remaining 90 minutes.

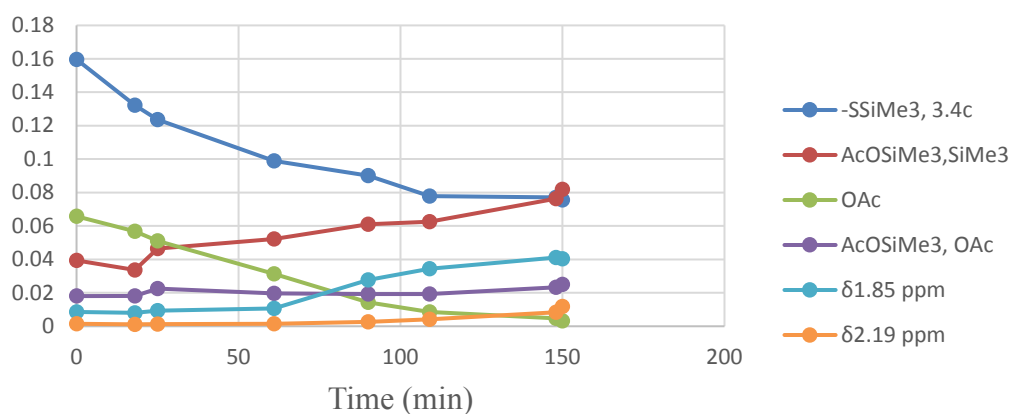


Figure 3.11 Scatter plot tracking changes in peak area for select resonances in **Figure 3.10**. $T = -25\text{ }^\circ\text{C}$ up to 60 min; $T = -10\text{ }^\circ\text{C}$ afterwards.

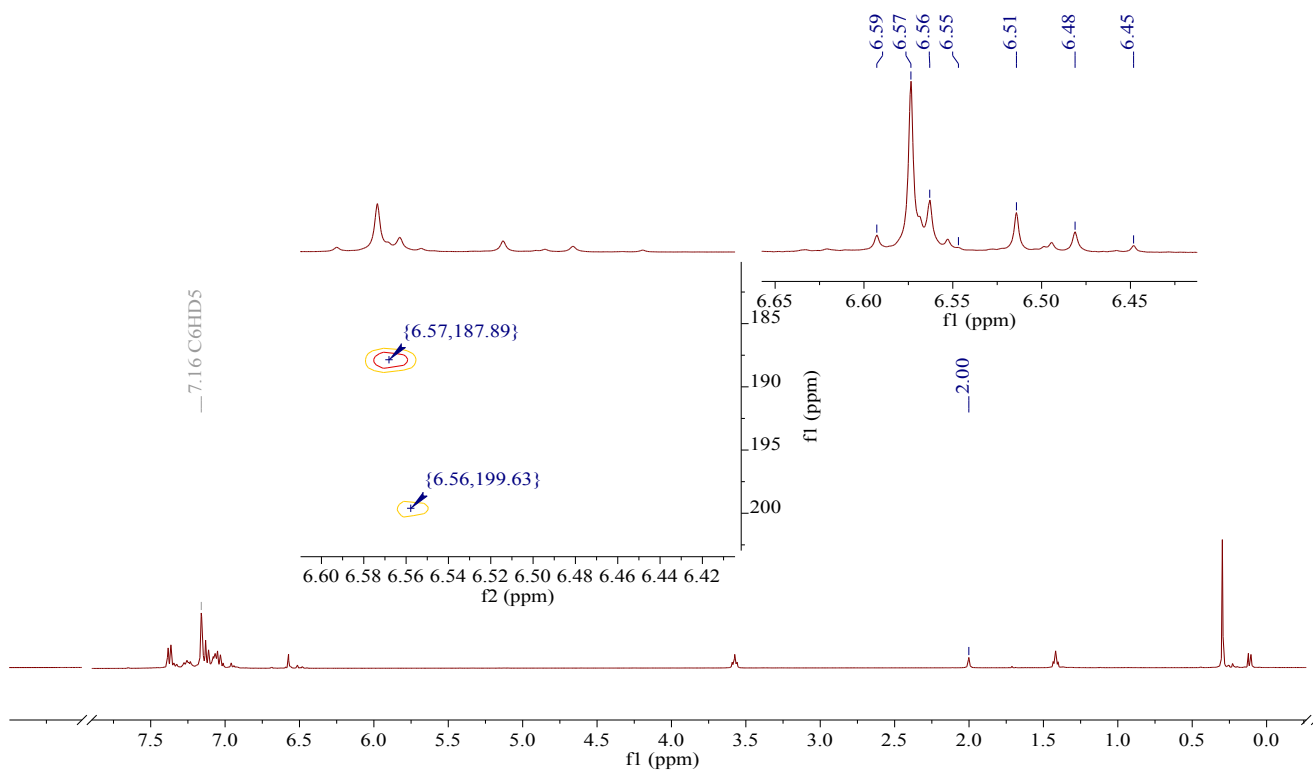


Figure 3.12: ^1H NMR spectrum of reaction of $[\text{ITrCuSeSiMe}_3]$ and $[\text{ITrAuOAc}]$ in C_6D_6 . Inset shows ^1H - ^{13}C HMBC for $\text{H}_{4,5\text{-imid}}$ region and expansion of the peaks in the f1 axis. Peak at $\delta 2.00$ ppm corresponds to $-\text{OAc}$ for $[\text{ITrCuOAc}]$.

The attempted syntheses of $[(\text{ITr})\text{Cu}(\mu_2\text{-E})\text{Au}(\text{ITr})]$ (**3.2ac** – **3.3ac**) were done first with $\text{E} = \text{Se}$, on the basis that reagents containing $-\text{Se}-\text{SiMe}_3$ would be more reactive than their thiolate counterparts. Limited reactivity with this system would immediately negate the suitability of the thiolates towards these heterometallic systems because of the necessity to break more stable $\text{S}-\text{SiMe}_3$ bonds by this reaction chemistry. Though some of the reactions above were conducted in CDCl_3 , the results from the attempted syntheses of the homometallic compounds suggested avoiding the use of this solvent where possible. Thus, many of these subsequent reactions were conducted in THF, or C_6D_6 if low temperatures were not required. In general, it was found that addition of $[\text{ITrCuSeSiMe}_3]$ (**3.3a**) to $[\text{ITrAuOAc}]$ (**3.1c**) resulted in mixtures that were unpredictable; addition at -70 °C followed by storage at -25 °C overnight showed conversion of **3.1c** to $[\text{ITrCuOAc}]$ (**3.1a**, **Figure 3.12**). While ^1H and ^{13}C NMR data corroborate this observation, peaks in the ^1H NMR spectra that would normally be assigned to **3.3a** and $[\text{ITrAuSeSiMe}_3]$ (**3.3c**) in the $\text{H}_{4,5\text{-imid}}$ region ($\delta 6.48$ ppm; $\delta 6.45$ ppm) were present, with no corresponding evidence of the respective $-\text{SiMe}_3$ resonance in the $^1\text{H} - ^{13}\text{C}$ HMBC NMR spectra of this mixture (**3.3a** $\delta_{\text{H}} 0.30$ ppm, $\delta_{\text{C}} 7.1$ ppm; **3.3c** $\delta_{\text{H}} 0.25$ ppm, $\delta_{\text{C}} 7.4$ ppm. See **Figure 3.12**). An unassigned peak at $\delta 6.51$ ppm showed

very weak correlation by ^1H - ^{13}C HMBC to a carbenic resonance at δ 199.6 ppm, however, any attempt to isolate single crystals for analysis has thus far been unfruitful.

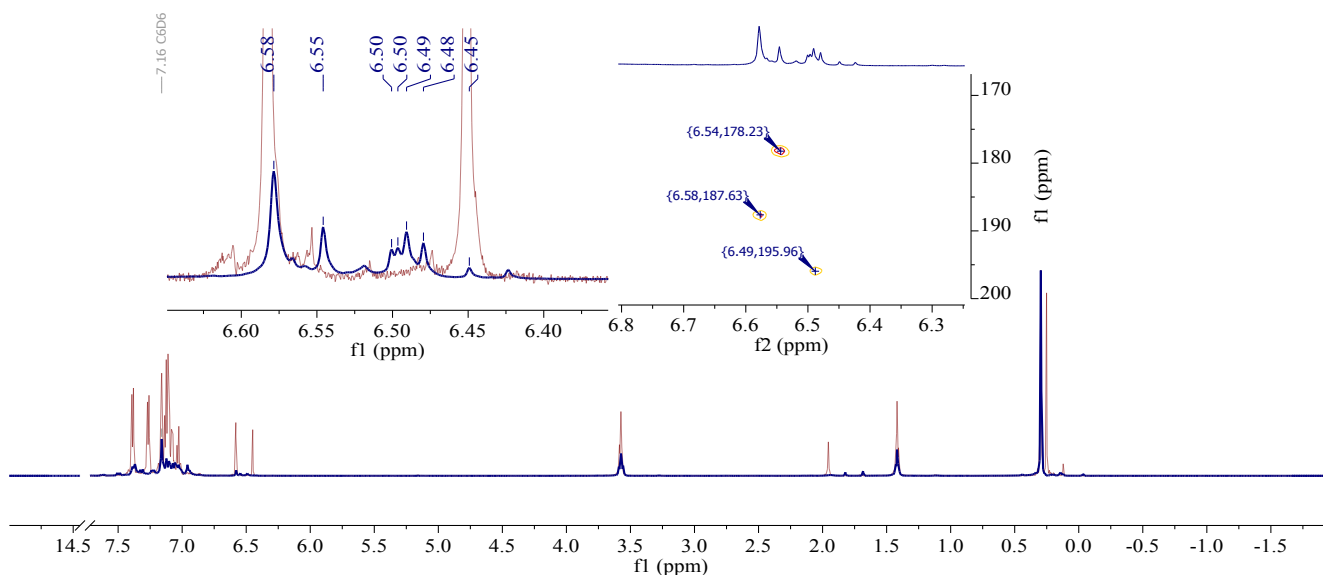


Figure 3.13: ^1H NMR spectra of the reaction of $[\text{ITrAuSeSiMe}_3]$ and $[\text{ITrCuOAc}]$. Spectra in C_6D_6 after 1 hour at $-25\text{ }^\circ\text{C}$ (red) and 24 hours at $25\text{ }^\circ\text{C}$ (blue) superimposed to illustrate disappearance of $-\text{SeSiMe}_3$.

Attempting the reaction by adding $[\text{ITrCuOAc}]$ (**3.1a**) to a solution of $[\text{ITrAuSeSiMe}_3]$ (**3.3c**) at low temperature ($\leq -65\text{ }^\circ\text{C}$) and slowly warming to room temperature showed evidence of a slower reaction as both compounds remained in solution, as confirmed by ^1H and ^{13}C NMR data (**Figure 3.13**). Stirring the reaction at room temperature for a few hours showed minimal changes, however, at room temperature for ≥ 24 hours ^1H and ^{13}C NMR data showed consumption of **3.3c**, as confirmed by the absence of the $-\text{SeSiMe}_3$ resonance in the ^1H NMR spectrum (δ 0.25 ppm). Evidence of both **3.1a** and $[\text{ITrAuOAc}]$ (**3.3a** $\delta_{\text{H}} 6.54$ ppm, $\delta_{\text{C}} 178.2$ ppm see **Figure 3.13**) were also present in these data. Complicating matters further, the $\text{H}_{4,5\text{-imid}}$ region showed the presence of a peak at δ 6.49 ppm, which showed correlation to a carbenic resonance at δ 196.0 ppm, different than anything that has been seen thus far (**Figure 3.13** inset). At first glance this suggested the persistence of **3.3c**, but without corroborating evidence of the $-\text{SeSiMe}_3$ moiety, or SCXRD data of these reaction products, it is unclear as to what compound this $[\text{ITr-Au-Se}]$ fragment belongs.

3.2.3. The Inability to Synthesize Homometallic and Heterometallic [(ITr)₂M(μ₂-E)M'].

The inability to selectively access the compounds of this work was an unexpected result, especially in the attempted syntheses of homometallic [(ITr)₂M₂(μ₂-E)] (M = Cu, Au). On closer review of the literature, however, the limitations of the silyl deprotection strategy (i.e. using [(NHC)MESiMe₃] and [(NHC)M'X]) may have been demonstrated in the synthesis of [(IPr*)₂Cu₂(μ₂-S)] (**3.I**), where the reaction of [(IPr*)CuSSiMe₃] and [(IPr*)CuF] produced **3.I** in an unextractable mixture.² The researchers commented that this result was in stark contrast to their prior work that demonstrated the selective reaction of [(IPr)₂Cu₂(μ₂-SSiMe₃)]BF₄ and [IPrCuF] to make [(IPr)₃Cu₃(μ₃-S)]⁺ (**3.II**).^{1,2} Attempts toward an IPr analogue of **3.I** by this strategy also proved unsuccessful, resulting in a slow reaction that ultimately produced a mixture of compounds, including the unconfirmed [(IPr)₂Cu₂(μ₂-S)].^{1,2} The synthesis of [(7Dipp)₂Cu₂(μ₂-S)] (**3.III**), the only other example of this type of compound, was described by the salt metathesis and the acid – base deprotection strategies, while the silyl deprotection strategy was seemingly not investigated.³ Attempts made in this thesis help corroborate a working hypothesis that the silyl deprotection strategy is hindered by the presence of very sterically demanding NHCs. The difference in steric bulk between IPr, IPr*, 7Dipp, and ITr (%V_{bur}, = 44.5%, 50.4%, 52.6%, 57.3% respectively) correlated with this idea, however, electronic differences between ITr and IPr* (TEP_{ITr} vs. TEP_{IPr*} = 2034.0 cm⁻¹ vs. 2052.7 cm⁻¹) made it difficult to argue that steric contribution alone was the only limiting factor in this chemistry.^{7,25,31}

In addition, the use of metal acetates in this work differed from the use of metal fluorides by Zhai *et al.*, which may have had an impact on the reactions in this work.^{1,2} At first glance, it was thought that the use of a ITr-stabilized metal fluoride could be too reactive for the reactions in this work. The use of [ITrM'OAc] was proposed based on previous precedent suggesting it may have been a less reactive alternative.³² Ironically, many of the results above suggested that [ITrM'OAc] was not reactive enough to selectively cleave the E-Si bond in [ITrMESiMe₃] under conditions of kinetic control (T ≤ 0 °C) (see **Figure 3.2**, **Figure 3.9**, **Figure 3.12** for examples). The use [NHCCuF], by Zhai *et al.*, took advantage of the very high bond enthalpy of Si-F bonds and the volatility of the F-SiMe₃ to push the deprotection reaction forward.^{1,2} In comparison, the -OAc used in this work was not as thermodynamically favoured for -SiMe₃ because of a relatively weaker Si-O bond strength (452 kJ/mol vs. 565 kJ/mol), made less favorable also because of the delocalized nature of the electron density about oxygen. This thermodynamically less favoured product, AcOSiMe₃, was also less volatile than the F-SiMe₃ generated in previous examples, apparently slowing the reactions in this work to an extent where they would not

occur appreciably at lower temperatures.^{1,2} Thus, the inability to observe selective product formation by the silyl deprotection strategy may have been due to the combination of excessive steric bulk from ITr and the limited reactivity of [(ITr)M'OAc].^{1,2}

Though the discussion so far attempts to explain the inability to access the dinuclear molecular chalcogenides by the silyl deprotection strategy, it does not provide any explanation on the failure to selectively obtain the homometallic products by salt metathesis, a supposedly straightforward method.¹⁻³ In addition to the syntheses of [(IPr*)₂Cu₂(μ₂-S)] (**3.I**) and [(7Dipp)₂Cu₂(μ₂-S)] (**3.III**) discussed above, the synthesis of phosphine-stabilized analogues, for instance [(Ph₃P)₂Au₂(μ₂-S)] (**3.IV**), have been realized by salt metathesis.^{2,3,33} The ability to selectively isolate **3.I**, **3.III**, and **3.IV** by this direct method suggested that the failure to do so in this work was not a function of the reaction method, rather, something inherent to the nature of [(ITr)₂M₂(μ₂-E)] must have limited the ability to isolate these compounds. Barring the electronic differences between **3.IV** and **3.I – 3.III**, the inability to isolate [(ITr)₂M₂(μ₂-E)] (M= Cu, Au; E=S, Se) in light of the successes for **3.I** and **3.III** suggested that the steric profile of ITr played a role.^{2,3} In this vein, failure to isolate [(ITr)₂Cu₂(μ₂-S)] (**3.2a'**) by salt metathesis helped suggest that excessive steric crowding about the metal centre could have caused unfavorable steric interactions and limited selective product formation in this work.

Comparison of the %V_{bur} calculated about the Cu centre in [(IPr*)₂Cu₂(μ₂-S)] (**3.I**), [(IPr)₂Cu₂(μ₃-S)SiMe₃]⁺ (**3.II**), [(7Dipp)₂Cu₂(μ₂-S)] (**3.III**), and [ITrCuSSiMe₃] (**3.2a**) showed a dramatic difference, with the metal being most sequestered in **3.2a** (See Appendix)^{2,3,34} This suggested that the steric demand of ITr on the metal centre was far greater than has been observed previously in literature.¹⁻³ This comparison was made carefully, however, given the subtle difference in the coordination geometry about the metals in multinuclear compounds **3.I – 3.III** and the mononuclear **3.1b**.^{2,3} Therefore, this quantity helped to give some measure of the steric demand on the copper centre, but could not alone be used to argue that the ligand was too large to allow for the formation of [(ITr)₂Cu₂(μ₂-S)] (**3.2a'**). Ironically, the isolation of one of the compounds in the series [(ITr)₂M₂(μ₂-E)] would have been the best comparator to **3.I – 3.III**, to discuss the limitations of ITr and help explain the inability to selectively form any other compound in the series. Fortunately, a single crystal of what was presumed to be [(ITr)₂Au₂(μ₂-Cl)]OTf (**3.7**) was recently isolated from reactions using [ITrAuSSiMe₃] and Bi(OTf)₃ in chlorinated solvent, conducted for an unrelated work. The structural details of **3.7** allowed an investigation into the coordination profiles of bulky NHCs in dinuclear molecules bridged by a (μ₂-S) or (μ₂-Cl). By comparing the molecular structures of [(NHC)₂Cu₂(μ₂-S)] (NHC=IPr*, **3.I**; 7Dipp, **3.III**) and [(NHC)Au₂(μ₂-Cl)]⁺

(NHC=ITr, **3.7**; 7Dipp, **3.V**) any structural differences observed between the compounds could be carefully extrapolated to the structures of $[(ITr)_2M_2(\mu_2-E)]$, helping shed some light as to why they were not selectively made by even the most direct methods available.

The presumption on the identity of $[(ITr)_2Au_2(\mu_2-Cl)]^+$ (**3.7**) was due to the presence of additional electron density in the crystallographic data that could not be satisfactorily modeled during structure refinement, which initially suggested a molecular sulfide, $[(ITr)_2Au_2(\mu_2-S)]$. After many attempts at modelling this unassigned electron density as disordered solvent molecules, it was thought to try to model the density as a triflate counterion, suggesting instead a molecular gold chloride compound. With no suitable model obtained, comparison between the Au–Cl bond lengths in the molecular structure of **3.7** with those in analogous $[(7Dipp)_2Au_2(\mu_2-Cl)]^+$ (**3.V**) and $[(Ph_3P)_2Au_2(\mu_2-Cl)]^+$ (**3.VI**) showed very little statistical difference, while comparison to the molecular structure of a sulfido analogue, $[(Ph_3P)_2Au_2(\mu_2-S)]$ (**3.VII**) showed a larger difference, precluding **3.7** as the gold sulfide molecule ($r_{Au-X_{ave}}$: **3.7** = 2.3036(6)Å; **3.V** = 2.313(5)Å; **3.VI** = 2.339(5)Å; **3.VII** = 2.159(5)Å).^{35–37}

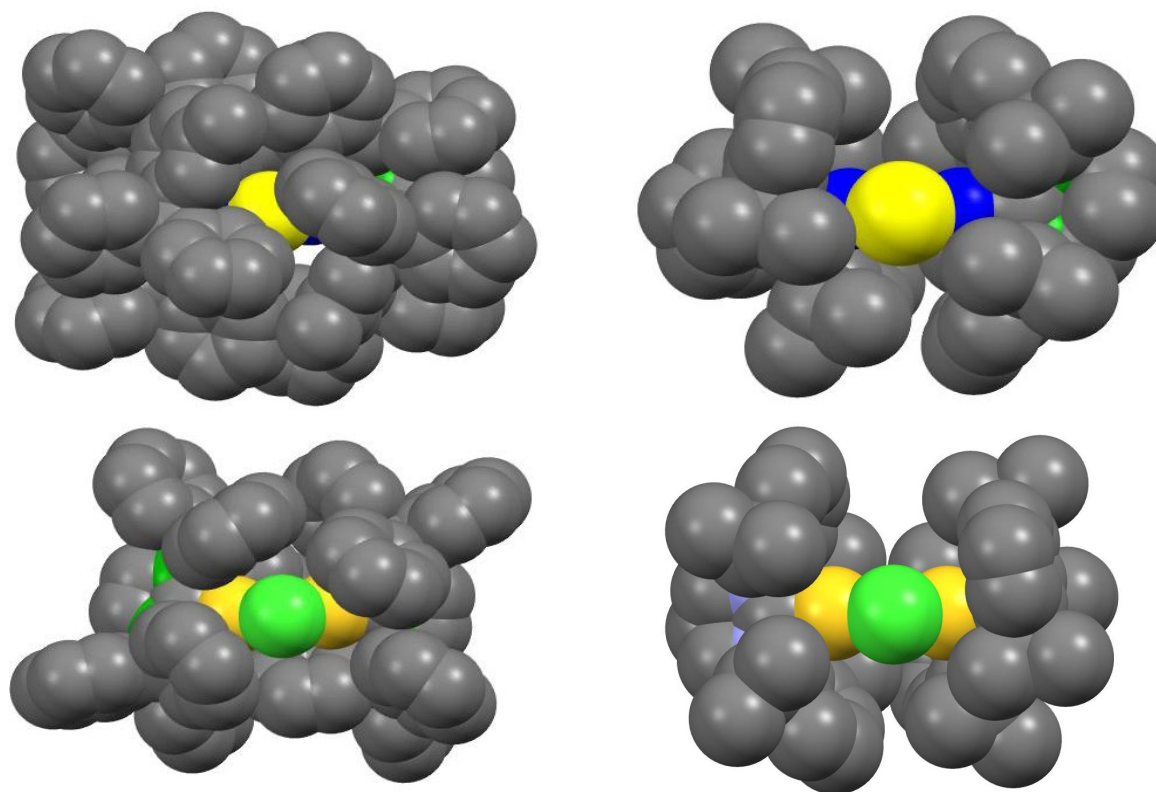


Figure 3.14: Space Filling Models of $[(IPr^*)_2Cu_2(\mu_2-S)]$, (**3.I**, top left), $[(7Dipp)_2Cu_2(\mu_2-S)]$ (**3.III**, top right), $[(7Dipp)_2Au_2(\mu_2-Cl)]^+$ (**3.V** bottom right) and $[(ITr)_2Au_2(\mu_2-Cl)]^+$ (**3.7**, bottom left). Solvent and counter ions omitted for clarity. Cl = lime green, S = yellow, Au = gold, N = green, C = grey, Cu = blue.

The molecular structures of $[(\text{NHC})_2\text{Cu}_2(\mu_2\text{-S})]$ (NHC=IPr*, **3.I**; 7Dipp, **3.III**) and $[(\text{NHC})\text{Au}_2(\mu_2\text{-Cl})]^+$ (NHC=ITr, **3.7**; 7Dipp, **3.V**) were compared to ascertain any structural differences that could help explain the inability to selectively make $[(\text{ITr})_2\text{M}_2(\mu_2\text{-E})]$, with a focus on $[(\text{ITr})_2\text{Cu}_2(\mu_2\text{-S})]$ (**3.2a'**) as the simplest compound not selectively made (**Figure 3.14**). Attempting to use the structure of **3.7** to discuss the targeted compounds of this work was done with the understanding that structural changes would occur as the $[\text{Au}_2(\mu_2\text{-Cl})]^+$ fragment is exchanged for $[\text{Cu}_2(\mu_2\text{-S})]$. Though the general structural framework was proposed to be similar, the difference in atomic radii, M – X bond length (X = S, Cl) and the M – X – M bond angles were expected to cause structural differences that would not be immediately obvious in the molecular structure of **3.7**. The differences between **3.7** and **3.I**, for example, suggest that replacing the $[\text{Au}_2(\mu_2\text{-Cl})]^+$ framework with $[\text{Cu}_2(\mu_2\text{-S})]$ could result in a more obtuse M–X–M bond angle, shorter NHC–Cu bonds and shorter Cu–S bonds.² Combined with a smaller copper centre, these differences could result in the metals buried deeper in the NHC “pocket” and swung out closer to the plane in which the bridging ligand sat. Comparison of **3.III** and **3.V**, which both feature the same NHC, suggested all of the same structural changes, with the exception of a more acute Cu–S–Cu bond angle (**3.III** = 110.66(6)° vs. **3.V** = 121.07(7)°), which could bring the bulky ITr ligands in closer proximity to each other.^{3,35} Though this is partially reflected in the space filling models of these compounds (**Figure 3.14** right), attempting to predict the structural properties of $[(\text{ITr})_2\text{Cu}_2(\mu_2\text{-S})]$ without any comparable data on $[(\text{ITr})_2\text{M}_2(\mu_2\text{-E})]$ would be non-trivial and difficult to imagine with structural data and space – filling models alone.

In an attempt to better understand the coordination profile of the compounds discussed in this work, steric maps were generated using the *SambVca* web application, available online for the calculation of %V_{bur} for quantification of the steric bulk of NHCs and other (ancillary) ligands.³⁴ These maps have been used previously to discuss and “evaluate the role of steric hindrance on the IPr NHC ligand”, wherein researchers generated these maps to show how substitution of the phenyl rings in IPr* resulted in a ligand with similar %V_{bur} but different coordination characteristics.³⁸ Using SCXRD data, the steric maps of $[(\text{NHC})_2\text{Cu}_2(\mu_2\text{-S})]$ (**3.I** = IPr*, **3.III** = 7Dipp), $[(\text{IPr})_2\text{Cu}_2(\mu_3\text{-SSiMe}_3)]^+$ (**3.II**), $[(\text{ITr})\text{CuSSiMe}_3]$ (**3.2a**) and $[(\text{NHC})_2\text{Au}_2(\mu_2\text{-Cl})]^+$ (**3.V** = 7Dipp, **3.7** = ITr) were generated and the %V_{bur} of the coordination sphere used to generate each image was calculated, along with the free volume within certain “pockets” (see Appendix). The maps for **3.II** were generated by eliminating the –SiMe₃ moiety from the calculations, to probe the effect of the R groups of IPr on a five-membered framework in contrast to their behaviour on the seven-membered 7Dipp.^{2,3,34}

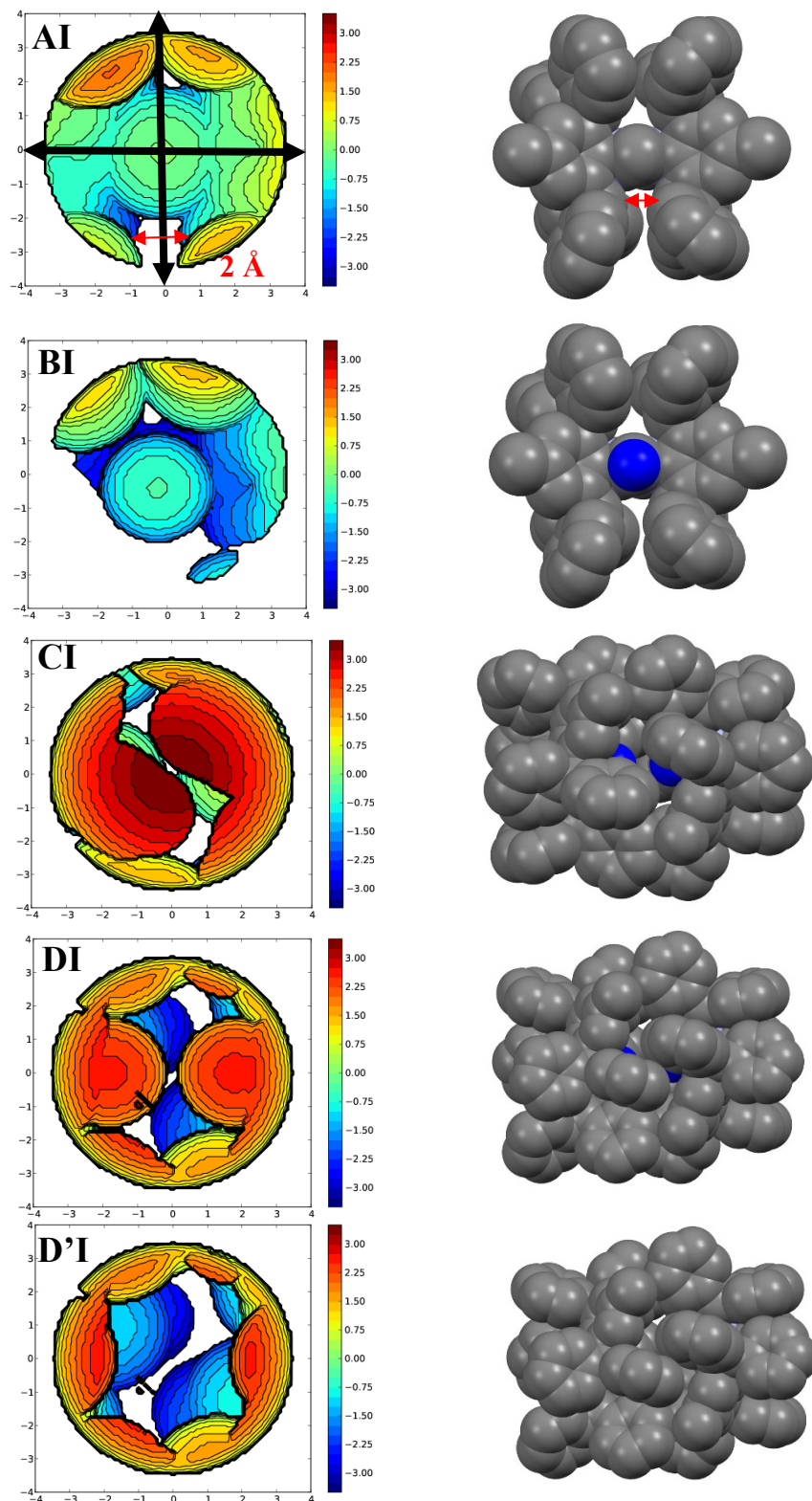


Figure 3.15: Steric maps of $[(IPr^*)_2Cu_2(\mu_2-S)]$ (**3.I**) generated from crystallographic data. Space filling model next to each image shows the molecule in the same orientation, with the appropriate atoms deleted. C = grey, Cu^I = blue. See Appendix for details.

An example of the steric maps generated is shown in **Figure 3.15** along with space – filling models of **3.I** in the corresponding orientation used for the generation of each image (See Appendix).^{2,34} These images behaved like detailed space–filling models, with scales and contours to help quantify the space around a centre of choice. For instance, **Figure 3.15 – AI** was generated by setting a copper atom (not shown in the space filling model) as the centre of a coordination sphere with a 3.5Å diameter. The contour plots helped to visualize the steric hindrance offered by the IPr* R groups, especially in quadrant I and II (on the Cartesian plane of **AI**), and show that a space of ~2Å is available for access to the copper atom in this “pocket” (**Figure 3.15**). It should be noted that these “distances” are actually generated by the crystallographic data, which has been modified to account for the atomic radii of the elements given by the Bondi radii and scaled by a theoretically determined multiplier.³⁴ Thus, a single figure on its own was not very informative, however, comparison of a number of images of related structures could offer some insight on the effect of the NHC in each structure.

By studying these plots generated for [(IPr)₂Cu₂(μ₃-SSiMe₃)]⁺ (**3.II**) and [(7Dipp)₂M₂(μ₂-X)]ⁿ⁺ (**3.III** M =Cu^I, X =S, n = 0; **3.V** M=Au^I, X=Cl, n=1), it was ultimately found that the larger backbone (7Dipp vs. IPr) resulted in the R groups swinging closer to the metal centre, extending beyond the Cu atoms in **3.III** to partially cover the bridging μ₂-S ligand (see **Figure 3.16**). The molecular structure of **3.II** required the -SiMe₃ to protect the compound from further degradation because IPr was unsuitable at protecting the bridging sulfido ligand. Interestingly, replacement of the [Cu₂(μ₂-S)] subunit in **3.III** with [Au₂(μ₂-Cl)]⁺ in **3.V** resulted in structural changes that ultimately led to a more exposed, less protected inorganic core (see **Figure S.3**). Because **3.V** was isolated as an intermediate in the abstraction of chloride from [(7Dipp)AuCl] by Na[BAr^f₄], one could imagine that this structure was less stable than the final [(7Dipp)₂Au₂(μ-Ar^f)]⁺ molecule formed, which featured a completely buried inorganic core. In the context of this work, the maps generated for **3.V** and **3.III** suggest that a similar change with ITr should result in a more encumbered inorganic core, on going from [(ITr)₂Au₂(μ₂-Cl)]⁺ (**3.7**) to [(ITr)₂Cu₂(μ₂-S)] (**3.2a'**). The analysis of similar images generated for **3.7** and [ITrCuSSiMe₃] **3.2a** suggest that such a structural change could result in excessive steric clashing, likely preventing the formation of **3.2a'** and other analogues. Further support for this hypothesis was the more encapsulated metal centre in **3.2a** and the observation that **3.7** featured steric interactions between opposing trityl groups that could not be resolved at the level of calculation done to generate these images (**Figure S.4 – D7/D'7**).

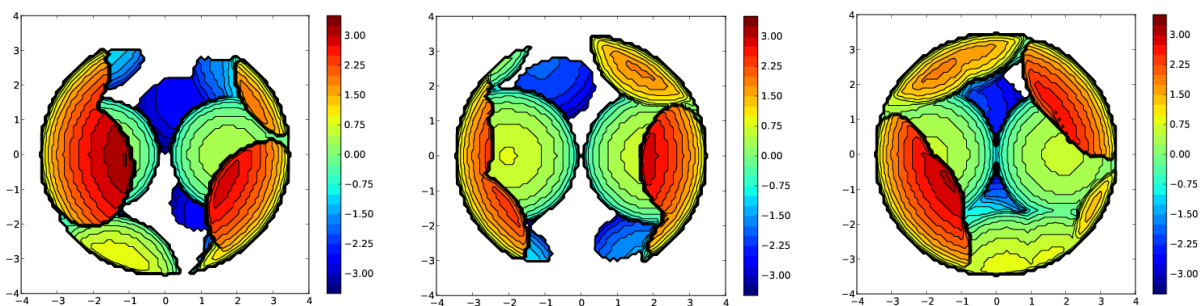


Figure 3.16: Steric Maps of $[(7\text{Dipp})_2\text{Cu}_2(\mu_2\text{-S})]$ (**3.III**) and $[(\text{NHC})_2\text{Au}_2(\mu_2\text{-Cl})]^+$ (NHC = 7Dipp, **3.V**; ITr, **3.7**) in the same orientation seen in **Figure 3.14** (Orientation C, see Appendix)

While this analysis provided some explanation on the inability to access $[(\text{ITr})_2\text{Cu}_2(\mu_2\text{-E})]$, the space filling models of **3.6** and **3.V** suggested that the gold analogues should have been easily accessible (**Figure 3.14** and **Figure 3.16**). The NMR data shown in **Figure 3.5** and **Figure 3.8** had suggested that $[(\text{ITr})_2\text{Au}_2(\mu_2\text{-E})]$ (**3.2c'** – **3.3c'**) was sensitive to the presence of chlorinated solvent and may have been prone to the formation of $[(\text{ITr})_3\text{Au}_3(\mu_3\text{-E})]^+$ during the salt metathesis reactions. Assuming minimal structural change between **3.6** and **3.2c'** – **3.3c'**, the analysis of the steric maps suggests the bridging chalcogenido moiety in the gold compounds of this work would be more exposed than most of the other compounds analyzed in this work (see **Figure 3.16**). If the chalcogenido moiety in $[(\text{ITr})_2\text{Au}_2(\mu_2\text{-E})]$ (**3.2c'** – **3.3c'**) remained as nucleophilic as $[(\text{IPr}^*)_2\text{Cu}_2(\mu_2\text{-S})]$, this could help explain the difficulty in obtaining **3.2c'** and **3.3c'**, as the dinuclear subunits could coordinate to any $[\text{ITrAu}]^+$ fragments that may be formed *in situ*.²

3.3 Conclusions

The methods discussed above were unsuccessful in the isolation of dinuclear metal chalcogenide molecules. The full characterization of the products proposed to be $[(\text{ITr})_2\text{Au}_2(\mu_2\text{-E})]$ (E = S, **3.2c'**; Se, **3.3c'**) has not been accomplished due to the mixture of compounds inevitably obtained during their attempted synthesis. ESI – MS data from experiments using the silyl deprotection strategy (**Scheme 3.1**) have been the only indicators that **3.2b'** and **3.3c'** may have been made. Attempting to access these proposed compounds by salt metathesis led to a mixture of products when mixed at room temperature, following the darkening of the reaction mixtures due to a small amount of colloidal gold being formed.

Ultimately, this represented one of the only marginal success in this work. Salt metathesis reactions toward $[(\text{ITr})_2\text{Cu}_2(\mu_2\text{-E})]$ (E = S, **3.2a'**; Se, **3.3a'**) showed no progress when stirred at room temperature for 48 hours. Reactions attempted according to **Scheme 3.2** behaved erratically depending on the system studied. The ligand exchange apparent in the ^1H NMR data of reactions between $[(\text{ITr})\text{CuESiMe}_3]$ (E = S, **3.2a**; Se, **3.3a**) and $[(\text{ITr})\text{M}'\text{OAc}]$ (M' = Ag, **3.1b**; Au, **3.1c**) (**Figure 3.12**, **Figure 3.15**) had no literature precedent and was not studied any further. While reactions between **3.3a** and **3.1c** showed the presence of $[(\text{ITr})\text{CuOAc}]$ (**3.1a**), there was no indication of $[(\text{ITr})\text{AuSeSiMe}_3]$ (**3.3c**) in the NMR data of these mixtures. Attempting the reaction towards $[(\text{ITr})\text{Cu}(\mu_2\text{-E})\text{Au}(\text{ITr})]$ (E = S, **3.2ac**; Se, **3.3ac**) using $[(\text{ITr})\text{AuESiMe}_3]$ (E = S, **3.2c**; Se, **3.3c**) and **3.1a** often resulted in no reaction at low temperature, with reactions stirred at room temperature for extended periods of time forming a mixture of products. The most promising reactions attempted were of **3.2c** – **3.3c** with $[(\text{ITr})\text{AgOAc}]$ (**3.1b**), however, suitable crystals for SCXRD have not been isolated and ESI-MS has not shown evidence of the product molecular ion. Attempting to track reaction progress *in situ* by ^1H NMR spectroscopy showed these reactions proceed very slowly at $-25\text{ }^\circ\text{C}$ and suffer unknown side reactions when warmed to $-10\text{ }^\circ\text{C}$. The absence of any structural data precludes any conclusion being made on the viability of these reactions.

A closer analysis of the molecular structure of $[(\text{ITr})_2\text{Au}_2(\mu_2\text{-Cl})]^+$ (**3.6**) and comparison with the structure of other dinuclear metal chalcogenides from previous literature helped to suggest part of the reason the compounds in this work were not isolated selectively was due to the steric profile of the ITr ligand.^{1-3,35} $[(\text{ITr})_2\text{Cu}_2(\mu_2\text{-E})]$ (E = S, **3.2a'**; Se, **3.3a'**) and $[(\text{ITr})_2\text{Au}_2(\mu_2\text{-E})]$ (E = S, **3.2c'**; Se, **3.3c'**) could not be isolated selectively for different reasons by this analysis. Excessive steric crowding around the copper centres likely precluded the synthesis of **3.2a'** – **3.3a'**, especially under the conditions of salt metathesis. Further investigations could be made as to whether these molecules would become accessible with some other synthetic technique that was not kinetically hindered, however, the analysis in this work suggested the ITr ligand would be too large to fit. Ironically, the coordination profile of **3.6** suggested that **3.3'b** – **3.3'c** could be prone to further reactivity, making their synthesis possible but complicated by issues of unselective reactivity. Given the unsuitable nature of the silyl deprotection strategy toward the compounds targeted in this work, syntheses attempted by salt metathesis were likely prone to excessive reaction at the chalcogen bridge and the formation of a $[\text{Au}_3(\mu_3\text{-E})]^+$ inorganic framework. These claims are made tentatively, however, given the fact that no structural characterization on these proposed products has been conducted. While NHCs provide stability to many of the structures targeted by inorganic chemists, further work is required to understand the nuances of these ligands and how they affect metal chalcogenide chemistry.

3.4 Experimental

3.4.1. General Considerations

All syntheses described were carried out using standard double-manifold Schlenk-line techniques, under an atmosphere of high-purity dry nitrogen. Non-chlorinated solvents (tetrahydrofuran, toluene, hexanes, pentane) were dried and collected using an MBraun MB-SP Series solvent purification system and stored over 3 Å molecular sieves. Tetrahydrofuran was often degassed further by three to five freeze-pump-thaw cycles just prior to use. Deuterated chloroform and deuterated benzene were purchased from Caledon and dried over P₂O₅ and NaK alloy respectively, refluxing under N₂ prior to collecting by distillation. Celite® was dried under dynamic vacuum at 220°C for 24 hours and stored under nitrogen in a sealed flask. Many chemicals required for the syntheses of starting materials were used as received from commercial sources (Alfa Aesoar, Sigma Aldrich, Caledon). S(SiMe₃)₂, Se(SiMe₃)₂, ITr·HOTf, and [ITrAuCl] were synthesized according to previous literature preparations.^{11,25} All NMR spectra were recorded on Inova 400 and Inova 600 spectrometers. ¹H and ¹³C{¹H} NMR chemical shifts are reported relative to SiMe₄ at 25 °C using either the residual solvent signals or silicone grease as internal references. Heteronuclear Multiple Bond Correlation Experiments were performed for ¹³C-¹H to confirm peak assignments or to improve signal to noise for the detection of carbenic carbons. Electrospray Ionization-Mass Spectrometry was conducted at the Mass Spectrometry Facility by Mr. Doug Hairsine.

3.4.2. Syntheses

Synthesis of [ITrCuCl] (3.4) – In a 100 mL round-bottom flask, ITr·HOTf (0.542 g, 0.771 mmol) and KHMDS (0.154 g, 0.770 mmol) were suspended in 25 mL toluene and the yellow slurry was left stirring overnight. The mixture was filtered over Celite and the filtrate dropped directly onto excess CuCl (0.100 g, 1.01 mmol) to get a cloudy mixture. The mixture was stirred for 3 hours at room temperature and filtered over Celite; the Celite pad was washed with a total of 25 mL CH₂Cl₂, and the filtrate dried *in vacuo* to obtain an off-white solid (0.243 g, 49% yield). **M.p.** 180 °C. **¹H NMR (C₆D₆, 399.76 MHz, 25 °C):** δ 7.23 – 7.28 (o-ArH, 12H), δ 7.07 – 7.13 (m - ArH, 12H), δ 7.01 – 7.07 (p - ArH, 6H), δ 6.54 ppm (s, H_{4,5-imid}, 2H). **¹³C{¹H} NMR (C₆D₆, 100.53 MHz, 25 °C):** δ 188.7 (NCN), δ 142.7 (ArC), δ 130.3 (ArC), δ 128.6 (ArC), δ 120.3 (ArC), δ 78.4 (CPh₃) ppm.

Attempted Syntheses of [(ITr)₂M₂(μ₂-E)] (E = S, 3.1'b – 3.3'b; Se, 3.1'c – 3.3'c): Reactions toward the homometallic compounds outlined in this work were attempted by two general methods. *Method I:*

Two equivalents of [ITrMOAc] were dissolved and the mixture cooled to allow for the addition of E(SiMe₃)₂. The reaction was stirred per the protocol established in Chapter 2 for the synthesis of the respective [(ITr)MESiMe₃] complex; for [(ITr)AuESiMe₃] addition of the chalcogen reagent was done at -60 °C and the reaction stirred between -50 °C to -40 °C for 1 – 2 hours and then allowed to warm to room temperature. For reactions conducted in CDCl₃ aliquots were taken for analysis by ¹H NMR and ¹H – ¹³C HMBC NMR spectroscopy. Reactions conducted in THF were analyzed by evacuating an aliquot (~5 mg theoretical) in a pre-dried NMR tube, followed by dissolution in the appropriate NMR solvent. Often, reactions that had become turbid from stirring at room temperature were filtered over Celite through a glass frit, washed with the appropriate reaction solvent 1 – 3 times and the filtrate analyzed or worked up further. Crystals of [ITrMCl] (M = Cu, **3.4**; Ag, **3.5**; Au, **3.6**) were grown from reactions conducted in CDCl₃ by slow diffusion of pentane into the reaction mixture at -25 °C over 2 – 3 days. *Method II*: [ITrMCl] was dissolved in THF or toluene and added to a slurry of Na₂E in the same solvent. Some attempts were made by initiating the reaction at low temperatures (T ≤ -40 °C) by cooling the slurry down and adding the chlorido complex dropwise. The mixtures were warmed to room temperature and reaction aliquots analyzed by transferring to an NMR tube, evacuating the reaction solvent and dissolving in the appropriate NMR solvent. Where the solids generated were analyzed by SEM-EDX, the mixture was left to sit, and precipitate allowed to settle. The mother liquor was decanted, and the precipitate washed 3 – 5 times before drying *in vacuo* and mounting onto SEM grids in the glovebox. Where the solids were not isolated, the reaction mixtures were filtered through Celite and the filtrate evacuated to dryness for subsequent analysis.

Attempted Syntheses of [(ITr)₂Ag(μ₂-E)M⁺] (M = Cu, **3.12b/c; Au, **3.23b/c**; E = S, **b**; Se, **c**):** Reactions toward **3.12b** and **3.12c** were conducted by the *in situ* generation of [ITrCuESiMe₃] (E = S, **3.1b**; Se, **3.1c**) per the protocols established in Chapter 2, followed by cooling the reaction mixture to T ≤ -50 °C for addition of [ITrAgOAc] (**3.2a**). These reactions were conducted in CDCl₃ and analyzed by taking aliquots for analysis at various points in the reaction. Reactions toward **3.23b** and **3.23c** were conducted by adding a solution of **3.2a** to [(ITr)AuESiMe₃] (E = S, **3.3b**; Se, **3.3c**). A reaction toward **3.23b** was conducted in CDCl₃ by the addition of **3.3b** (0.031 g, 0.036 mmol) and **3.2a** (0.024g, 0.033 mmol) to a J. Young Tube followed by distillation of ~ 2 mL CDCl₃ into the tube at -70 °C. The frozen sample was inserted into an INOVA 400 spectrometer pre-cooled to -25 °C and allowed to thaw in the machine; full melting and equilibration to this temperature was confirmed by monitoring lock and shim values. After conducting the variable temperature NMR experiments, the sample was ejected and stored at -25 °C. The sample was emptied into a pre-cooled Schlenk tube under a flow of nitrogen and attempts

were made to grow single crystals for analysis by SCXRD experiments. Crystals have thus far not been isolated suitable for SCXRD experiments.

Attempted Syntheses of [(ITr)₂Cu(μ_2 -E)Au] (E = S, **3.13b; Se, **3.13c**):** Reactions were attempted by varying the acetates from [(ITr)CuOAc] (**3.1a**) to [(ITr)AuOAc] (**3.3a**) as well as the metallochalcogenolates from **3.1b/3.1c** – **3.3b/3.3c**, respectively. For those reactions conducted with **3.1b/3.1c**, the cuprachalcogenolates were synthesized *in situ* following the protocols set in Chapter 2, the reactions cooled back down to $T \leq -50$ °C and **3.3a** added to initiate the reaction. For reactions with **3.3b/3.3c** the aurachalcogenolates were synthesized separately, dissolved in the appropriate reaction solvent and a solution of **3.1a** was added to this at $T \leq -50$ °C to initiate the reaction. In either case, reactions in CDCl₃ were monitored by taking reaction aliquots and transferring them to NMR tubes, while reactions in non-deuterated solvent were transferred to NMR tubes, the reaction solvent evacuated, and the sample dissolved in deuterated solvent.

3.4 References

- (1) Zhai, J.; Hopkins, M. D.; Hillhouse, G. L. *Organometallics* **2015**, *34*, 4637–4640.
- (2) Zhai, J.; Filatov, A. S.; Hillhouse, G. L.; Hopkins, M. D. *Chem. Sci.* **2016**, *7*, 589–595.
- (3) Jordan, A. J.; Walde, R. K.; Schultz, K. M.; Bacsa, J.; Sadighi, J. P. *Inorg. Chem.* **2019**, *58*, 9592–9596.
- (4) Bagherzadeh, S.; Mankad, N. P. *Chem. Commun.* **2018**, *54*, 1097–1100.
- (5) Hopkinson, M. N.; Richter, C.; Schedler, M.; Glorius, F. *Nature* **2014**, *510*, 485–496.
- (6) Nelson, D. J.; Nolan, S. P. *Chem. Soc. Rev.* **2013**, *42*, 6723–6753.
- (7) Gómez-Suárez, A.; Nelson, D. J.; Nolan, S. P. *Chem. Commun.* **2017**, *53*, 2650–2660.
- (8) Huynh, H. V. *Chem. Rev.* **2018**, *118*, 9457–9492.
- (9) Fard, M. A.; Weigend, F.; Corrigan, J. F. *Chem. Commun. (Camb)*. **2015**, *51*, 8361–8364.
- (10) Azizpoor Fard, M.; Levchenko, T. I.; Cadogan, C.; Humenny, W. J.; Corrigan, J. F. *Chem. –Eur. J.* **2016**, *22*, 4543–4550.
- (11) Polgar, A. M.; Weigend, F.; Zhang, A.; Stillman, M. J.; Corrigan, J. F. *J. Am. Chem. Soc.* **2017**, *139*, 14045–14048.
- (12) Polgar, A. M.; Zhang, A.; Mack, F.; Weigend, F.; Lebedkin, S.; Stillman, M. J.; Corrigan, J. F. *Inorg. Chem.* **2019**, *58*, 3338–3348.
- (13) DeGroot, M. W.; Corrigan, J. F. *Organometallics* **2005**, *24*, 3378–3385.
- (14) Tran, D. T. T.; Corrigan, J. F. *Organometallics* **2000**, *19*, 5202–5208.
- (15) Borecki, A.; Corrigan, J. F. *Inorg. Chem.* **2007**, *46*, 2478–2484.
- (16) Polgar, A. M.; Khadka, C. B.; Azizpoor Fard, M.; Nikkel, B.; O'Donnell, T.; Neumann, T.; Lahring, K.; Thompson, K.; Cadogan, C.; Weigend, F.; Corrigan, J. F. *Chem. –Eur. J.* **2016**, *22*, 18378–18382.
- (17) DeGroot, M. W.; Corrigan, J. F. *Angew. Chem., Int. Ed.* **2004**, *43*, 5355–5357.
- (18) DeGroot, M. W.; Taylor, N. J.; Corrigan, J. F. *J. Am. Chem. Soc.* **2003**, *125*, 864–865.
- (19) DeGroot, M. W.; Taylor, N. J.; Corrigan, J. F. *J. Am. Chem. Soc.* **2003**, *125*, 864–865.

- (20) Tran, D. T. T.; Beltran, L. M. C.; Kowalchuk, C. M.; Trefiak, N. R.; Taylor, N. J.; Corrigan, J. F. *Inorg. Chem.* **2002**, *41*, 5693–5698.
- (21) Thurston, J. H.; Trahan, D.; Ould–Ely, T.; Whitmire, K. H. *Inorg. Chem.* **2004**, *43*, 3299–3305.
- (22) Sculfort, S.; Braunstein, P. *Chem. Soc. Rev* **2011**, *40*, 2741–2760.
- (23) Gu, Y.–N.; Chen, Y.; Wu, Y.–L.; Zheng, S.–T.; Li, X.–X. *Inorg. Chem.* **2018**, *57*, 2472–2479.
- (24) Polgar, A. M.; Zhang, A.; Mack, F.; Weigend, F.; Lebedkin, S.; Stillman, M. J.; Corrigan, J. F. *Inorg. Chem* **2019**, *58*, 53.
- (25) Roy, M. M. D.; Lummis, P. A.; Ferguson, M. J.; McDonald, R.; Rivard, E. *Chem. –Eur. J.* **2017**, *23*, 11249–11252.
- (26) Roy, M. M. D.; Ferguson, M. J.; Mcdonald, R.; Rivard, E. *Chem. Commun.* **2018**, *54*, 483–486.
- (27) Gardea–Torresdey, J. L.; Tiemann, K. J.; Gamez, G.; Dokken, K.; Tehuacanero, S.; José–Yacamán, M. *J. Nanoparticle Res.* **1999**, *1*, 397–404.
- (28) Vorobyev, S.; Likhatski, M.; Romanchenko, A.; Maksimov, N.; Zharkov, S.; Krylov, A.; Mikhlin, Y. *Minerals* **2018**, *8*, 492.
- (29) Koelle, U.; Laguna, A. *Inorg.Chim. Acta* **1999**, *290*, 44–50.
- (30) Kowala, C.; Swan, J. M. *Aust. J. Chem.* **1966**, *19*, 547–554.
- (31) Clavier, H.; Nolan, S. P. *Chem. Commun.* **2010**, *46*, 841–861.
- (32) Dehnen, S.; Eichhöfer, A.; Fenske, D. *Eur. J. Inorg. Chem.* **2002**, *2002*, 279–317.
- (33) Canales, F.; Gimeno, C.; Laguna, A.; Villacampa, M. D. *Inorg. Chim. Acta* **1996**, *244*, 95–103.
- (34) Falivene, L.; Cao, Z.; Petta, A.; Serra, L.; Poater, A.; Oliva, R.; Scarano, V.; Cavallo, L. *Nat. Chem.* **2019**, *11*, 872–879.
- (35) Phillips, N.; Dodson, T.; Tirfoin, R.; Bates, J. I.; Aldridge, S. *Chem. – Eur. J.* **2014**, *20*, 16721–16731.
- (36) Jones, P. G.; Sheldrick, G. M.; Uson, R.; Laguna, A. *Acta Crystallogr., Sect. B: Struct. Crystallogr. Cryst. Chem.* **1980**, *36*, 1486–1488.
- (37) Lensch, C.; Jones, P. G.; Sheldrick, G. M. *Z. Naturforsch. B* **1982**, *37*, 944–949.
- (38) Poater, A.; Falivene, L.; Urbina–Blanco, C. A.; Manzini, S.; Nolan, S. P.; Cavallo, L. In *Procedia Computer Science*; Elsevier B.V., 2013; Vol. 18, pp 845–854.

Chapter 4

4 Conclusions and Outlook

4.1. Summary and Conclusions

The work in this thesis described the synthesis and characterization of a new series of NHC-stabilized trimethylsilyl metallochalcogenolates, using *bis*-1,3-tritylimidazole-2-ylidene (ITr), and the subsequent investigation into their reactivity toward dinuclear metal chalcogenide compounds.¹ Building on previous work, the syntheses of the metallochalcogenolate reagents were carried out by the 1:1 reaction of [ITrMOAc] with E(SiMe₃)₂, with reactions for the gold chalcogenolates conducted by the generation of [LiESiMe₃] followed by subsequent reaction with [ITrAuCl]. ¹H and ¹³C NMR spectroscopic data of these compounds, in comparison to previously synthesized analogues, confirm the electronically different nature of ITr to other NHCs previously used.²⁻⁴ The increased electron donating character and smaller HOMO-LUMO gap of ITr had important implications on understanding the NMR spectroscopic data for the metallochalcogenolates made in this work. SCXRD data of the copper chalcogenolate compounds showed the effect of the impressive steric bulk of the ITr ligand, compared to previously used NHCs, with some indication of η₂ interactions between Cu and the aryl rings on the ligand. The compounds made were thermally robust when isolated from solution, with solution stability of the copper and gold compounds being similar to, or better than, previous analogues made.²⁻⁵ The use of the more sterically demanding ITr had little effect on the solution stability of [ITrAgESiMe₃], given the weaker NHC – Ag bond more greatly affecting the stability of this species in solution.⁶

Subsequent attempts to isolate dinuclear metal chalcogenides of the group 11 metals using these newly synthesized compounds were unsuccessful. The general reaction strategy used for the attempted syntheses of the homometallic compounds mimicked the syntheses of the metallochalcogenolates, using a 2:1 ratio of [ITrMOAc] and E(SiMe₃)₂, in the hopes that the metallochalcogenolate generated *in situ* would react with the additional equivalent of the acetate, removing the –SiMe₃ group to form the desired compounds. The reactions failed to proceed selectively, yielding residual [ITrMOAc] and [ITrMESiMe₃]. The lack of selective product formation made product isolation and characterization difficult. The results described in this thesis work suggest compounds of the general formula [(ITr)₂M₂(μ₂-E)] (M = Cu, Ag, Au; E = S, Se) may be prone to decomposition in the presence of chlorinated solvents, mimicking the reactivity of previously synthesized dicopper sulfide molecules (see **Figure 4.1** for examples).⁷⁻⁹ For those reactions attempted in chlorinated solvents, some of the single crystals isolated were consistent

with the formation of [ITrMCl], though these data were evaluated on a preliminary basis and full structural solutions were not obtained, given the lack of novelty of these compounds.¹⁰ The closest indication of success was the identification of compounds whose NMR and ESI-MS spectra suggested the chemical formulae [(ITr)₂Au₂(μ₂-E)] (E = S, Se). These reactions appeared to be more successful when conducted in chlorinated solvents, however, the compounds were produced in a mixture with the respective metallochalcogenolate; avoiding chlorinated solvents seemed to affect reaction progress and only the [ITrAuESiMe₃] compounds were observed. Given the inability to selectively obtain dinuclear homometallic chalcogenide compounds by this general method, salt metathesis was also attempted toward the synthesis of the dinuclear chalcogenides of copper and gold. Analysis of the reactions of [ITrCuCl] and Na₂E suggested little to no reaction, while data from the analogous reaction with gold suggested unselective reactivity, with solutions left stirring for 24 hours at room temperature containing a mixture of [ITrAuCl] and other potential products.

Reactions toward the heterometallic compounds were attempted by the same silyl deprotection strategy cited above, reacting [ITrMESiMe₃] with [ITrM'OAc] at low temperatures in an attempt to selectively remove the -SiMe₃ moiety. Many of the reactions done in CDCl₃ suffered from unwanted side reactions, generating a mixture of products including [ITrMCl]. Reactions toward [(ITr)₂Ag(μ₂-E)Cu] were attempted by *in situ* generation of the cuprachalcogenolate and addition of [ITrAgOAc], with preliminary results suggesting ligand transfer to form the respective argentochalcogenolates and [ITrCuOAc]. The attempted synthesis of [(ITr)₂Ag(μ₂-E)Au] did not yield one product selectively, with reactions monitored by ¹H NMR spectroscopy in CDCl₃ suggesting unwanted side reactivity of [ITrAgOAc] that resulted in reaction mixtures containing [ITrAuESiMe₃] and other unidentified side products. The attempted synthesis of [(ITr)₂Au(μ₂-E)Cu] was done by varying the metal acetate and metallochalcogenolate reagents. Reactions using [ITrCuOAc] did not progress under conditions of kinetic control (i.e. lower temperatures) and produced a mixture of products when warmed to room temperature; reactions with [ITrAuESiMe₃] often resulted in the formation of [ITrAuOAc] as confirmed by ¹H and ¹³C NMR, with no indication of the corresponding [ITrCuESiMe₃] being formed.

4.2. Future Work

While the compounds in this work were not successful in obtaining the dinuclear metal chalcogenides, their synthesis contributed to the growing library of NHC – stabilized group 11 trimethylsilyl metallochalcogenolates, featuring ITr as a ligand that was very electron donating and sterically demanding.¹⁰ In the interest of expanding this library of compounds further, future work could focus on the synthesis of group 11 trimethylsilyl metallochalcogenolates with other NHCs. **Figure 4.1** featured the NHCs used to date in the synthesis of some of these compounds, however, not all of these ligands have been used to develop the full library of compounds ($M = \text{Cu}^I, \text{Ag}^I, \text{Au}^I$; $E = \text{S}, \text{Se}, \text{Te}$). By completing this library of compounds, their properties could be better understood, perhaps revealing new ways in which they may be used. In this vein, a quantum chemical investigation into the electronic structure of this class of compounds may help shed some light on their reactivity patterns.

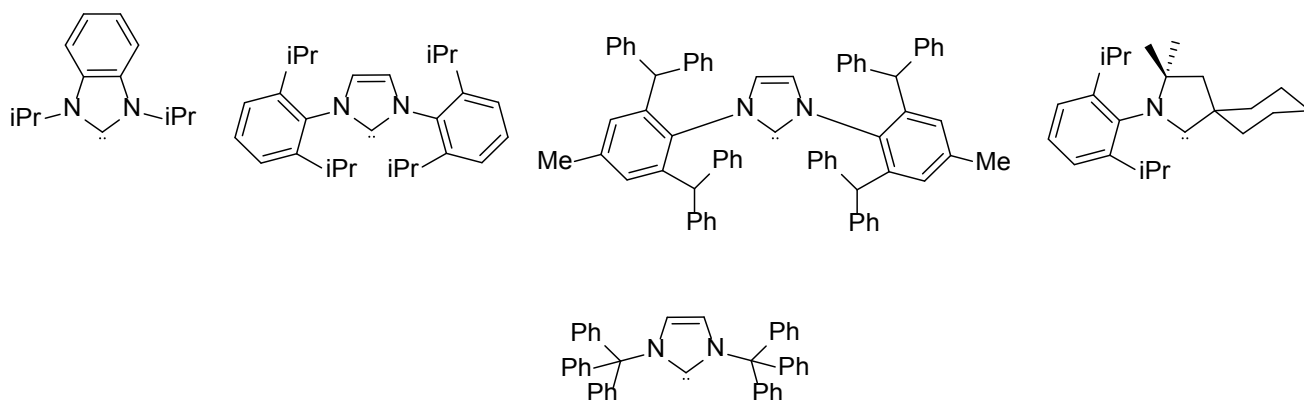


Figure 4.2: *N*-Heterocyclic Carbenes (NHCs) used in the isolation of group 11 trimethylsilyl metallochalcogenolates.

Although NHC-stabilized group 11 trimethylsilyl metallochalcogenolates have been used successfully in reactions with heterometallic compounds stabilized featuring weaker ancillary ligands (i.e. PR_3 , OPR_3 , etc.), or no ligand at all, this work was a second example to showcase the unselective reactivity of these compounds when involved in reactions with ternary reagents that also feature NHCs.^{2-5,7} It was thought that the steric bulk of ITr was a limiting factor in this chemistry, as similar challenges were faced when using *bis*-1,3-(2,6-(diphenylmethyl)-4-methylphenyl)imidazole-2-ylidene (IPr*) stabilized cuprathiolate $[\text{IPr}^*\text{CuSSiMe}_3]$.⁷ Though sterically less demanding, similar reactions involving *bis*-1,3-(2,6-diisopropylphenyl)imidazole-2-ylidene (IPr) were thought to proceed, albeit in a very slow and unselective manner; complete characterization of the product of this reaction was not done. In contrast to these shortcomings, the use of $[\text{IPr}^*\text{CuSH}]$ was shown to proceed by a clean reaction with $[\text{IPr}^*\text{CuO}^t\text{Bu}]$

toward the dinuclear copper sulfide molecule. Though the final product was, again, not completely characterized, the use of [IPrCuSH] and [IPrCuO^tBu] resulted in the formation of a single product after five minutes in an NMR experiment. These results suggested that the acid – base deprotection strategy is a more straightforward method toward the synthesis of dinuclear metal chalcogenide molecules. Future work could focus on the use of [NHCM – EH] compounds, likely of copper and gold, in reactions with heterometallic NHC-stabilized alkoxides to attempt the synthesis of new and interesting molecules.

Despite the previously reported utility of the NHC-stabilized metallochalcogenol compounds, their relative instability and the limited reports of their synthesis make them a less attractive option as synthons for the pursuit of heterometallic compounds.⁷ Additionally, adapting this methodology to compounds of silver (i.e. [NHCAg-EH]) would be a challenge given the limited solution stability of even the NHC-stabilized trimethylsilyl argentochalcogenolates.² Thus, the use of the trimethylsilyl metallochalcogenolates should continue to be investigated, to find the reaction conditions that favour the selective formation of low – nuclearity, homoleptic, heterometallic chalcogenide molecules targeted herein. A review of this work, and the previous works that inspired it, suggested the use of trimethylsilyl protecting groups may favour reactions that are limited by the surprising challenge of cleaving the E – Si bond on the metallochalcogenolate molecule. Quantum chemical investigations into the electronic structure of these compounds have not been done; these studies, along with *in silico* studies on the reaction mechanisms favoured by these reagents, may give some indication on how best to proceed with this research in the future.

In conjunction with these theoretical studies, the reaction of NHC-stabilized trimethylsilyl metallochalcogenolates and heterometal reagents should continue to be investigated with various [NHCM – X] reagents, where X is a nucleophilic anion. Though the previously reported use of [NHCCuF] (NHC = IPr, IPr*) featured a very nucleophilic fluoride, these previous reaction data, in light of the results from this work, suggest that these reagents favour the formation of compounds that may have resulted from the generation of [(NHC)Cu]⁺ cations.⁷ Though these claims can only amount to speculation, they follow the observation that these previously reported reactions proceeded unselectively, and certain reactions in this work involved ligand transfer that could have occurred by some transient [ITrM]⁺ species in solution.^{11,12} A review of the Supporting Information from Zhai *et al.* suggested reactions involving IPr* formed an unknown compound whose ¹H NMR chemical shifts bore a striking resemblance to that of [IPr*CuF], as though a [(IPr*)₂Cu₂(μ₂-F)]F complex was formed.⁷ The use of IPr led to an unknown compound whose ¹H NMR spectrum featured a singlet that the researchers interpreted as the presence of

a -SiMe₃ group, perhaps suggesting [(IPr)₂Cu₂(μ₂-SSiMe₃)]F^{7,9}. By Pearson Hard/Soft Acid Base Theory (PSAB), the soft/hard interaction between Cu^I and F⁻, coupled with the presence of the stabilizing NHC ligands, may bias these reactions to proceed through a dissociative mechanism. The culmination of this discussion, then, is the proposed use of [NHC–M–X] reagents whose X groups are more tightly bound to the metal centre. While the use of metal acetates in this work was in line with this vision, the delocalized nature of the carbonyl lone pair made it difficult to undergo nucleophilic attack, with data suggesting it was prone to ligand transfer instead. The use of NHC-stabilized metal alkoxides could mitigate these challenges by featuring an alkoxy moiety with more localized electron density and a stronger propensity to bond to silicon centres. Another specific example for future work in this regard featured compounds of the general formula [(NHC)Au(CH₂COCH₃)], which has demonstrated reactivity with ^tBuPh₂SiCl despite excessive steric crowding about the silicon centre (see **Figure 4.2**).¹³ Though reported only for the gold molecules, these compounds can be investigated in the reaction toward [NHCM'ESiMe₃], to first probe whether selective transformations could be conducted toward heterometallic gold chalcogenide molecules and then subsequent work applying this motif to the other group 11 metals.

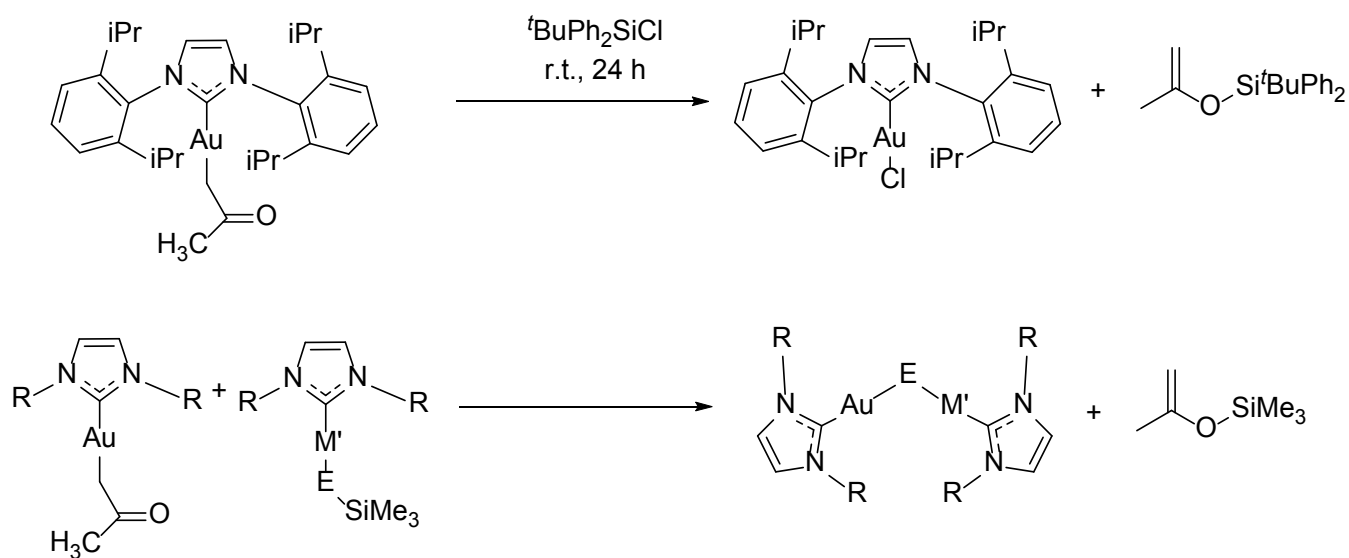


Figure 4.3: Example of silyl deprotection of [(NHC)Au(CH₂COCH₃)] from Nolan *et al.* (NHC = IPr, top). Proposed use for future work toward synthesis of heterometallic dinuclear gold chalcogenides (bottom).

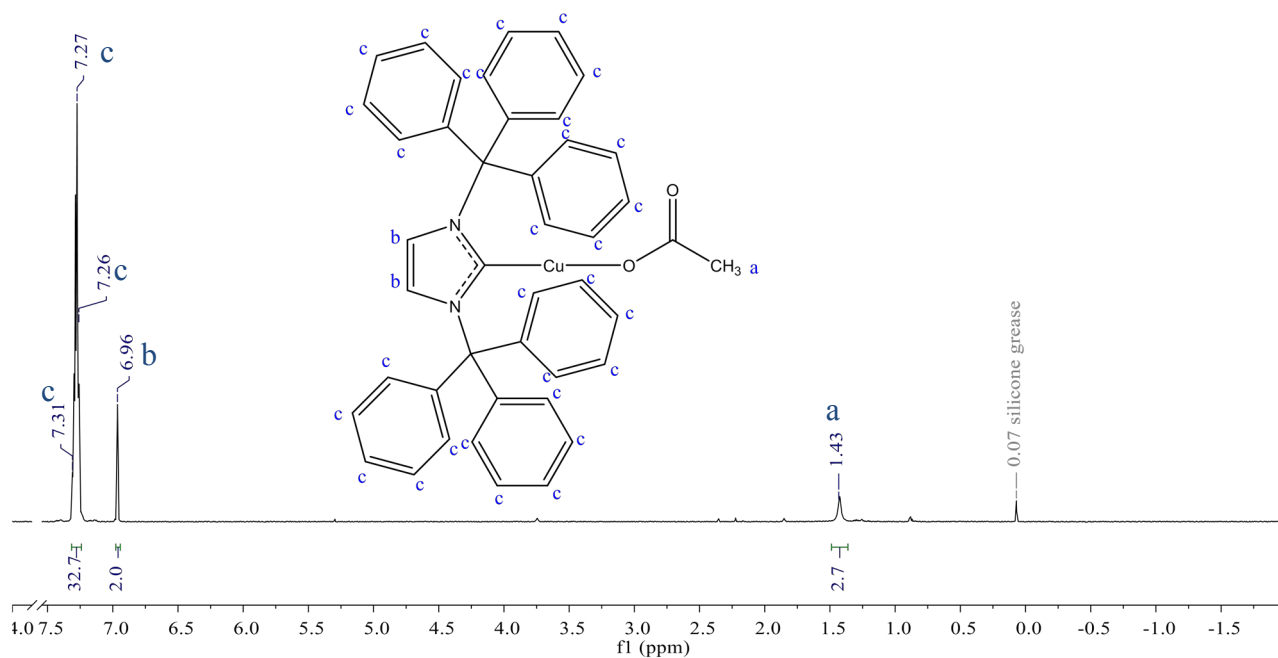
4.3. References

- (1) Roy, M. M. D.; Lummis, P. A.; Ferguson, M. J.; McDonald, R.; Rivard, E. *Chem. - Eur. J.* **2017**, *23*, 11249–11252.
- (2) Azizpoor Fard, M.; Levchenko, T. I.; Cadogan, C.; Humenny, W. J.; Corrigan, J. F. *Chem. - Eur.*

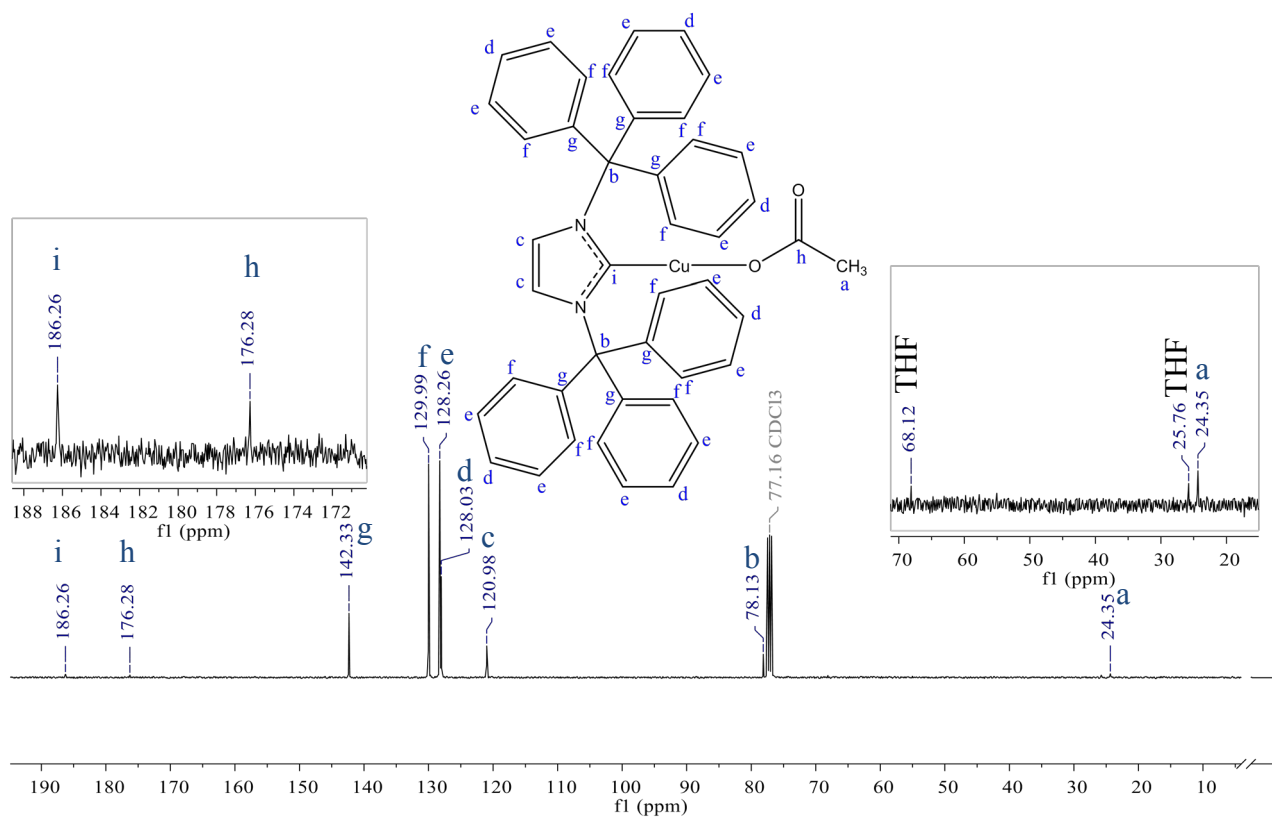
- J.* **2016**, *22*, 4543–4550.
- (3) Fard, M. A.; Weigend, F.; Corrigan, J. F. *Chem. Commun. (Camb)*. **2015**, *51*, 8361–8364.
 - (4) Polgar, A. M.; Weigend, F.; Zhang, A.; Stillman, M. J.; Corrigan, J. F. *J. Am. Chem. Soc.* **2017**, *139*, 14045–14048.
 - (5) Polgar, A. M.; Zhang, A.; Mack, F.; Weigend, F.; Lebedkin, S.; Stillman, M. J.; Corrigan, J. F. *Inorg. Chem.* **2019**, *58*, 3338–3348.
 - (6) Wong, V. H. L.; White, A. J. P.; Hor, T. S. A.; Hii, K. K. (Mimi). *Chem. Commun.* **2015**, *51*, 17752–17755.
 - (7) Zhai, J.; Filatov, A. S.; Hillhouse, G. L.; Hopkins, M. D. *Chem. Sci.* **2016**, *7*, 589–595.
 - (8) Jordan, A. J.; Walde, R. K.; Schultz, K. M.; Bacsa, J.; Sadighi, J. P. *Inorg. Chem.* **2019**, *58*, 9592–9596.
 - (9) Zhai, J.; Hopkins, M. D.; Hillhouse, G. L. *Organometallics* **2015**, *34*, 4637–4640.
 - (10) Roy, M. M. D. D.; Lummis, P. A.; Ferguson, M. J.; McDonald, R.; Rivard, E. *Chem. - Eur. J.* **2017**, *23*, 11249–11252.
 - (11) Phillips, N.; Dodson, T.; Tirfoin, R.; Bates, J. I.; Aldridge, S. *Chem. - Eur. J.* **2014**, *20*, 16721–16731.
 - (12) Roy, M. M. D.; Ferguson, M. J.; McDonald, R.; Rivard, E. *Chem. Commun.* **2018**, *54*, 483–486.
 - (13) Gasperini, D.; Collado, A.; Gómez-Suárez, A.; Cordes, D. B.; Slawin, A. M. Z.; Nolan, S. P. *Chem. - Eur. J.* **2015**, *21*, 5403–5412.

Appendix 1. Supporting Information for Chapter 2

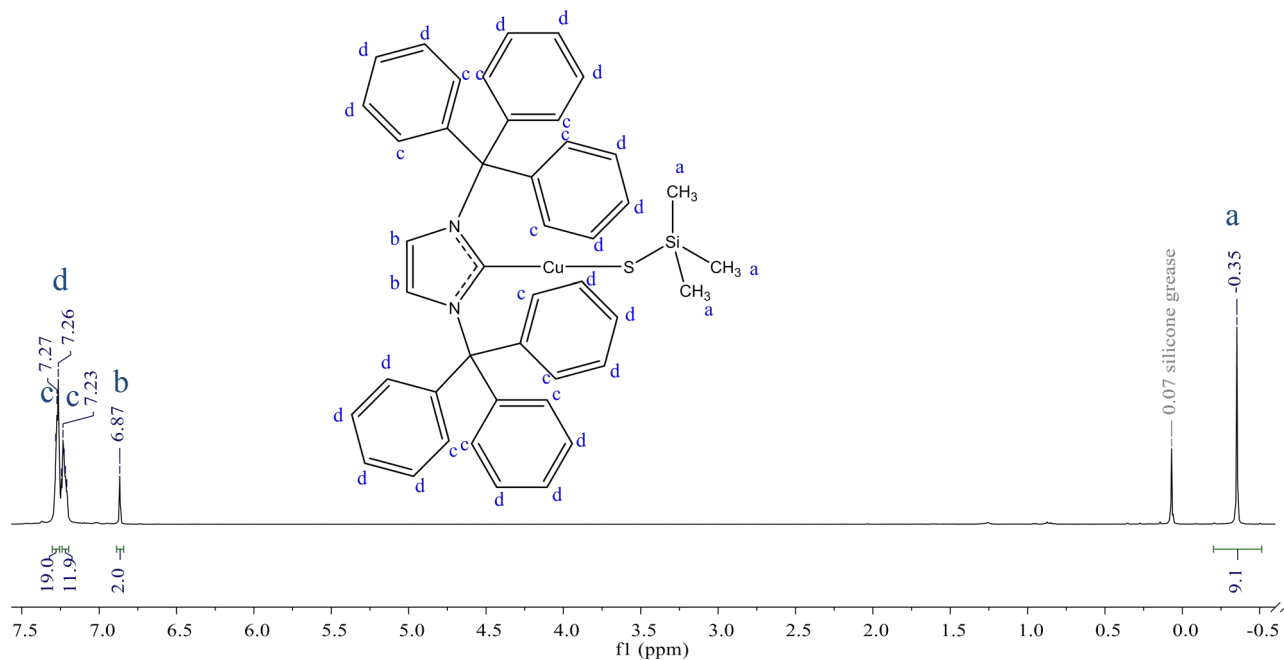
2.1a – ^1H NMR CDCl_3 – 298 K



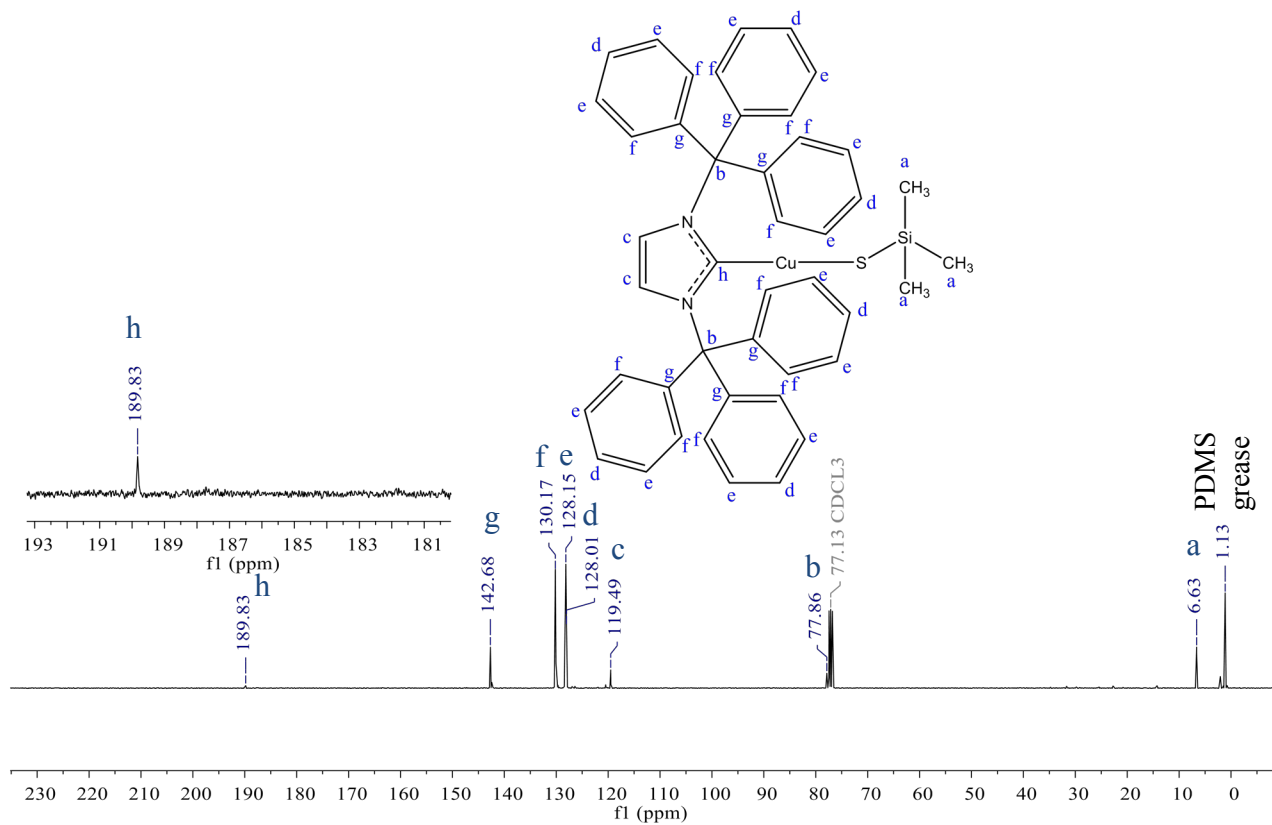
2.1a – $^{13}\text{C}\{^1\text{H}\}$ NMR CDCl_3 – 298 K



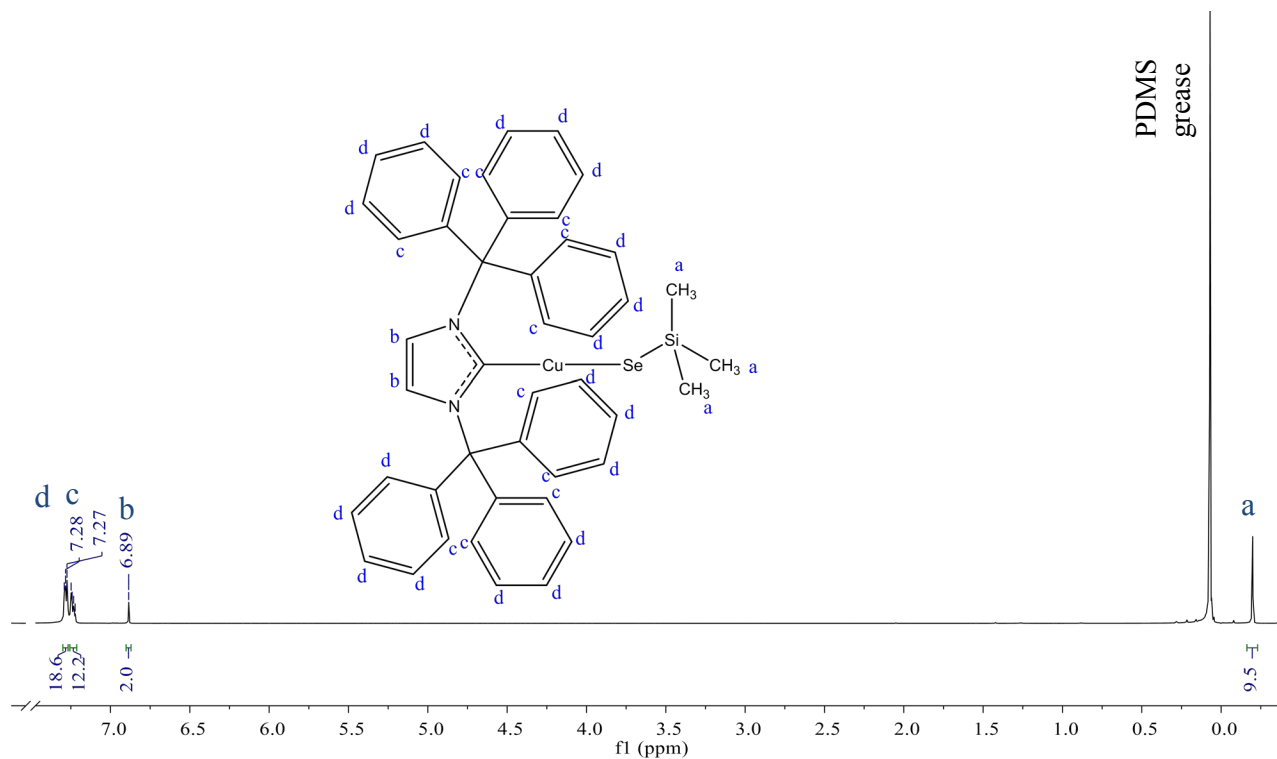
2.2a – ^1H NMR CDCl_3 – 298 K



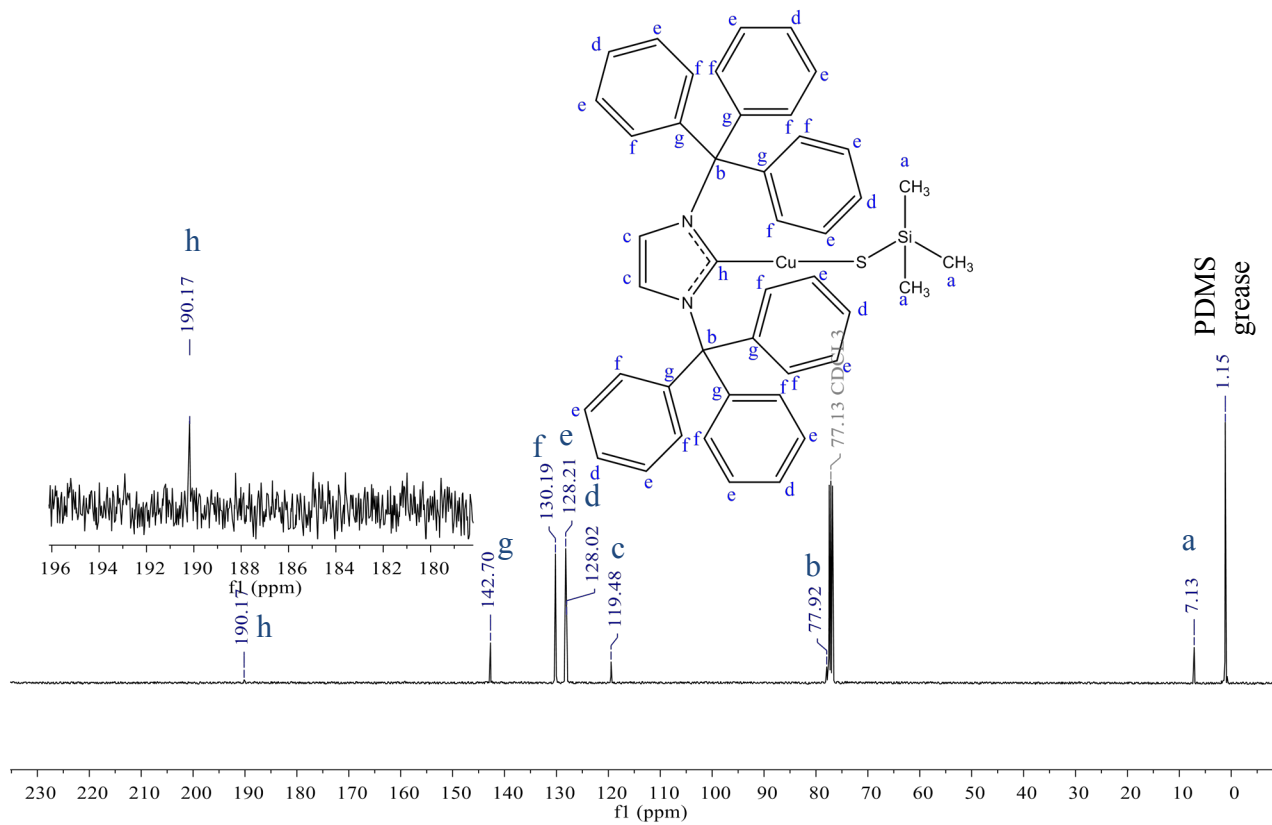
2.2a – $^{13}\text{C}\{^1\text{H}\}$ NMR CDCl_3 – 298 K



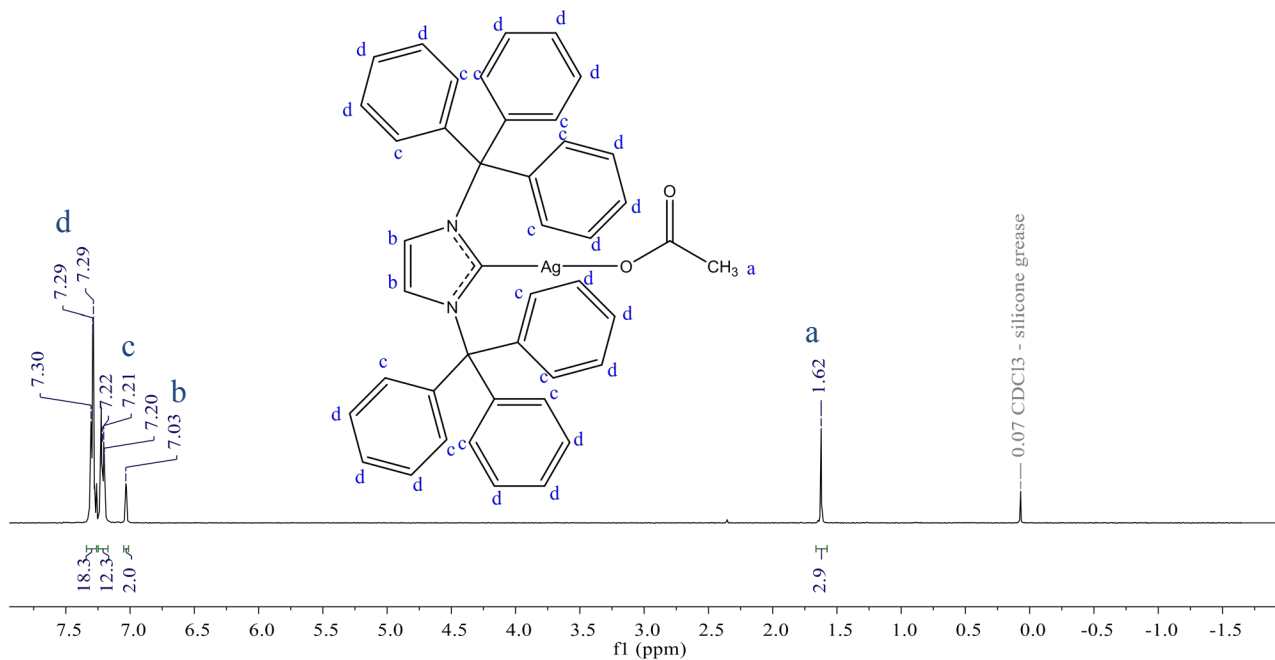
2.3a – ^1H NMR CDCl_3 – 298 K



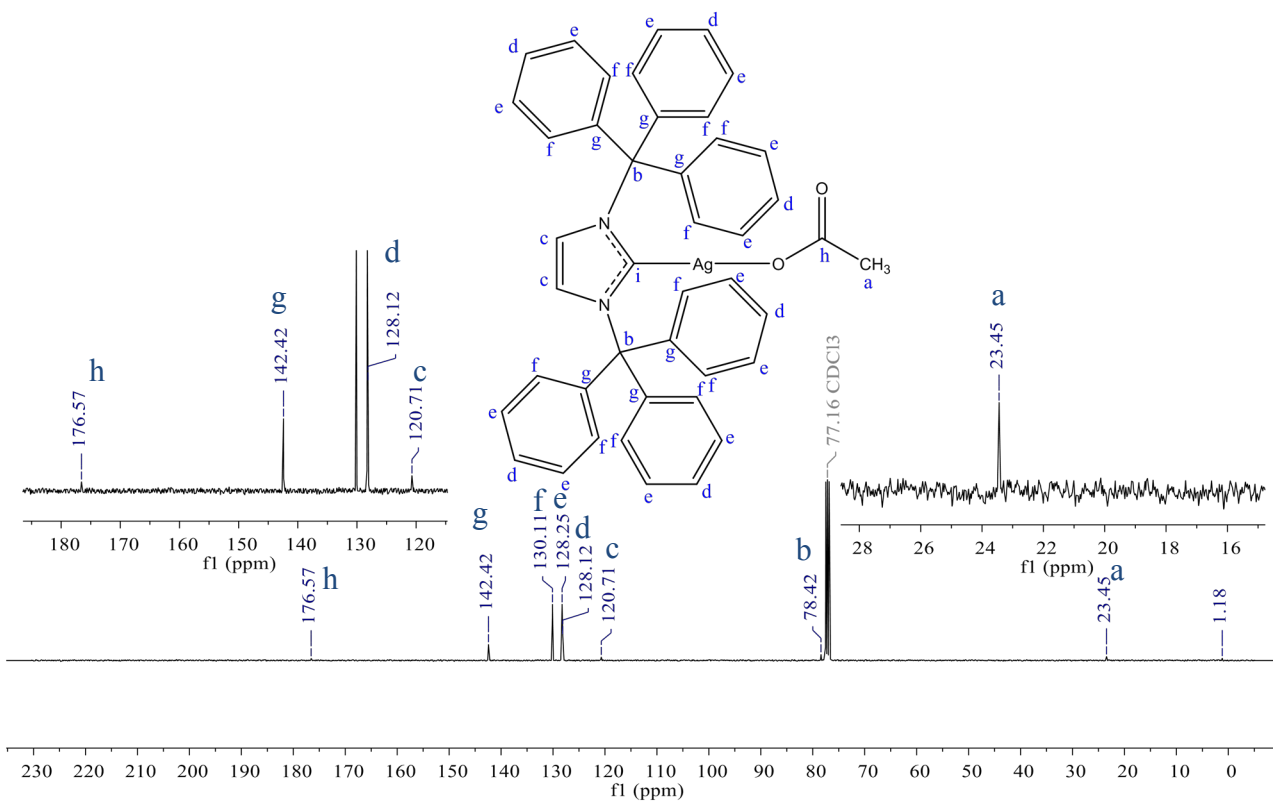
2.3a – $^{13}\text{C}\{^1\text{H}\}$ NMR CDCl_3 – 298 K



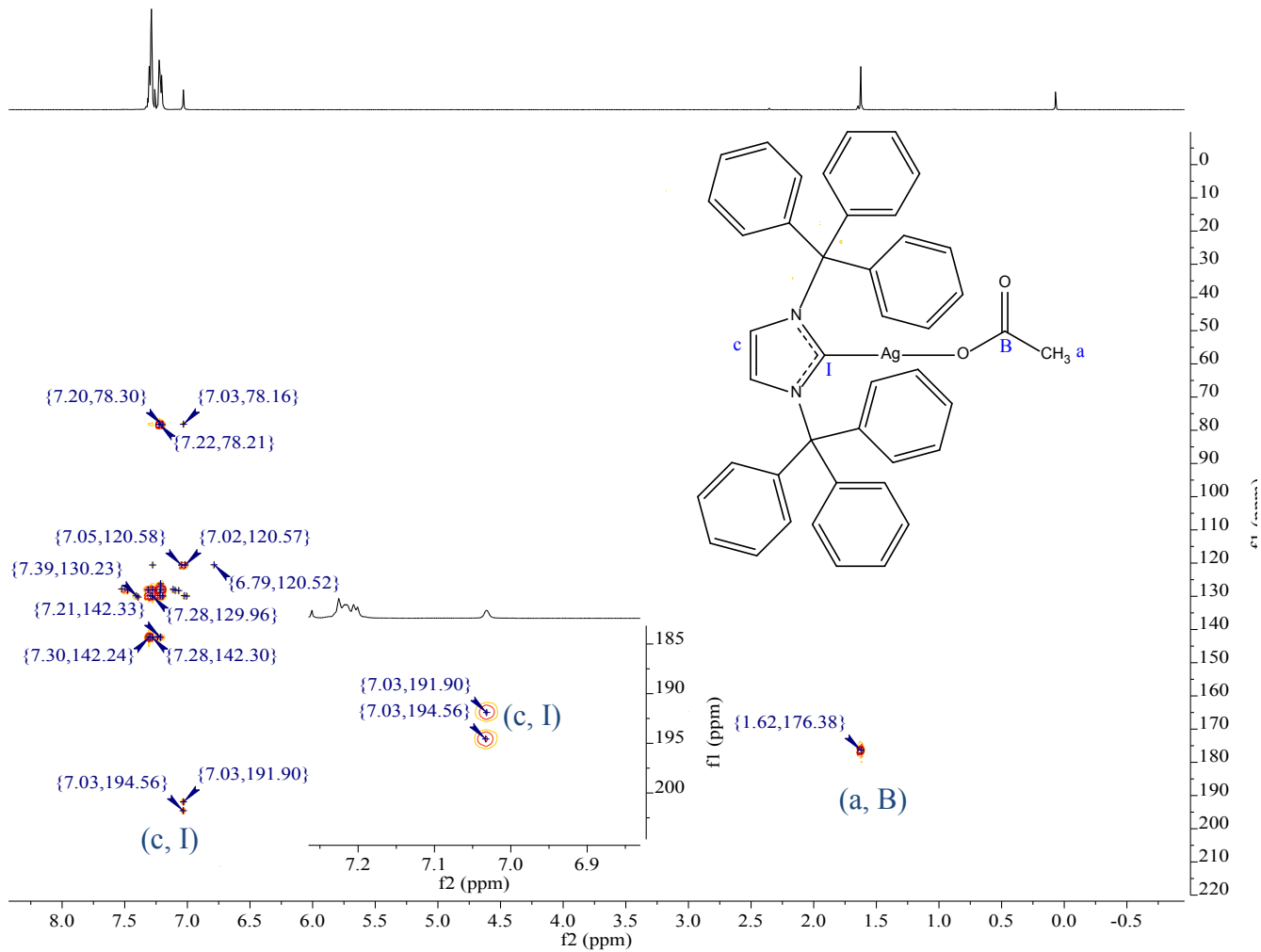
2.1b – ^1H NMR CDCl_3 – 298 K



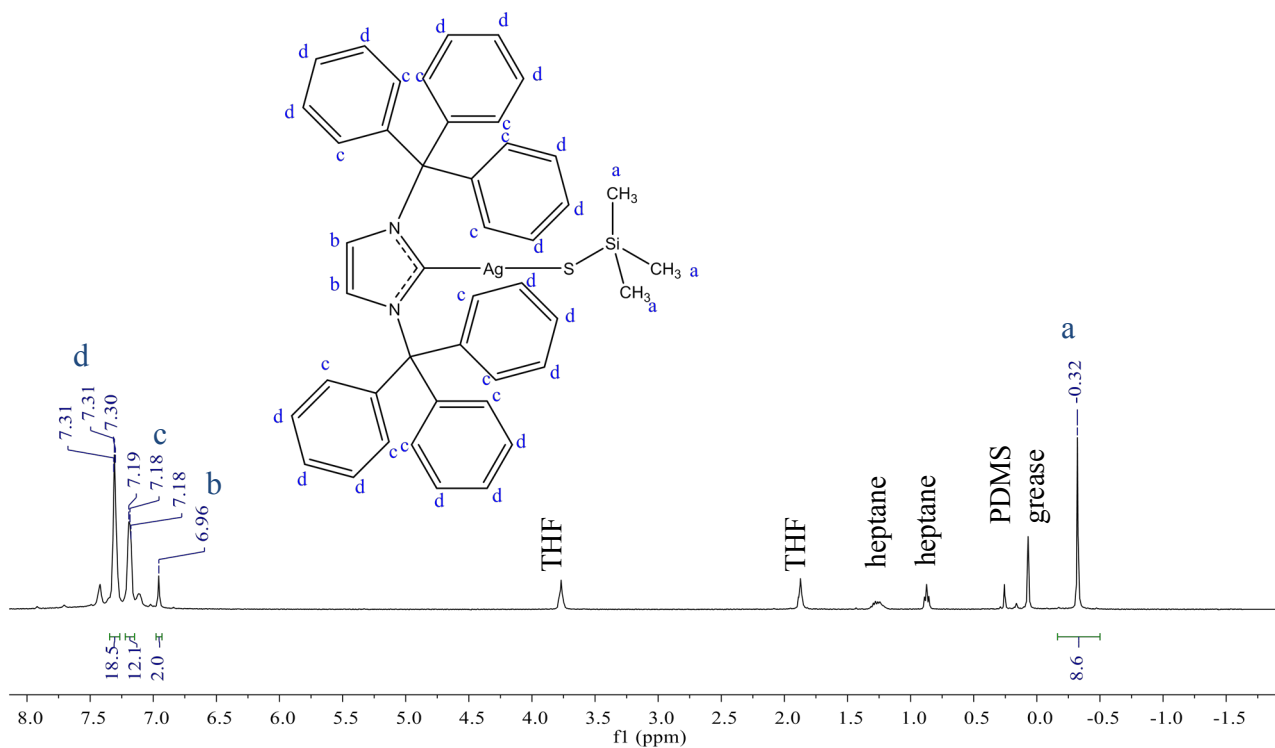
2.1b – $^{13}\text{C}\{^1\text{H}\}$ NMR CDCl_3 – 298 K



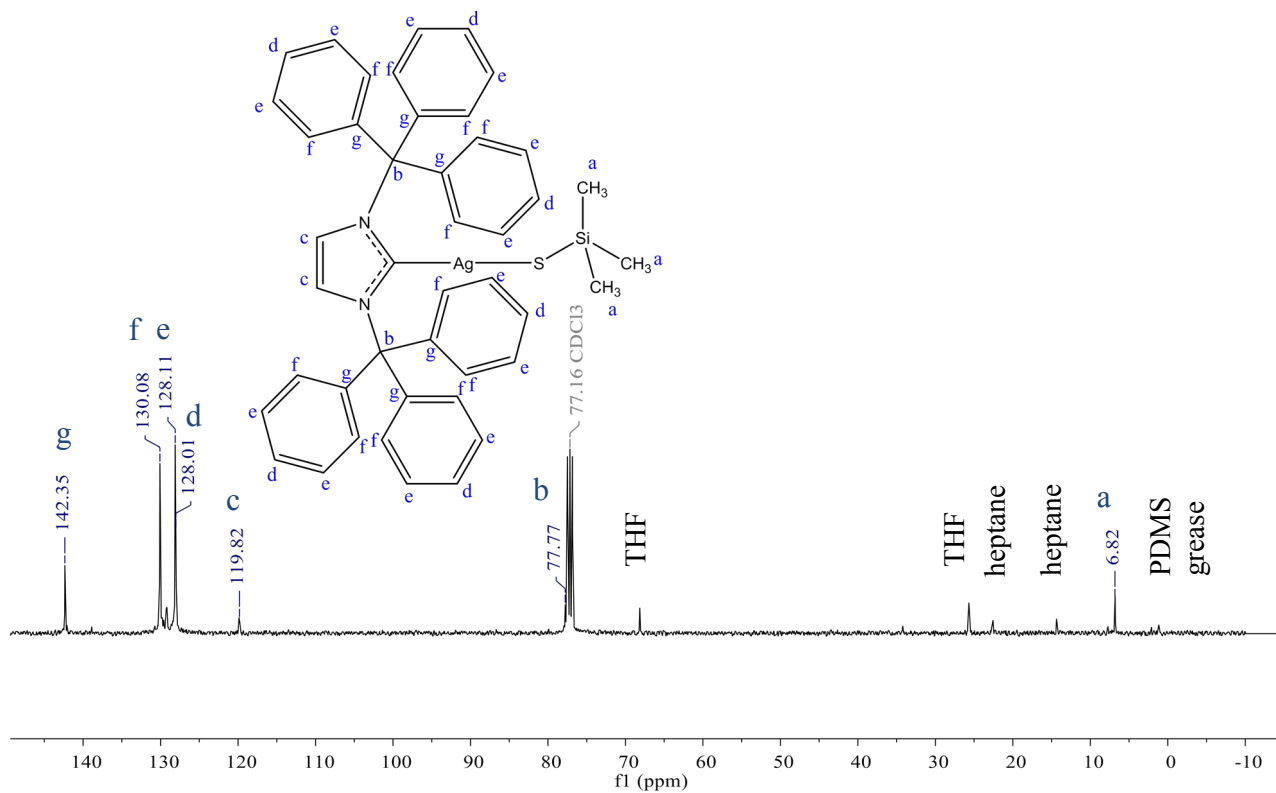
2.1b – ^1H – ^{13}C HMBC NMR CDCl_3 – 298 K



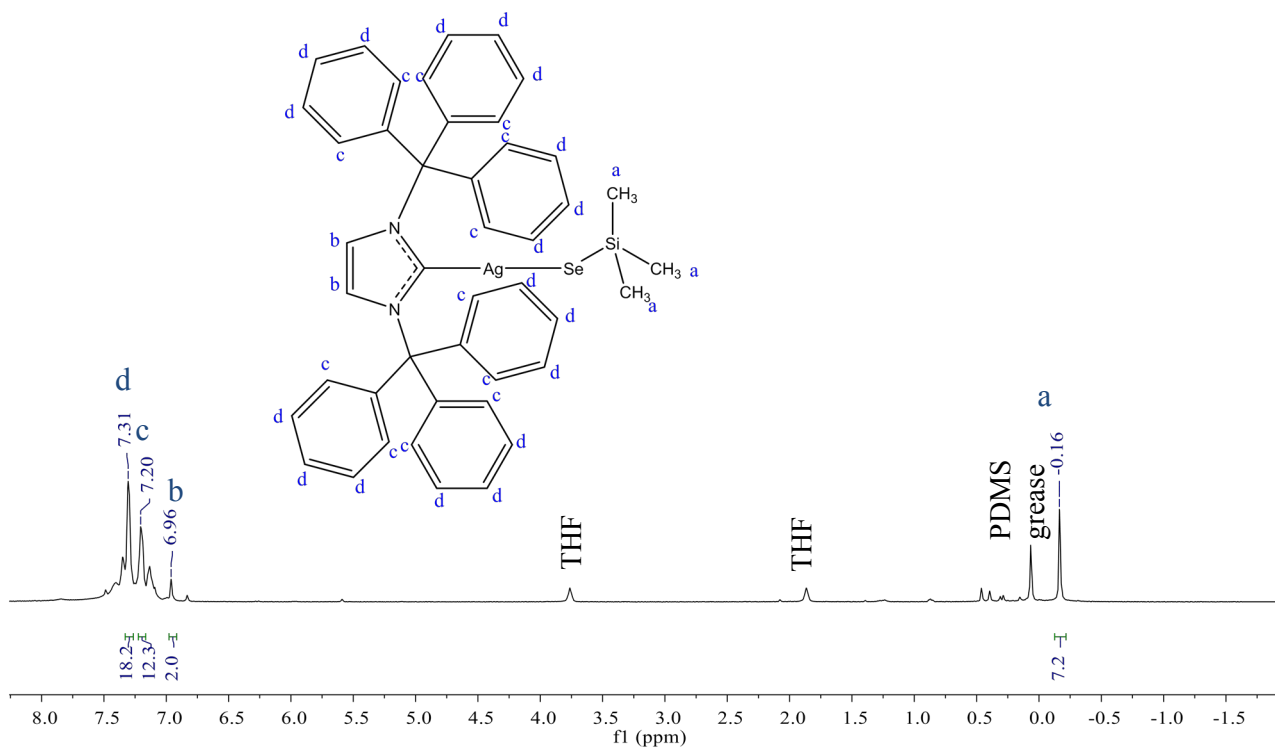
2.2b – ^1H NMR CDCl_3 – 243 K



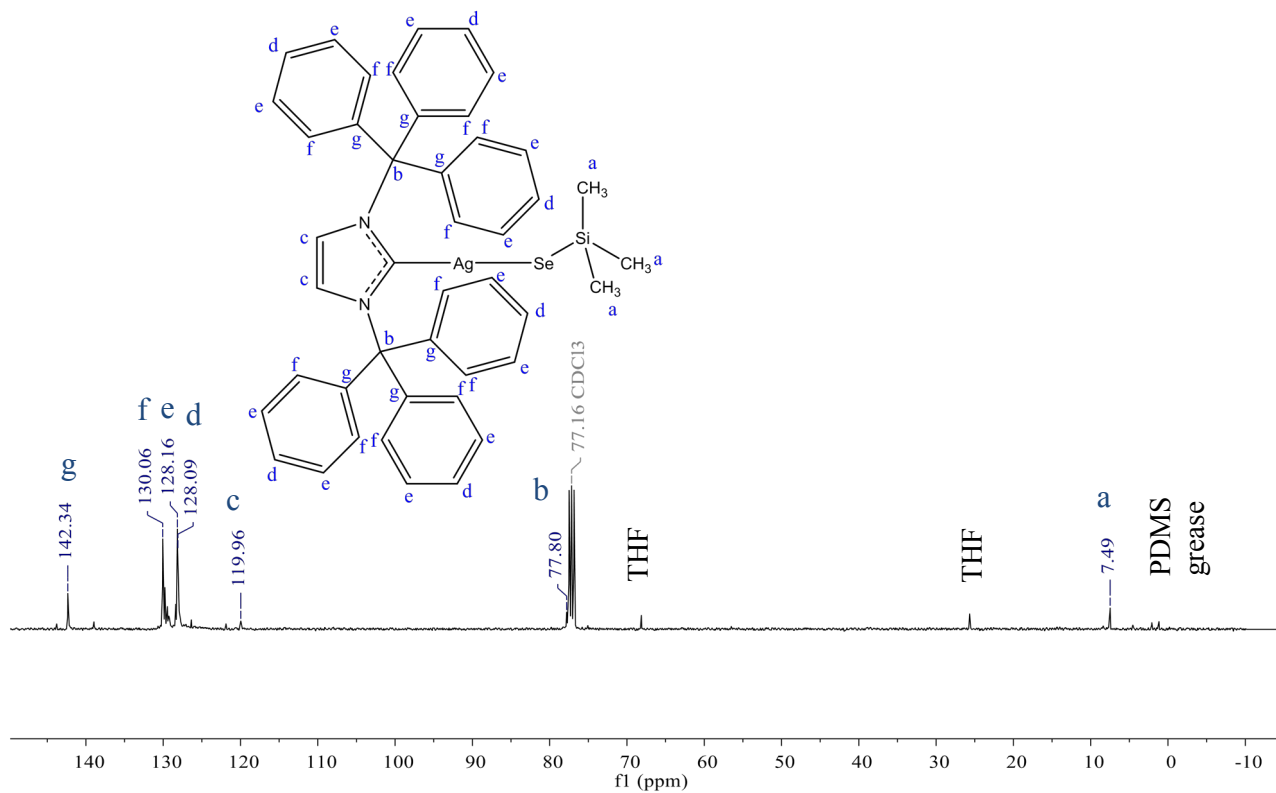
2.2b – $^{13}\text{C}\{^1\text{H}\}$ NMR CDCl_3 – 243 K



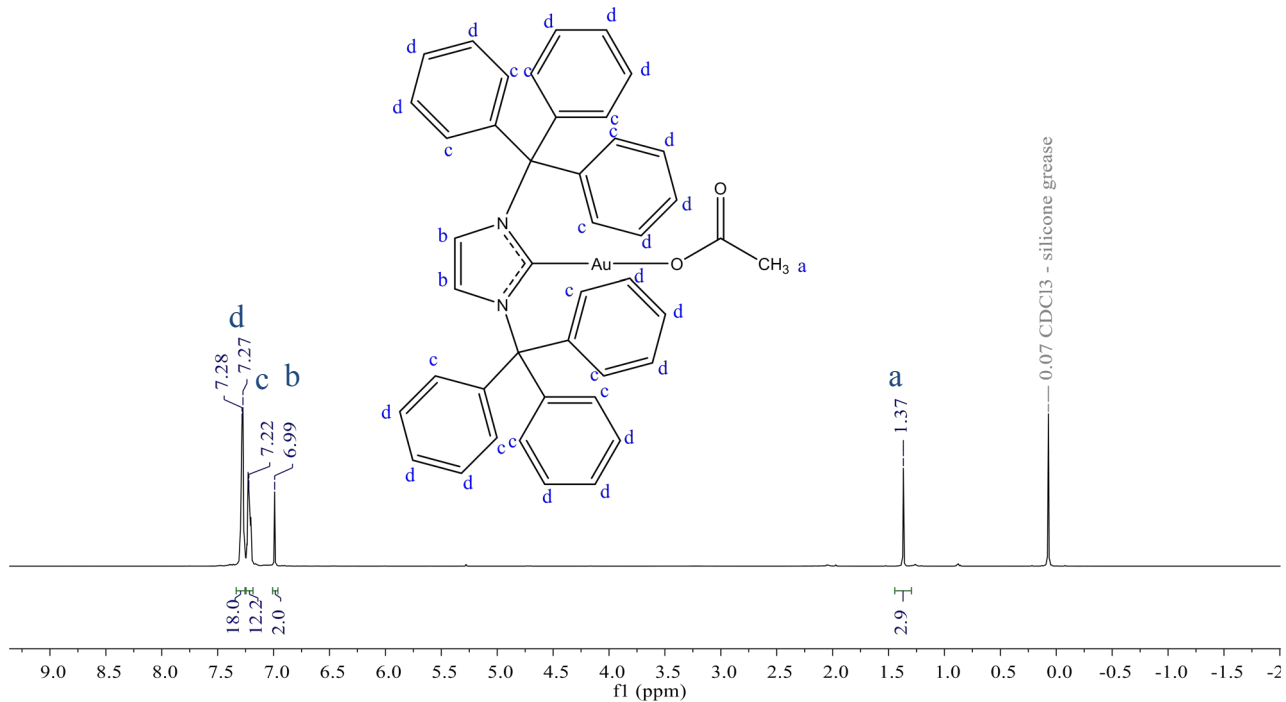
2.3b – ^1H NMR CDCl_3 – 243 K



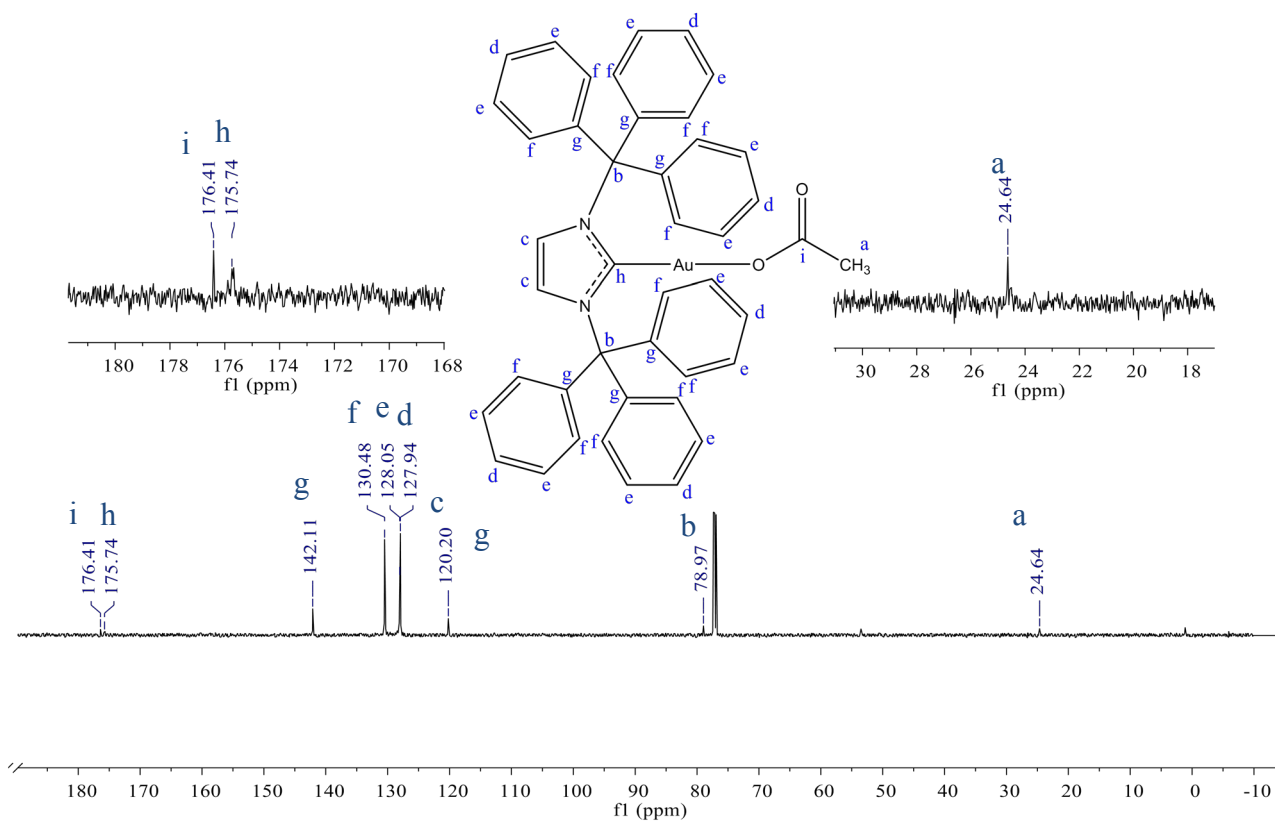
2.3b – $^{13}\text{C}\{^1\text{H}\}$ NMR CDCl_3 – 243 K



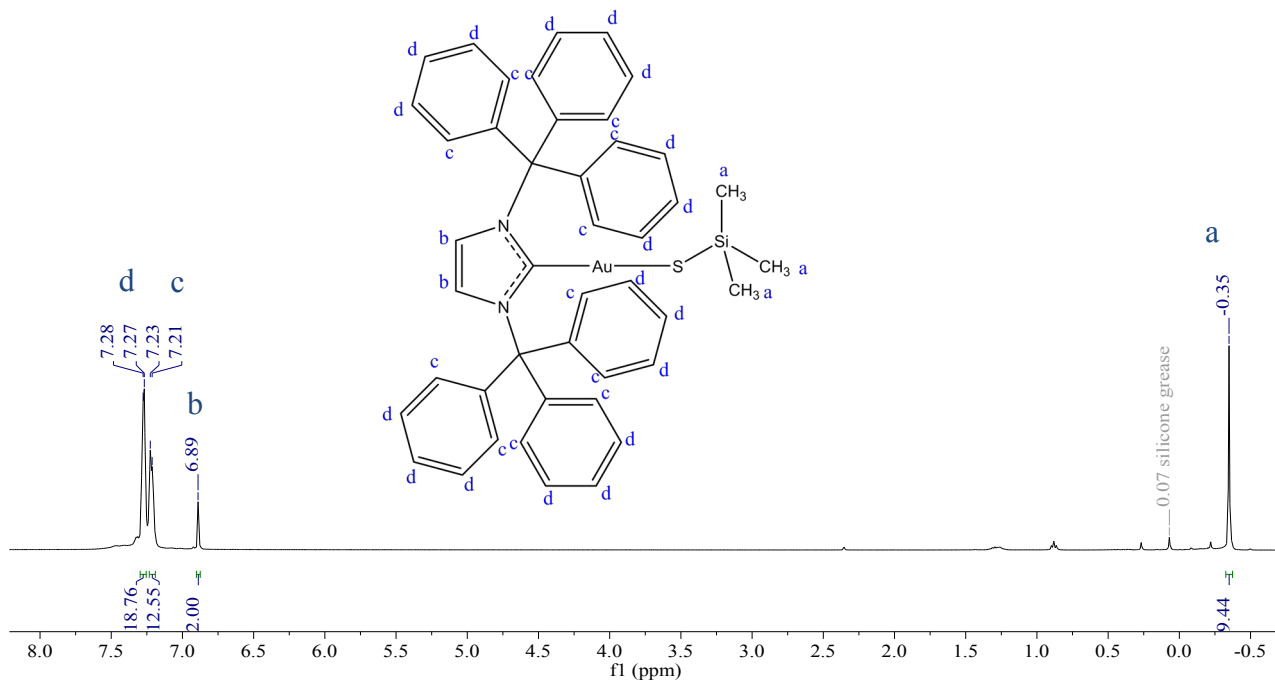
2.1c – ^1H NMR CDCl_3 – 298 K



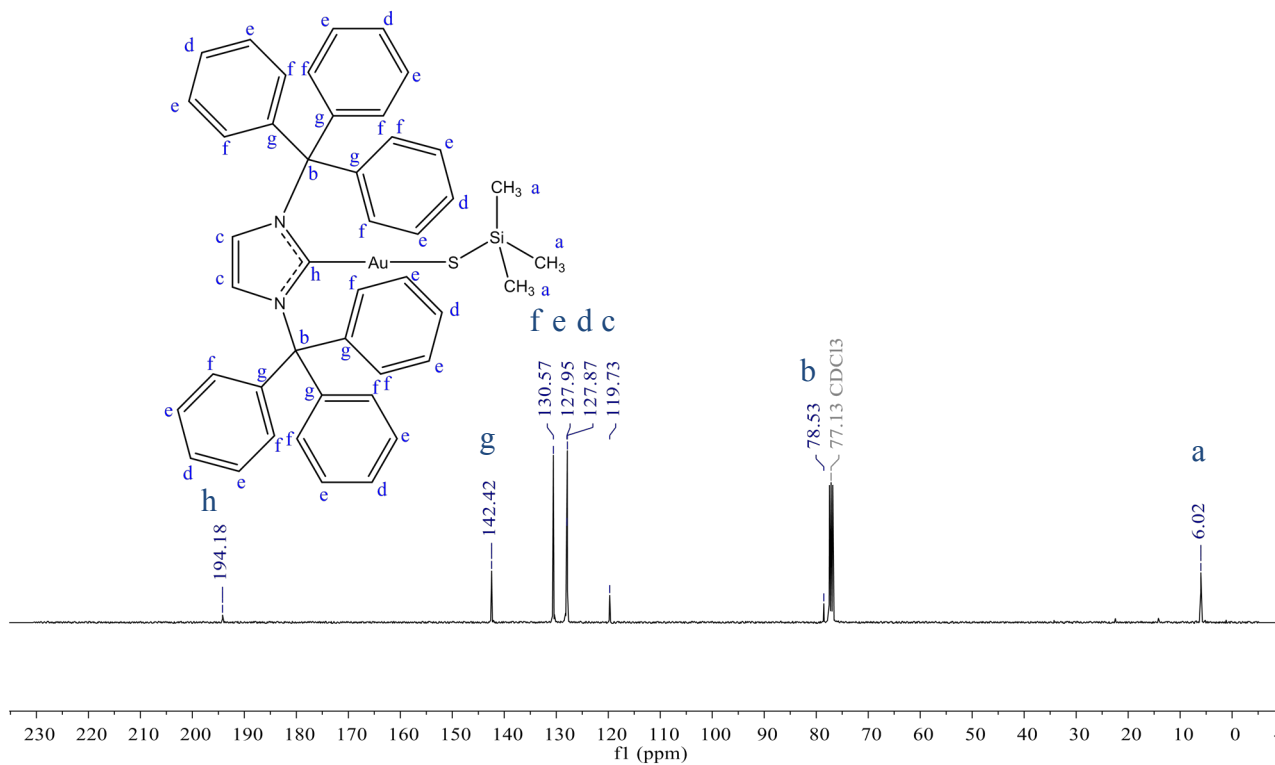
2.1c – $^{13}\text{C}\{^1\text{H}\}$ NMR CDCl_3 – 298 K



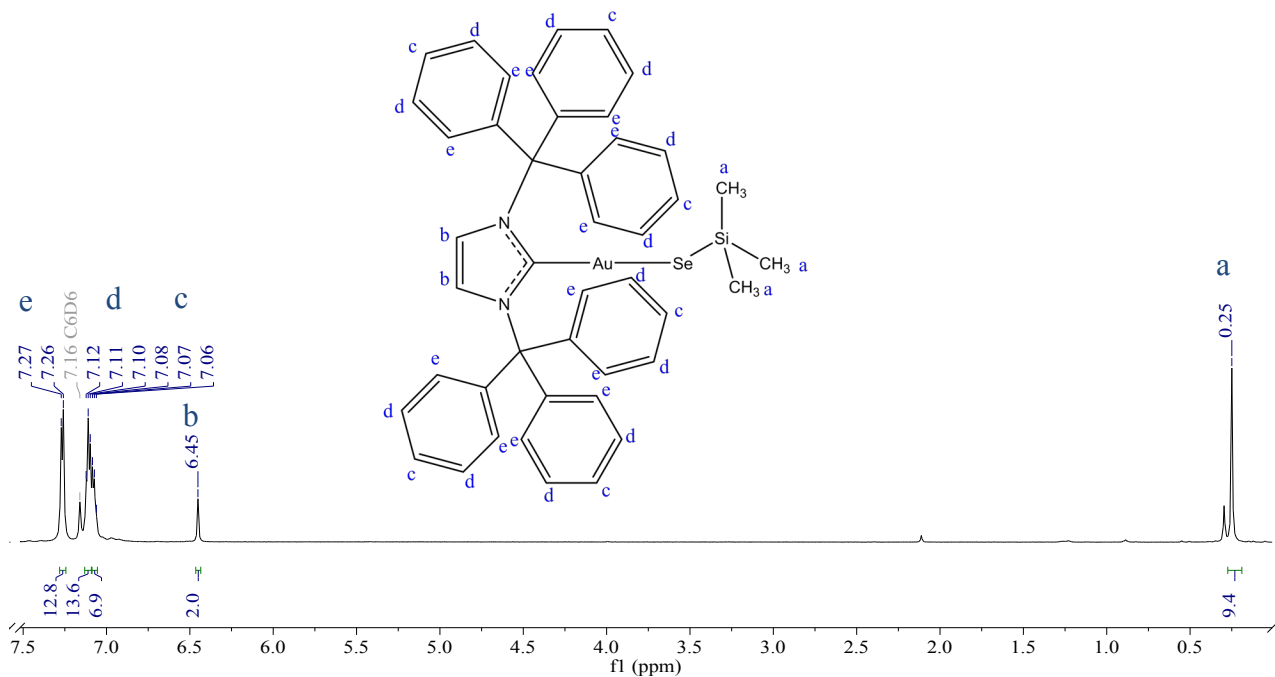
2.2c – ^1H NMR CDCl_3 – 298 K



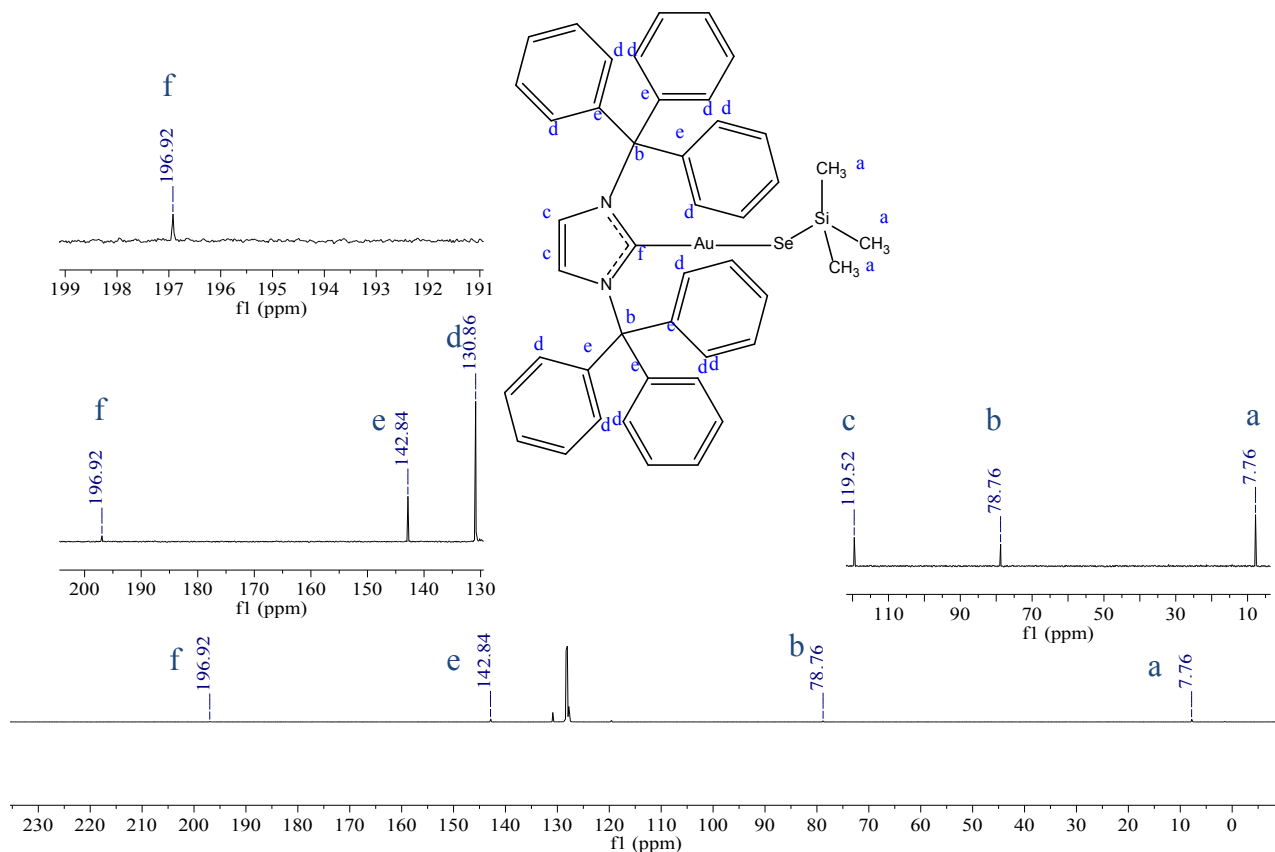
2.2c – $^{13}\text{C}\{^1\text{H}\}$ NMR CDCl_3 – 298 K



2.3c – ^1H NMR C_6D_6 – 298 K



2.3c – $^{13}\text{C}\{^1\text{H}\}$ NMR C_6D_6 – 298 K



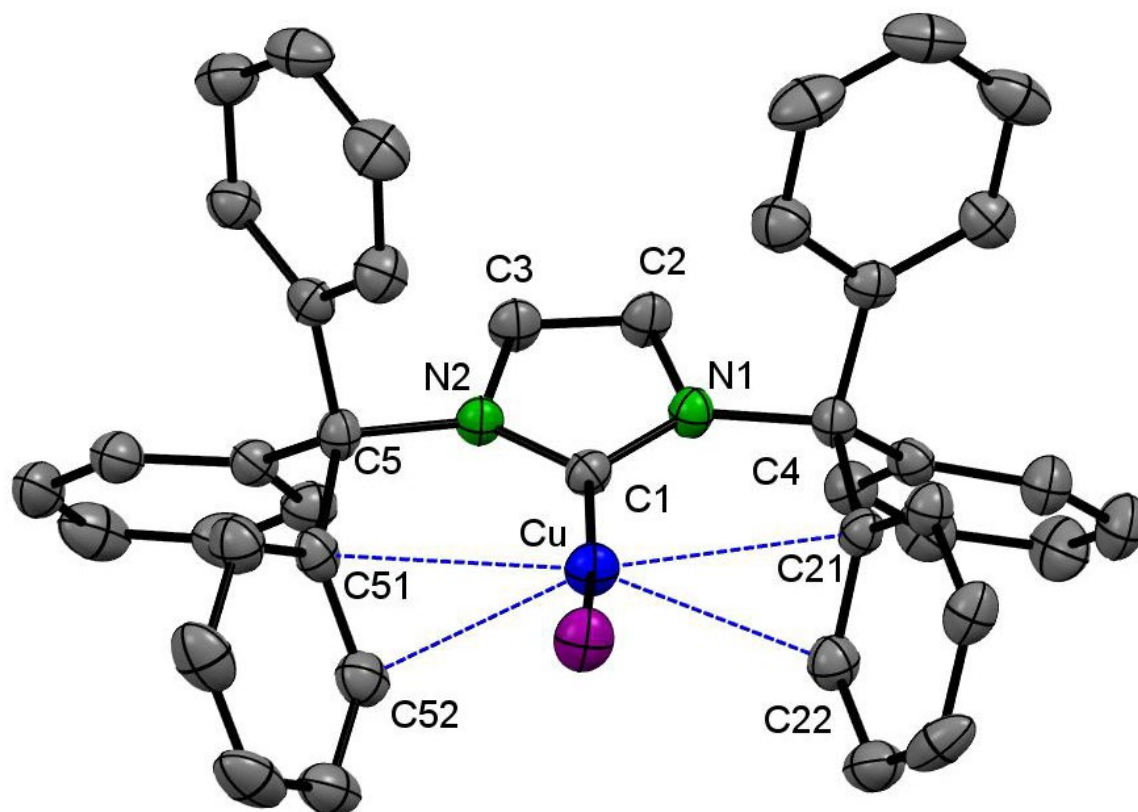


Figure S2.1: Molecular structure of [ITrCuI] showcasing intramolecular Ph - Cu contacts, implying η_2 coordination.¹ Cu = blue, N = green, C = grey, I = purple. C1 - Cu: 1.917(3)Å. Cu - I: 2.4336(4) Å. C1 - N1: 1.367(4) Å. C1 - N2: 1.369(4) Å. N1/2 - C2/3: 1.394(4)Å. N1/2 - C4/5: 1.492(4)Å. C51 - Cu: 2.942(3)Å. C52 - Cu: 2.894(3)Å. C21 - Cu: 2.910(3)Å. C22 -Cu: 2.92(3)Å. C1 - Cu - I: 165.91(9)°. Cu - C1 - N1: 128.0(2)°. Cu - C1 - N2: 126.7(2)°. C1 - N1 - C4: 127.6(2)°. C1 - N2 - C5: 127.4(2)°.

Table S2.1: Summary of Crystal Data for [ITrCuSSiMe₃] · 1.5 THF (**2.1b**)

Formula	C ₄₉ H ₅₁ CuN ₂ O _{1.25} SSi
Formula Weight (<i>g/mol</i>)	811.60
Crystal Dimensions (<i>mm</i>)	0.314 × 0.186 × 0.125
Crystal Color and Habit	colourless needle
Crystal System	triclinic
Space Group	P -1
Temperature, K	110
<i>a</i> , Å	15.016(2)
<i>b</i> , Å	15.844(2)
<i>c</i> , Å	18.062(3)
α , °	84.158(5)
β , °	81.579(6)
γ , °	87.220(10)
<i>V</i> , Å ³	4226.3(11)
Number of reflections to determine final unit cell	9927
Min and Max 2 θ for cell determination, °	5.0, 54.88
<i>Z</i>	4
F(000)	1712
ρ (<i>g/cm</i> ⁻³)	1.276
λ , Å, (MoK α)	0.71073
μ , (<i>cm</i> ⁻¹)	0.634
Diffractometer Type	Bruker Kappa Axis Apex2
Scan Type(s)	phi and omega scans
Max 2 θ for data collection, °	56.734
Measured fraction of data	0.998
Number of reflections measured	20983
Unique reflections measured	20983
R _{merge}	0.0428
Number of reflections included in refinement Cut	20983
off Threshold Expression	I > 2sigma(I)
Structure refined using	full matrix least-squares using F ²
Weighting Scheme	w=1/[sigma ² (Fo ²)+(0.0926P) ² +5.724 2P] where P=(Fo ² +2Fc ²)/3

Number of parameters in least-squares	961
R ₁	0.0789
wR ₂	0.1888
R ₁ (all data)	0.1371
wR ₂ (all data)	0.2147
GOF	1.114
Maximum shift/error	0.001
Min & Max peak heights on final DF Map (e ⁻ /Å)	-1.074, 1.060

Where:

$$R_1 = S(|F_o| - |F_c|) / S F_o$$

$$wR_2 = [S(w(F_o^2 - F_c^2)^2) / S(w F_o^4)]^{1/2}$$

$$GOF = [S(w(F_o^2 - F_c^2)^2) / (No. of reflns. - No. of params.)]^{1/2}$$

Table S2.2. Atomic Coordinates for [(ITr)CuSSiMe₃] · 1.5 THF (**2.1b**)

Atom	x	y	z	U _{iso/equiv}
Cu1	0.29862(3)	0.17070(3)	0.85080(3)	0.02203(13)
S1	0.35266(8)	0.09461(7)	0.76136(6)	0.0266(2)
Si1	0.42403(9)	-0.01112(8)	0.80593(7)	0.0317(3)
N1	0.2791(2)	0.32533(19)	0.93114(18)	0.0189(7)
N2	0.1808(2)	0.2336(2)	0.98085(18)	0.0184(7)
C1	0.2510(3)	0.2456(2)	0.9243(2)	0.0191(8)
C2	0.2268(3)	0.3608(3)	0.9900(2)	0.0271(9)
C3	0.1658(3)	0.3036(3)	1.0217(2)	0.0257(9)
C4	0.1274(3)	0.1543(2)	0.9934(2)	0.0192(8)
C5	0.1795(3)	0.0828(2)	1.0358(2)	0.0203(8)
C6	0.2674(3)	0.0889(3)	1.0487(2)	0.0246(9)
C7	0.3109(3)	0.0234(3)	1.0875(2)	0.0318(10)
C8	0.2669(3)	-0.0503(3)	1.1144(2)	0.0305(10)
C9	0.1783(3)	-0.0570(3)	1.1032(2)	0.0280(9)
C10	0.1342(3)	0.0089(2)	1.0651(2)	0.0234(9)
C11	0.1101(3)	0.1325(3)	0.9158(2)	0.0224(8)
C12	0.1131(3)	0.0503(3)	0.8957(2)	0.0234(9)
C13	0.0892(3)	0.0326(3)	0.8273(2)	0.0278(9)

C14	0.0631(3)	0.0976(3)	0.7776(2)	0.0294(10)
C15	0.0623(3)	0.1803(3)	0.7954(2)	0.0308(10)
C16	0.0847(3)	0.1976(3)	0.8637(2)	0.0272(9)
C17	0.0365(3)	0.1723(2)	1.0435(2)	0.0212(8)
C18	0.0369(3)	0.1815(2)	1.1200(2)	0.0231(8)
C19	-0.0428(3)	0.1983(3)	1.1664(2)	0.0271(9)
C20	-0.1238(3)	0.2029(3)	1.1382(3)	0.0317(10)
C21	-0.1254(3)	0.1921(3)	1.0641(3)	0.0338(10)
C22	-0.0458(3)	0.1767(3)	1.0163(2)	0.0265(9)
C23	0.3466(3)	0.3702(2)	0.8722(2)	0.0192(8)
C24	0.3131(3)	0.3605(2)	0.7968(2)	0.0227(8)
C25	0.2232(3)	0.3835(3)	0.7897(3)	0.0293(10)
C26	0.1881(4)	0.3726(3)	0.7244(3)	0.0395(12)
C27	0.2413(4)	0.3379(3)	0.6659(3)	0.0413(13)
C28	0.3297(4)	0.3147(3)	0.6721(2)	0.0394(12)
C29	0.3661(3)	0.3269(3)	0.7368(2)	0.0283(9)
C30	0.4425(3)	0.3328(3)	0.8754(2)	0.0219(8)
C31	0.4636(3)	0.2614(3)	0.9207(2)	0.0278(9)
C32	0.5523(3)	0.2325(3)	0.9229(3)	0.0353(11)
C33	0.6215(3)	0.2755(3)	0.8781(3)	0.0394(12)
C34	0.6017(3)	0.3473(3)	0.8319(3)	0.0366(11)
C35	0.5135(3)	0.3754(3)	0.8305(3)	0.0295(10)
C36	0.3489(3)	0.4646(2)	0.8881(2)	0.0222(8)
C37	0.3245(3)	0.5319(3)	0.8392(3)	0.0304(10)
C38	0.3299(3)	0.6155(3)	0.8562(3)	0.0394(12)
C39	0.3585(3)	0.6318(3)	0.9223(3)	0.0355(11)
C40	0.3853(3)	0.5656(3)	0.9703(3)	0.0317(10)
C41	0.3816(3)	0.4825(3)	0.9532(2)	0.0246(9)
C42	0.4228(4)	-0.0184(4)	0.9084(3)	0.0578(16)
C43	0.5460(3)	-0.0070(4)	0.7621(3)	0.0468(13)
C44	0.3819(4)	-0.1127(3)	0.7823(4)	0.0557(16)
Cu1A	0.17839(3)	0.28047(3)	0.34215(3)	0.02188(13)
Si1A	0.10349(8)	0.32932(7)	0.25334(6)	0.0285(2)
Si1A	-0.02043(8)	0.37695(7)	0.30698(7)	0.0260(3)

N1A	0.2500(2)	0.17681(19)	0.46908(17)	0.0174(7)
N2A	0.3424(2)	0.2703(2)	0.41264(17)	0.0177(7)
C1A	0.2587(3)	0.2404(2)	0.4124(2)	0.0180(8)
C2A	0.3822(3)	0.2286(3)	0.4710(2)	0.0232(9)
C3A	0.3252(3)	0.1703(2)	0.5059(2)	0.0218(8)
C4A	0.1677(2)	0.1245(2)	0.4865(2)	0.0161(7)
C5A	0.1872(2)	0.0434(2)	0.5378(2)	0.0168(7)
C6A	0.2016(3)	0.0503(2)	0.6116(2)	0.0186(8)
C7A	0.2186(3)	-0.0218(3)	0.6598(2)	0.0243(9)
C8A	0.2160(3)	-0.1010(3)	0.6348(2)	0.0280(9)
C9A	0.1999(3)	-0.1094(3)	0.5627(2)	0.0284(9)
C10A	0.1860(3)	-0.0374(2)	0.5144(2)	0.0204(8)
C11A	0.0898(3)	0.1754(2)	0.5300(2)	0.0183(8)
C12A	0.0158(3)	0.1315(3)	0.5674(2)	0.0212(8)
C13A	-0.0562(3)	0.1734(3)	0.6071(2)	0.0282(9)
C14A	-0.0546(3)	0.2602(3)	0.6108(3)	0.0335(11)
C15A	0.0187(3)	0.3046(3)	0.5742(3)	0.0300(10)
C16A	0.0904(3)	0.2625(2)	0.5338(2)	0.0228(8)
C17A	0.1450(3)	0.1004(2)	0.4115(2)	0.0171(7)
C18A	0.0575(3)	0.1019(2)	0.3948(2)	0.0201(8)
C19A	0.0401(3)	0.0740(3)	0.3272(2)	0.0255(9)
C20A	0.1095(3)	0.0457(3)	0.2762(2)	0.0272(9)
C21A	0.1975(3)	0.0442(3)	0.2921(2)	0.0258(9)
C22A	0.2153(3)	0.0708(2)	0.3589(2)	0.0226(8)
C23A	0.3747(3)	0.3481(2)	0.3637(2)	0.0184(8)
C24A	0.4730(3)	0.3628(2)	0.3718(2)	0.0205(8)
C25A	0.5394(3)	0.2996(3)	0.3553(2)	0.0270(9)
C26A	0.6287(3)	0.3149(3)	0.3542(3)	0.0367(11)
C27A	0.6565(3)	0.3929(3)	0.3676(3)	0.0380(11)
C28A	0.5913(3)	0.4573(3)	0.3826(3)	0.0361(11)
C29A	0.5008(3)	0.4416(3)	0.3850(3)	0.0271(9)
C30A	0.3764(3)	0.3342(3)	0.2803(2)	0.0214(8)
C31A	0.4018(3)	0.4020(3)	0.2269(2)	0.0291(10)
C32A	0.4090(3)	0.3942(3)	0.1509(2)	0.0348(11)

C33A	0.3921(4)	0.3176(3)	0.1261(2)	0.0374(12)
C34A	0.3693(3)	0.2491(3)	0.1780(3)	0.0350(11)
C35A	0.3624(3)	0.2570(3)	0.2545(2)	0.0266(9)
C36A	0.3103(3)	0.4203(2)	0.3910(2)	0.0196(8)
C37A	0.3001(3)	0.4317(3)	0.4676(2)	0.0279(9)
C38A	0.2398(3)	0.4933(3)	0.4974(3)	0.0302(10)
C39A	0.1917(3)	0.5459(3)	0.4508(3)	0.0327(10)
C40A	0.2012(3)	0.5356(3)	0.3755(3)	0.0365(11)
C41A	0.2594(3)	0.4725(3)	0.3462(2)	0.0271(9)
C42A	-0.0098(3)	0.4717(3)	0.3574(3)	0.0364(11)
C43A	-0.0818(3)	0.2976(3)	0.3764(3)	0.0368(11)
C44A	-0.0933(3)	0.4107(3)	0.2332(3)	0.0393(12)
O1S	0.4279(6)	0.0009(6)	0.4441(5)	0.065(2)
C1S	0.4397(5)	-0.0490(4)	0.5093(4)	0.0674(18)
C2S	0.5122(5)	0.0205(5)	0.4359(4)	0.080(2)
O3S	0.8261(6)	0.3847(6)	0.8129(5)	0.148(3)
C12S	0.8815(11)	0.3301(11)	0.8470(9)	0.196(6)
C13S	0.9411(7)	0.3915(6)	0.8819(6)	0.105(3)
C14S	0.8124(8)	0.4610(8)	0.8527(7)	0.138(4)
C15S	0.8769(8)	0.4552(8)	0.9162(7)	0.138(4)
O2S	0.5310(6)	0.2699(5)	0.6006(5)	0.055(2)
C3S	0.5598(8)	0.2042(10)	0.6559(8)	0.070(4)
C4S	0.6587(7)	0.1834(7)	0.6277(6)	0.048(3)
C5S	0.6834(10)	0.2595(8)	0.5762(9)	0.082(4)
C6S	0.6059(10)	0.3224(10)	0.5869(13)	0.078(6)
O2SA	0.5522(7)	0.2428(6)	0.5670(6)	0.071(3)
C3SA	0.6040(10)	0.3153(9)	0.5642(9)	0.062(5)
C4SA	0.6243(17)	0.3166(13)	0.6419(11)	0.140(9)
C5SA	0.6336(16)	0.2238(13)	0.6706(13)	0.140(8)
C6SA	0.5694(10)	0.1824(9)	0.6291(8)	0.061(4)
H2	0.232765	0.415561	1.005361	0.033
H3	0.121124	0.309983	1.063969	0.031
H6	0.298586	0.139292	1.030560	0.029
H7	0.371287	0.029196	1.095528	0.038

H8	0.296857	-0.095735	1.140336	0.037
H9	0.147361	-0.107430	1.121827	0.034
H10	0.073028	0.003825	1.058787	0.028
H12	0.131791	0.004956	0.929254	0.028
H13	0.091025	-0.024397	0.814914	0.033
H14	0.045649	0.085572	0.731411	0.035
H15	0.046428	0.225498	0.760523	0.037
H16	0.082783	0.254798	0.875659	0.033
H18	0.092167	0.176216	1.140119	0.028
H19	-0.041658	0.206707	1.217563	0.033
H20	-0.178401	0.213531	1.170166	0.038
H21	-0.181336	0.195144	1.045056	0.041
H22	-0.047795	0.169186	0.965081	0.032
H25	0.185707	0.406871	0.830088	0.035
H26	0.127272	0.389124	0.720222	0.047
H27	0.217244	0.329891	0.621372	0.050
H28	0.366338	0.290207	0.631770	0.047
H29	0.427635	0.311964	0.739783	0.034
H31	0.416370	0.231113	0.951300	0.033
H32	0.565166	0.183488	0.954932	0.042
H33	0.682175	0.256000	0.878929	0.047
H34	0.649117	0.377229	0.801183	0.044
H35	0.500827	0.424518	0.798461	0.035
H37	0.303946	0.521305	0.793837	0.036
H38	0.313761	0.661256	0.822038	0.047
H39	0.359799	0.688606	0.934584	0.043
H40	0.406335	0.576688	1.015330	0.038
H41	0.401477	0.437204	0.986145	0.030
H42A	0.458017	-0.068904	0.924380	0.087
H42B	0.360558	-0.022409	0.933661	0.087
H42C	0.449179	0.032382	0.921842	0.087
H43A	0.579123	-0.057287	0.781461	0.070
H43B	0.572112	0.044245	0.774731	0.070
H43C	0.550001	-0.005853	0.707370	0.070

H44A	0.419060	-0.160426	0.800958	0.084
H44B	0.385217	-0.111702	0.727595	0.084
H44C	0.319202	-0.119183	0.805840	0.084
H2A	0.439386	0.239377	0.483894	0.028
H3A	0.334415	0.131537	0.548034	0.026
H6A	0.199784	0.104799	0.629463	0.022
H7A	0.231653	-0.016227	0.708881	0.029
H8A	0.225408	-0.150276	0.667707	0.034
H9A	0.198332	-0.164211	0.546059	0.034
H10A	0.175436	-0.043470	0.464671	0.024
H12A	0.014609	0.071855	0.565780	0.025
H13A	-0.106565	0.142524	0.631753	0.034
H14A	-0.103584	0.289052	0.638355	0.040
H15A	0.020125	0.364103	0.576567	0.036
H16A	0.140291	0.293685	0.508575	0.027
H18A	0.009150	0.122016	0.429270	0.024
H19A	-0.020086	0.074588	0.316594	0.031
H20A	0.097378	0.027234	0.230319	0.033
H21A	0.245627	0.024766	0.256934	0.031
H22A	0.275524	0.069117	0.369422	0.027
H25A	0.522389	0.245520	0.344860	0.032
H26A	0.672498	0.270776	0.343954	0.044
H27A	0.718575	0.402611	0.366724	0.046
H28A	0.609031	0.511841	0.391144	0.043
H29A	0.456959	0.485520	0.395994	0.033
H31A	0.414286	0.454662	0.243340	0.035
H32A	0.425670	0.441459	0.115641	0.042
H33A	0.395981	0.312128	0.073774	0.045
H34A	0.358348	0.196166	0.161286	0.042
H35A	0.347978	0.209103	0.289604	0.032
H37A	0.334708	0.397098	0.499633	0.033
H38A	0.231794	0.498965	0.549809	0.036
H39A	0.152106	0.589150	0.470843	0.039
H40A	0.167989	0.571737	0.343398	0.044

H41A	0.264302	0.465068	0.294206	0.032
H42D	-0.069761	0.491795	0.379088	0.055
H42E	0.019064	0.516687	0.322073	0.055
H42F	0.026953	0.456447	0.397680	0.055
H43D	-0.141903	0.320809	0.394160	0.055
H43E	-0.048354	0.284432	0.419045	0.055
H43F	-0.087471	0.245649	0.352467	0.055
H44D	-0.151505	0.432853	0.256898	0.059
H44E	-0.102971	0.361854	0.206462	0.059
H44F	-0.063842	0.455085	0.197539	0.059
H1S1	0.469896	-0.102783	0.494101	0.081
H1S2	0.378891	-0.063525	0.535358	0.081
H2S1	0.519848	0.064738	0.392857	0.096
H2S2	0.546584	-0.030376	0.418492	0.096
H12B	0.919086	0.295903	0.810533	0.235
H12C	0.847551	0.291628	0.886642	0.235
H13B	0.973448	0.359441	0.920460	0.127
H13C	0.985837	0.419255	0.842357	0.127
H14B	0.748736	0.466354	0.876063	0.165
H14C	0.826179	0.511836	0.816902	0.165
H15B	0.905218	0.509721	0.919076	0.166
H15C	0.845897	0.434010	0.966406	0.166
H3SA	0.523275	0.153222	0.659236	0.084
H3SB	0.553382	0.225402	0.706166	0.084
H4SA	0.695243	0.176244	0.669415	0.057
H4SB	0.665486	0.131464	0.600847	0.057
H5SA	0.694398	0.245085	0.523489	0.098
H5SB	0.738825	0.283266	0.588126	0.098
H6SA	0.609316	0.355100	0.630197	0.094
H6SB	0.603766	0.362254	0.541218	0.094
H3SA	0.569614	0.367364	0.548748	0.074
H3SB	0.660239	0.310736	0.528345	0.074
H4SA	0.574748	0.345564	0.673222	0.168
H4SB	0.680915	0.346037	0.642105	0.168

H5SA	0.615416	0.215081	0.725722	0.168
H5SB	0.696103	0.201568	0.658000	0.168
H6SA	0.596905	0.129135	0.610468	0.073
H6SB	0.512649	0.169100	0.662738	0.073

Table S2.3: Summary of Crystal Data for [(ITr)CuSeSiMe₃] · 1.5 THF (**2.1c**)

Formula	C ₄₉ H ₅₁ CuN ₂ O _{1.25} SeSi
Formula Weight (<i>g/mol</i>)	858.51
Crystal Dimensions (<i>mm</i>)	0.598 × 0.184 × 0.109
Crystal Color and Habit	colourless needle
Crystal System	triclinic
Space Group	P -1
Temperature, K	110
<i>a</i> , Å	15.1218(7)
<i>b</i> , Å	15.8816(7)
<i>c</i> , Å	18.0881(7)
α , °	83.753(2)
β , °	81.279(2)
γ , °	87.308(2)
<i>V</i> , Å ³	4266.2(3)
Number of reflections to determine final unit cell	9964
Min and Max 2 θ for cell determination, °	4.58, 55.24
<i>Z</i>	4
F(000)	1784
ρ (<i>g/cm</i> ⁻³)	1.337
λ , Å, (MoK α)	0.71073
μ , (<i>cm</i> ⁻¹)	1.432
Diffractometer Type	Bruker Kappa Axis Apex2
Scan Type(s)	phi and omega scans
Max 2 θ for data collection, °	50.0
Measured fraction of data	0.972
Number of reflections measured	36585
Unique reflections measured	14597

R _{merge}	0.0312
Number of reflections included in refinement	14597
Cut off Threshold Expression	I > 2sigma(I)
Structure refined using	full matrix least-squares using F ²
Weighting Scheme	w=1/[sigma ² (Fo ²)+(0.0753P) ² +6.24 13P] where P=(Fo ² +2Fc ²)/3
Number of parameters in least-squares	961
R ₁	0.0533
wR ₂	0.1397
R ₁ (all data)	0.0759
wR ₂ (all data)	0.1481
GOF	1.085
Maximum shift/error	0.001
Min & Max peak heights on final ΔF Map (e ⁻ /Å) -	0.913, 1.787

Where:

$$R_1 = \sum (|F_o| - |F_c|) / \sum F_o$$

$$wR_2 = [\sum (w (F_o^2 - F_c^2)^2) / \sum (w F_o^4)]^{1/2}$$

$$GOF = [\sum (w (F_o^2 - F_c^2)^2) / (\text{No. of reflns.} - \text{No. of params.})]^{1/2}$$

Table S2.4. Atomic Coordinates for [(ITr)CuSeSiMe₃] · 1.5 THF (**2.1c**)

Atom	x	y	z	U _{iso/equiv}
Se1	0.10932(3)	0.33299(3)	0.24498(2)	0.02633(13)
Cu1	0.18251(4)	0.27892(3)	0.34077(3)	0.02148(14)
Si1	-0.02278(9)	0.37998(8)	0.30576(7)	0.0268(3)
N1	0.3423(2)	0.2696(2)	0.41447(17)	0.0158(7)
N2	0.2498(2)	0.1753(2)	0.46994(16)	0.0144(7)
C1	0.2604(3)	0.2394(3)	0.4121(2)	0.0157(9)
C2	0.3805(3)	0.2281(3)	0.4741(2)	0.0222(10)
C3	0.3237(3)	0.1691(3)	0.5082(2)	0.0205(9)
C4	0.1677(3)	0.1239(3)	0.4870(2)	0.0160(9)
C5	0.1860(3)	0.0416(3)	0.5378(2)	0.0146(9)
C6	0.1983(3)	0.0469(3)	0.6124(2)	0.0195(9)
C7	0.2135(3)	-0.0255(3)	0.6594(2)	0.0237(10)

C8	0.2131(3)	-0.1044(3)	0.6343(2)	0.0251(10)
C9	0.1996(3)	-0.1103(3)	0.5610(2)	0.0253(10)
C10	0.1867(3)	-0.0384(3)	0.5134(2)	0.0202(9)
C11	0.0902(3)	0.1748(3)	0.5305(2)	0.0162(9)
C12	0.0155(3)	0.1320(3)	0.5677(2)	0.0202(9)
C13	-0.0553(3)	0.1741(3)	0.6065(2)	0.0274(11)
C14	-0.0526(3)	0.2606(3)	0.6097(2)	0.0332(12)
C15	0.0207(3)	0.3042(3)	0.5729(2)	0.0285(11)
C16	0.0924(3)	0.2616(3)	0.5334(2)	0.0213(10)
C17	0.1453(3)	0.1015(2)	0.4110(2)	0.0151(9)
C18	0.0589(3)	0.1025(2)	0.3951(2)	0.0175(9)
C19	0.0407(3)	0.0751(3)	0.3282(2)	0.0219(10)
C20	0.1100(3)	0.0473(3)	0.2769(2)	0.0252(11)
C21	0.1970(3)	0.0459(3)	0.2923(2)	0.0251(10)
C22	0.2150(3)	0.0726(3)	0.3586(2)	0.0200(9)
C23	0.3754(3)	0.3473(3)	0.3649(2)	0.0177(9)
C24	0.3113(3)	0.4196(3)	0.3928(2)	0.0186(9)
C25	0.2582(3)	0.4694(3)	0.3480(3)	0.0302(11)
C26	0.2003(4)	0.5316(3)	0.3773(3)	0.0396(13)
C27	0.1914(3)	0.5426(3)	0.4528(3)	0.0347(12)
C28	0.2421(3)	0.4918(3)	0.4989(3)	0.0312(11)
C29	0.3016(3)	0.4317(3)	0.4685(2)	0.0266(10)
C30	0.4734(3)	0.3612(3)	0.3728(2)	0.0196(9)
C31	0.5018(3)	0.4401(3)	0.3850(3)	0.0278(11)
C32	0.5919(3)	0.4542(3)	0.3826(3)	0.0394(13)
C33	0.6545(4)	0.3908(4)	0.3693(3)	0.0404(13)
C34	0.6279(3)	0.3122(4)	0.3572(3)	0.0386(13)
C35	0.5377(3)	0.2976(3)	0.3583(2)	0.0293(11)
C36	0.3777(3)	0.3347(3)	0.2818(2)	0.0181(9)
C37	0.4009(3)	0.4031(3)	0.2287(2)	0.0314(12)
C38	0.4082(4)	0.3960(3)	0.1520(2)	0.0376(13)
C39	0.3920(4)	0.3203(3)	0.1277(2)	0.0379(13)
C40	0.3711(4)	0.2517(3)	0.1787(2)	0.0375(13)
C41	0.3649(3)	0.2580(3)	0.2559(2)	0.0257(10)

C42	-0.0984(4)	0.4111(3)	0.2341(3)	0.0420(13)
C43	-0.0125(4)	0.4741(3)	0.3556(3)	0.0364(12)
C44	-0.0792(4)	0.2993(3)	0.3774(3)	0.0382(12)
Se1A	0.35381(3)	0.09883(3)	0.75351(2)	0.02768(13)
Cu1A	0.29603(4)	0.17431(3)	0.84988(3)	0.02102(14)
Si1A	0.42607(10)	-0.01439(9)	0.80482(8)	0.0349(3)
N1A	0.1791(2)	0.2346(2)	0.98102(17)	0.0174(8)
N2A	0.2774(2)	0.3264(2)	0.93171(17)	0.0168(8)
C1A	0.2494(3)	0.2470(3)	0.9246(2)	0.0172(9)
C2A	0.1645(3)	0.3041(3)	1.0222(2)	0.0235(10)
C3A	0.2249(3)	0.3613(3)	0.9908(2)	0.0232(10)
C4A	0.1265(3)	0.1552(3)	0.9943(2)	0.0191(9)
C5A	0.1101(3)	0.1331(3)	0.9160(2)	0.0190(9)
C6A	0.0846(3)	0.1988(3)	0.8640(2)	0.0278(11)
C7A	0.0618(3)	0.1816(3)	0.7960(2)	0.0314(12)
C8A	0.0625(3)	0.0986(3)	0.7786(2)	0.0299(11)
C9A	0.0887(3)	0.0342(3)	0.8289(2)	0.0287(11)
C10A	0.1126(3)	0.0513(3)	0.8969(2)	0.0223(10)
C11A	0.0359(3)	0.1723(3)	1.0439(2)	0.0185(9)
C12A	-0.0458(3)	0.1768(3)	1.0164(2)	0.0275(11)
C13A	-0.1258(3)	0.1918(3)	1.0630(3)	0.0312(11)
C14A	-0.1256(3)	0.2026(3)	1.1379(3)	0.0300(11)
C15A	-0.0452(3)	0.1973(3)	1.1659(2)	0.0247(10)
C16A	0.0345(3)	0.1808(3)	1.1203(2)	0.0228(10)
C17A	0.1779(3)	0.0841(3)	1.0363(2)	0.0182(9)
C18A	0.1337(3)	0.0097(3)	1.0660(2)	0.0229(10)
C19A	0.1774(3)	-0.0564(3)	1.1038(2)	0.0274(11)
C20A	0.2662(3)	-0.0488(3)	1.1138(2)	0.0296(11)
C21A	0.3096(3)	0.0246(3)	1.0863(2)	0.0298(11)
C22A	0.2654(3)	0.0908(3)	1.0476(2)	0.0269(11)
C23A	0.3454(3)	0.3716(3)	0.8728(2)	0.0180(9)
C24A	0.4403(3)	0.3337(3)	0.8771(2)	0.0185(9)
C25A	0.4600(3)	0.2611(3)	0.9225(2)	0.0242(10)
C26A	0.5479(3)	0.2332(3)	0.9246(3)	0.0323(11)

C27A	0.6177(3)	0.2759(3)	0.8809(3)	0.0360(12)
C28A	0.5995(3)	0.3479(3)	0.8350(3)	0.0336(12)
C29A	0.5121(3)	0.3763(3)	0.8332(2)	0.0268(10)
C30A	0.3479(3)	0.4652(3)	0.8887(2)	0.0188(9)
C31A	0.3803(3)	0.4845(3)	0.9530(2)	0.0245(10)
C32A	0.3847(3)	0.5662(3)	0.9693(2)	0.0304(11)
C33A	0.3591(3)	0.6327(3)	0.9205(3)	0.0347(12)
C34A	0.3298(4)	0.6160(3)	0.8557(3)	0.0364(12)
C35A	0.3236(3)	0.5324(3)	0.8394(3)	0.0298(11)
C36A	0.3134(3)	0.3627(3)	0.7969(2)	0.0203(10)
C37A	0.3673(4)	0.3305(3)	0.7372(2)	0.0283(11)
C38A	0.3326(4)	0.3181(3)	0.6719(2)	0.0368(13)
C39A	0.2447(4)	0.3390(3)	0.6661(3)	0.0405(14)
C40A	0.1905(4)	0.3719(3)	0.7248(3)	0.0360(13)
C41A	0.2241(3)	0.3838(3)	0.7900(2)	0.0268(11)
C42A	0.3830(5)	-0.1153(4)	0.7828(4)	0.069(2)
C43A	0.4241(5)	-0.0194(5)	0.9068(3)	0.071(2)
C44A	0.5481(4)	-0.0121(4)	0.7612(3)	0.0558(16)
O1S	0.4396(6)	-0.0527(6)	0.5132(5)	0.059(2)
C1S	0.4857(6)	-0.0226(6)	0.5633(5)	0.098(3)
C2S	0.4339(8)	-0.0023(7)	0.4492(6)	0.121(3)
O2S	0.5572(7)	0.2455(6)	0.5664(5)	0.063(3)
C3S	0.5995(11)	0.3248(10)	0.5883(13)	0.081(6)
C4S	0.6826(13)	0.2637(11)	0.5820(12)	0.128(7)
C5S	0.6632(10)	0.1849(10)	0.6310(9)	0.085(5)
C6S	0.5633(11)	0.2065(15)	0.6512(9)	0.110(7)
O2SA	0.5338(9)	0.2687(8)	0.6007(8)	0.108(4)
C3SA	0.6114(11)	0.3184(12)	0.5605(9)	0.079(6)
C4SA	0.6274(14)	0.3161(10)	0.6407(9)	0.099(6)
C5SA	0.6248(13)	0.2242(9)	0.6764(9)	0.086(5)
C6SA	0.5801(10)	0.1812(8)	0.6213(9)	0.066(4)
O3S	0.8301(9)	0.3733(9)	0.8106(7)	0.213(5)
C7S	0.8821(13)	0.4480(12)	0.9261(10)	0.230(8)
C8S	0.9357(8)	0.3913(8)	0.8804(7)	0.134(4)

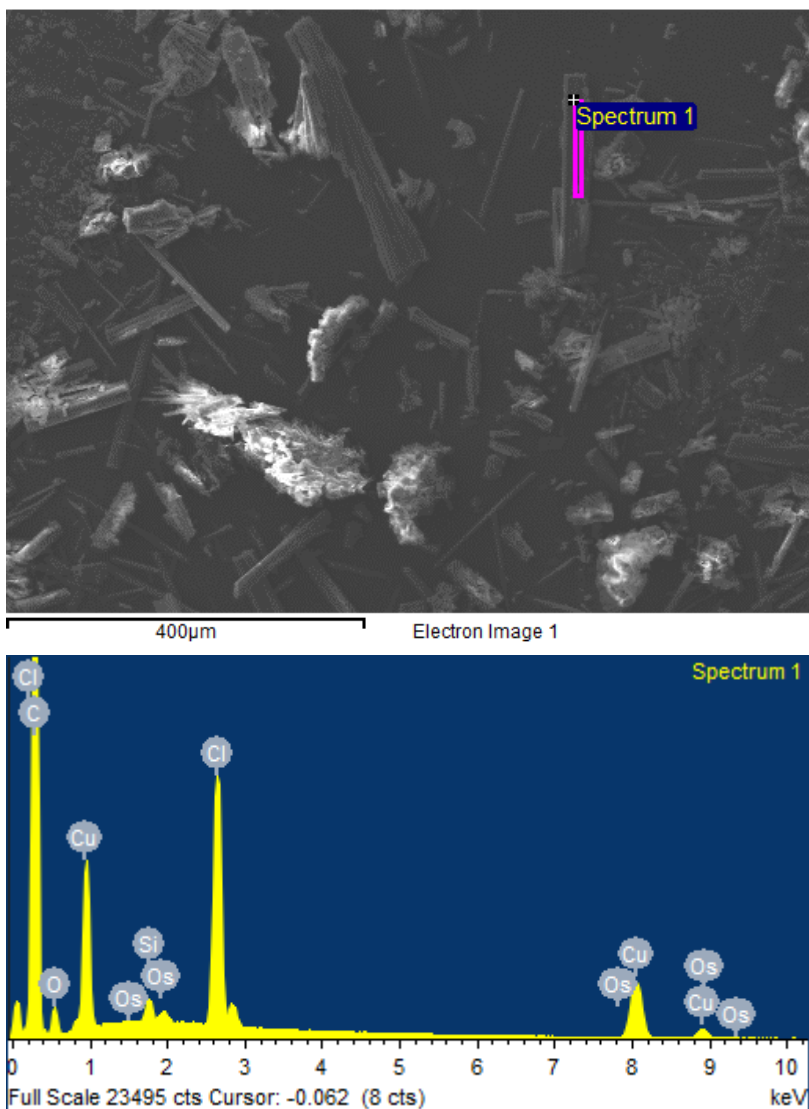
C9S	0.8762(18)	0.3228(17)	0.8492(14)	0.316(13)
C10S	0.8137(12)	0.4449(12)	0.8570(10)	0.216(7)
H2	0.436544	0.239545	0.487987	0.027
H3	0.332048	0.130188	0.550556	0.025
H6	0.196214	0.100775	0.630908	0.023
H7	0.224285	-0.020733	0.709125	0.028
H8	0.222007	-0.154089	0.666909	0.030
H9	0.199198	-0.164508	0.543433	0.030
H10	0.178203	-0.043646	0.463116	0.024
H12	0.013261	0.072553	0.566321	0.024
H13	-0.106100	0.143865	0.631004	0.033
H14	-0.100954	0.289675	0.637077	0.040
H15	0.022368	0.363695	0.574528	0.034
H16	0.142844	0.292084	0.508473	0.026
H18	0.011100	0.122026	0.430075	0.021
H19	-0.019141	0.075705	0.318113	0.026
H20	0.098015	0.029206	0.231199	0.030
H21	0.244646	0.026410	0.257152	0.030
H22	0.274927	0.071432	0.368634	0.024
H25	0.261647	0.460779	0.296516	0.036
H26	0.166376	0.566806	0.345359	0.048
H27	0.150979	0.584773	0.473036	0.042
H28	0.235898	0.498294	0.550999	0.037
H29	0.336781	0.397734	0.500261	0.032
H31	0.458962	0.484644	0.394988	0.033
H32	0.610265	0.508577	0.390289	0.047
H33	0.716164	0.400787	0.368428	0.048
H34	0.671280	0.267927	0.347984	0.046
H35	0.520003	0.243503	0.349074	0.035
H37	0.412044	0.455870	0.245206	0.038
H38	0.424381	0.443430	0.116631	0.045
H39	0.395186	0.315462	0.075447	0.046
H40	0.360667	0.199062	0.161677	0.045
H41	0.351833	0.209401	0.290656	0.031

H42A	-0.155050	0.434470	0.258632	0.063
H42B	-0.109959	0.361158	0.209992	0.063
H42C	-0.069772	0.453943	0.195975	0.063
H43A	-0.071468	0.490520	0.381563	0.055
H43B	0.010682	0.521073	0.319281	0.055
H43C	0.028645	0.460473	0.392497	0.055
H44A	-0.139717	0.320058	0.395816	0.057
H44B	-0.044873	0.288719	0.419500	0.057
H44C	-0.082747	0.246443	0.354753	0.057
H2A	0.120129	0.309864	1.064680	0.028
H3A	0.230570	0.415843	1.006242	0.028
H6A	0.083030	0.255777	0.875697	0.033
H7A	0.045576	0.226680	0.761139	0.038
H8A	0.045257	0.086276	0.732716	0.036
H9A	0.090395	-0.022688	0.816992	0.034
H10A	0.130894	0.005983	0.930626	0.027
H12A	-0.046847	0.169613	0.965056	0.033
H13A	-0.180816	0.194513	1.043396	0.037
H14A	-0.180041	0.213583	1.169586	0.036
H15A	-0.044610	0.204942	1.217192	0.030
H16A	0.088776	0.175328	1.140992	0.027
H18A	0.072899	0.004410	1.060156	0.027
H19A	0.146813	-0.106951	1.122874	0.033
H20A	0.296441	-0.094069	1.139396	0.036
H21A	0.369852	0.030495	1.093526	0.036
H22A	0.296140	0.141316	1.028801	0.032
H25A	0.412775	0.230202	0.952402	0.029
H26A	0.560197	0.183986	0.956676	0.039
H27A	0.677729	0.256080	0.882354	0.043
H28A	0.647095	0.377864	0.804582	0.040
H29A	0.500406	0.425924	0.801360	0.032
H31A	0.399866	0.439601	0.986417	0.029
H32A	0.405371	0.577175	1.014233	0.036
H33A	0.361833	0.689482	0.931719	0.042

H34A	0.313543	0.661677	0.821378	0.044
H35A	0.302698	0.521695	0.794462	0.036
H37A	0.428470	0.316643	0.740445	0.034
H38A	0.370075	0.295061	0.631413	0.044
H39A	0.221315	0.330828	0.621585	0.049
H40A	0.129725	0.386659	0.720677	0.043
H41A	0.186014	0.406406	0.830266	0.032
H42A	0.419922	-0.163049	0.801252	0.104
H42B	0.385351	-0.114350	0.728315	0.104
H42C	0.320909	-0.121559	0.807398	0.104
H43A	0.461645	-0.067691	0.923442	0.106
H43B	0.362503	-0.026395	0.932233	0.106
H43C	0.447172	0.033085	0.919311	0.106
H44A	0.579402	-0.063660	0.779783	0.084
H44B	0.575405	0.037631	0.774983	0.084
H44C	0.552505	-0.008982	0.706400	0.084
H1S1	0.448883	0.025787	0.582487	0.118
H1S2	0.483659	-0.067355	0.606022	0.118
H2S1	0.419595	-0.034176	0.408669	0.145
H2S2	0.389818	0.045211	0.457015	0.145
H3SA	0.602650	0.374633	0.550126	0.098
H3SB	0.577314	0.340199	0.639583	0.098
H4SA	0.699040	0.250767	0.529215	0.154
H4SB	0.733824	0.291038	0.596678	0.154
H5SA	0.695325	0.179341	0.675118	0.102
H5SB	0.674626	0.133831	0.603661	0.102
H6SA	0.550569	0.248716	0.688151	0.132
H6SB	0.526517	0.155961	0.667476	0.132
H3SA	0.595994	0.374927	0.536168	0.095
H3SB	0.656208	0.286529	0.527565	0.095
H4SA	0.580643	0.350871	0.668963	0.119
H4SB	0.686361	0.339779	0.642441	0.119
H5SA	0.685854	0.200114	0.679709	0.103
H5SB	0.589056	0.219366	0.727148	0.103

H6SA	0.538126	0.136831	0.645459	0.080
H6SB	0.622306	0.160215	0.579451	0.080
H7SA	0.908778	0.503507	0.927401	0.276
H7SB	0.856788	0.422682	0.976913	0.276
H8SA	0.978957	0.360140	0.910080	0.161
H8SB	0.970197	0.424620	0.837007	0.161
H9SA	0.914284	0.283751	0.817926	0.379
H9SB	0.838362	0.289631	0.890684	0.379
H10A	0.750696	0.443665	0.881848	0.260
H10B	0.820669	0.498218	0.823099	0.260

Appendix 2. Supporting Information for Chapter 3



Element	Weight%	Atomic%
C K	78.95	91.15
O K	5.04	4.37
Si K	0.40	0.20
Cl K	5.60	2.19
Cu K	9.37	2.05
Os M	0.64	0.05

Figure S3.1: Example of SEM - EDX data of solids isolated from 2:1 reaction of [ITrCuCl] and Na₂Se. Characteristic X – ray detected for each element listed (K shell, M shell, etc.).

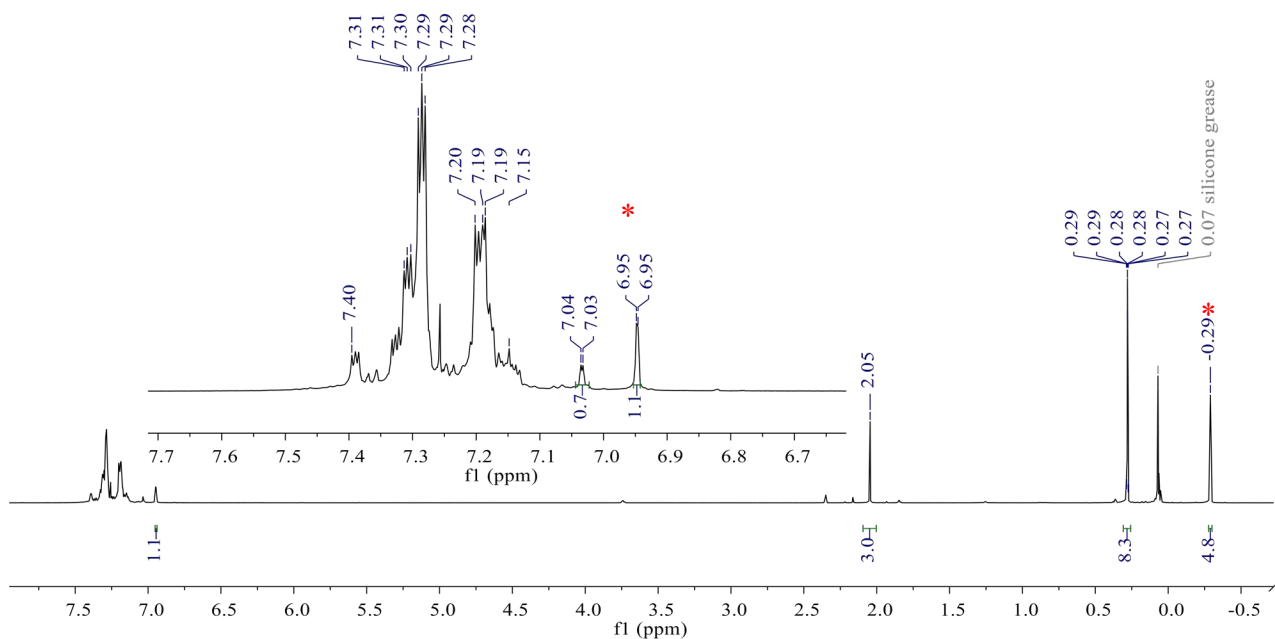


Figure S3.2: ^1H NMR spectrum of a 2:1 reaction of $[\text{ITrAgOAc}]$ and $\text{S}(\text{SiMe}_3)_2$ in CDCl_3 , after 1 hour at -45°C . Data collected at room temperature. * - $[\text{ITrAgSSiMe}_3]$

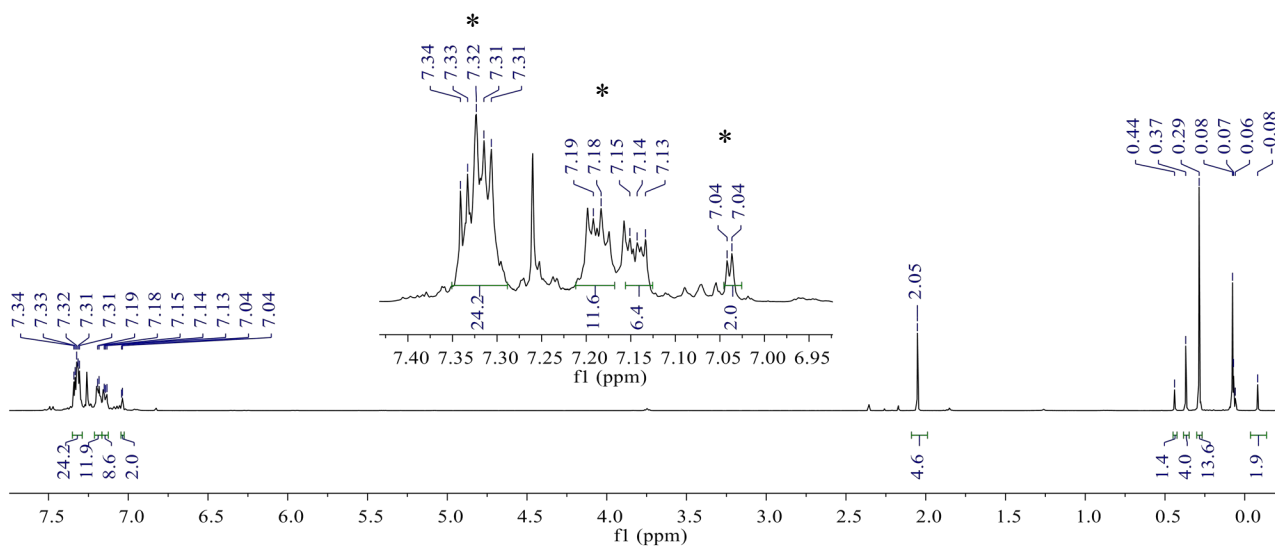


Figure S3.3: ^1H NMR spectrum of the sample from Figure S3.2 after overnight at room temperature * - $[\text{ITrAgCl}]$ (proposed)

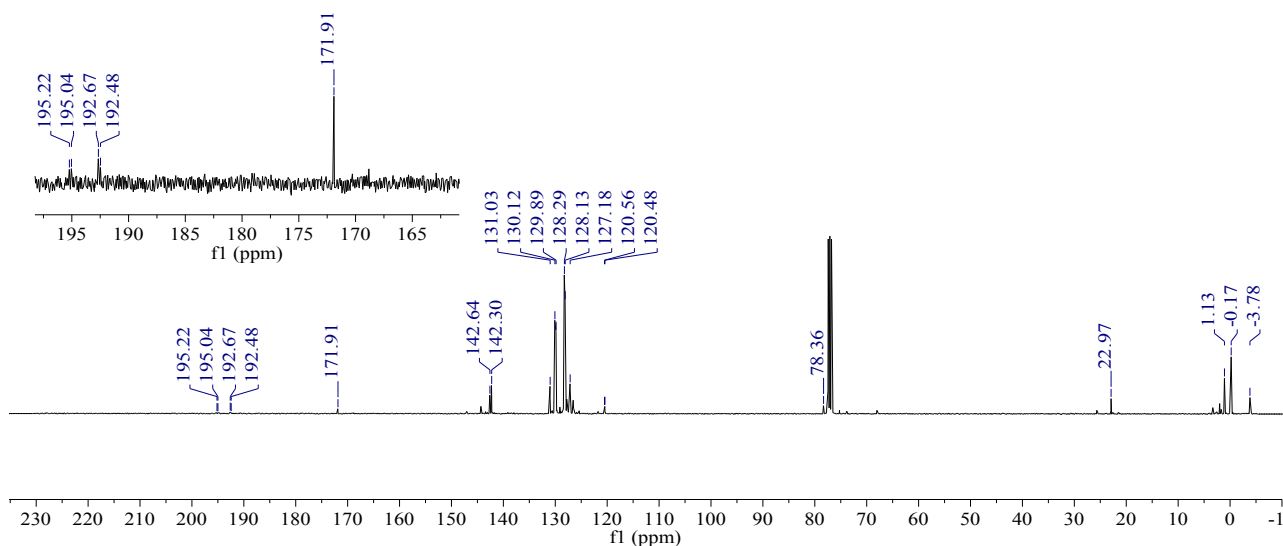


Figure S3.4: $^{13}\text{C}\{^1\text{H}\}$ NMR spectrum of the sample from Figure S3.3. Inset shows doublet of doublets for carbenic carbon (δ 193.9 ppm, $^1J_{109\text{Ag}-^{13}\text{C}} = 277$ Hz, $^1J_{107\text{Ag}-^{13}\text{C}} = 239$ Hz).

Table S3.1: Summary of Crystal Data for $[\text{ITrAgCl}] \cdot 2\text{CHCl}_3$ (**3.5**)

Formula	$\text{C}_{86}\text{H}_{68}\text{Ag}_2\text{Cl}_{14}\text{N}_4$
Formula Weight (g/mol)	1869.48
Crystal Dimensions (mm)	$0.187 \times 0.076 \times 0.021$
Crystal Color and Habit	colourless Needle
Crystal System	monoclinic
Space Group	$P 2_1/c$
Temperature, K	100
a , Å	11.410(2)
b , Å	17.840(4)
c , Å	19.930(4)
α , °	90
β , °	100.77(3)
γ , °	90
V , Å ³	3985.4(14)
Number of reflections to determine final unit cell	9857
Min and Max 2θ for cell determination, °	4.76, 55.1
Z	2
$F(000)$	1888
ρ (g/cm ³)	1.558
λ , Å, (MoK α)	0.71073
μ , (cm ⁻¹)	1.010
Diffractometer Type	Bruker Kappa Axis Apex2

Scan Type(s)	phi and omega scans
Max 2 θ for data collection, °	55.07
Measured fraction of data	0.999
Number of reflections measured	70235
Unique reflections measured	9157
R _{merge}	0.0582
Number of reflections included in refinement	9157
Cut off Threshold Expression	I > 2sigma(I)
Structure refined using	full matrix least-squares using F ²
Weighting Scheme	w=1/[sigma ² (Fo ²)+(0.0612P) ² +5.86 06P] where P=(Fo ² +2Fc ²)/3
Number of parameters in least-squares	478
R ₁	0.0374
wR ₂	0.1029
R ₁ (all data)	0.0538
wR ₂ (all data)	0.1179
GOF	1.067
Maximum shift/error	0.001
Min & Max peak heights on final DF Map (e ⁻ /Å)	-0.955, 0.762

Where:

$$R_1 = S(|F_o| - |F_c|) / S F_o$$

$$wR_2 = [S(w(F_o^2 - F_c^2)^2) / S(w F_o^4)]^{1/2}$$

$$GOF = [S(w(F_o^2 - F_c^2)^2) / (No. of reflns. - No. of params.)]^{1/2}$$

Table S3.2: Atomic Coordinates for [ITrAgCl]·2CHCl₃ (**3.5**)

Atom	x	y	z	U _{iso/equiv}
Ag1	0.39122(2)	0.62236(2)	0.17454(2)	0.01490(8)
Cl1	0.41456(8)	0.67231(5)	0.06809(4)	0.02282(18)
N1	0.2924(2)	0.57642(13)	0.30841(12)	0.0082(5)
N2	0.4719(2)	0.53736(13)	0.31215(12)	0.0084(5)
C1	0.3804(3)	0.57517(16)	0.27127(15)	0.0098(6)
C2	0.3264(3)	0.53884(16)	0.37002(15)	0.0112(6)
C3	0.4388(3)	0.51500(16)	0.37265(15)	0.0108(6)
C4	0.1633(2)	0.59669(15)	0.28564(14)	0.0074(5)
C5	0.1425(3)	0.64364(16)	0.21969(15)	0.0096(6)
C6	0.2073(3)	0.70980(16)	0.21824(15)	0.0115(6)
C7	0.1834(3)	0.75750(17)	0.16253(16)	0.0161(6)
C8	0.0925(3)	0.74080(18)	0.10761(16)	0.0182(7)
C9	0.0267(3)	0.67640(19)	0.10924(17)	0.0198(7)
C10	0.0504(3)	0.62779(17)	0.16489(16)	0.0144(6)
C11	0.1013(3)	0.51963(16)	0.27765(15)	0.0092(5)
C12	0.1258(3)	0.47258(17)	0.22579(16)	0.0138(6)
C13	0.0831(3)	0.39907(18)	0.21949(17)	0.0164(6)
C14	0.0174(3)	0.37179(17)	0.26594(18)	0.0174(7)
C15	-0.0057(3)	0.41736(18)	0.31798(17)	0.0166(6)
C16	0.0356(3)	0.49119(17)	0.32393(15)	0.0118(6)
C17	0.1231(3)	0.64841(16)	0.33875(14)	0.0092(6)

C18	0.0015(3)	0.66289(16)	0.33362(15)	0.0120(6)
C19	-0.0377(3)	0.71529(17)	0.37626(16)	0.0155(6)
C20	0.0428(3)	0.75520(17)	0.42300(16)	0.0157(6)
C21	0.1645(3)	0.74248(16)	0.42851(15)	0.0143(6)
C22	0.2041(3)	0.68919(16)	0.38644(15)	0.0109(6)
C23	0.5923(3)	0.52411(16)	0.29351(15)	0.0094(6)
C24	0.5842(3)	0.46284(16)	0.23829(15)	0.0108(6)
C25	0.4793(3)	0.44307(17)	0.19467(16)	0.0145(6)
C26	0.4798(3)	0.39150(18)	0.14185(17)	0.0204(7)
C27	0.5848(3)	0.35792(18)	0.13287(17)	0.0209(7)
C28	0.6897(3)	0.37577(18)	0.17719(16)	0.0180(7)
C29	0.6899(3)	0.42783(17)	0.22867(15)	0.0144(6)
C30	0.6339(3)	0.59976(16)	0.26857(15)	0.0109(6)
C31	0.6945(3)	0.60406(18)	0.21383(16)	0.0151(6)
C32	0.7321(3)	0.67331(19)	0.19326(17)	0.0184(7)
C33	0.7101(3)	0.73831(19)	0.22625(18)	0.0225(7)
C34	0.6500(3)	0.73432(19)	0.28060(18)	0.0218(7)
C35	0.6131(3)	0.66560(17)	0.30178(16)	0.0156(6)
C36	0.6769(3)	0.49669(17)	0.35889(14)	0.0103(6)
C37	0.7641(3)	0.54216(18)	0.39681(16)	0.0145(6)
C38	0.8370(3)	0.5143(2)	0.45590(16)	0.0185(7)
C39	0.8232(3)	0.4417(2)	0.47771(16)	0.0183(7)
C40	0.7361(3)	0.39673(19)	0.44108(16)	0.0162(6)
C41	0.6641(3)	0.42321(17)	0.38181(15)	0.0130(6)
C01S	0.6460(3)	0.70740(19)	0.53285(17)	0.0212(7)
Cl02	0.75801(9)	0.65336(5)	0.58408(5)	0.0304(2)
Cl03	0.53514(9)	0.64858(6)	0.48737(5)	0.0331(2)
Cl04	0.71071(10)	0.76280(6)	0.47674(5)	0.0358(2)
C02S	0.7503(3)	0.4858(2)	0.00994(18)	0.0280(8)
Cl05	0.86748(9)	0.46261(6)	0.07815(5)	0.0370(2)
Cl06	0.64664(9)	0.54482(6)	0.03792(5)	0.0308(2)
Cl07	0.81062(12)	0.52877(9)	-0.05560(6)	0.0566(4)
H2	0.279031	0.531401	0.403920	0.013
H3	0.486495	0.488052	0.408911	0.013
H6	0.268341	0.722260	0.255882	0.014
H7	0.229340	0.801808	0.161769	0.019
H8	0.075946	0.773547	0.069426	0.022
H9	-0.035592	0.664906	0.071955	0.024
H10	0.003792	0.583778	0.165514	0.017
H12	0.172169	0.490930	0.194408	0.017
H13	0.099007	0.367985	0.183539	0.020
H14	-0.011819	0.321806	0.262043	0.021
H15	-0.050098	0.398265	0.350058	0.020
H16	0.018643	0.522074	0.359767	0.014
H18	-0.054882	0.636781	0.300776	0.014
H19	-0.120761	0.723603	0.373105	0.019
H20	0.015239	0.791356	0.451418	0.019
H21	0.220307	0.769846	0.460685	0.017

H22	0.287285	0.680523	0.390264	0.013
H25	0.406070	0.464878	0.200767	0.017
H26	0.407226	0.379478	0.111907	0.025
H27	0.585110	0.323097	0.096842	0.025
H28	0.762173	0.352071	0.172191	0.022
H29	0.762898	0.440091	0.258043	0.017
H31	0.710085	0.559705	0.190615	0.018
H32	0.773323	0.675743	0.156084	0.022
H33	0.735853	0.785320	0.211921	0.027
H34	0.634125	0.778875	0.303422	0.026
H35	0.572979	0.663509	0.339449	0.019
H37	0.774052	0.592191	0.382566	0.017
H38	0.896654	0.545621	0.481314	0.022
H39	0.873396	0.423126	0.517675	0.022
H40	0.725232	0.347242	0.456397	0.019
H41	0.605414	0.391218	0.356482	0.016
H01S	0.608730	0.741044	0.563079	0.025
H02S	0.708901	0.438609	-0.008294	0.034

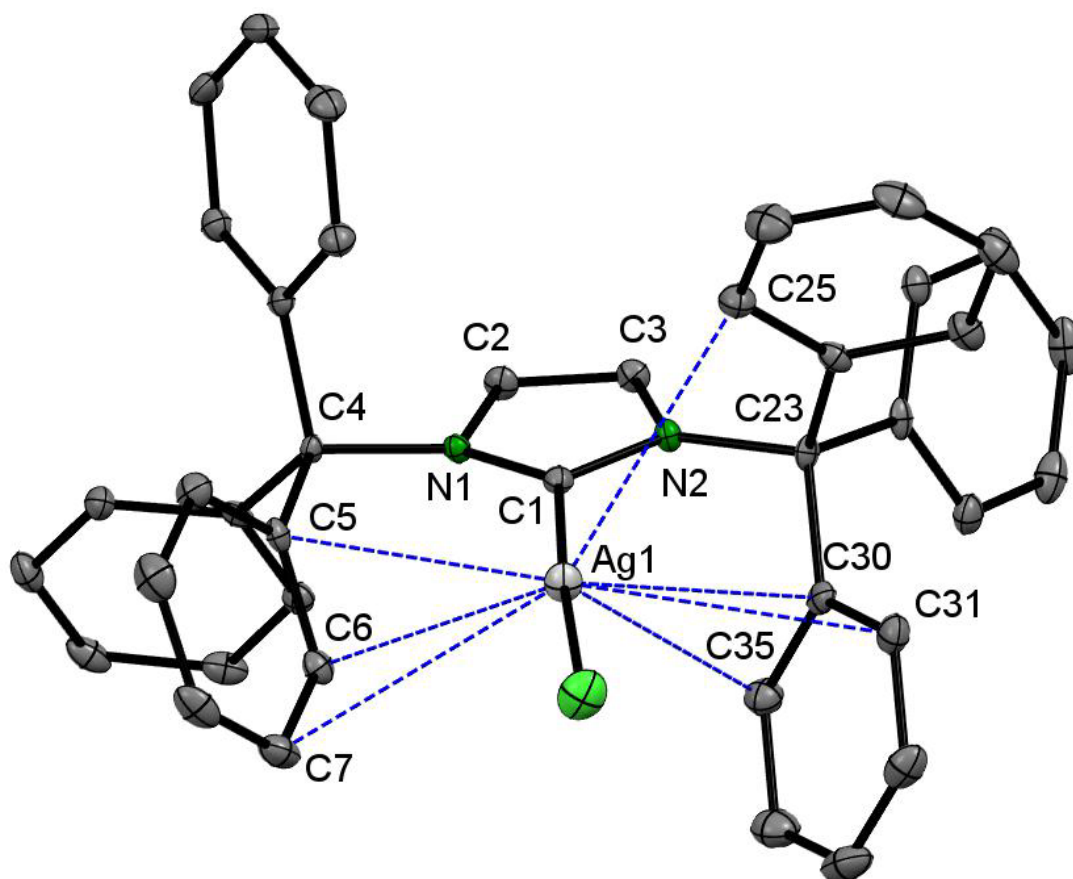


Figure S3.5: Molecular structure of [ITrAgCl] (**3.5**) showcasing intramolecular Ph - Ag contacts, implying η_3 and η_2 coordination. Ag = silver, N = dark green, C = grey, Cl = lime green. C1 - Ag1: 2.128(3)Å. Ag - Cl: 2.3615(9) Å. C1 - N1: 1.354(4) Å. C1 - N2: 1.375(4) Å. N1 - C2: 1.389(4)Å. N2 - C3: 1.387(4)Å. N1 - C4: 1.502(4)Å. N2 - C23:1.508(4)Å. C5 - Ag1: 3.156(3)Å. C6 - Ag1: 2.878(3)Å. C7 - Ag1: 3.358(3)Å. C25 - Ag1: 3.354(3)Å. C30 - Ag1: 3.067(3)Å. C31 - Ag1: 3.418(3)Å. C35 - Ag1: 3.322(3)Å. C1 - Ag1 - Cl: 176.74(8)°. Ag1 - C1 - N1: 131.5(2)°. Ag1 - C1 - N2: 124.4(2)°. C1 - N1 - C4: 128.6(2)°. C1 - N2 - C23: 123.8(2)°.

Table S3.3: Summary of Crystal Data for [ITrAuCl]₇·2CHCl₃ (**3.6**)

Formula	C ₄₃ H ₃₄ AuCl ₇ N ₂
Formula Weight (<i>g/mol</i>)	1023.84
Crystal Dimensions (<i>mm</i>)	0.157 × 0.134 × 0.054
Crystal Color and Habit	colourless Prism
Crystal System	trigonal
Space Group	P -3
Temperature, K	110
<i>a</i> , Å	25.8840(9)
<i>b</i> , Å	25.8840(9)
<i>c</i> , Å	11.0393(6)
α, °	90
β, °	90
γ, °	120
<i>V</i> , Å ³	6405.2(6)
Number of reflections to determine final unit cell	9741
Min and Max 2θ for cell determination, °	5.18, 55.62
<i>Z</i>	6
F(000)	3024
ρ (<i>g/cm</i>)	1.593
λ, Å, (MoKα)	0.71073
μ, (<i>cm</i> ⁻¹)	3.916
Diffractometer Type	Bruker Kappa Axis Apex2
Scan Type(s)	phi and omega scans
Max 2θ for data collection, °	55.842
Measured fraction of data	0.998
Number of reflections measured	92324
Unique reflections measured	10136
R _{merge}	0.0646
Number of reflections included in refinement	10136
Cut off Threshold Expression	I > 2σ(I)
Structure refined using	full matrix least-squares using F ²
Weighting Scheme	w=1/[σ(F _o ²)+(0.0412P) ² +7.2902P] where P=(F _o ² +2F _c ²)/3
Number of parameters in least-squares	478
R ₁	0.0336
wR ₂	0.0817
R ₁ (all data)	0.0479
wR ₂ (all data)	0.0867
GOF	1.064
Maximum shift/error	0.003
Min & Max peak heights on final ΔF Map (<i>e</i> ⁻ /Å)	-1.170, 2.179

Where:

$$R_1 = \frac{\sum (|F_o| - |F_c|)}{\sum F_o}$$

$$wR_2 = \left[\frac{\sum w(F_o^2 - F_c^2)^2}{\sum w F_o^4} \right]^{1/2}$$

$$GOF = \left[\frac{\sum w(F_o^2 - F_c^2)^2}{(\text{No. of reflns.} - \text{No. of params.})} \right]^{1/2}$$

Table S3.4. Atomic Coordinates for [ITrAuCl]·2CHCl₃ (**3.6**)

Atom	x	y	z	U _{iso} /equiv
Au1	0.73302(2)	0.13515(2)	0.79637(2)	0.02021(6)
Cl1	0.66350(5)	0.10245(5)	0.94696(11)	0.0378(3)
N1	0.81430(13)	0.13832(13)	0.5938(3)	0.0180(7)
N2	0.83088(13)	0.22667(13)	0.6364(3)	0.0174(6)
C1	0.79613(16)	0.16832(16)	0.6666(3)	0.0161(7)
C2	0.86090(16)	0.17814(16)	0.5191(4)	0.0209(8)
C3	0.87134(16)	0.23274(16)	0.5470(3)	0.0194(8)
C4	0.78928(16)	0.07171(16)	0.6001(3)	0.0181(8)
C5	0.81052(17)	0.05544(17)	0.7172(3)	0.0207(8)
C6	0.84288(17)	0.09642(18)	0.8076(4)	0.0229(8)
C7	0.8605(2)	0.0786(2)	0.9104(4)	0.0345(11)
C8	0.8467(2)	0.0198(2)	0.9244(4)	0.0387(11)
C9	0.8155(2)	-0.0211(2)	0.8330(4)	0.0359(11)
C10	0.7983(2)	-0.00307(18)	0.7319(4)	0.0292(10)
C11	0.81441(17)	0.05209(16)	0.4932(3)	0.0197(8)
C12	0.77923(18)	0.01944(17)	0.3940(4)	0.0241(9)
C13	0.8038(2)	0.00222(18)	0.3007(4)	0.0293(10)
C14	0.8626(2)	0.0160(2)	0.3054(4)	0.0350(11)
C15	0.8978(2)	0.04840(19)	0.4039(4)	0.0304(10)
C16	0.87400(18)	0.06582(17)	0.4967(4)	0.0249(9)
C17	0.72080(16)	0.04314(16)	0.5932(4)	0.0204(8)
C18	0.69715(18)	0.06212(18)	0.5013(4)	0.0244(9)
C19	0.63609(19)	0.03817(19)	0.4877(4)	0.0308(10)
C20	0.5978(2)	-0.0043(2)	0.5673(5)	0.0351(11)
C21	0.62007(19)	-0.02303(19)	0.6600(4)	0.0342(11)
C22	0.68179(18)	0.00019(17)	0.6744(4)	0.0274(9)
C23	0.84028(16)	0.27906(16)	0.7131(3)	0.0182(8)
C24	0.89100(16)	0.28786(16)	0.7998(3)	0.0184(8)
C25	0.87936(17)	0.24987(17)	0.8983(4)	0.0215(8)
C26	0.92559(19)	0.25413(19)	0.9710(4)	0.0275(9)
C27	0.98425(19)	0.29629(19)	0.9446(4)	0.0290(9)
C28	0.99605(17)	0.33325(19)	0.8444(4)	0.0285(10)
C29	0.95034(17)	0.32911(17)	0.7725(4)	0.0220(8)
C30	0.85547(16)	0.33346(16)	0.6330(4)	0.0200(8)
C31	0.88144(17)	0.38993(17)	0.6882(4)	0.0238(9)
C32	0.88865(18)	0.43895(18)	0.6233(4)	0.0298(10)
C33	0.86968(19)	0.43269(19)	0.5057(4)	0.0335(11)
C34	0.84334(19)	0.3772(2)	0.4496(4)	0.0323(10)
C35	0.83665(17)	0.32815(17)	0.5138(4)	0.0241(9)
C36	0.78209(16)	0.26706(16)	0.7754(4)	0.0208(8)
C37	0.78182(18)	0.28414(17)	0.8944(4)	0.0264(9)
C38	0.7298(2)	0.27740(19)	0.9461(5)	0.0350(11)
C39	0.6786(2)	0.2559(2)	0.8776(5)	0.0414(13)
C40	0.67856(19)	0.24123(19)	0.7572(5)	0.0396(12)
C41	0.73006(17)	0.24609(17)	0.7054(4)	0.0285(10)

C1S	0.53719(19)	0.0799(2)	1.0915(4)	0.0302(10)
C12	0.46579(5)	0.05673(6)	1.03234(11)	0.0395(3)
C13	0.53215(6)	0.03833(6)	1.22143(11)	0.0409(3)
C14	0.57371(5)	0.15665(5)	1.12417(11)	0.0403(3)
C2S	0.7699(2)	0.1885(2)	0.1768(5)	0.0390(11)
C16	0.82443(7)	0.26431(5)	0.19796(12)	0.0549(4)
C17	0.80157(6)	0.14277(6)	0.19517(14)	0.0509(3)
C18	0.71099(7)	0.16900(7)	0.27842(15)	0.0616(4)
H2	0.881196	0.168260	0.459928	0.025
H3	0.901037	0.269116	0.512049	0.023
H6	0.852981	0.136916	0.798746	0.027
H7	0.882257	0.106904	0.971931	0.041
H8	0.858379	0.007544	0.995436	0.046
H9	0.806141	-0.061397	0.840806	0.043
H10	0.777337	-0.031313	0.669719	0.035
H12	0.738474	0.009014	0.390320	0.029
H13	0.779850	-0.019233	0.233317	0.035
H14	0.878938	0.003692	0.242321	0.042
H15	0.938493	0.058514	0.407094	0.036
H16	0.898362	0.087350	0.563603	0.030
H18	0.723478	0.092173	0.446757	0.029
H19	0.620954	0.051204	0.423508	0.037
H20	0.555899	-0.020830	0.558526	0.042
H21	0.593226	-0.052228	0.715336	0.041
H22	0.696613	-0.013235	0.738535	0.033
H25	0.839326	0.220562	0.916264	0.026
H26	0.916828	0.228203	1.038333	0.033
H27	1.015900	0.299900	0.994128	0.035
H28	1.036169	0.361783	0.825066	0.034
H29	0.959373	0.354500	0.704150	0.026
H31	0.894097	0.394512	0.770185	0.029
H32	0.906855	0.477115	0.660629	0.036
H33	0.874529	0.466475	0.462065	0.040
H34	0.830055	0.372863	0.368112	0.039
H35	0.818854	0.290255	0.475321	0.029
H37	0.817435	0.300560	0.940961	0.032
H38	0.729542	0.287607	1.028720	0.042
H39	0.643063	0.251137	0.913315	0.050
H40	0.643555	0.227848	0.709676	0.048
H41	0.729904	0.235255	0.623166	0.034
H1S	0.560875	0.072847	1.028871	0.036
H2S	0.754011	0.183384	0.092440	0.047

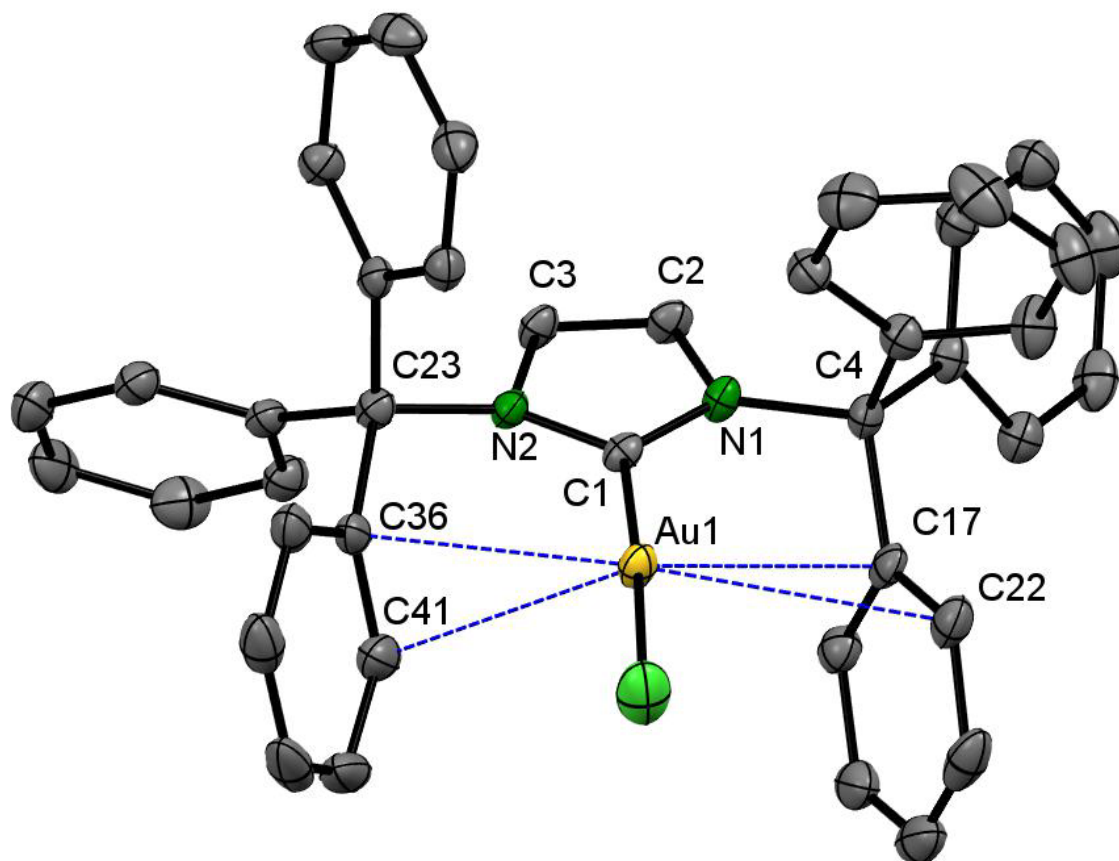


Figure S3.6: Molecular structure of [ITrAuCl] (**3.6**) showcasing intramolecular Ph - Au contacts, implying η_2 coordination. Au = yellow, N = dark green, C = grey, Cl = lime green. C1 - Au1: 2.014(4)Å. Au - Cl: 2.2793(11)Å. C1 - N1: 1.354(5)Å. C1 - N2: 1.357(4)Å. N1 - C2: 1.398(5)Å. N2 - C3: 1.390(5)Å. N1 - C4: 1.510(4)Å. N2 - C23: 1.511(5)Å. C17 - Au1: 3.170(4)Å. C22 - Au1: 3.338(4)Å. C36 - Au1: 2.998(4)Å. C41 - Au1: 3.079(4)Å. C1 - Au1 - Cl: 177.07(10)°. Au1 - C1 - N1: 128.1(3)°. Au1 - C1 - N2: 126.4(3)°. C1 - N1 - C4: 123.6(3)°. C1 - N2 - C23: 125.5(3)°.

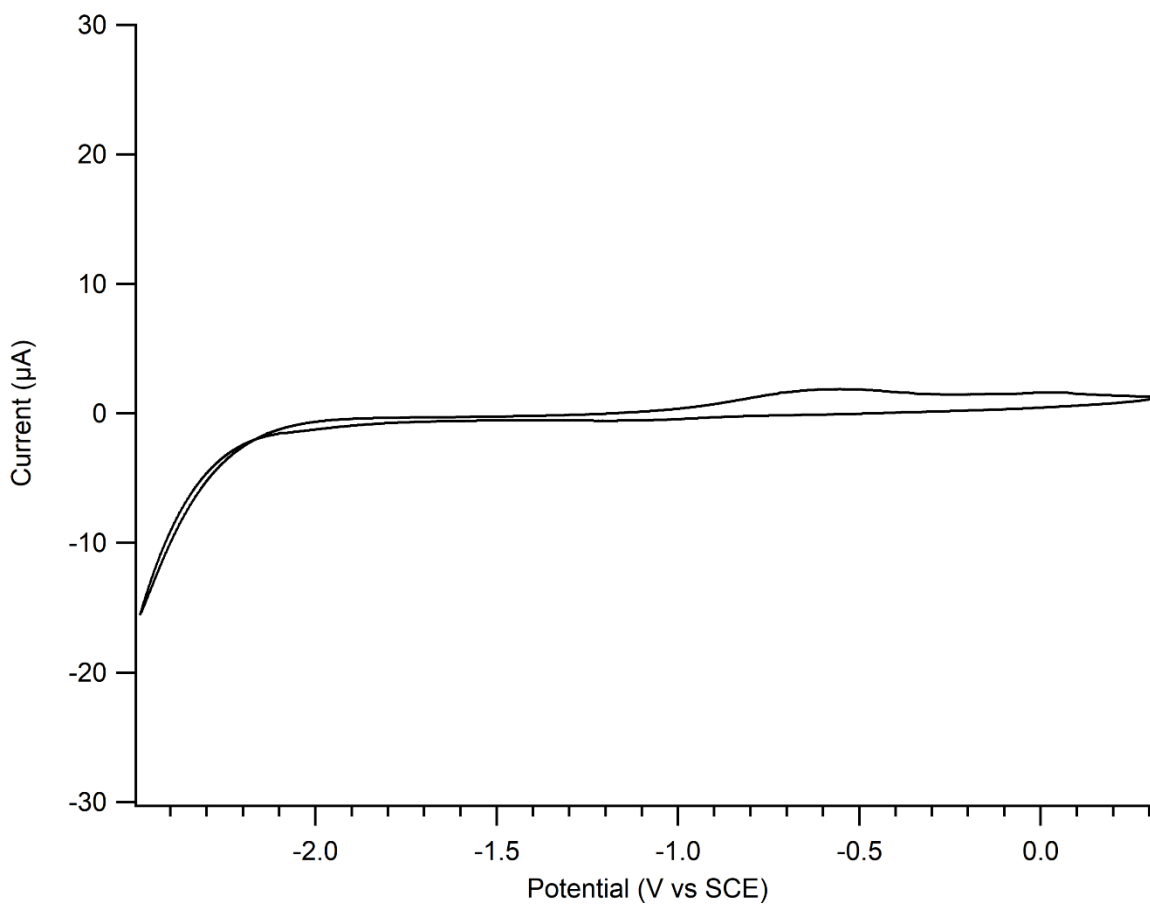
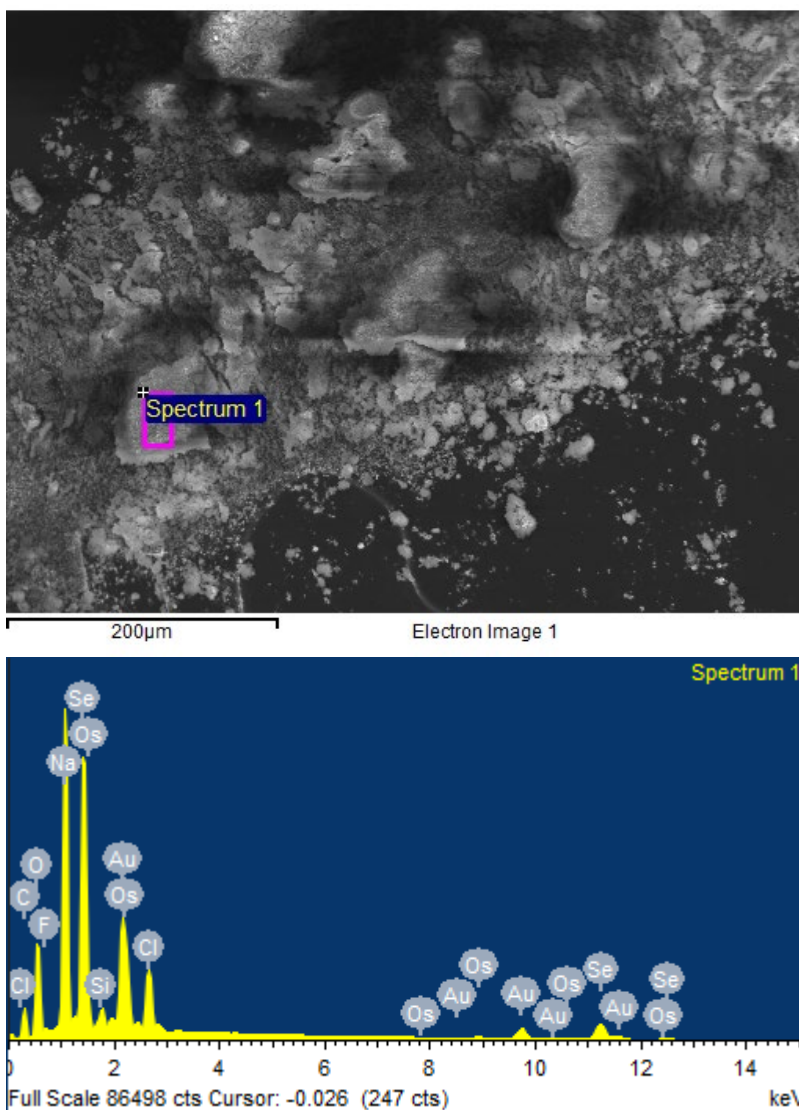


Figure S3.7: Cyclic voltammogram of [ITrAuCl] (**3.6**) in 3 mL MeCN (1mM sample, 0.1M TBAPF₆). Potential window of 0.316 to -2.484 V vs. SCE at scan rate of 0.1V/s. Pt disc working electrode and Pt wire counter electrode



Element	Weight%	Atomic%
C K	16.83	36.54
O K	18.49	30.12
F K	1.28	1.75
Na K	15.67	17.77
Si K	1.05	0.98
Cl K	3.88	2.85
Se L	21.79	7.19
Os M	1.81	0.25

Figure S3.8: Example of SEM - EDX data of solids isolated from 2:1 reaction of [ITrAuCl] and Na₂Se. Characteristic X – ray detected for each element listed (K shell, M shell, etc.).

Table S3.5: Crystal Structure Data for [(ITr)₂Au₂(μ₂-Cl)]OTf · 1.5 THF

Formula	C ₈₉ H ₇₆ Au ₂ ClF ₃ N ₄ O _{4.50} S
Formula Weight (g/mol)	1791.98
Crystal Dimensions (mm)	0.213 × 0.110 × 0.102
Crystal Color and Habit	colourless Fragment
Crystal System	triclinic
Space Group	P -1
Temperature, K	110
<i>a</i> , Å	14.0120(13)
<i>b</i> , Å	14.7021(14)
<i>c</i> , Å	22.266(2)
α, °	104.838(5)
β, °	97.263(5)
γ, °	112.970(5)
<i>V</i> , Å ³	3948.2(7)
Number of reflections to determine final unit cell	9840
Min and Max 2θ for cell determination, °	5.14, 55.48
<i>Z</i>	2
F(000)	1784
ρ (g/cm)	1.507
λ, Å, (MoKα)	0.71073
μ, (cm ⁻¹)	3.833
Diffractometer Type	Bruker Kappa Axis Apex2
Scan Type(s)	phi and omega scans
Max 2θ for data collection, °	55.478
Measured fraction of data	0.999
Number of reflections measured	67955
Unique reflections measured	18342
R _{merge}	0.0321
Number of reflections included in refinement	18342
Cut off Threshold Expression	I > 2σ(I)
Structure refined using	full matrix least-squares using F ²
Weighting Scheme	w=1/[σ(F _o ²)+(0.0777P) ² +29.5 829P] where P=(F _o ² +2F _c ²)/3
Number of parameters in least-squares	895
R ₁	0.0526
wR ₂	0.1429
R ₁ (all data)	0.0687
wR ₂ (all data)	0.1539
GOF	1.047
Maximum shift/error	0.001
Min & Max peak heights on final ΔF Map (e ⁻ /Å)	-2.521, 5.775 (disordered triflate)

Where:

$$R_1 = \frac{\sum (|F_o| - |F_c|)}{\sum F_o}$$

$$wR_2 = \left[\frac{\sum w(F_o^2 - F_c^2)^2}{\sum w F_o^4} \right]^{1/2}$$

$$GOF = \left[\frac{\sum w(F_o^2 - F_c^2)^2}{(\text{No. of reflns.} - \text{No. of params.})} \right]^{1/2}$$

Table S3.6: Atomic Coordinates for [(ITr)₂Au₂(μ₂-Cl)]OTf · 1.5 THF

Atom	x	y	z	U _{iso/equiv}
Au1	0.46558(2)	0.38161(2)	0.71720(2)	0.02675(8)
Cl1	0.45304(14)	0.42894(14)	0.82190(8)	0.0305(3)
Au2	0.40186(2)	0.56206(2)	0.84708(2)	0.02220(8)
C1	0.4619(6)	0.3139(6)	0.6248(3)	0.0335(16)
C2	0.4973(7)	0.2428(8)	0.5340(4)	0.047(2)
C3	0.3940(7)	0.2193(8)	0.5200(4)	0.048(2)
C4	0.2699(6)	0.2717(7)	0.5825(3)	0.0377(18)
C5	0.1796(6)	0.1974(8)	0.5215(4)	0.047(2)
C6	0.1561(7)	0.0905(8)	0.4994(4)	0.057(3)
C7	0.0726(8)	0.0215(10)	0.4462(5)	0.069(3)
C8	0.0114(7)	0.0565(10)	0.4157(5)	0.071(4)
C9	0.0308(7)	0.1590(11)	0.4372(4)	0.067(3)
C10	0.1172(7)	0.2315(9)	0.4906(4)	0.056(3)
C11	0.3012(5)	0.3888(7)	0.5927(3)	0.0367(17)
C12	0.3363(6)	0.4276(7)	0.5442(4)	0.0423(19)
C13	0.3724(7)	0.5311(8)	0.5508(4)	0.050(2)
C14	0.3744(7)	0.6031(8)	0.6062(4)	0.045(2)
C15	0.3408(6)	0.5665(7)	0.6554(4)	0.0409(18)
C16	0.3053(6)	0.4620(7)	0.6485(3)	0.0361(17)
C17	0.2336(6)	0.2321(7)	0.6375(4)	0.046(2)
C18	0.1517(7)	0.2526(8)	0.6597(4)	0.054(2)
C19	0.1175(8)	0.2175(9)	0.7106(5)	0.071(4)
C20	0.1599(9)	0.1611(8)	0.7360(5)	0.063(3)
C21	0.2319(8)	0.1332(7)	0.7099(4)	0.055(3)
C22	0.2672(7)	0.1687(7)	0.6610(4)	0.046(2)
C23	0.6557(6)	0.3509(7)	0.6347(3)	0.0365(17)
C24	0.6600(6)	0.3350(7)	0.7017(3)	0.0354(16)
C25	0.5907(7)	0.2400(7)	0.7057(4)	0.0386(17)
C26	0.5935(8)	0.2234(7)	0.7646(4)	0.047(2)
C27	0.6649(8)	0.3017(7)	0.8194(4)	0.047(2)
C28	0.7332(7)	0.3957(7)	0.8158(4)	0.045(2)
C29	0.7328(6)	0.4131(7)	0.7575(3)	0.0365(16)
C30	0.7101(6)	0.2921(8)	0.5947(4)	0.046(2)
C31	0.7236(7)	0.2098(8)	0.6072(4)	0.053(2)
C32	0.7673(9)	0.1534(10)	0.5685(5)	0.069(3)
C33	0.7961(9)	0.1818(11)	0.5160(5)	0.075(3)
C34	0.7834(8)	0.2647(10)	0.5029(5)	0.068(3)
C35	0.7418(7)	0.3204(8)	0.5425(4)	0.051(2)
C36	0.7036(6)	0.4659(7)	0.6388(3)	0.0403(18)
C37	0.8136(7)	0.5265(8)	0.6609(4)	0.050(2)
C38	0.8607(9)	0.6295(10)	0.6655(5)	0.070(3)
C39	0.7991(10)	0.6776(9)	0.6489(5)	0.068(3)
C40	0.6887(8)	0.6197(8)	0.6259(4)	0.055(2)
C41	0.6426(7)	0.5158(7)	0.6219(3)	0.045(2)
C42	0.3729(5)	0.6852(5)	0.8835(3)	0.0255(13)

C43	0.2983(6)	0.7863(6)	0.9307(4)	0.0331(16)
C44	0.4013(6)	0.8491(6)	0.9393(4)	0.0325(15)
C45	0.5666(5)	0.8288(5)	0.9240(3)	0.0260(13)
C46	0.5954(5)	0.8316(6)	0.9936(3)	0.0283(14)
C47	0.6415(7)	0.9240(7)	1.0452(4)	0.0419(18)
C48	0.6547(8)	0.9244(8)	1.1082(4)	0.056(2)
C49	0.6188(8)	0.8293(9)	1.1192(4)	0.055(3)
C50	0.5743(6)	0.7371(7)	1.0685(4)	0.0397(18)
C51	0.5623(6)	0.7380(6)	1.0070(4)	0.0328(15)
C52	0.6005(5)	0.7597(5)	0.8757(3)	0.0252(13)
C53	0.5631(5)	0.7392(6)	0.8101(3)	0.0303(15)
C54	0.5966(5)	0.6823(6)	0.7654(3)	0.0331(16)
C55	0.6693(6)	0.6465(6)	0.7858(4)	0.0337(16)
C56	0.7070(5)	0.6676(6)	0.8501(4)	0.0305(15)
C57	0.6749(5)	0.7268(5)	0.8954(3)	0.0260(13)
C58	0.6194(6)	0.9383(6)	0.9166(4)	0.0327(15)
C59	0.7315(6)	0.9935(6)	0.9384(5)	0.0420(19)
C60	0.7851(7)	1.0899(7)	0.9309(5)	0.048(2)
C61	0.7300(7)	1.1318(6)	0.9019(4)	0.045(2)
C62	0.6210(7)	1.0765(7)	0.8775(4)	0.045(2)
C63	0.5654(6)	0.9789(6)	0.8840(4)	0.0383(17)
C64	0.1789(5)	0.5876(5)	0.8860(3)	0.0260(13)
C65	0.1236(5)	0.5257(6)	0.8145(3)	0.0334(16)
C66	0.0250(6)	0.4383(7)	0.7998(4)	0.044(2)
C67	-0.0334(7)	0.3810(9)	0.7369(4)	0.058(3)
C68	0.0049(7)	0.4124(10)	0.6874(4)	0.060(3)
C69	0.1000(7)	0.5009(10)	0.7019(4)	0.059(3)
C70	0.1605(6)	0.5571(8)	0.7651(4)	0.044(2)
C71	0.2153(5)	0.5258(6)	0.9224(3)	0.0271(14)
C72	0.1941(6)	0.4218(6)	0.8932(4)	0.0351(16)
C73	0.2343(7)	0.3721(7)	0.9279(5)	0.044(2)
C74	0.2925(7)	0.4230(7)	0.9899(4)	0.0427(19)
C75	0.3137(6)	0.5266(6)	1.0195(4)	0.0349(16)
C76	0.2759(5)	0.5780(6)	0.9859(3)	0.0303(14)
C77	0.0981(5)	0.6229(6)	0.9134(4)	0.0316(15)
C78	0.0651(5)	0.6041(5)	0.9668(4)	0.0305(15)
C79	-0.0106(6)	0.6367(6)	0.9883(4)	0.0388(18)
C80	-0.0509(6)	0.6871(6)	0.9571(5)	0.045(2)
C81	-0.0193(6)	0.7049(7)	0.9021(5)	0.050(2)
C82	0.0541(6)	0.6722(7)	0.8812(4)	0.0436(19)
N1	0.5391(5)	0.3005(5)	0.5995(3)	0.0359(14)
N2	0.3719(5)	0.2627(5)	0.5762(3)	0.0379(15)
N3	0.2796(4)	0.6859(4)	0.8956(3)	0.0257(11)
N4	0.4468(4)	0.7878(5)	0.9086(3)	0.0279(12)
O1S	0.2917(11)	0.0739(11)	0.3695(7)	0.066(4)
C2S	0.2085(17)	0.0155(19)	0.3173(9)	0.080(7)
C3S	0.2419(16)	-0.0354(16)	0.2671(10)	0.064(5)
C4S	0.3631(18)	0.0388(19)	0.2842(10)	0.079(7)

C5S	0.3852(16)	0.0922(19)	0.3517(10)	0.073(6)
O2S	-0.049(4)	0.562(3)	0.5177(17)	0.24(2)
C6S	-0.068(2)	0.487(3)	0.4604(14)	0.082(8)
C7S	0.007(3)	0.442(3)	0.4581(13)	0.105(10)
C8S	0.0520(16)	0.4670(18)	0.5310(9)	0.047(4)
C9S	-0.002(2)	0.527(2)	0.5582(13)	0.082(8)
O3S	-0.0596(9)	0.9263(9)	0.9092(5)	0.044(3)
C10S	-0.0913(13)	0.9168(13)	0.8468(7)	0.045(4)
C11S	-0.008(2)	0.993(2)	0.8292(12)	0.104(9)
C12S	0.0688(16)	1.0692(14)	0.8950(9)	0.057(5)
C13S	0.0469(13)	0.9891(15)	0.9236(10)	0.062(5)
S1	0.6612(3)	0.1331(3)	0.27429(19)	0.0907(10)
O1	0.6165(6)	0.0206(6)	0.2483(4)	0.0671(19)
O2	0.6530(8)	0.2005(8)	0.2377(5)	0.100(3)
O3	0.6435(13)	0.1509(13)	0.3413(7)	0.171(6)
C1A	0.8012(13)	0.1732(17)	0.2961(10)	0.220(13)
F1	0.8430(13)	0.2772(13)	0.3269(8)	0.194(6)
F2	0.8234(13)	0.1611(13)	0.2403(8)	0.207(6)
F3	0.8047(17)	0.1164(17)	0.3365(10)	0.263(9)
H2	0.535895	0.223878	0.504896	0.056
H3	0.344481	0.180039	0.479148	0.057
H6	0.198061	0.065560	0.521201	0.068
H7	0.058097	-0.050357	0.431116	0.083
H8	-0.045564	0.009002	0.378873	0.085
H9	-0.014120	0.181946	0.416050	0.080
H10	0.131509	0.303362	0.504957	0.067
H12	0.334803	0.380386	0.505490	0.051
H13	0.396632	0.554502	0.517124	0.060
H14	0.398057	0.674877	0.610368	0.054
H15	0.342358	0.614052	0.694004	0.049
H16	0.282808	0.438837	0.682608	0.043
H18	0.120119	0.288896	0.641141	0.065
H19	0.064589	0.233202	0.727344	0.085
H20	0.139132	0.141529	0.771515	0.075
H21	0.257513	0.090053	0.725023	0.067
H22	0.316715	0.148372	0.643045	0.055
H25	0.540974	0.185921	0.667912	0.046
H26	0.546066	0.158020	0.766955	0.057
H27	0.666973	0.290724	0.859628	0.056
H28	0.781707	0.449885	0.853965	0.054
H29	0.781965	0.478096	0.755627	0.044
H31	0.702887	0.191063	0.642953	0.064
H32	0.776890	0.097502	0.577758	0.083
H33	0.824787	0.143998	0.488679	0.090
H34	0.803259	0.283022	0.466822	0.082
H35	0.734932	0.378093	0.534256	0.062
H37	0.857449	0.495391	0.673198	0.059
H38	0.936377	0.668444	0.680202	0.085

H39	0.832046	0.749749	0.653236	0.082
H40	0.645601	0.651203	0.613175	0.066
H41	0.566906	0.476834	0.607116	0.054
H43	0.246933	0.806773	0.945916	0.040
H44	0.437065	0.922322	0.962102	0.039
H47	0.664744	0.988882	1.037419	0.050
H48	0.687666	0.988612	1.143133	0.067
H49	0.625016	0.828121	1.161917	0.066
H50	0.551758	0.672257	1.076275	0.048
H51	0.530691	0.673313	0.972486	0.039
H53	0.514566	0.764603	0.796207	0.036
H54	0.570112	0.667556	0.720892	0.040
H55	0.692613	0.607523	0.755143	0.040
H56	0.755310	0.641785	0.863852	0.037
H57	0.704434	0.744497	0.939962	0.031
H59	0.770956	0.964578	0.958461	0.050
H60	0.860870	1.126849	0.946226	0.058
H61	0.766721	1.199222	0.898564	0.054
H62	0.582964	1.104939	0.855868	0.054
H63	0.490220	0.940620	0.866018	0.046
H66	-0.002337	0.417957	0.833660	0.053
H67	-0.099343	0.320476	0.727506	0.070
H68	-0.034193	0.373100	0.643954	0.072
H69	0.124641	0.524100	0.668259	0.071
H70	0.226979	0.616781	0.774158	0.052
H72	0.152634	0.384964	0.849998	0.042
H73	0.220632	0.301362	0.907705	0.053
H74	0.318668	0.387810	1.013001	0.051
H75	0.354190	0.562322	1.063009	0.042
H76	0.291374	0.649174	1.006124	0.036
H78	0.093373	0.569315	0.989060	0.037
H79	-0.033539	0.623332	1.024846	0.047
H80	-0.100522	0.710376	0.972443	0.053
H81	-0.048195	0.739111	0.879645	0.059
H82	0.074988	0.683711	0.843821	0.052
H2SA	0.180534	0.060906	0.303110	0.096
H2SB	0.150202	-0.037349	0.328158	0.096
H3SA	0.204542	-0.040847	0.224612	0.077
H3SB	0.229525	-0.106395	0.267368	0.077
H4SA	0.405693	-0.001056	0.275569	0.095
H4SB	0.377927	0.088463	0.259909	0.095
H5SA	0.427741	0.067264	0.376273	0.087
H5SB	0.427831	0.168461	0.361500	0.087
H6SA	-0.066114	0.518263	0.425997	0.099
H6SB	-0.140661	0.429640	0.450880	0.099
H7SA	0.064073	0.475683	0.438050	0.125
H7SB	-0.029384	0.365257	0.434808	0.125
H8SA	0.032216	0.402498	0.542550	0.057

H8SB	0.130841	0.508697	0.544608	0.057
H9SA	-0.057473	0.484195	0.575645	0.099
H9SB	0.050981	0.589281	0.594732	0.099
H10A	-0.157065	0.927189	0.840167	0.054
H10B	-0.108345	0.845375	0.818873	0.054
H11A	-0.037026	1.029784	0.805990	0.125
H11B	0.028495	0.960227	0.802176	0.125
H12A	0.144514	1.101999	0.893164	0.068
H12B	0.047051	1.123626	0.915480	0.068
H13A	0.084150	0.946281	0.908012	0.075
H13B	0.074966	1.021847	0.970763	0.075

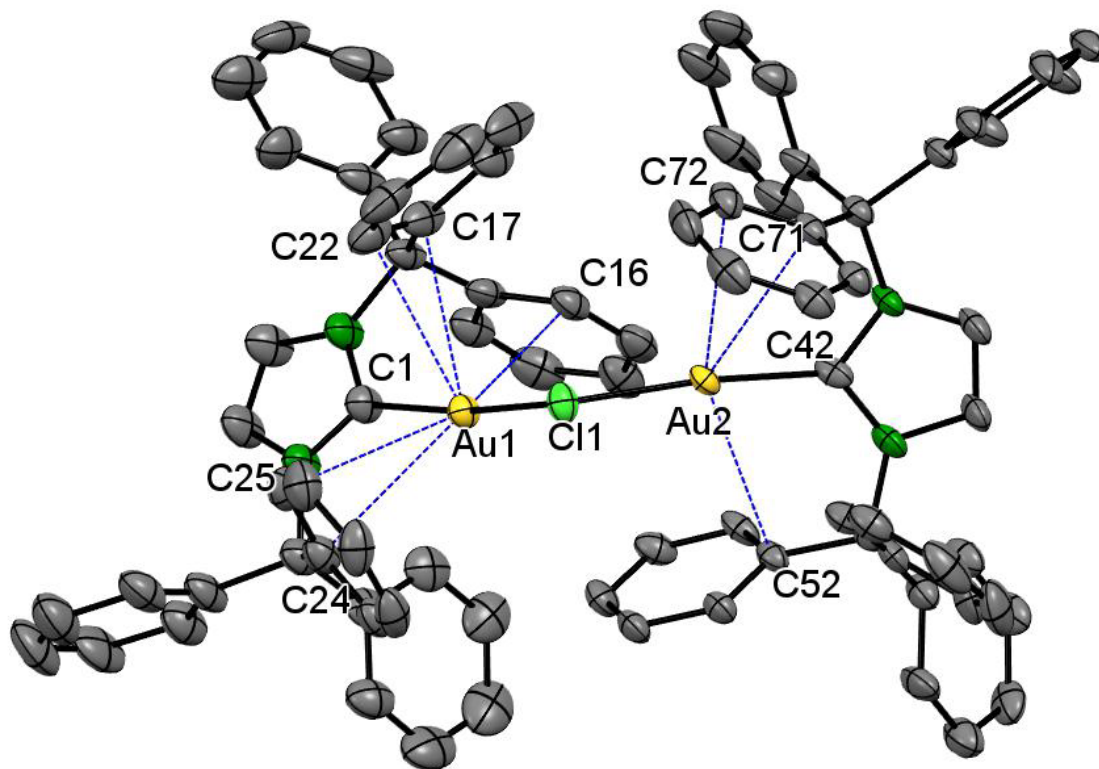


Figure S3.9: Molecular structure of $[(ITr)_2Au_2(\mu_2-Cl)]^+$ (**3.7**) showcasing intramolecular Ph - Au contacts, implying η_2 coordination. Au = yellow, N = dark green, C = grey, Cl = lime green. C1 - Au1: 2.028(7) Å. C42 - Au2: 2.001(7)Å. Au1 - Cl1: 2.3061(16). Au2 - Cl1: 2.3010(17)Å. C16 - Au1: 3.300(7)Å. C17 - Au1: 3.087(8)Å. C22 - Au1: 3.069(8)Å. C24 - Au1: 3.095(7) Å. C25 - Au1: 3.198(8)Å. C52 - Au2: 2.982(6)Å. C71 - Au2: 3.230(6)Å. C72 - Au2: 3.307(7)Å. Au1 - Cl1 - Au2: 113.07(7)°. C1 - Au1 - Cl1: 170.0(2)°. C42 - Au2 - Cl1: 170.58(18)°. Au1 - C1 - N1: 130.0(5)°. Au1 - C1 - N2: 123.9(5)°. C1 - N1 - C4: 122.4(6)°. C42 - N3 - C64: 123.8(5)°. C1 - N2 - C23: 124.7(6)°. C42 - N4 - C45: 126.8(5)°.

Appendix 2.1 – Calculation of Percent Buried Volume and Steric Maps

The *SambVca* web application was used for the calculation of percent buried volume ($\%V_{\text{bur}}$) to quantify the steric contributions of the various *N*-heterocyclic carbenes (NHC) discussed in this work. Using SCXRD data, the web application generates a coordination sphere of pre-defined radius about an atom of choice and calculates the volume of this sphere that has been occupied by other atoms from the ligand using the atomic coordinates and the Bondi radii of the atoms. The application allows for the generation of steric contour plots by allowing the user to define the *z* direction and the *xz* plane. For this work, various “coordination spheres” were investigated with the orientations of the molecules in each shown in **Figure S3.10**.

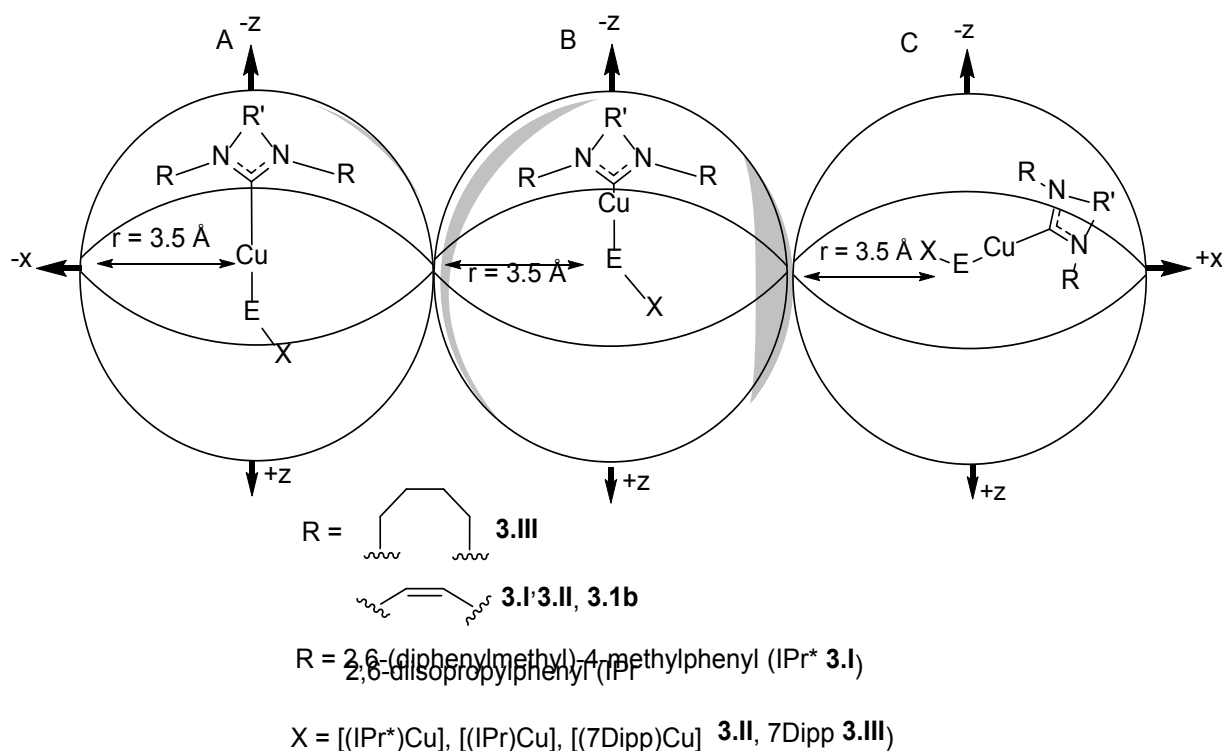


Figure S3.10: Orientations used to generate steric maps in Figure S.2. Orientation D is the map generated from observing from *-z* for orientation C. Labels are included for literature compounds visualized by this method in Figure S3.7 – Figure S3.9.

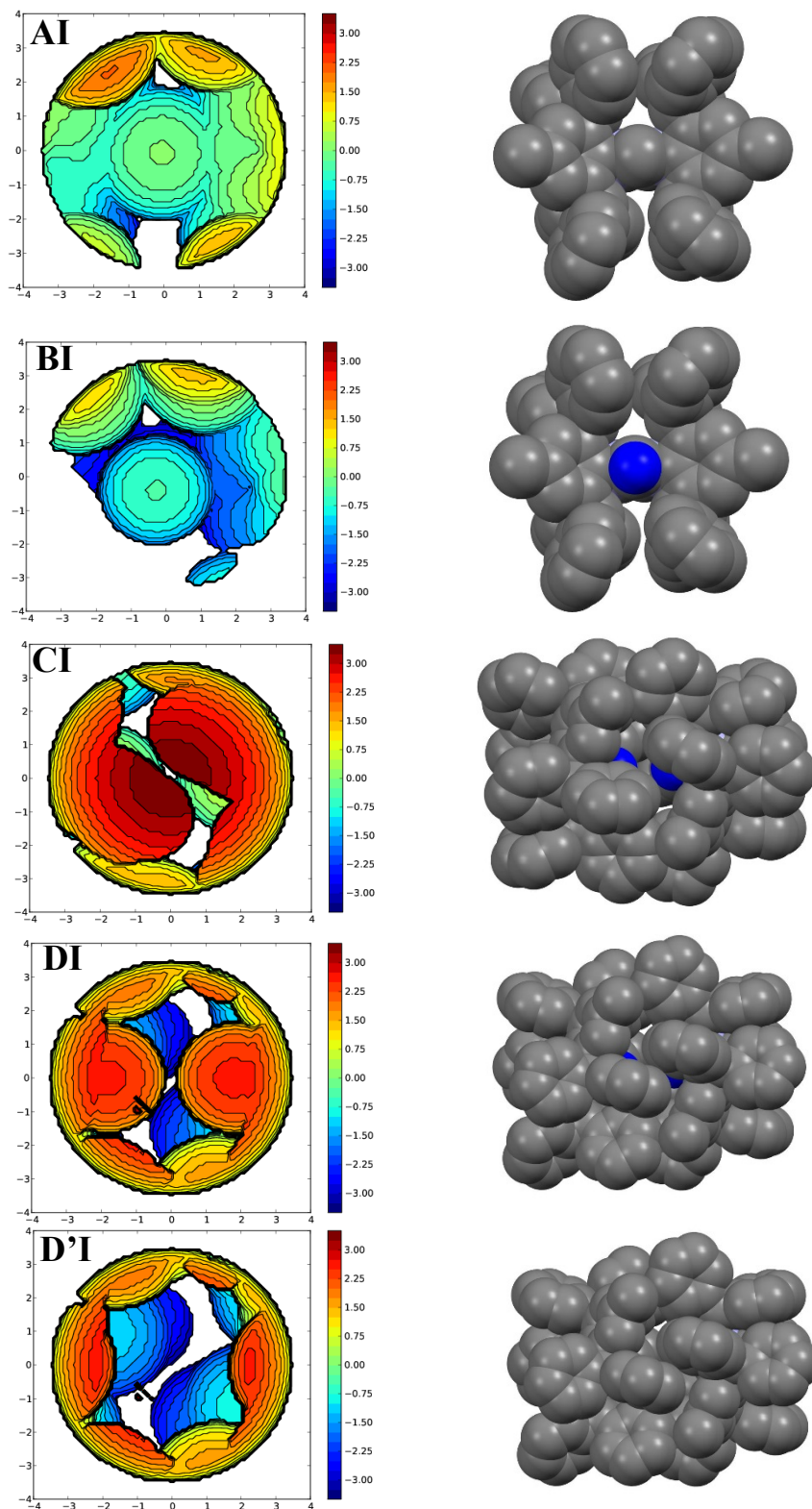


Figure S3.11: Steric Maps and Space Filling Models of $[(IPr^*)_2Cu_2(\mu_2-S)]$ (**3.I**). Space-Filling models illustrate orientation. blue = Cu^I , grey = C. Hydrogen and solvent omitted for clarity

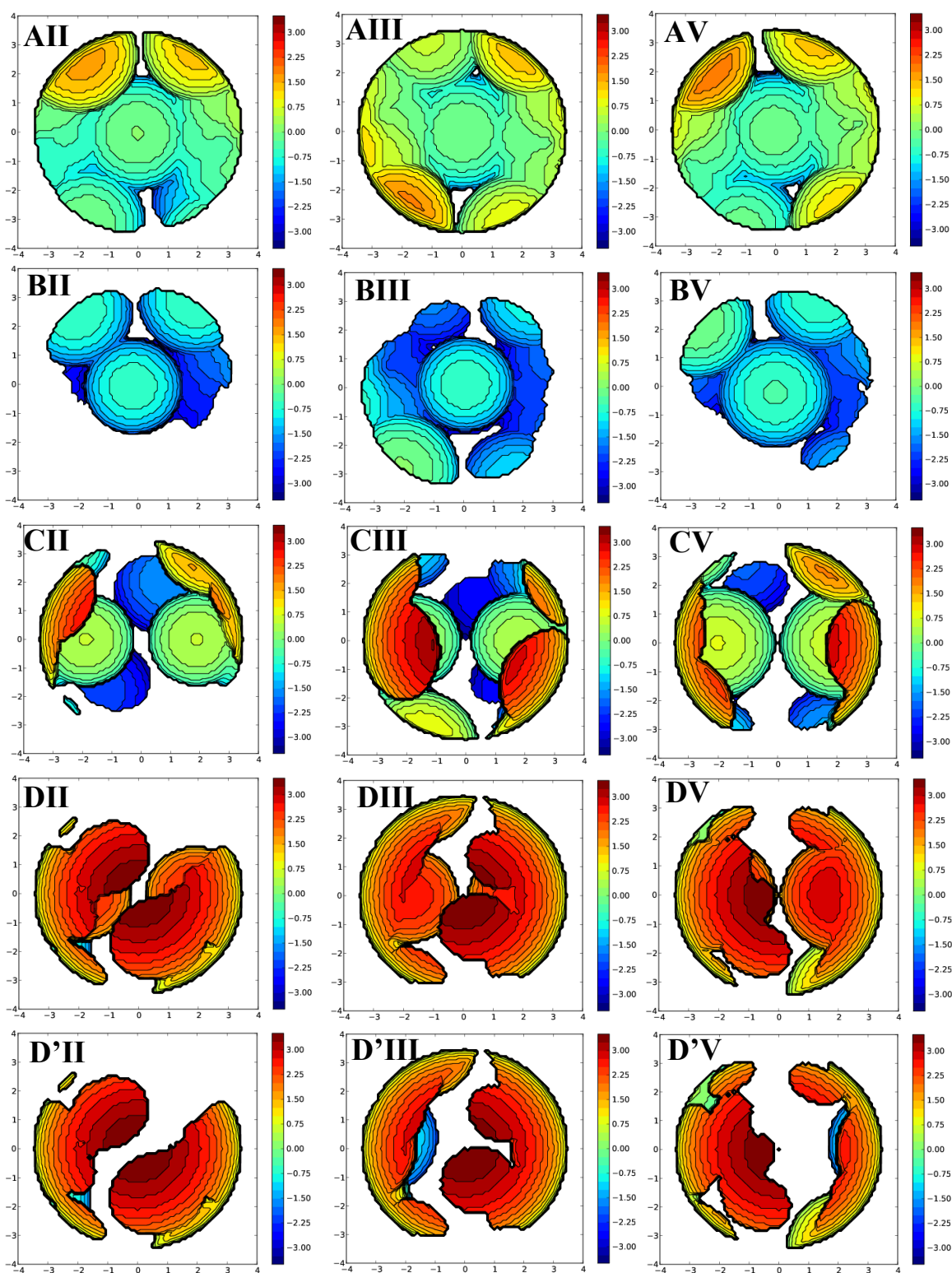


Figure S3.12: Steric maps of dinuclear compounds stabilized by 2,6-diisopropylphenyl containing NHCs, $[(\text{IPr})_2\text{Cu}_2(\mu_3\text{-SSiMe}_3)]^+$ (**3.II**), $[(7\text{Dipp})_2\text{Cu}_2(\mu_2\text{-S})]$ (**3.III**), and $[(7\text{Dipp})_2\text{Au}_2(\mu_2\text{-Cl})]^+$ (**3.V**).

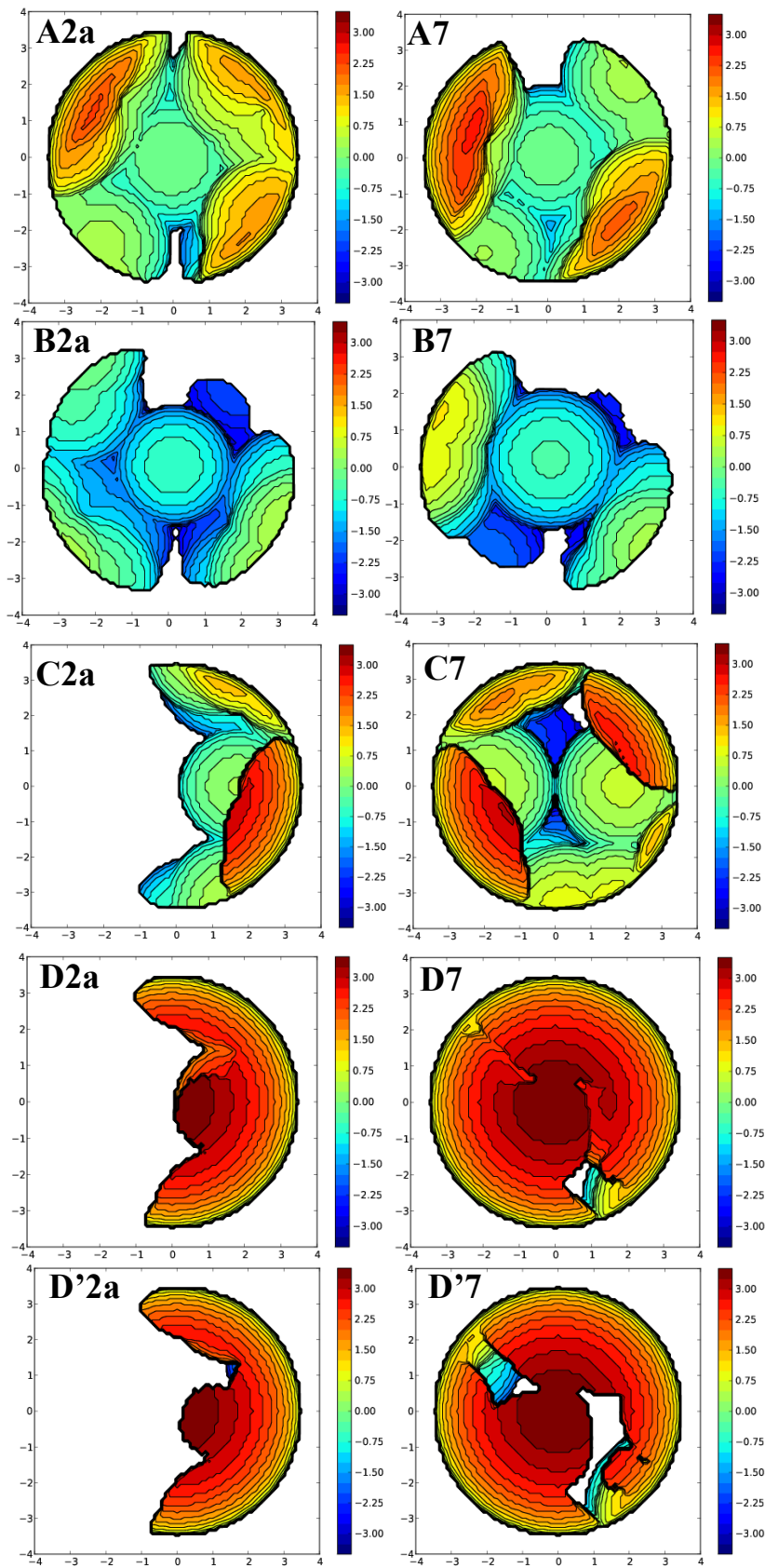


Figure S3.13: Steric maps of $[(\text{ITr})\text{CuSSiMe}_3]$ (**3.2a**) and $[(\text{ITr})_2\text{Au}_2(\mu_2\text{-Cl})]^+$ (**3.7**).

Table S3.2: %Vbur of coordination spheres generated about the central atom in **Figure S3.11 -Figure S3.13**. Values calculated using SambVca. Values for orientation C and D are identical.

	A	B	C	D'
3.I	50.1	28.2	55.2	42.8
3.II	48.0	17.9	33.4	21.0
3.III	55.6	20.7	44.3	31.8
3.V	52.6	22.8	42.4	21.2
3.1b	61.0	27.9	27.8	22.1
3.7	58.8	30.9	61.3	42.9

Curriculum Vitae

Dickron Richard Nahhas

Education

The University of Western Ontario London, ON
M. Sc candidate, Department of Chemistry, Sep. 2017 – Present
Thesis: *N*-Heterocyclic Carbene Ligated Group 11 Trimethylsilylchalcogenolates:
Building Blocks for Heterometallic Chalcogenide Molecules

York University Toronto, ON
B. Sc Hons. Chemistry, Sep. 2008 – Apr. 2016
Thesis: The Hydrothermal Preparation of Cu₃S₂/ZnS Core – Shell Nanoparticles

Volunteer & Work Experience

Indigenous Services at The University of Western Ontario London, ON
Chemistry & Math Graduate Student Tutor, Fall 2018 - Present

Science Rendezvous at The University of Western Ontario London, ON
Volunteer, Spring 2017

Surface Instrumentation & Engineering Laboratory at York University Toronto, ON
Research Assistant, Jan. 2017 – July 2017

Pietro Group at York University Toronto, ON
Undergraduate Research Assistant, Summer 2016

Conference Presentations

Oral Presentation (National). **D. R. Nahhas**, J. F. Corrigan*, *N*-Heterocyclic Carbene Ligated Group 11 Trimethylsilylchalcogenolates: Building Blocks for Heterometallic Chalcogenide Molecules, 102nd Canadian Chemistry Conference and Exhibition, Quebec, QC, 3rd June – 7th June, 2019.

Teaching Assistantships

The University of Western Ontario		London, ON
CHEM 2213A	Organic Chemistry for Life Sciences	Fall 2017
CHEM 2223B	Organic Chemistry of Biological Molecules	Winter 2018
CHEM 2213A	Organic Chemistry for Life Sciences	Fall 2018
CHEM 2223B	Organic Chemistry of Biological Molecules	Winter 2019

Graduate Courses Completed

CHEM 9503R	Advanced NMR Spectroscopy I
CHEM 9603T	Advanced NMR Spectroscopy II
CHEM 9541A	Crystallography I
CHEM 9657Y	Graduate Seminar Course